3D Hydrodynamic and Morphodynamic Modelling of Offshore Sandbanks

Stephen Andrew Clee

School of Engineering

Cardiff University, Wales, UK

Supervised by:
Professor Shunqi Pan and Dr Catherine Wilson

This thesis is submitted in partial fulfilment of the requirements for the degree of:

Doctor of Philosophy (Ph.D.)

September 2020

In memory of a very kind friend, who was so proud to see me start this journey.

Acknowledgements

There is one author's name on the front of this thesis, but this thesis is the result of the efforts of many people.

Primarily I must thank my supervisor, Professor Shunqi Pan, who has provided a tremendous amount of advice, support and guidance to me throughout the course of my PhD, both academically and personally. He has gone above and beyond expectations to help me succeed. I would also like to thank my second supervisor, Dr Catherine Wilson, for the time and help she has given me during this project.

I would also like to thank the many members of academic staff in the School of Engineering with whom I have had the opportunity to work with. They have provided a positive atmosphere to work in as well as guidance and experience which I shall always value. I must also thank all the staff in the Research Office who have not only helped navigate the administrative complexities of a PhD but have also provided sandwiches, cakes and other provisions to a hungry student.

This research was supported by the Engineering and Physical Sciences Research Council in the UK via grant EP/L016214/1 awarded for the Water Informatics: Science and Engineering (WISE) Centre for Doctoral Training and the British Council Newton Fund, which is gratefully acknowledged. The support and assistant received from Supercomputing Wales (SCW) in running some of the larger models is also gratefully acknowledged.

During my time studying, I had the privilege of travelling to Hohai University in China for a research visit. I am very grateful to Professor

Yongping Chen and his colleagues and students for their hospitality and for the knowledge and skills they imparted to me.

I have been supported by a wide variety of people throughout my time studying and to name them all could be a thesis in itself. I am particularly grateful for all my friends at WISE and Cardiff University. I am also grateful to the Australia Road crew who have endured the challenge of living with me over the past few years and to Joe and Dan for their many years of friendship. More so I am extremely thankful for my family especially my parents, who have provided me an unimaginable amount of support throughout this journey, for my siblings and for my "little monkeys" (my niece and nephew) who spread joy wherever they go.

My faith is a core part of my identity, so I remain thankful to God, whom I believe has provided me with the gifts and graces to succeed in what will be one of my life's greatest achievements.

Cardiff, 2020 Stephen Clee

Abstract

Offshore sandbanks are large sedimentary bodies observed on the bed of tidal seas around the world. They play a number of important roles in coastal environments including coastal protection, sediment sources for dredging, natural habitats and sites for offshore wind farms. Sandbanks are actively dynamic; formed and maintained by intensive currents and the local tidal regime. Understanding their response to hydrodynamic conditions and sediment transport processes is important for coastal management. Numerical modelling is seen as an important tool to study this. Simple numerical models can be easily developed to simulate and predict the response of sandbanks to a variety of physical processes. However, hydrodynamic and sediment transport processes are very complex and oversimplifying numerical models can lead to them becoming unreliable. For example, many numerical models use 2D hydrodynamics therefore neglecting the vertical velocity components - which are known to influence sediment transport.

This research aims to develop an advanced numerical model to study the effect of 3D hydrodynamics and morphodynamics on the offshore sandbanks in the southern North Sea.

The model results showed that in general the 2D model simulated lower velocities compared to the 3D model. The difference in the 2D and 3D depth averaged velocities was greatest during peak flows and the spring tidal cycles. The 3D vertical profiles showed that the near bed velocities at these times tended to be larger than the 2D depth averaged velocity. Since sediment transport is influenced more by the near bed currents, this implies that consideration of 2D hydrodynamics may in turn underestimate sediment transport rates and sandbank evolution.

Morphodynamic modelling showed that sediment was eroded in the sandbanks troughs and transported towards the crests. With consideration of a simple normal wave condition there was reduced deposition on the crest and some of the shallower crests exhibited areas of erosion. This pattern was not visible without the wave condition and highlights the need to consider all of these factors in tandem.

The publications derived from the work undertaken in this thesis are one journal paper and one conference paper. In addition, oral and poster presentations have been given to academics and industry representatives at number of events.

Journal paper

1. Chen, Y., Li, J., Pan, S., Gan, M., Pan, Y., Xie, D. and **Clee, S.** (2019). Joint probability analysis of extreme wave height and surges along China's coasts. *Ocean Engineering 177, 97-107.* [DOI: 10.1016/j.oceaneng.2018.12.010]

Conference paper

1. **Stephen Clee**, Shunqi Pan. 2D and 3D Modelling of Offshore Sandbank Dynamics. *38th IAHR World Congress.* Panama City, Panama. 2019

Nomenclature

Abbreviations

1D	One Dimensional
2D	Two Dimensional
3D	Three Dimensional
ASDIC	Anti-Submarine Detection Investigation Committee
CP	Coriolis Parameter
CSL	Coefficient to calibrate Sea Level
CTR	Coefficient to calibrate Tidal Range
CTV	Coefficient to calibrate Tidal Velocities
DR	Deposition Rate
ER	Erosion Rate
HAT	Highest Astronomical Tide
JONSWAP	Joint North Sea Wave Project
MAD	Mean Absolute Difference
MAE	Mean Absolute Error
NSE	Nash-Sutcliffe Efficiency
RMSE	Root Mean Square Error
SLR	Sea Level Rise
SPM	Suspended Particulate Matter

Dimensionless parameters

ϕ	Dimensionless current induced sediment transport
D_*	Non-dimensional grain diameter
s	Sediment density ratio
S_h	Fluid source or sink terms

Greek Symbols

α	Angle between defined axes
α_{ks}	Roughness height coefficient
α_{sc}	Secondary currents coefficient
α_{sf}	Angle between sediment transport and flow directions
β	Empirical coefficient for slope effect
β_2	Empirical coefficient for shape function
δ^*	Direction of bed shear stress
δ_{sc}	Direction of secondary currents
κ	von Karman coefficient
Λ	Latitude
λ	Bed porosity
μ	Friction factor
ν	Dynamic viscosity
ω	Angular velocity/angular frequency
ρ	Density
σ	Relative angular frequency
τ	Shear stress
τ_{cw}	Shear stress due to combined currents and waves
τ_c	Shear stress due to currents
τ_{sf}	Shear stress due to skin friction
τ_w	Shear stress due to waves
Θ	Shields number
θ	Wave propagation direction
υ	Kinematic viscosity
ε_s	Turbulent diffusivity of the sediment
φ	Wave phase

Roman Symbols

$\tilde{G}_n$	Gradient function in the normal direction
$\tilde{G}_t$	Gradient function in the tangential direction
A	Spiral flow coefficient
a	Tidal amplitude
A_0	Semi-orbital excursion

A_{bed}	Bedload coefficient
A_{ss}	Empirical sediment transport factor
A_{susp}	Suspended load coefficient
C	Depth Averaged concentration
C_D	Quadratic drag coefficient
C_f	Coefficient of friction
C_g	Group velocity of waves
C_{cf}	Chezy's friction coefficient
C_{eq}	Equilibrium near bed concentration
C_{sf}	Coefficient of friction due to skin friction
C_{zref}	Near bed concentration
d_{50}	Median sediment diameter
d_{90}	90% cumulative percentile sediment diameter
E	Directional spectrum of energy
E_w	Wave energy per unit area
F	Variance density directional spectrum
f	Wave frequency
F^c	Coriolis force
F^f	Friction force
f_r	Wave frequency
f_w	Wave friction factor
g	Acceleration due to gravity
h	Water depth
H_s	Significant wave height
H_{m0}	Significant spectral wave height
i	Hydraulic gradient
k	Wave number
k_s	Roughness height
L	Wave length
l	Vertical layer number
m_n	nth order moment
N	Directional spectrum of wave action
p	Pressure

p_d	Dynamic pressure
Q	Sediment transport rate
Q^*	Corrected sediment transport rate
R	Rouse number
r_s	Local radius of curvature
S	Source or sink term
T	Tracer concentration
t	Time
T_p	Peak period
U	Depth averaged velocity in the x-direction
u	Velocity in the x-direction
u_*	Friction velocity
U_c	Norm of the depth averaged velocity
U_w	Wave orbital velocity
V	Depth averaged velocity in the y-direction
v	Velocity in the y-direction
v_T	Tracer diffusion coefficient
v_t	Momentum diffusion coefficient
W	Depth averaged velocity in the z-direction
w	Velocity in the z-direction
w_s	Settling velocity
x	Cartesian space in the longitudinal direction
y	Cartesian space in the transverse direction
Z	Free surface elevation
z	Cartesian space in the vertical direction
z_0	Bed roughness
z_b	Bottom elevation
z_{rb}	Reference elevation above the bed
z_{ref}	Elevation at the bedload/suspended load interface

Superscripts

$\dot{(\cdot)}$	Transfer rate of variable
$\overline{(\cdot)}$	Time-averaged variable

Subscripts

$(\cdot)_0$	Initial variable value
$(\cdot)_{atm}$	Atmospheric variable value
$(\cdot)_{bed}$	Variable relating to bedload
$(\cdot)_{cr}$	Critical variable value
$(\cdot)_h$	Variable relating to water depth
$(\cdot)_i$	Variable relating to tidal component i
$(\cdot)_l$	Variable relating to layer l
$(\cdot)_{mod}$	Modelled variable value
$(\cdot)_m$	Variable relating to monochromatic wave component m
$(\cdot)_{obs}$	Observed variable value
$(\cdot)_{susp}$	Variable relating to suspended load
$(\cdot)_s$	Variable relating to sediment
$(\cdot)_T$	Variable related to tracer
$(\cdot)_t$	Variable at time t
$(\cdot)_x$	Variable along the x-direction
$(\cdot)_y$	Variable along in the y-direction
$(\cdot)_z$	Variable along in the z-direction

List of Figures

List of Tables

Contents

Chapter 1

Introduction

1.1 Context

Coastal zones are important social and economic resources. Globally, coastal zones are under increasing threat from the effects of climate change, erosion and flooding. Understanding the mechanisms of individual coastal processes is key to the successful long term management and protection of coastal zones and their resources. The coastal zone has always been of great importance for economic, cultural and recreational activities. Over past decades coastlines have undergone immense socio-environmental changes that are projected to continue into the foreseeable future. Population densities are much higher in coastal regions and there is an observed ongoing trend of migration to coastal areas [Neumann et al., 2015].

The United Nations estimated that by the year 2020, nearly 75% of the world's population will live in or near to coastal zones. Coastal environments offer a variety of important economic, residential and recreational functions which all depend on its physical characteristics. With increased pressure on coastal regions due to the effects of climate change and sea level rise, there is great scope to expand current coastal management schemes and improve our understanding of the complex governing processes in order to protect this vital resource for future generations [Chadwick et al., 2012]. The size of coastal communities is set to

dramatically increase making coastal erosion and retreat an important social and economic factor [Brooks, 2010]. Given the importance of the coastal zone to society as a whole, coupled with the threats that it faces, a great deal of work is needed in order to determine the most effective way of managing and protecting this vital resource.

Primarily, coastal modelling is undertaken using either physical models or numerical models. In recent years numerical modelling has become a useful tool in studying coastal environments and the various hydrodynamic and morphodynamic processes that affect them. Numerical models have several advantages over conventional physical models. They can be relatively simple to set up and take up a lot less space compared to a physical model. They are more adaptable and can easily be applied to a variety of domains. Advancements in computational power and efficiency, particularly the rise of supercomputing, means that much larger spatial and temporal time scales can be modelled more quickly. However, there are some drawbacks of numerical modelling. Most importantly, numerical models need to be calibrated and validated in order to be accurate. This often requires field measurements and/or the use of a physical model anyway. Coastal hydrodynamics and morphodynamics are highly complex processes which can sometimes therefore be oversimplified in numerical models. Finally, numerical models can be limited by their scope. Whilst short term trends can be quickly modelled, this does not necessarily mean that the model is applicable to long term trends. For example, modelling the effects of dredging on sandbank equilibrium could reveal a limited impact in the short term, but could neglect a significant impact in the long term.

It is suggested by van Maanen et al. [2016] that effective coastal management requires morphological modelling at a decadal to centennial time periods and a spatial length scale in the order of 10-100km. Reduced complexity models that can represent critical processes are proving effective at describing coastal behaviour. Developing qualitative models can aid the development of quantitative models which can be supplemented with data driven models. These modelling approaches have been considered in isolation but van Maanen et al. [2016] suggests that an integrated approach would present the best tool for coastal management.

1.2 Sandbanks

Sandbanks are the largest sedimentary body observed in tidally dominated continental shelves [Collins et al., 1995]. For consistency, this thesis will use the term sandbank, but in the literature other terms used include: Tidal ridges ([Off, 1963],[Liu and Xia, 1985]), Sand ridges ([Amos and King, 1984]), Open shelf ridges ([Dyer and Huntley, 1999] and Linear Sandbanks ([Collins et al., 1995].

1.2.1 Features

The dimensions of sandbanks can vary according to a variety of factors. The dimensions of sandbanks used throughout the literature are summarised in Table 1.1.

Table 1.1: Dimensions of sandbanks

Length	Width	Height	Spacing	Reference
8-64km	-	8-30m	1.6-10km	Off [1963]
55km	6km	up to 40m	-	Collins et al. [1995]
up to 60km	0.7-8km	1-30m	-	Amos and King [1984]
2-100km	5-10km	7-30m	1-10km	Liu and Xia [1985]
80km	13km	10s of m	-	Dyer and Huntley [1999]
5-70km	2-30km	13-43m	2-30km	Berne [2003]
1-10km	-	40m	5km	van der Veen et al. [2006]

Sandbanks are present on open shelf tidal seas where there is a supply of sediment and strong enough tidal currents to move that sediment. The current velocities required for the presence of sandbanks varies in the literature from between 0.5-3.5m/s ([Off, 1963], [Amos and King, 1984], [Liu and Xia, 1985], [Dyer and Huntley, 1999],[Carbajal and Montano, 2001]). Larger ridges require stronger

currents near the top end of this range to form and be maintained. Sandbanks tend to be orientated to the prevailing tidal flow. The angle of orientation varies with maximum values of 20-30° ([de Swart and Yuan, 2018],[Hulscher and van den Brink, 2001],[Collins et al., 1995] and typical values of 7-15° ([Amos and King, 1984]). The majority of sandbanks in the Northern hemisphere are rotated anti-clockwise to the tidal flow but some are rotated clockwise [Besio et al., 2005]. As a result of asymmetric tidal currents, sandbanks are often asymmetric in profile with a steep slope inclined at 6° to the horizontal ([Collins et al., 1995],[Dyer and Huntley, 1999]) and a gentle slope inclined at 1° to the horizontal. Sandbanks consist of a core material of coastal deposits [Berne, 2003]. The material is made up of well sorted homogeneous sediment, usually very fine to medium sands with a particle size varying between 62.5µm to 300µm ([Liu and Xia, 1985],[Huntley et al., 1993],[Collins et al., 1995],[Roos et al., 2004]).

Other recognisable features include linear to sinusoidal crest lines [Amos and King, 1984]. The majority of crestlines are flat with some observations of meandering crestlines [de Swart and Yuan, 2018]. Some sandbanks have the presence of sand waves or megaripples on the flanks [Amos and King, 1984].

1.2.2 Formation and Maintenance

Carbajal and Montano [2001] suggests that sandbanks are a time averaged response to the local hydrodynamic regime. Multiple processes including surface gravity waves, storm driven currents and tidal currents may be capable of transporting sediment, or even dominate the sediment mobility, but they are not necessarily all relevant to the process of sandbank formation. Pattiaratchi and Collins [1987] concludes that there are several different mechanisms that could be responsible for the formation and maintenance of offshore tidal sandbanks. These are summarised in the following sections:

1.2.2.1 Spiral Flow Concept

It was observed by Houbolt [1968] that the tidal currents were slower over the crest of a sandbank compared to in the channels between them. It was theorised

that the water would flow in two counter-rotating spirals to compensate for this. This results in the near bed currents being directed outwards from the channels and towards the sandbank crest. Asymmetry in the cross-section of the sandbanks is then a result of dominance on one side of the bank of these secondary spiral currents. Helical flows are caused by channels which are laterally constricted, suggesting that in unbound channels these helical flows may not exist. Therefore, this concept was more applicable to the maintenance of already formed linear sandbanks and the proposed model is not necessarily a mechanism by which these sandbanks were originally formed from a plane seabed.

1.2.2.2 Stability Model (Smith)

The mechanism proposed in Smith [1969] for the formation of large tidal sandbanks is an extension of a theory that was developed for the formation of smaller sand waves. It is indicated that as shear stress decreases in the x-direction, deposition occurs and similarly as shear stress increases in the x-direction erosion occurs. This theory proposes that in order for the growth of a sand wave to occur the maximum shear stress must occur upstream of the crest of a sand wave. The positive shear stress gradient extends from the windward slope up to the point of maximum shear stress. Then a negative shear stress gradient extends from the point of maximum shear stress over the crest and down the leeside slope. This effect causes erosion in the area of the windward slope and deposition along the crest and leeside slope. Although this theory was developed initially for bedforms such as sand waves where the height to width ratio is small, it was argued by Smith [1969] that this mechanism is still applicable to large sandbanks because of the transverse flow driven by the cross-bank pressure gradient.

1.2.2.3 Lateral Migration

Through detailed sand wave and current observations, it has been shown that on one side of a sandbank the tidal currents are flood-dominant whilst on the other they are ebb-dominant. On the sandbank itself, the crestline shows an area of stronger near-bed currents and a convergence of sand transport towards the crestline. This provides material for sandbank growth which proceeds both laterally

and vertically, the latter being limited by the water depth. The growth results from upslope movements of sand by near bed currents and downslope dispersion of sand due to sand wave action. Again, it was observed that asymmetry results from dominance of these processes on one side of the bank compared to the other. Caston [1972] proposed further theories for the sequence of sandbank migration, suggesting that initially a linear sandbank is present between an ebb and flood channel on either side. The dominance of sand transport in one particular channel causes the crestline to become kinked and the resultant curvature develops into a pair of ebb and flood channels. Next, these channels lengthen until a time when the central ridge becomes separated from the two kinks either side. This cycle then repeats but now there are three banks present. This process increases the number of banks whilst decreasing the spacing between them, although there is a larger spacing between offshore banks compared to nearshore banks. This theory is displayed in Figure 1.1 and applies to the maintenance of sandbanks rather than the origin.

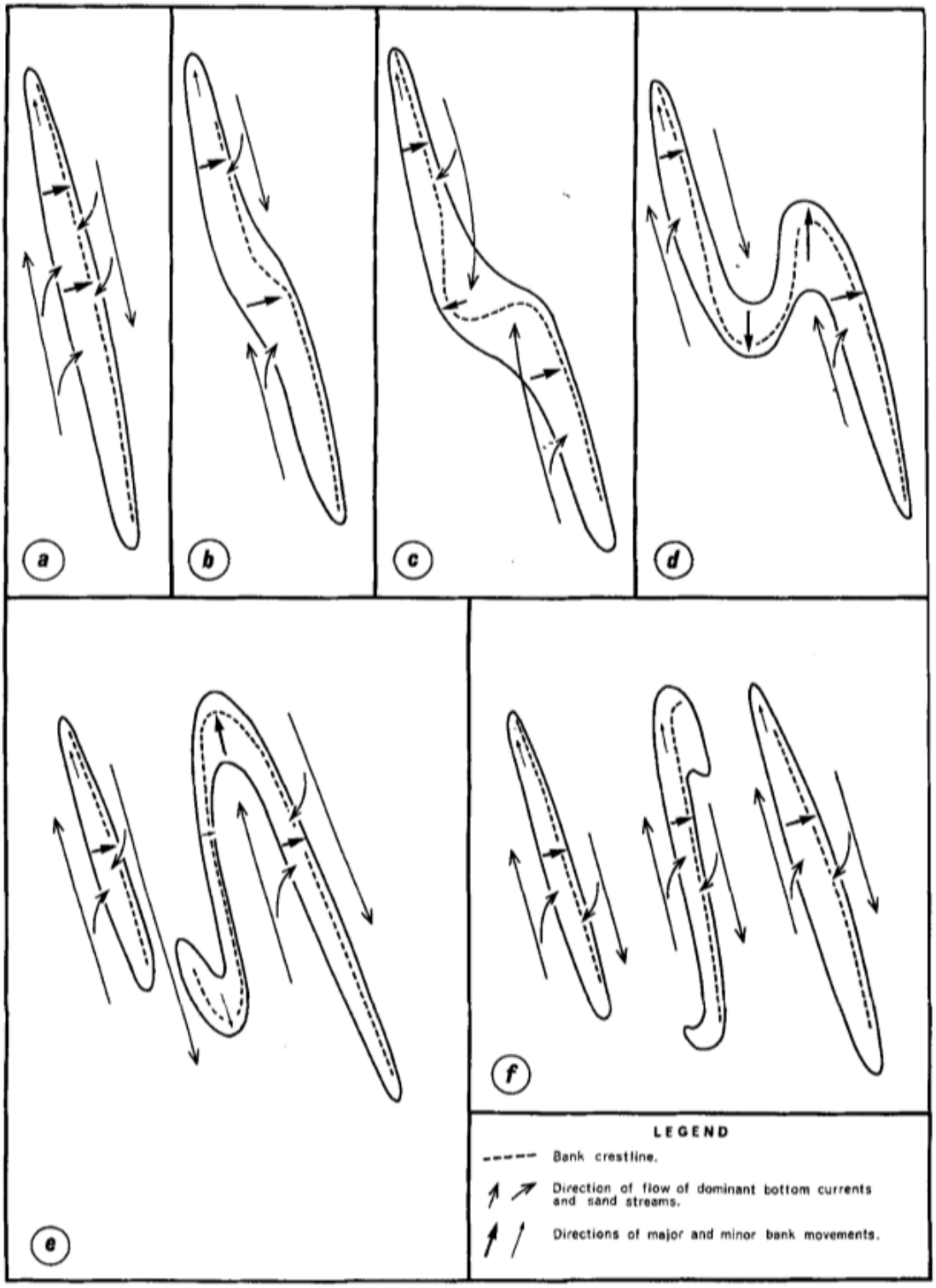

Figure 1.1: Sequence of bank migration (taken from Caston [1972])

1.2.2.4 Detachment from the Coastline

This proposed mechanism considers the formation of sandbanks which initially are connected to the shore-face. The sandbank can become detached from the shore-face under storm dominated conditions (as considered by Duane et al. [1972]) or by tidally dominated conditions (as considered by Belderson et al. [1982]). The hydraulic model considered by Duane et al. [1972] based on observations on the North American Atlantic shelf suggested that sandbanks formed as a result of increasing sea level. The rise in sea level and the associated shore-face retreat, intense storm generated currents and wave surges causes erosion at the landward end of the bank eventually resulting in the detachment of the sandbank from the coastline. These isolated banks continue to be maintained by helical flows created by storm currents or by the prevailing hydraulic regime. More efficient sand transport by wave action nearer to the coastline compared to offshore results in the angle of the banks being towards the coast. The sandbanks are then able to migrate as the water column becomes more constricted due to a reduction in water depth as the sandbank grows in height. For tidally dominated shelves, Belderson et al. [1982] proposed a mechanism whereby a sand spit becomes detached from a headland as a result of reversing tidal currents as they flow past the headland.

1.2.2.5 Tidal Stirring

The interaction between the tidal flow and a headland results in the creation of residual eddies. By considering the balance of forces and accounting for bottom friction and Coriolis forces, the circulation creates a low pressure region at the centre of the eddy. This causes convergence of flow at the seabed and divergence of flow at the surface. This flow convergence was presumed to cause accumulation of sand at the centre of the eddy resulting in another possible method of sandbank formation and maintenance. The model in Pingree [1978] shows this flow pattern of near bed convergence and surface divergence which results in a flow field similar to the helical flow model proposed by Houbolt [1968]. Numerical studies identified these flow patterns confirming this mechanism as one by which sandbanks can be formed and maintained.

1.2.2.6 Stability Model (Huthnance)

The stability model developed by Huthnance [1982a] investigated the growth of seabed topographic irregularities considering parallel depth columns. The model considered the growth rate of a sandbank as a function derived from depth averaged flow and sand transport rates. The growth rate was shown to be dependent on the angle between a bedform contour and the current direction, the normalised wave number, bedform spacing, water depth and seabed drag coefficient. Huthnance predicted that in the absence of wave action and with an unlimited sediment supply, sandbank growth would continue until it reached the water surface. Banks with a limited supply of sediment would be narrower and shorter and banks where wave action was a factor would present flatter and broader crests. Figueiredo Jr et al. [1981] found good qualitative agreement between the predictions of this model and the observed data in the mid Atlantic Bight and Parker et al. [1982] concludes that observations relating to sandbanks on the Argentine shelf were most adequately explained through this mechanism.

1.2.3 Classification

Sandbanks could be classified as a function of their core material and migration - "younger" ridges retain the initial nucleus of material whereas "fully-evolved" ridges have migrated sufficiently that their origin material is no longer present [Berne, 2003]. The most widely accepted classification of sandbanks used in the literature today was undertaken by Dyer and Huntley [1999]. At the time, Dyer and Huntley [1999] suggested that confusion in the terminology of sandbanks was due to the fact that many were described in terms of their hydrodynamic and morphodynamic context without consideration of their geology, origin or development. The proposed classification by Dyer and Huntley [1999] grouped sandbanks into three categories shown in Figure 1.2. Figure 1.2b shows the distribution of sandbanks in the North Sea according to this classification. The Norfolk Offshore Banks (area highlighted in red in Figure 1.2b) consist mainly of Type 1 (Open Shelf Ridges) and Type 3B (Alternating Ridges).

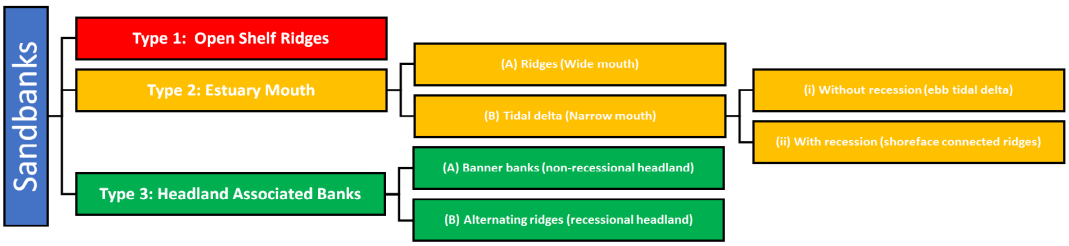

(a) Classification of sandbanks

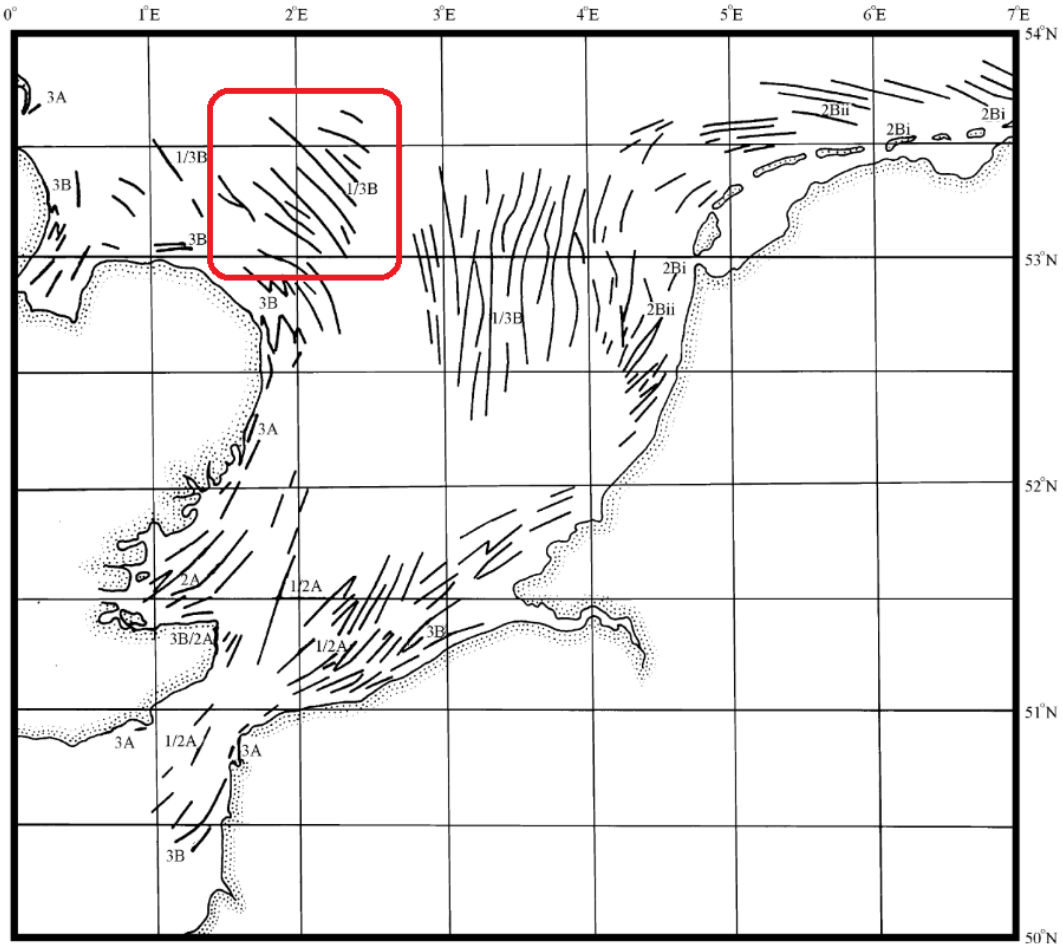

(b) Distribution of sandbanks in the North Sea

Figure 1.2: Classification and distribution of sandbanks in the North Sea according to Dyer and Huntley [1999]

Dyer and Huntley [1999] suggests that sandbanks can also be further categorised by two types: active and moribund. Yuan and de Swart [2017] classified their present behaviour similarly into three groups: active (those with sand transport everywhere), quasi-active (sand transport on parts of the bank) and inactive (those without sand transport). Active sandbanks are those which are maintained by the present tidal regime [Collins et al., 1995]. They are associated with areas of intense tidal currents and sediment supply. Active sandbanks are also characterised by imposed sand waves [Amos and King, 1984].

Moribund sandbanks tend to occur in areas where the water depth exceeds 200m, areas where tidal currents are too weak to cause sediment movement or areas where there is no sediment supply ([Collins et al., 1995],[de Swart and Yuan, 2018]). They are much larger with length scales of up to 200km, width scales of 55km, height of 55m and spacing of 20km. They have flatter cross sections and gentler slopes (around 1° or less) [Dyer and Huntley, 1999]. The crests are also more rounded compared to active sandbanks [Amos and King, 1984]. It is suggested that these sandbanks were formed at periods of lower sea level and have become isolated from the intense currents and sediments that formed them as the sea level has risen [Dyer and Huntley, 1999]. Examples of moribund ridges can be seen on the continental shelf of the Celtic Sea and in the deeper regions of the North Sea.

1.3 Purpose of Sandbanks

Sandbanks are a vital feature of shelf seas and fulfil a variety of important roles as follows:

1.3.1 Coastal Defence

The primary role of sandbanks is as a natural method of coastal defence [Lewis et al., 2014]. Sandbanks reduce the height of incoming waves providing a measure of protection for the adjacent stretches of shoreline. The protection provided by offshore sandbanks to the adjacent coastline is limited compared to the protection offered by sandbanks nearer the shoreline. This gives potential to the idea

of constructing artificial sandbanks as a sustainable method of coastal defence. Another option would be to dump large quantities of dredged material offshore to increase the height of already developed sandbanks.

1.3.2 Navigational Channels

Due to the fact that the crest of a sandbank can often be within a few metres of the water surface they can present a real hazard for shipping. Accurate understanding of the local and potential migration of offshore sandbanks is therefore necessary to help ensure the safe operation of shipping in coastal waters especially in the North Sea, a busy shipping lane where sandbanks are a common occurrence.

1.3.3 Biodiversity and Ecology

Sandbanks are an important environmental feature for a wide variety of organisms and as a means of encouraging biodiversity. The majority of sandbanks in the UK are defined as Special Areas of Conservation (SACs) due to their massive ecological and environmental importance [JNCC, 2017a]. Sandbanks provide a habitat for many different species such as worms, molluscs and crustaceans [JNCC, 2017b]. Sandbanks are also a feeding ground and spawning area for some species of fish [Lewis et al., 2014]. The importance of this ecological habitat extends to the larger organisms that depend on these species for survival.

1.3.4 Offshore Installation

The North Sea region contains large oil and gas reserves. As of January 2015, there were 173 active drilling rigs in the North Sea. These platforms and their associated pipelines are often constructed near or on sandbanks because of the reduced water depths. However, dynamically active sandbanks can present problems of scour and erosion. More recently, the North Sea is being considered as a suitable site for offshore wind farms due to favourable wind conditions. Table 1.2 (created from information taken from 4C Offshore Ltd [2018]) details some of the projects in the southern North Sea. Many of the current and newly planned

offshore windfarms are sited on sandbanks due to engineering efficiency and the positions of shipping routes. Again this raises questions about how these projects will impact existing sand transport pathways and the effects sandbanks could have on factors such as scour, erosion and deposition in the existing environment.

Table 1.2: Offshore Wind Projects in the Southern North Sea (sourced from 4C Offshore Ltd [2018]

Number of Projects	Stage	Number of Turbines	Capacity (MW)
5	Concept/Early Planning	426-494	3658-3858
4	Application Submitted	374-714	6340
2	Consent Authorised	176-248	2160
6	Pre-Construction	484	4216.5
2	Under Construction	125	933
1	Partial Generation	174	1218
24	Fully Commissioned	1451	5989.4

1.3.5 Sand Mining

Nearshore and offshore sandbanks can be used as a sediment source for a variety of purpose. Sand is a vital material for many industries. Finer well sorted sediments such as those found on sandbanks are ideal for use in the production of construction materials such as concrete and glass but also for silicon used in electronics. In addition to this, beach nourishment, shore protection, sandscaping and land reclamation projects all require sand as an aggregate in large volumes. Sandbanks are a possible source of the sediment required for these beach nourishment and land reclamation projects [Besio et al., 2005]. The success of these schemes requires the nourished sediment to be of a similar size and quality to the site sediment. This makes offshore sandbanks an ideal source since some of the sediment supplied to them is originally sourced from the nearby coast. The

Bacton to Walcott sandscaping scheme for example, will use approximately 1.8 million cubic metres of sand to construct an artificial sandbank in order to protect the coastline and vital infrastructure nearby [North Norfolk District Council, 2018]. In 2002, it was estimated that the UK extracted 12.8 million cubic metres of sand from coastal waters [Garel et al., 2009]. If intense dredging is carried out on sandbanks, it is important to predict their dynamics and responses to these human interventions [Besio et al., 2005].

1.4 Aims and Objectives

The primary aim of this research is to use an advanced numerical model to study the effect of 3D hydrodynamics and morphodynamics on the offshore sandbanks in the southern North Sea. The aim of this is to reveal whether the 3D hydrodynamics, particularly the vertical flow components have a significant impact on the behaviour and dynamics of established sandbank systems. This research aims to develop further knowledge in the field of coastal dynamics by highlighting the potential importance of developing numerical 3D models. Another aim is to attempt to combine physical processes, such as sediment transport and wave modelling, into the final model.

The main aims of this research will be achieved by the following specific objectives:

1. Develop and set up a 2D and a 3D TELEMAC model and apply the models to the offshore sandbanks in the southern North Sea

2. Calibrate and validate the model against observational data.

3. Analyse the hydrodynamic results of the 2D and 3D models and compare the differences between the 3D vertical profiles and the 2D hydrodynamics

4. Further develop the models to include sediment transport processes and morphological changes. Analyse the results of the sediment transport model to determine the influence and effects of 3D hydrodynamics on the morphological behaviour of sandbanks

5. Include a wave model to determine the influence of waves on the morphological behaviour, considering this in relation to both 2D and 3D hydrodynamics.

1.5 Outline

This thesis comprises of eight chapters organised as follows:

Chapter 2 details a comprehensive review of the published literature in order to ascertain the current state of knowledge with respect to hydrodynamic and morphodynamic modelling and their applications to sandbanks. This is organised chronologically in order to better reflect how the knowledge has changed and developed over time from early research to more recent developments.

Chapter 3 describes the theory and governing equations behind the software used to form a technical foundation for the numerical modelling.

Chapter 4 describes the early model development along with the study site to which it is applied.

Chapter 5 presents the results of the 2D hydrodynamic model testing in terms of its calibration, validation and sensitivity.

Chapter 6 details the development of the 3D hydrodynamic model as well as presenting the results and the comparison between the 2D and 3D hydrodynamics along with discussion of the impacts and significance of this.

Chapter 7 develops the 2D and 3D hydrodynamic models previously described to include sediment transport processes and the effects of a simple normal wave condition. Again it compares the differences between the 2D and the 3D models with a focus on the bed level changes in the region of the Norfolk Banks.

Chapter 8 concludes the results of this research and recommends several areas where the work could be improved or expanded.

Chapter 2

Literature review

2.1 Introduction

The aim of this literature review is to determine and evaluate the body of literature and research that covers the field of 2D and 3D modelling in coastal engineering relating more specifically to sandbanks both regionally and globally. The aim is to establish the progress and limitations of previous studies and identify potential areas that this research can build upon and/or identify the gaps that this research can fill. This literature review is ordered chronologically starting at some of the earlier research and progressing on to more recent studies. However, successive studies by the same author are grouped together for continuity purposes.

2.2 Studies on Sandbanks

2.2.1 Early Studies

Stride [1963] noted that there was a lack of published information of sediment transport pathways on continental shelves. The majority of early understanding of sediment movement in the North Sea was obtained by using sand traps to measure the amount of sediment moving and relating this to tidal current data.

For example VanVeen's 1936 study cited in Stride [1963] had concluded that in the channels off the coast of Belgium, some channels would see sediment movements induced by the ebb currents and others by the flood currents. Later, by using echo-sounding, the presence of a number of large underwater sand dunes was revealed. It was interpreted that the steep northern slopes corresponded to a northward transport of sand. Robinson [1960] identified similar features near the English coast. Stride [1963] expanded this thinking by studying these features and expanding the search for such features in the North Sea. In the southern North Sea, a front approximately 40 miles wide was identified as one of the most important sand streams. Sand transport rates across this front were estimated as $4 \times 10^6 m^3$ per year. Another such sand stream is located near the Norfolk banks extending south contributing to the sandbanks in the Thames Estuary. A second stream extends northwards from the Norfolk banks although the sand moved here is relatively small based on the structure and occurrence of the sand waves there.

By studying bathymetric charts in coastal areas characterised by large tidal ranges (greater than 3m) and strong tidal currents (0.5-2.5m/s), Off [1963] noted that there were two types of sand accumulation that could be observed. The first type referred to as tidal ridges, are rhythmic bedforms orientated parallel to the tidal currents. Their composition is mainly sand but some also contain mud and silt. The second observed feature was sand waves. These are larger ripples orientated perpendicular to the current direction. Although generally a small scale feature, evidence suggests that in the open ocean they can have heights exceeding 8m. At this time, it was unclear what the relationship between the smaller scale sand waves and large scale tidal ridges was, although they were observed in the same environments. They are a common feature observed globally with the North Sea, Bay of Korea and Gulf of Cambay displaying well developed examples of these features.

Robinson [1966] assessed the importance of residual currents in fashioning the seabed configuration from hydrographic data such as marine surveys, drogue runs and current observations. The pattern of banks, sediment circulation and morphological changes closely reflect the residual current movements. Robinson [1966] noted that the assumption that nearshore velocities are too small to move sediment led to the role of tidal currents in coastal evolution being neglected.

However, under certain conditions it is stated that even velocities as low as 0.5m/s are capable of moving heavier grades of sediment. It was also estimated that offshore currents in the North Sea range from 1.2-1.7m/s at the surface and are 10% lower near the bed. Dominant deposit in the shoal area is medium sand of 200-300µm. It was concluded that the net movement of sediment is in the direction of residual currents and that this leads to evolution of offshore sandbanks with both lateral and longitudinal movements occurring. This residual current pattern and associated sandbanks are conducive to sediment arriving on the shoreline and the degree of erosion and accretion experienced by a coastline is related to this as well as the available sediment supply.

In 1968 Houbolt studied the characteristics of sandbanks in the southern North Sea. This work showed the effect of the environment on the formation and structure of sandbanks. Subsequently many authors have commented on this pioneering work. Houbolt suggested that the complicated internal structure of these sandbanks was down to the fact that the flood and ebb currents do not follow the same path. It was also concluded that the sediment material was derived from the seabed and originated from post glaciation deposits or sand deposited during times when the sea level was lower [Houbolt, 1968].

Later work by Smith [1969] showed that sand waves would grow if sediment was deposited on the crest. In order for this to happen, the maximum boundary shear stress would have to occur upstream of the crest. This theory for sand waves also applies to sandbanks provided that the sandbank is broad relative to its height. Further growth occurs when the maximum rotary currents are parallel to the orientation of the sandbank. It was suggested that theoretically the limit of sandbank growth would be continuous, i.e. the sandbank would grow until it reaches the free surface. However, the presence of wind waves at the surface causes sediment erosion thus the true limit of growth is determined by a balance between erosion caused by wind wave induced velocities and deposition caused by tidal currents.

Caston and Stride [1970] outlined sand wave areas by using detailed echo-sounding surveys and side-scan ASDIC equipment to determine their crest orientation. Current measurements were obtained from a combination of direct readings from anchored vessels, drilling barges, production platforms and subsur-

face buoys. This sand wave and current data was analysed and suggested that the long sandbanks in the southern bight of the North Sea experience a northerly flow of sand on the western slopes and a southerly flow of sand on the eastern slopes. The steeper north-eastern slopes of the sandbanks indicate that the north-westerly flow of sand on the west side of the sandbanks must be of greater impact than the opposite south-easterly flow on the east side of the sandbanks. The asymmetry in the sandbanks could provide an indication of the extent of the long term dominance of the net sand flow since small changes would not move enough sand to alter the asymmetry of the banks. The presence of an internal structure within the sandbanks also confirms this observation and suggests a lateral migration of the sandbanks in that direction. They concluded that at present there was no general explanation as to why the peak tidal flows to north or south are limited to opposite sides of the channels. This localised sand transport pattern is also in keeping with the wider regional sand transport patterns observed earlier by Stride [1963].

Caston [1972] observed that the majority of the linear sand banks in the Norfolk Banks area of the southern North Sea are considered to be large-scale mobile bed forms in dynamic equilibrium with the environment, thus confirming much of the earlier work of Houbolt [1968]. Sand streams moving in opposing directions on either side of a bank were shown to be deflected upslope, and therefore converge at the crestline. The asymmetry of a sandbank was considered to be a result of the dominance of one of these streams. Convergence of sand streams causes an accumulation of sand which results in the growth of the bank parallel to the direction of flow of the tidal currents. This study confirmed that sand streams are deflected towards the crest on both sides of a bank. This explains how the crestline is emphasized and perpetuated. In addition, it was clearly demonstrated that sand streams move in opposing directions on either side of the bank which agrees with the observations made in previous studies. Vertical growth will be limited by the depth of water, but the method of lengthways growth is not proven. It was suggested that lengthways growth could be a result of oblique movements of sand upslope induced by tidal currents. Houbolt [1968] has suggested migration rates of around 1.6km over a period of around 70 years, however, Caston [1972] suggested migration rates of between 300-700m over a period of 100 years.

Research by McCave [1978] studied the grain size distribution on the East Anglian coast. The apparent coarsening of sediment in the net wave driven transport direction was ascribed to the finer sediments being dispersed offshore by tidal current. McCave suggested that the coastline nesses are points where sediment is lost offshore rather than gained, especially during storm surges and periods of abnormal wave and tidal activity. This was directly opposed to the view expressed in Robinson [1966]. Robinson [1980] expanded the original study ([Robinson, 1966]) indicating that "both tidal currents and wave action play a part in shoreline change". The author concluded that offshore sandbank systems play a complex role in coastal evolution which relies on both tidal current and wave processes to transport bed sediment. These effects have greater impact for offshore sandbanks that lie close to the shoreline where the influence on wave energy is greater. Carr [1981] also reviewed these opposing views using more recent data available from the East-Anglian coastal zone. Carr [1981] concluded that neither argument is proven but it is more likely that nesses are places where sediment is lost from the nearshore rather than gained from offshore. This aligned more with the view of McCave but the author conceded that "It is clear that further research is warranted especially into the way in which onshore/offshore transfer of the varies grades of sediment takes place.". The various offshore sandbanks studied have migrated differently over time. The author suggested that the majority of the Norfolk banks have remained stable over the last few centuries but some banks are slowly migrating offshore.

Zimmerman [1981] concluded that although the existence of residual tidal eddies could be explained by quasi 2D dynamics and bottom morphology, this theory does not necessarily explain the bottom morphological features from the residual current pattern. It was suggested that a 2D approach would require incorporation of the interaction between time varying seabed morphology and the tidal current pattern, indicating that for suspended sediment transport the vertical structure of the velocity field is important for producing residual transport. Dimensionality of the theory can be a limiting factor. Observational evidence of residual currents on sandbanks was scarce and what observations were available could not necessarily be explained by 2D theories. At the time, there was also a lack of development of the relevant 3D theories.

Stride et al. [1982] noted that offshore sandbank formation was often attributed to pairs of helical circulations rotating in opposite senses to the axes parallel to the direction of the peak tidal current. However, Stride et al. [1982] suggested that these circulations may in fact play a bigger role in the building up of already formed sandbanks.

Another main contribution to the body of early research in the area of sandbanks was done by Huthnance. Huthnance [1973] implemented a 2D analytic model for oscillatory tidal flow over parallel sandbanks. This concluded that Coriolis force and bottom friction are both responsible for distinct mechanisms of mean current generation. The model was applied to tidal current data which resulted in an indication of clockwise current circulation around the Norfolk Sandbanks. In Huthnance [1982a] a model was created whereby the fluid depth depended on both horizontal co-ordinates, quasi-steady flow depended on inertial pressure and bottom friction and sand transport was proportional to the instantaneous current and wind-wave action. This model concluded that low parallel bars grow fastest and support the calculations of linear banks in spatially extensive uniform seas. Therefore, sandbanks could be interpreted in terms of vorticity generation and advection of flow over a hump. This hump would then evolve into an equilibrium bank depending on the supply of sediment and the limitations on growth imposed by wind-wave erosion. It was suggested that the sandbanks studied were in the late state of evolution whereby they are slowly lengthening due to net current sediment transport occurring along the side of sandbanks causing deposition as it turns around the bank ends. Stability in evolution is then reached with exception of when an overall bed slope is in the direction of the mean current or when the sediment supply in abundant. The model predicted that the maximum growth rate occurs when the ratio between the sandbank spacing and the water depth was 250. This relationship showed good agreement between the model predictions and observed data. Huthnance [1982b] expanded this model stating the combination of effects described previously results in a stronger upslope current. This would transport sediment onto the sandbank faster than the reverse tidal current would transport it off. Assuming the sediment is more easily transported downhill, the growth of short wavelength perturbation of the sea bed are suppressed and the maximum growth rate of a bed form is related to its wave-

length and orientation. The orientation is likely to be sensitive to the behaviour of adjacent coastlines. In friction dominated tidal currents, sandbanks evolve to a profile that is flatter rather than sinusoidal owing to wind-wave induced erosion and inclination to the tidal currents. Where sediment supply is limited, banks narrow to approximately one fifth of their spacing and further restrictions on sediment supply limit their height. In the Norfolk banks area, the observed steeper slopes on the downstream side of the banks relate to the dominance of the ebb tidal currents over the flood tidal currents. The results suggested that a bank would rotate to align itself with the axis of greatest deposition. A sandbank would grow lengthways providing that the angle between the tidal currents and the bank was between 18° and 48° with the maximum volume growth occurring at an angle of 27°. The model also predicted reversal of the mean tidal current at the ends of a sandbank which has been supported by observational evidence. Both of these models predict features of sandbanks including bank inclination to tidal flow, asymmetric profiles and the veering of tidal currents and sediment transport across sandbanks. All of these features have been confirmed by field observations from several other researchers [Pattiaratchi and Collins, 1987].

Robinson [1983] discussed the generation of tidally induced residual flows and the vorticity mechanisms around parallel sandbanks. It was theorised that as fluid columns move onto the sandbanks they are squeezed. This generates clockwise anticyclonic vorticity (for sandbanks located in the northern hemisphere). Then as the column moves off the sandbanks they spin up cyclonically. This effect occurs independent of the tidal flow direction and the net effect is that over a tidal cycle there is a negative vorticity in the shallow water area and a positive vorticity in the deep water areas. Bottom friction also enhances vorticity and the frictional stress has a greater effect on shallow water columns compared to deep water columns. The resulting current pattern has residual flows parallel to the sandbanks which manifests as an asymmetric flood/ebb tidal flow.

Howarth and Huthnance [1984] used current data measurements of the Well bank in order to determine the locally generated tidal asymmetries. It was noted that the semi-diurnal components were dominant and also rectilinear and inclined to the bank axis. The fourth diurnal currents were consistent with measurements with the area overall. They appeared to be generated by the tides but only a small

part locally. Averaged over a tidal cycle, the residual currents were circulating clockwise around the bank which is consistent with simple numerical models. This gives strong evidence towards the thinking that they are necessary and important for the generation of sandbanks. The circulation combines with the semi-diurnal tidal currents to help maintain the sandbanks. Finally it was concluded that a persistent component of the residual current onto the bank 7 metres above the bottom may indicate distortion of the friction layer by the sloping bottom or by bank curvature.

Pattiaratchi and Collins [1987] used surface bed morphology data, sediment size data and current meter data in order to calculate and predict the sediment transport rates for sandbanks located in the Swansea Bay region. The data showed that water circulation in the vicinity of a headland associated sandbank was governed by the instantaneous flow across it and the residual flow around it. The instantaneous flow pattern depends on the tidal state. The residual flow is generated by a combination of bottom friction and the Coriolis effect due to the water column stretching and squeezing as it travels over the bank. The observed currents in this region are consistent with active sandbanks in dynamic equilibrium with the tidal conditions. The same behaviour does not correlate to moribund sandbanks which tend to be located in much deeper waters. Pattiaratchi and Collins [1987] concluded that "Although patterns of sand and water movement have been identified, using a variety of techniques and approaches, they do not appear to be associated with a single mechanism for sandbank maintenance. Rather, the field observations can be explained in terms of the combination of a number of possible mechanisms" (which are detailed in section 1.2.2).

Huntley et al. [1993] measured the seabed drag coefficients at the Norfolk banks in the North Sea using pressure sensors and current meter data. The results showed that drag coefficient increases with wind conditions. The results suggest that the consideration of sediment movements is important for numerical models that consider wave/current interactions. The sand movements in the region were also studied using fluorescent sand tracing. This showed evidence of the early stages of development of a new bank between the Broken and Well banks.

Hulscher et al. [1993] used a modified version of the models used by Huthnance

[1982a,b] and Huthnance [1982b]. It was noted that the models previously used by Huthnance did not describe a mode with a finite wave length which would become unstable with variations in hydraulic parameters. This is supported by the observation that bedforms will not be present if water depths are too large or tidal amplitudes are too low for example. Hulscher et al. [1993] stated that the model is also limited by neglecting the vertical structure of the current. However it is known that the secondary circulations in the vertical plane have an effect on sediment transport. The inclusion of these factors into the developed models then predicted the formation and growth of sand waves and ridges. The ellipticity of the tide introduces a critical parameter below which bed form growth is prevented. The values of the numerical parameters applied to the North Sea indicated a critical wave length of approximately 8km which is consistent with regional observations. Limitations of this study were that the linear stability analysis presented was only valid for small bed perturbations, providing information only on the initial stages of growth and development. In order to assess long term morphodynamic behaviours, a non-linear approach was suggested. However, Hulscher et al. [1993] suggested that a non-linear analysis would result in a more complex topography with varying length scales which is contrary to the rhythmic patterns that have been observed. Hulscher [1996] described a 3D model that calculated the bottom shear stress explicitly but also studies vertical flow effects. The model was similar to others previously described in that it consists of coupled hydrodynamic and sediment transport parts, but with the vertical effects considered by a constant viscosity and a slip condition. Depending on the parameter values, the model could accurately predict the development of all the bedforms observed (sandbanks, sand waves and parallel ridges). Hulscher [1996] concluded that a 3D model that captures the vertical profiles is necessary to predict the formation or absence of all large scale bedforms. Hulscher and van den Brink [2001] then expanded this work and tested the predictions of a numerical model against observations of sandbanks and sand waves in the North Sea. Developing the original 3D model, Hulscher and van den Brink [2001] derived a model based on parameters (specifically water depth, tidal velocity, level of zero intercept and an eddy viscosity variation parameter). By using spatially varying values of these latter two parameters, the model was able to accurately predict the bedforms in

the southern North Sea, but there were other factors not included in the model that would explain whether or not bedform features would develop.

Berne et al. [1994] noted that since the initial studies done by Houbolt [1968] very little progress had been made on analysing the internal structure of tidal sandbanks. Seismic records indicated that the bedding material in the Norfolk banks consisted of inclined reflectors parallel to the banks steep face. From a stratigraphical point of view there are two main types of tidal sandbank. The first are sandbanks whereby bank growth is related to the convergence of sand transport which have cores consisting of Holocene deposits. The second are sandbanks where the cores consist of eroded fluvial or estuarine sediments (typically Holocene deposits for nearshore banks and Pleistocene deposits for offshore banks). The sediment composition of the internal structure may have an impact on sediment transport processes and the development and migration of sandbanks, but this angle does not appear to be incorporated into numerical models thus far.

Lanckneus et al. [1994] analysed the behaviour of sediments on a sandbank in a macrotidal environment over medium and long terms to determine the interactions between water movement, sediment transport and bedform mobility. Results specific to the Middelkerke Bank off the coast of Belgium showed that the overall volume of the bank decreases during periods of heavy weather and rebuilds itself during periods of fair weather. Seasonal variations showed a volumetric change of $-21\% - +26\%$ over a winter-summer cycle. However, these values were considered as extreme values and observed changes may in fact be less pronounced.

Collins et al. [1995] recorded current velocities at 2m above the bed and mid depth at 10 minutes intervals to determine tidal current patterns. Artificial sand tracers were used to determine sediment transport patterns. The use of tracer data was limited by insufficient spatial sampling meaning that the results could only be used qualitatively. South-easterly currents are stronger than the opposite North-westerly currents in the swales between sandbanks. This tidal current pattern is consistent with the known regional sediment transport pattern. However, in the swale between the Well and Broken banks the residual current is in a North-easterly direction which directly contradicts the observations of Caston

and Stride [1970]. This contradiction could be the result of meteorological conditions. Offshore transport pathways cause the sandbanks to grow both vertically and laterally. Lateral migration from studying bathymetric charts appears limited. Sediment composition of the sandbanks also does not provide evidence of lateral migration. Magnitude of current speeds and particle size suggest that the transport mode lies between material moving in suspension and bedload. Tidal currents alone result in transport via bedload but small increase in near bed currents caused by wave induced currents or storm surges is enough to cause mobilisation of sediment and transport in suspension. This in turn has a significant impact on the localised sediment transport pathways.

Kamphuis [1995] concluded that using 2D wave-flume experiments over of 3D wave-basin experiments to model beach profiles did not influence the time scale of morphological changes. However, the resultant long term profiles were substantially different. It was also demonstrated that although equilibrium conditions could be reached with respect to fluid flow and sediment transport rate, an equilibrium profile does not necessarily develop in either the field or in laboratory experiments.

2.2.2 Recent Studies

Recently, Williams et al. [2000] stated that little is known about the sediment transport patterns within a sandbank system over long term periods or the response of such systems to severe storms or long term climate change. Currently, the numerical modelling of sandbank systems includes tidal and hydrodynamic components. The effects of natural changes (e.g. sea level rise) and anthropogenic changes (e.g. commercial dredging) are neglected. The paper discussed field investigations and numerical modelling studies of hydrodynamics and sediment dynamics of the Middelkerke Bank. In low wind stress conditions, a 3D model was able to predict clockwise residual currents around the bank consistent with established theories. The strong current refraction was attributed to the reduction in water depth over the crests of sandbanks. The spatial and temporal variations of the drag coefficient were also found to be strongly correlated to the tidal current. By using fluorescent sand tracers, the field investigation showed

clockwise sediment movement around the bank, a feature that was replicated by the numerical model and also consistent with theory. The results suggested that the Middelkerke bank has a small influence on the nearshore wave heights.

Reeve et al. [2001] used historic bathymetric surveys coupled with a Geographical Information System to construct a detailed seabed topography. With this, the study focused on using an Eigenfunction analysis to examine temporal changes in sandbank morphology specifically relating to the Great Yarmouth banks. One particular finding was that there was a gradual upward trend in the volume of the upper sections of sandbanks. This suggests that the sandbanks have been growing steadily taller over long periods of time. However, based on the assumption that the sandbanks have already developed into a dynamic equilibrium, this growth must therefore be down to a morphological response to changing sea levels. Using crude calculations to estimate the volume of the sandbanks from simple geometry, the author was able to equate the annual change in height, noting that this was an order of magnitude greater than the sea level rise over the same time period and therefore there were other factors involved in contributing to this growth. The lack of volumetric change at lower depths suggests that the banks are fed by material directly from the coastline or by retention of material moving across open boundaries.

At the time of Carbajal and Montano [2001], no previous attempts had been carried out to describe the relationships between tidal velocities, latitude, horizontal length scales and the orientations of sand ridges. Carbajal and Montano [2001] attempted to fill this gap by using the model described by Hulscher and van den Brink [2001] along with elliptical tidal currents and Coriolis forces to determine if this would cause significant changes in the predicted sandbank orientation and wavelength. Additionally this would observe how realistically these models could predict sandbank wavelength under a variety of tidal conditions. The results revealed that there was a linear dependence between the orientation and wavelength of sandbanks and the latitude of the Coriolis term, provided that the water depth and tidal conditions were fixed. The model was applied to theoretical curves from a number of global sites with good agreement between the two. It was concluded that this model could contribute to the understanding of sandbank systems in a variety of tidal regimes.

Idier and Astruc [2003] studied linear and non-linear behaviour of sandbanks using a combination of linear stability analysis and numerical modelling. The numerical modelling approach used depth averaged hydrodynamic equations, a quadratic friction law and bedload sediment transport. The numerical model appeared to underestimate the growth rates of the most unstable modes due to hydrodynamic inaccuracies. The characteristics of continental shelf sandbanks showed good agreement with the model's estimation of temporal dynamics. A comparison with North Sea field data gave a slight overestimation of the saturation height, likely due to processes that were neglected in the numerical modelling. Estimations of the migration rates appeared reasonable with historic observations. Although morphodynamic modelling provides insight in the dynamic behaviour of sandbanks, it is still in part limited by computational resources.

Roos and Hulscher [2003] used simple models to describe the large scale bed evolution in shelf seas. The model accounts for bedload and suspended load. It was concluded that the behaviour of large scale features was dependent on the inclusion of Coriolis and friction mechanisms. The bedload transport can be seen as a limiting case of suspended load transport. The model was considered in 2D and thus limited in its application to the horizontal length scale of sandbanks. Also the effects of wave interactions was neglected which limited the models applicability to offshore conditions. The author recommends that long term observational data could benefit the area of study involving morphological responses of sandbank systems. Roos et al. [2004] developed a non-linear morphodynamic model that resolved the dynamics on a tidal timescale allowing for asymmetric tidal flows. It was attempted to model the sandbank profiles in ways not considered before by addressing the morphodynamic evolution to an equilibrium profile, the influence of different tidal components on bank profiles and a comparison with observed bank profiles in the North Sea. It was shown that bedload transport under symmetric tidal conditions leads to high, spiky banks which become lowered and smoothed by processes including suspended sediment transport, wind wave stirring and asymmetric tidal flow. Bathymetric data gives fair agreement with the modelled profiles but the results are limited by the small number of banks observed and uncertainty in the input parameters.

Besio [2004] and Besio et al. [2005, 2006, 2008] proposed a 3D model to de-

scribe the generation and evolution of tidal sandbanks. A 2D horizontal flow with Coriolis effects was resolved in the vertical direction from the seabed to the surface. The flow regime considered was a turbulent flow following the Boussinesq approach. Sediment transport was modelled as bedload and suspended load and the effects of wind waves were considered. This work points out that the direction of the rotation of the tidal wave plays a predominant role in the formation of a tidal sandbank. However, the model could not predict whether these tidal ellipses were clockwise or counter-clockwise because it did not solve tidal propagation. The model suggests that the orientation of the sandbank is opposite to the orientation of the tidal ellipse (i.e. clockwise rotating tides produce counter-clockwise orientated sandbanks and vice versa). This behaviour seems to be independent of the strength of the tidal currents and the water depth. However, variation in these parameters produced bedforms of different scales. Similarly, increasing the sediment size parameter did not produce significant qualitative changes. Limitations of this 3D model were that the amplitudes of the bedform considered were small and a linear approach used. As previously discussed this means that only the initial formation and growth can be simulated, not the long term morphological behaviour. The model predictions were accurate when compared to other morphodynamic stability analyses [Besio et al., 2006].

Horillo-Caraballo [2005] and Horrillo-Caraballo and Reeve [2005] developed a tidal model for the South North Sea with particular attention to the Great Yarmouth sandbanks. The authors state that it was the most detailed analysis of tidal hydrodynamics for that area at the time in terms of both tidal harmonics and grid resolution. The numerical model was used to investigate the changes in time averaged flow statistic near coastal sandbanks. The model computed residual currents, Reynolds stresses, eddy statistics and vorticity and investigated whether these hydrodynamic parameters had an impact on morphological change. The preliminary results suggested that this hydrodynamic information was necessary to explain the configuration and development of offshore sandbanks in the long term, which proves a vital tool for coastal management [Horrillo-Caraballo and Reeve, 2005]. The Reynolds stresses showed a coherent spatial and temporal structure which enabled the interpretation of the action of tidal eddies in driving residual current patterns and sediment transport and morphological changes.

Horillo-Caraballo [2005] concluded that there was scope to extend these results by comparison with historic bathymetric charts to calibrate and validate morphological changes. In addition to this the model could be expanded to include 3D effects, storm surge and wave effects as well as having the sea bed morphology and current velocity feedback each other.

Kenyon and Cooper [2005] stated that sandbanks will be maintained where the peak current is greater than 0.9m/s and the near bed currents are greater than 0.55m/s. As water depth increases over time (e.g. due to the effects of sea level rise) active sandbanks can become stranded in areas of weak currents causing them to become moribund. A proposed evolutionary theory is that sandbanks will form at a retreating coastline as a banner bank, develop into an equilibrium state as an open shelf ridge and finally end up as moribund when the sediment supply cannot keep up with the pace of coastal retreat [Dyer and Huntley, 1999]. Sandbank movement should be considered separately from the movement of other bedforms such as sand waves. Despite being much larger scale bedforms, the migration rates of sandbanks can vastly exceed that of the much smaller sand waves. Open shelf sandbanks have been recorded as moving laterally at a rate of up to 40m/year. The relationship between offshore sandbanks and their adjacent coastline is poorly understood but of pivotal importance when relating to the supply of sediment to and from the coastline and also for consideration of schemes such as offshore windfarms. Bedload transport moves more slowly and less widespread compared to suspended sediment and therefore the local transport pathways are considered most important.

Grunnet and Ruessink [2005] studied the response of a nearshore sandbank system to shoreface nourishment in the Netherlands. Under normal conditions, the system is characterised by a state of dynamic equilibrium whereby a morphological feedback mechanism engenders a cyclic offshore directed migratory behaviour. The implementation of the nourishment scheme was shown to greatly impact the stability of this dynamic behaviour resulting in a 6-7 year postponement in the cross-shore bank development. Eventually however, the system recovered its pre-nourishment dynamic equilibrium. The nourishment scheme also altered the onshore/offshore sediment transport balance with an observed increase in onshore sediment transport at the expense of offshore sediment trans-

port. Hence offshore sandbanks which are reliant on this sediment supply for maintenance would be greatly impacted by such schemes.

The work by Stansby et al. [2006] and Kuang and Stansby [2006a,b] aimed to determine whether sandbanks of increased height, whether naturally or artificially, would reduce or reverse the effects of sea level rise on coastal erosion. The question raised by the dumping of dredged material onto offshore sandbanks was - to what extent the material remains on the bank or alternatively is washed away by the tidal regime. It is theorised that if the tidal regime is causing erosion of offshore sandbanks, then it will also simply erode any dumped material. Accurate numerical modelling of hydrodynamic and morphological conditions could give an indication of whether the hypothesis proposed by Stansby et al. [2006] are plausible, although it is accepted that the modelling of some processes, namely sediment transport, involves high levels of empiricism and is therefore far from precise. One key factor proposed by Stansby et al. [2006] is that the effects and influence of storm waves should be considered. The results showed that wind speeds of 10m/s had negligible effects but wind speeds of 20m/s produced much higher wave heights across the domain. An assumed increase in sea level of 1m caused an increase in wave height of 4-40cm with an average increase of 30cm. Since erosion processes are proportional to the square of the wave height, this greatly impacts the effects of coastal erosion. Results analysed in Kuang and Stansby [2006a] showed that the model was insensitive to Mannings friction coefficient. They also showed that the peak tidal currents occur one hour either side of the high and low tides and the dominant mode of sediment transport was by suspended load. The Coriolis force had a significant impact on the average accretion across the domain as a whole, amplified in areas of shallow water. This was attributed to the centrifugal forces driving sediment towards the centre of the sandbanks and the generation of residual circulation. Sediment would enter the domain during the flood tides and leave during the ebb tides. The model used different mesh sizes across the computations. It was noted that the evolution results of the fine and intermediate mesh (with a cell size of 360-1530m) were comparable, but the results from the coarse mesh (with a cell size of 1000m) was significantly different. This was attributed to the failure of the coarse mesh to resolve these recirculating flows around the sandbanks [Kuang and Stansby,

2006a]. One limitation of this study was that there was no experimental data on sandbank morphodynamics that could be used to validate these numerical models. The authors appreciated that numerical convergence and simulation accuracy are not the same thing [Kuang and Stansby, 2006b]. Stansby et al. [2006] concluded that artificially increasing the heights of sandbanks is an effect counter to the effects of sea level rise and coastal erosion, but the effects are drastically reduced when considering offshore sandbanks compared to nearshore sandbanks.

The model of Hulscher [1996] was extended by van der Veen et al. [2006]to include a grain size dependency. This improved the predictions of the model especially when it comes to predicting sand waves. When grain size was accounted for, larger areas of flat bed are predicted. This is because for larger grain sizes the critical shear stress increases and the bed shear stress is no longer larger than the critical shear stress. This results in no sediment transport and thus a flat bottom topography. Inclusion of the grain size into the model was seen to increase its overall correct prediction rate from 51% to 62%. The same original model ([Hulscher, 1996]) was used by van der Veen and Hulscher [2009] to predict the occurrence of sandbanks in the North Sea. In general the model predictions agree with sandbank observations in the North Sea, quantitatively giving a correct prediction in 64.5% of the study area. It was shown that the model had a tendency to over-predict sandbank occurrence. Overestimation of sediment transport was down to sediment transport being proportional to the total bed stress rather than the bed stress minus the critical shear stress. However, in this model that would not influence the prediction of bedform types only their growth rates. Differences between the prediction and observation could be down to other factors such as friction and bed slope coefficients. Another reason for the difference in the predictions and observations could be that smaller amplitude banks are being underestimated by the model.

Dolphin et al. [2007] stated that sandbanks are difficult to study because of the large spatial domain they occupy and the fact that their response to hydrodynamic and morphodynamic processes occurs over long time periods. Historic bathymetric charts are useful for studying sandbanks because they can span long term periods showing the cyclical trends. However, the drawback of this is that often large time intervals between successive published charts can give no indica-

tion of behaviour in the interim period. Furthermore lack of field datasets makes the validation of numerical models difficult. Dolphin et al. [2007] created a new digitised dataset based on a 182 year historic survey record to study bank behaviour in the North Sea region. The analysis showed that the Newcombe Sands bank exhibited cyclic morphological behaviour, relating to its migration, overall volume and elevation, over a period of 70-80 years. Survey data also indicated that shorter periods of gradual and episodic change occurred. The proximity to the shoreline, elevation and bank shape all have a significant influence on wave energy distribution. This is a major contributing factor to sediment transport and coastal erosion. Bank shape is determined by a combination of wave and tidal processes. Dolphin et al. [2007] noted that at the time, there was no hydrodynamic data of a sufficient duration to investigate the behaviour of sandbanks. Using historic survey records also relies on the accuracy of these surveys which is not necessarily verifiable.

Tonnon et al. [2007] used a 3D model to study an artificial sand wave in the North Sea under tidal currents of 0.5-1m/s with a sediment size of 200-500µm. It concluded that the bed roughness coefficient has a significant effect on the ratio between the bedload and the suspended load. The 3D model results showed that accretion occurs under dominant bedload conditions (weak tidal currents, coarse sediment, small roughness and low waves) and erosion occurs under dominant suspended load conditions (strong tidal currents, fine sediment, large roughness and storm waves). It also indicated that provided the tidal currents are symmetric, the direction of migration would be along the ebb flow. When the tidal currents are asymmetric, the direction of migration is along the flood flow, provided that the flood current is dominant.

Jacoub et al. [2007] sought to study the effects of the wave climate and tidal currents coupled with a rising sea level on the morphodynamics of offshore sandbanks. By increasing the mean sea level by 0.6m, the wave breaking height was increased by approximately 10% and the rate of erosion was increased by approximately 12%. The effects of sea level rise are insignificant when considering offshore waves height less than 5m. However, an increase of 3-10% was seen for higher offshore wave heights. Wave action is a more significant factor when calculating sediment transport rates compared to tidal action by itself. Modelling

was conducted over short time periods and the results suggested that there was also a need to simulate sandbank evolution and coastal erosion over long time scales (e.g. periods of 20-30 years).

Coughlan et al. [2007] stated that waves play an important role in sediment transport and coastal morphology. Wave climate near sandbanks is determined by current interactions, refraction, diffraction and shoaling. This study used numerical modelling to examine the importance of the tidal stage on the sediment transport inshore of a sandbank, applied specifically to the Norfolk coast portion of the North Sea. Over the crests of sandbanks where water depth is small, the differences between high and low tide become significant. This controls the wave heights and longshore currents. The wave climate model showed that the waves coming from the south had the largest impact on the coastline, but only one in nine waves came from that direction. The majority of the waves approached from the North-northeast direction. Tidal currents can be deflected over a sandbank which could aid upslope sediment transport and bank growth. The creation of anticyclonic eddies during periods of high water are unlikely to have a significant impact on sediment transport by themselves. However, when coupled with wave conditions they may become significant. The patterns of erosion and accretion vary more with wave direction rather than tidal stage, but tidal stage does play a significant role in the magnitude of wave energy.

Pan et al. [2007] described a quasi-3D model developed to study the medium and long term morphological evolution of offshore sandbanks. The model consists of a 3D tidal module using the Galerkin-eigenfunction method with sub-modules to compute bedform characteristics, suspended sediment concentrations, sediment fluxes and morphological change. The model also includes wave current interaction and wind wave effects. The model results showed that the friction factor varies according to the bedform characteristics and the sediment size. Higher friction factors are located at the sandbank crest and lower friction factors occur in areas of deeper water. Friction factors doubled during spring tides compared to neap tides. The steep topography and non-linear tidal dynamics creates local asymmetric flow fields. Sandbank development is then controlled by the local flow field and wave climate. Pan et al. [2007] highlighted the importance of long term monitoring and detailed field measurements in the development and validation

of numerical models. Coverage of large coastal domains, the interaction between groups of sandbanks and the imposition of boundary conditions are important in the modelling future. Theoretical work on sandbanks that have been studied previously account for hydrodynamic effects, sediment transport patterns and the effects of morphodynamic changes on the hydrodynamics but neglect to consider all these factors simultaneously. Numerical models developed predict the long term evolution of sandbanks but largely ignore the effects of wave climate and wave-current interactions.

Sanay et al. [2007] used a series of process-orientated numerical simulation to evaluate the role of residual flow and overtides on sediment transport over sandbanks. The simulations showed that the magnitudes of residual flow and overtides are highly sensitive to the bottom roughness parametrisation. Although both play a part in bank orientation and sediment transport, the residual flow has a higher magnitude than the locally generated overtides and is therefore probably more significant. Net sediment transport was dominated by the interaction between the residual flow and the semi-diurnal tidal currents. Cross bank sediment transport can exist even when the cross bank residual flow was zero, suggesting that the magnitude and phase difference between the major tidal constituents and the overtides was what controls cross bank sediment transport. The net bedload transport described a gyre that converges on the crest of banks. The findings showed that more active banks are those which are smoother (i.e. smaller roughness coefficients) or those with a greater rotation with respect to the main tidal currents.

Reeve et al. [2008] used a data-driven morphological model that used empirical orthogonal function analysis and other statistical analysis techniques to determine a forecast and the associated uncertainty of the morphological conditions of the Great Yarmouth sandbanks. This type of modelling is an alternative method to simple equilibrium or behavioural models normally used to predict morphological evolution. The predictions were compared against survey measurements showing that the model was able to capture the variability well in regions where the variation was similar to standing wave behaviour but suffered in regions where chance events (e.g. storm surges) have a greater effect on the sandbank morphology.

Horrillo-Caraballo and Reeve [2008] used a depth integrated tidal model to

calculate the residual currents around sandbanks with a nested model covering the Great Yarmouth region of the North Sea. The model was calibrated and validated against tidal predictions and field measurements. The model used a coarse resolution of 1045m increasing to a resolution of 104.5m in the sandbank region. The model performance was considered to be in good agreement with the field measurements. Sediment movements were determined to be driven by the residual currents and bottom morphology, a view supported by other investigators. As the currents are modifying the bottom morphology, the changes in the bottom morphology are in turn modifying the flow. This suggests that there is a complex interaction and feedback between the flow and the bathymetry. In this case, the sandbanks are areas where sediment accumulates between opposing flows creating a gyre. The Great Yarmouth sandbanks are active sandbanks migrating at rates of around 1km over a period of around 150 years. The approach used by Horrillo-Caraballo and Reeve [2008] had wider applicability to other sandbank systems not just those considered specifically by this model.

Knaapen [2009] suggested that sandbanks could be more commonly widespread than previously noted in some areas of the Dutch continental shelf because their relatively low height caused them to be ignored in some bathymetric analyses. It was observed that there is a large region of the Dutch continental shelf where no sandbanks were observed. This region coincides with the mouth of a river suggesting that the freshwater outflow impacts the tidal ellipse and the residual currents in a way that suppressed the formation of sandbanks. The newly identified sandbanks support previous authors' predictions, strengthening the idea that the sandbanks in the North Sea are a result of instability between the tidal currents and the bed. Human activity on continental shelves is rapidly increasing. It is noted that although marine construction and dredging can have an impact on local scour, this is not likely to have an impact on hydrodynamics and the surrounding bathymetry, at least not over the short timescales considered. However, large scale activities, such as gas or sand mining, are likely to show some impact on the sandbank pattern. Knaapen [2009] suggests that this interaction could lead to an increase in sandbank height, more prominently for smaller banks. The long term impact of this is an area that needs greater study and it is necessary to consider the impact of human activity on continental shelves.

The morphological model described by Neill and Scourse [2009] showed that reduced bed friction as a consequence of sea level rise was a major factor in the formation of headland sandbanks but less so for sandbanks formed under tidal flow. However the model was limited by using idealistic bathymetry over realistic bathymetry, suggesting that idealistic bathymetry was enough to model the mechanisms behind sandbank formation.

Giardino et al. [2010] noted that the majority of investigations into sandbank behaviour were done from a point of view of tide related parameters, bathymetry and Coriolis force. The impact of wave conditions on sediment fluxes and sandbanks would often be neglected because of the short duration of significant wave activity. It is known that the interaction between waves and tidal currents leads to a large increase in bottom shear stress particularly at the sandbank crests, leading to an increase in the sediment transport rate. Giardino et al. [2010] carried out numerous wave simulations to determine their effect on the evolution of a sandbank. The results showed that wave activity is responsible for a large increase in sediment transport but also for a change in direction of the net flux of sediments. This is significant because in the specific case of the Kwinte Bank, the evolution pattern was directed to its westward side under combined waves and currents, in contrast to the expected transport pattern due to currents alone. However, over long periods of time these opposite transports patterns would balance each other leading to a dynamic equilibrium. This is of particular interest when considering sandbank migration because by only considering short term trends a sandbank could appear to be migrating unilaterally in a particular direction. However, in reality, it is part of a more cyclic migration pattern. The morphological analysis of several sand banks supports the idea that wave activity might also have an impact on the shape of sandbanks. It is also suggested that wave climate data could be a useful tool when studying the evolution of sandbanks.

The model of Chini et al. [2010] suggested that expected sea level rises of 3.5, 7 and 19mm/year can increase the 100 year return wave height by 2%, 4% and 12% respectively. This increase in wave energy is likely to have a direct impact on the evolution of sandbanks. Jenkins et al. [2010] projects a sea level rise of 93-190cm over the next 100 years which correlates with the top end of the predictions by Chini et al. [2010]. However, Jenkins et al. [2010] also suggested that storm

surges are not expected to increase by more than 9cm for a less than 1 in 50 year return period anywhere along the UK coastline. Wahl et al. [2013] estimated that observed sea level rise over the period of 1900-2011 was 1.5mm/year for the North Sea region. Idier et al. [2017] noted that sea level rise affects tidal dynamics in addition to total water levels. Modelling under uniform sea level rises up to 10m above present level showed significant increases in the high tide levels in the southern North Sea. The magnitude of the change was proportional to the sea level rise up to 2m. There were also notable changes in behaviour and patterns of tidal components. Analysis of the largest tidal components showed that the M_2,S_2,N_2,M_4, MS_4 and MN_4 exhibit the most significant changes with sea level rise, with the M_2 component being the most significant.

Garel [2010] observed there is no overall consensus on the processes behind the formation and maintenance of sandbanks, although many models have been created to evaluate this. Garel [2010] suggested that work by Huthnance [1982b] was the most promising when considering tidal sandbanks such as those in the North Sea. The tidally induced sediment transport over the Kwinte Bank showed a pattern of convergence towards the crests and occurs mainly on the upstream side. The precise convergence location varied according to the prevailing tidal flow. Deflection and growth of sandbanks is enhanced by the vorticity generated by the Coriolis force. Enhanced bottom friction during peak flood and ebb flows provides a mechanism by which sediment is moved towards the crest. Anthropogenic activities such as dredging impacts the local short term hydrodynamic and morphodynamic behaviour of the sandbank, but further investigation is needed to determine the long term impacts of such activities. However, long term sandbank dynamic processes can be difficult to estimate based on short term hydrodynamic measurements.

Brooks [2010] studied the link between coastal recession and bathymetric change on the East coast of the UK. The magnitude and orientation of recent bathymetric changes is significant for future cliff erosion. The Suffolk coastline has the fastest recession rate in the UK, reaching up to 5m/year. The development of the Sizewell-Dunwich sandbank reduced the recession rates of the nearby coastline by half. Sediment transport is generally in the Southerly direction although this was not proved. It was suggested that coastal recession would continue in

order to maintain a sediment supply for sandbanks. However, the dynamic issues of coastal recession were not considered.

Nabi et al. [2013] presented a 3D morphological model to simulate the evolution of sandbanks under 3D turbulent flow. The results showed that bedform development and the formation of turbulent eddies formed a coupled process amplifying each other until a steady state was reached. Smaller sediment sizes generate more superimposed ripples and more 2D bedforms. Larger sediment sizes were associated with more bed irregularities.

Lewis et al. [2014] studied the interannual variability of sandbanks in the Bristol Channel. The results showed that during stormier periods, the more wave exposed sandbanks decreased in volume but the less exposed bank increased in volume. It was noted that most studies assume that offshore sandbanks are dominated by the tidal processes without accounting for the changes induced by periods of intense wave activity. It was shown that natural variability exceeded the effects of human activities, such as dredging, by large factors. However, if the impacts of human activities on sandbanks are going to be assessed against their natural variability then the morphological models must account for wave and tidal processes. Fairley et al. [2016] also studied offshore sandbanks in the Bristol Channel using a 3D coastal numerical model to simulate the effects of storm surges. It was shown that for the sandbanks with greater wave exposure, the storm conditions were providing a mechanism for the maintenance of the crest position. In these cases the bed level changes over the crest were opposite to that of under tidal action alone. For the less exposed sandbank, there was similarity in the changes for storm conditions and tidal action alone. Under neap tidal conditions, volumetric changes for all the sandbanks were positive (i.e accretion). The amount of accretion increased with the maximum tidal currents. Under spring tide conditions, there is less accretion which changes into erosion as the maximum tidal current increases. Under storm conditions, the volumetric changes appeared to be more related to the geological setting and morphology rather than exposure and tidal forcing. The two headland associated banks, which have similar morphology, showed similar volumetric changes despite being at opposite exposure levels. Greater erosion was observed for a storm condition prescribed under a neap tidal for these banks.

Chatzirodou et al. [2016] described a fully calibrated and validated 3D hydrodynamic model combined with a morphological model to investigate the sediment dynamics in the Pentland Firth. The high resolution model showed that the sandbanks were dynamically active under the tidal flow regime. The highly energetic currents created bed shear stress values that greatly exceeded the value required to move sediment during the peak flood and ebb flows. Over time, the residual sediment transport rate would be in the direction of whichever direction of flow, flood or ebb, was more dominant. Two sandbanks studied in the regions showed opposite behaviour, in that one showed a sediment transport dominated by the flood flow. This bank showed erosion on the flanks with sediment being transported towards the crest. The second bank displayed an ebb dominated sediment transport. This was associated with a high degree of bank movement (although preserving its total volume) and a reshaping of the bank into a more elongated structure. It was concluded that since the highly energetic currents are controlling this morphodynamic behaviour and that they are also favourable sites for projects such as tidal stream turbines. Any change to the flow regime induced by a tidal stream turbine will significantly impact the dynamics of sandbanks.

The measurements of breaker bar morphodynamics presented by van der Zanden et al. [2017] specifically related to bedload and suspended load under laboratory wave conditions. At locations between the bar crest and trough, bedload transport rate correlates with bed slope and turbulent energy. The bedload and suspended load transport rates were observed to be of a similar magnitude but opposite sign. Bedload transport is directed onshore and is dominant in the shoaling zone. Bedload transport rate decreases over the bar crest and increases again on the shore-facing slope. Suspended transport rate is directed offshore and would become dominant after wave breaking. These both contribute significantly to bed profile evolution. This could explain the tendency for nearshore bars to migrate slowly offshore under normal wave conditions. Both bedload and suspended load contribute to bar morphodynmics but in notably difference ways. The bedload transport results in erosion of the offshore and nearshore slopes and accretion at the crest and trough. The suspended load contributes erosion at the trough, the offshore advection of sediment and a net deposition at the crest.

Yuan et al. [2017] developed an idealised non-linear numerical model to study

the long term evolution of tidal sandbanks. The model investigated the sensitivity of sandbanks, specifically their shape and growth time, 1D/2D configuration, tidal ellipticity and bed shear stress. For a 1D configuration, the model showed that bedform height grows exponentially until it reaches saturation, reaching a static equilibrium whereby height remains constant. To further understand the mechanisms behind the sandbanks reaching a static equilibrium the potential energy of the sandbanks was analysed. Potential energy was divided into two terms: the production term (as a result of advective sediment transport) and the damping term (as a result of slope induced sediment transport). Initially, the production term is larger than the damping term due to small bed slopes. This causes sandbank growth. As the bed slope increases, the damping term increases until it balances out the production term. It is suggested that the final equilibrium is down more to increases in the damping term rather than decreases in the production term. In contrast, the 2D configuration showed ridges in dynamic equilibrium, with meandering crests which oscillate in time. Meandering crests appeared when the vertical distance between the crest and the trough was greater than 80% of the maximum water depth. Global growth time was slightly larger for the 2D configuration compared to the 1D configuration. The global growth time also varied non-monotonically with the tidal ellipticity and it increases when bed shear stress is also accounted for. The model showed that the sandbank shape was sensitive to the tidal ellipticity but not sensitive to the bed shear stress. Near bed wave stirring was shown to cause the crests to become flatter as the water depth above the crest increases. A comparison between the model results and field observation showed the model was able to accurately simulate the characteristic of the southern North Sea sandbanks. It also suggested that these sandbanks may still be subject to growth. The dynamics of sandbanks are well documented, however the mechanism of long term evolution are still not fully understood [Yuan et al., 2017]. This knowledge would greatly benefit practical applications such as the stability of underwater structures and for sand mining. Yuan and de Swart [2017] stated that during their evolution, sandbanks are affected by changes in sea level and tidal currents. Using the same non-linear numerical model described in Yuan et al. [2017], the effects of sea level rise and changes in tidal currents (amplitude and direction) on the growth time and height of active sandbanks was

investigated. Generally, active sandbanks subject to sea level rise continue their growth trends and exhibit a larger height. If changes to tidal current direction is accounted for then the changes to growth time and height become less significant. The final morphology of a sandbank in equilibrium depended mainly on the initial formation conditions and the changes to the tidal current and sea level during its growth. In the case where the tidal current approximately matches the critical velocity for sediment transport, then the effects of sea level rise results in the generation of quasi-active sandbanks. The time scale for those quasi-active banks to develop into inactive banks (which are associated with increasing water depth and/or sea level rise) is inversely proportional to the rate of sea level rise. The model results were compared against sandbank observations qualitatively, but in general the height was overestimated and the bank spacing was underestimated.

The study by Glock et al. [2019] compared the consistency between the results of 1D, 2D and 3D simulations under different flow conditions. It showed that once calibrated against measured water levels, the ratios between 1D/2D and 1D/3D were almost the same. However it was shown that the simulated shear stress values in the 3D model were between 62%-86% of the simulated shear stress values in the 1D model. The corresponding ratio for the 2D/1D models was 90%-100%. Glock et al. [2019] accounts these differences to roughness definition, simplified geometry or the influence of turbulence. It is highlighted though that sediment transport calculations are based on shear stresses and therefore these differences are of importance in numerical modelling.

2.3 Knowledge Gaps

As pointed out by de Swart and Yuan [2018] there are several areas where sandbank research should be extended, these are summarised below:

- Most models consider depth averaged shallow water equations and neglect vertical flow structure. Since sediment transport is determined by near bed currents, whose magnitude and direction may differ from the depth averaged current then a 3D model could result in better agreement between numerical simulations and physical observations.

- Most models use a prescribed background tidal current which could be accurately replaced with a tidal current from large scale models also taking into account sea level rise.

- The modelling of wave conditions is often done with simple parametrisation. More insight about the effects of wave conditions on long term morphological behaviour could be gained by using more sophisticated wave models.

- Improvements made in the areas of sediment transport include accounting for both bedload and suspended load in the sediment transport equations. Often both are accounted for in isolated ways by prescribing coefficients to represent the relative importance of bedload to suspended load rather than calculating based on flow and sediment conditions. Another important consideration is to model non-uniform sediment to allow more accurate determination of how sediment sizes may be distributed across sandbanks.

- Limited progress has been made into the long term natural evolution of the wavelengths and orientation of sandbanks or consideration of models on a larger 2D domain scale. Similarly, while progress is made into the response of sandbanks to human intervention, again there is a lack of knowledge regarding the long term response of such interventions. There is also scope to study the behaviour of sandbanks in relation to how this impacts local ecology, noting that sediment composition and behaviour is a main driver in terms of habitat and diversity.

- There is potential to test numerical models against global domains. There has been a substantial amount of work completed focussing on the sandbanks on the European Shelf, mainly the North Sea, as these present ideal observational examples of sandbanks. However, the models developed could be applied to other shelf seas such as the Atlantic Ocean, East China Sea and Australian shelf seas where similar features are observed.

In conclusion, much has been written about the formation and maintenance of sandbanks and their effects of coastal morphology. Over the years research has progressed using field observations and measurements along with numerical

models to develop understanding of the mechanisms governing these processes. Numerical models have taken in a wide variety of factors including tidal patterns, Coriolis force, bed shear stress, sediment transport (in the form of bedload and suspended load), wave conditions and storm conditions. Computer modelling has progressed over the years to account for 1D, 2D and 3D hydrodynamics and morphodynamics as well as increasing spatial and temporal scales.

This research aims to develop knowledge in some of the limitations and gaps previously discussed. Particular notice is given to the fact that many authors have stated that models in 2D neglect the vertical flow structure which is important for sandbank formation and sediment transport processes. The models developed for this research will incorporate 3D hydrodynamics as a comparison against 2D hydrodynamics to highlight and discuss the impact of these differences. This research also considers a larger spatial domain compared to some of the previous models. It will also attempt to combine several of the physical processes together (i.e. sediment transport and wave conditions).

Chapter 3

Modelling Framework

3.1 Introduction

This chapter outlines the TELEMAC suite and the specific modules used in this research. It will briefly describe the governing equations behind each of the modules: TELEMAC2D, TELEMAC3D, SISYPHE and TOMAWAC.

3.2 The TELEMAC Suite

This research uses the TELEMAC-MASCARET software, also known simply as the TELEMAC suite. TELEMAC is an open source integrated suite of mathematical solvers used in the field of hydrodynamics. It consists of several different modules for free surface flows in 1D, 2D and 3D, sediment transport in 2D and 3D and wave propagation. Each of these can be used independently or coupled thereby allowing the combined effects of different modules to contribute to the model. Further information and access to the software is available from the website [HR Wallingford, 2016]. For the purposes of this research, the modules used are TELEMAC2D for 2D hydrodynamic modelling, SISYPHE for 2D morphodynamic modelling and TELEMAC3D for 3D hydrodynamic and morphodynamic modelling.

The information presented in the following sections provides a brief overview

of the principles and governing equations behind certain aspects of each module of the modelling software and is derived from the user manuals provided (see [Ata, 2017], [Tassi, 2017],[Mattic, 2017] and [Awk, 2017] and the references therein).

The model steering files are available in Appendices A to C, and refer to the computational options discussed here were chosen and the values of key parameters.

3.2.1 TELEMAC2D

3.2.1.1 Introduction

TELEMAC2D is the module used for deriving the 2D hydrodynamics. It achieves this through solving the depth averaged Saint-Venant equations for free surface flow. It is also able to take into account several important physical parameters. This section highlights the relevant options that were chosen for the final model. A complete description of the theoretical aspects behind these methods can be found in Hervouet [2007].

3.2.1.2 General Equations

The TELEMAC2D code solves four equations simultaneously: continuity, momentum along the x direction, momentum along the y direction, and conservation of tracers (see Equations 3.1 to 3.4).

$$\frac{\partial h}{\partial t} + u \cdot \nabla(h) + h div(u) = S_h \tag{3.1}$$

$$\frac{\partial u}{\partial t} + u \cdot \nabla(u) = -g\frac{\partial Z}{\partial x} + S_x + \frac{1}{h} div(h v_t \nabla u) \tag{3.2}$$

$$\frac{\partial v}{\partial t} + u \cdot \nabla(v) = -g\frac{\partial Z}{\partial y} + S_y + \frac{1}{h} div(h v_t \nabla u) \tag{3.3}$$

$$\frac{\partial T}{\partial t} + u \cdot \nabla(T) = S_T + \frac{1}{h} div(h v_T \nabla T) \tag{3.4}$$

where: h is the water depth, u and v are the velocity components, T is a passive tracer, g is the acceleration due to gravity, v_t and v_T are the momentum and tracer diffusion coefficients, t is time, x and y are the horizontal space components (in Cartesian space) and S_h is a source or sink of fluid, S_x and S_y are sources or sinks in the dynamic equations, and S_T is a source or sink of tracers.

Source terms, represented by S_x and S_y in equations 3.2 and 3.3, include the effects of bottom friction, Coriolis force, wind forces, atmospheric pressure, tide generating forces and other momentum sources. Tide generating forces can be neglected as it can be assumed that in a small tidal domain the tide originates from global tidal waves across the boundary. Wind driven flow can have an impact especially in storm conditions but was ignored here due to the model mainly considering normal tidal conditions and the absence of accurate wind data for this study. This leaves bottom friction and the Coriolis forces as the main source terms in the dynamic equations.

3.2.1.3 Physical Parameters

In environmental studies, bottom friction is a major unknown, leading to most friction laws being derived empirically. Friction stress acts in the direction of the current and can be split into the two components (see Equations 3.5 and 3.6).

$$\tau_{xz} = -\frac{u}{2} \rho C_f \sqrt{u^2 + v^2} \tag{3.5}$$

$$\tau_{yz} = -\frac{v}{2} \rho C_f \sqrt{u^2 + v^2} \tag{3.6}$$

However, the friction coefficient, C_f, is rarely used in free surface hydraulics

and is replaced by others such as Chezy's, Stricklers or Mannings. The models created in this study will used Chezy's coefficient which is related to C_f by the formula:

$$C_{cf} = \sqrt{\frac{2g}{C_f}} \tag{3.7}$$

Chezy's formula can then be expressed as follows:

$$F_x^f = -\frac{u}{cos(\alpha)} \frac{2g}{hC_{cf}^2} \sqrt{u^2 + v^2} \tag{3.8}$$

$$F_y^f = -\frac{v}{cos(\alpha)} \frac{2g}{hC_{cf}^2} \sqrt{u^2 + v^2} \tag{3.9}$$

In reality, the value of the Chezy's coefficient is not actually a constant but instead is dependent on the bottom roughness and the depth. However, due to the complexity and difficulty in getting accurate space varying field measurements, it was decided here to use a constant value. TELEMAC also presents options to account for sidewall friction on the solid boundaries and the effects of vegetation. These were both neglected for this study again partly due to lack of available field measurements but also to keep the model as simple as possible without significantly compromising its accuracy or applicability.

In 2D, the Coriolis force proportional to the degrees of latitude (Λ) and is calculated by the following equations:

$$F_x^c = 2\omega \sin(\Lambda) v \tag{3.10}$$

$$F_y^c = 2\omega \sin(\Lambda) u \tag{3.11}$$

In small domains this coefficient can be assumed to be constant. However, in larger domains the value of the Coriolis parameter varies spatially which can be an important consideration for the hydrodynamic modelling. The value of ω in equations 3.10 and 3.11 relates to the angular velocity of the Earth which is 7.292×10^{-5}rad/s (i.e. 2π radians over a sidereal day).

TELEMAC presents four options of varying complexity to model the turbulence in a hydrodynamic model: Constant viscosity, the Elder model, the k-Epsilon (k-ϵ) model and the Smagorinski model.

The constant viscosity option was used here. This option presents the simplest form of modelling turbulence and is ideal for the preliminary stages of developing a computational model. It is appreciated that as and if the model was developed further, using one of the other turbulence models may present a better insight to the hydrodynamic conditions. This option is applied by assigning a value to a constant viscosity coefficient which represents the molecular viscosity, turbulent viscosity and dispersion. This coefficient has a definite effect on the extent and shape of recirculation. Lower values tend to only dissipate small eddies. Larger values are capable of dissipating large recirculations. Values that result in the dissipation of eddies smaller than two meshes are observed to have virtually no effect on the computation. TELEMAC is able to have a constant value or a time-space varying value for the viscosity coefficient.

3.2.1.4 Numerical Parameters

It is necessary to specify in TELEMAC the type of equations to be solved. TELEMAC2D solves either the Saint-Venant equations, using either the finite element method or the finite volume method, or the Boussinesq equations. Since the finite element method represents the most traditional use of how TELEMAC2D is applied in numerical modelling, it was chosen here. In addition to this the discretisation in space must also be chosen. Velocity and depth can be discretised as

linear triangles (3 nodes), quasi-bubble triangles (4 nodes) or quadratic triangles (6 nodes). In practice, this results in 3 options for space discretisation: linear velocity and depth, quasi-bubble velocity and linear depth or quadratic velocity and linear depth. Each method has advantages and disadvantages over the others. The first method is the most efficient in terms of memory and computational time. The second method is recommended when observing free surface wiggles such as those induced by strong bathymetry gradients. The third method is recommended for the most accurate results (albeit at the cost of significant increases in memory and computational time). Linear velocity and depth was chosen here.

During computation, the user can choose whether to solve different steps of the equations using a fractional step method. These mainly concern the advection equations and propagation-diffusion equations. These steps can be activated or deactivated as desired. It is also possible to take into account the specific advection terms relating to depth, velocity components, turbulence energy and dissipation and tracers individually. Propagation and diffusion are calculated in the same step, so neglecting one term automatically excludes the other. However, the different diffusion terms can be similarly activated or deactivated individually as desired.

Finite element resolution is based on the primitive equations. It is possible to replace the original equations by a generalized wave equation obtained by eliminating the velocity from the continuity equation and using a value obtained from the momentum equation. This technique increases calculation speed but has the disadvantage of smoothing the results. It is important to stress that choosing the wave equation option automatically selects a number of other options: use of mass lumping on depth and velocities, and use of explicit velocity diffusion. In most cases, this option is recommended and offers the optimum in terms of stability and computational time.

When the linearised system is solved by an iterative method, it is necessary to give the accuracy that is to be achieved during the solving process and the maximum number of iterations permissible. This prevents the computation from entering unending loops if the required accuracy is not achieved. It is recommended to use an accuracy of between 1×10^{-3} and 1×10^{-6} with around 500 to 1000 iterations. Higher accuracy leads to increased computational time and lower

accuracy can lead to unstable results. These values give an optimal compromise between computational time and model accuracy.

Residual mass errors (of the order of a few percent) may appear when using boundary conditions with imposed depths. The continuity equation is not solved for these points and is replaced by the imposed value. Therefore, the resultant discharge is not properly computed and leads to error. Using continuity correction helps in correcting the velocity at these points so that the overall continuity is maintained.

During a model simulation, the Courant number value (number of grid cells crossed by a water particle during a time step) considerably influences the quality of the results. Irrespective of numerical schemes with a stability condition on the Courant number, experience shows that result quality decreases if the Courant number is above approximately 7 to 8. It is not so easy to estimate the value of the Courant number - especially in sea models with a large tidal range. To help, TELEMAC2D allows the user to check the Courant number during computation and the software automatically executes intermediate time steps so that the Courant number stays below a given value.

Tidal flats are areas that can become dry during the simulation. TELEMAC-2D offers several processing options for tidal flat areas when finite elements schemes are used. If the model does not contain tidal flats, all these options can be deactivated in order to save computational time.

Tidal flats can be processed in three different ways:

1. The tidal flats are detected and the free surface gradient is corrected,

2. The tidal flat areas are removed from the computation. Exposed elements still form part of the mesh but any contributions they make to the computations are cancelled by a so-called "masking" table. The data structure and the computations are thus formally the same to within the value of the masking coefficient. However, in this case, mass conservation may be slightly altered.

3. Processing is done in the same way as in the first case, but a porosity term is added to half-dry elements. Consequently, the quantity of water is changed

and is no longer equal to the depth integral over the entire domain but to the depth integral multiplied by the porosity.

The first option was used here.

The treatment of the negative depths can be specified using the following two methods:

1. Option 1 consists of smoothing the negative depths in a conservative way.
2. Option 2 consists of using a flux limitation that ensures strictly positive depths. This should be coupled with the advection schemes able to cope with tidal flats. This option is recommended when conservative tracers are modelled using distributive schemes since it still allows the model to obtain a perfect mass balance.

The second option was used here.

The threshold for negative depths is used only with the treatment option for smoothing the negative depths in a conservative way. It specifies the limit of the unchanged value. For example, a threshold of -0.01 means that depths greater than –1cm will be left unchanged. In certain cases, it may be advisable to limit the lower water depth value. The most common case involves eliminating negative values of depth (called H-Clipping). The minimum value of depth is used to fix the threshold below which clipping is performed. However, it should be noted that this latter option leads to an increase in the mass of water as it eliminates negative water depths.

3.2.2 TELEMAC3D

3.2.2.1 Introduction

TELEMAC3D is the module that calculates the 3D flow fields and the water depth. It also solves the transport of several tracers. These include active tracers, those which change the water density and/or act on the flow itself (such as temperature and salinity), and passive tracers, those which do not affect the flow and are merely transported. It is worth noting that several aspects of the

theory behind TELEMAC3D especially those relating to the physical parameters and numerical setup are similar if not the same as used in TELEMAC2D, with the only differences relating to the consideration of vertical components and will therefore not be duplicated.

3.2.2.2 3D Hydrostatic Version

TELEMAC3D solves the three-dimensional Navier-Stokes equations with a free surface changing in time. It also uses the assumption that the fluid is incompressible such that there is negligible variation of the density in the conservation of mass equations. The hydrostatic pressure hypothesis states that the pressure at a given depth is the sum of the air pressure at the fluid surface plus the weight of the overlying water body. It assumes the Boussinesq approximation for the momentum, specifically that density variations are only taken into account as buoyant forces. This gives the three-dimensional equations described in equations 3.12 to 3.16.

$$\frac{\partial u}{\partial x} + \frac{\partial v}{\partial y} + \frac{\partial w}{\partial z} = 0 \tag{3.12}$$

$$\frac{\partial u}{\partial t} + u\frac{\partial u}{\partial x} + v\frac{\partial u}{\partial y} + w\frac{\partial u}{\partial z} = -g\frac{\partial Z}{\partial x} + \upsilon\Delta(u) + S_x \tag{3.13}$$

$$\frac{\partial v}{\partial t} + u\frac{\partial v}{\partial x} + v\frac{\partial v}{\partial y} + w\frac{\partial v}{\partial z} = -g\frac{\partial Z}{\partial y} + \upsilon\Delta(v) + S_y \tag{3.14}$$

$$p = p_{atm} + \rho_0 g(Z - z) + \rho_0 g \int_z^Z \frac{\partial \rho}{\rho_0} dz' \tag{3.15}$$

$$\frac{\partial T}{\partial t} + u\frac{\partial T}{\partial x} + v\frac{\partial T}{\partial y} + w\frac{\partial T}{\partial z} = div(\upsilon gradT) + S_T \tag{3.16}$$

where: h is the water depth, Z is the free surface elevation, u, v and w are the three dimensional velocity components, T is an active or passive tracer, p is pressure, g is the acceleration due to gravity, ρ is the reference density, t is time, x, y and z are the three dimensional space coordinates and S_x, S_y and S_T are the sources terms for fluid and tracers.

Similar to TELEMAC2D, the source terms include processes such as the wind, Coriolis force, bottom friction.

The equations are solved in three fractional steps. The first step consists of finding out the advected velocity components by solving only the advection terms in the momentum equations. The second step uses these advected velocity components to compute new velocity components by taking into consideration the diffusion terms and the source terms in the momentum equations. These two solutions enable an intermediate velocity field to be calculated. The final step computes the water depth from the vertical integration of the continuity and momentum equations only including the pressure continuity terms (since all other terms are accounted for in the previous two steps). The resultant 2D equations are written as:

$$\frac{\partial h}{\partial t} + \frac{\partial (Uh)}{\partial x} + \frac{\partial (Vh)}{\partial y} = 0 \tag{3.17}$$

$$\frac{\partial U}{\partial t} = -g\frac{\partial Z}{\partial x} \tag{3.18}$$

$$\frac{\partial V}{\partial t} = -g\frac{\partial Z}{\partial y} \tag{3.19}$$

The upper case U and V denotes the two-dimensional variables of the vertically integrated velocities. These equations are solved by the TELEMAC2D libraries code and enable the calculation of the vertically averaged velocity and water depth. This vertically averaged water depth can be used to recalculate the free surface and elevations at the various mesh points within the layers of the 3D model. Finally the calculation of the u and v velocity components is achieved through a combination of the equations linking the velocities, while the vertical component, w, is calculated using the continuity equation.

3.2.2.3 3D Non-Hydrostatic Version

When not considering the hydrostatic hypothesis, the three-dimensional Navier-Stokes equations are solved with an additional equation for the vertical component, w, similar to those for the horizontal components (see equations 3.20 to 3.23).

$$\frac{\partial u}{\partial x} + \frac{\partial v}{\partial y} + \frac{\partial w}{\partial z} = 0 \tag{3.20}$$

$$\frac{\delta u}{\delta t} + u\frac{\delta u}{\delta x} + v\frac{\delta u}{\delta y} + w\frac{\delta u}{\delta z} = -\frac{1}{\rho}\frac{\partial p}{\partial x} + \upsilon\Delta(u) + S_x \tag{3.21}$$

$$\frac{\delta v}{\delta t} + u\frac{\delta v}{\delta x} + v\frac{\delta v}{\delta y} + w\frac{\delta v}{\delta z} = -\frac{1}{\rho}\frac{\partial p}{\partial y} + \upsilon\Delta(v) + S_y \tag{3.22}$$

$$\frac{\partial w}{\partial t} + u\frac{\partial w}{\partial x} + v\frac{\partial w}{\partial y} + w\frac{\partial w}{\partial z} = -\frac{1}{\rho}\frac{\partial p}{\partial z} - g + \upsilon\Delta(w) + S_z \tag{3.23}$$

In order to share as much of a common core as possible with the solutions that used the hydrostatic pressure hypothesis, the pressure is split up into hydrostatic

pressure and an addition dynamic pressure term described in equation 3.24.

$$p = p_{atm} + \rho_0 g(Z - z) + \rho_0 g \int_z^Z \frac{\partial \rho}{\rho_0} \delta z + p_d \tag{3.24}$$

The TELEMAC3D code then solves a hydrostatic step (the same as previously described) with the only differences arising in the continuity step, in which the dynamic pressure gradient alters the velocity field in order to provide zero divergence of velocity, and in the computation of the free surface.

3.2.2.4 Vertical Mesh Transformation

The 3D mesh is created by specifying a number of layers of 2D geometry. Each layer consists of a triangular mesh exactly the same as the mesh used in the TELEMAC2D model. The elements between two layers are joined together creating a 3D prism or tetrahedral structure depending on user preference. The layers are positioned such that the first layer corresponds to the bottom elevation of the model and the final layer corresponds to the free surface. The intermediate layers are then space depending on the water depth and can be defined in several ways. The first method is to have the layers equally spaced throughout the depth. For example, a model consisting of five layers will be structured as a bottom layer with the remaining four layers spaced at 25% of the water depth. The second method is to fix the location of each layer as a proportion of the water depth. This is done through editing the mesh transformation subroutine in the code. This method is useful for example to refine layers closer to the bed to determine near-bed velocity flows. A third method is available, where the user is able to fix the altitude of each layer at a specific elevation. It is also possible to merge each of these options together in the mesh transformation subroutine in order to construct the vertical mesh (i.e assign a specific elevation to particular layer and have the remaining layers equally spaced around them or at assigned proportions of the depth). An example showing the difference between the arrangement of the vertical layers using the first two methods is shown in Figure 3.1 (the third method was not implemented for this research).

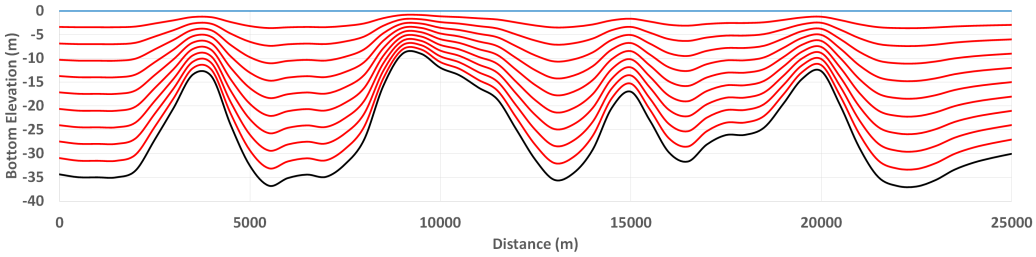

(a) Layers equally spaced

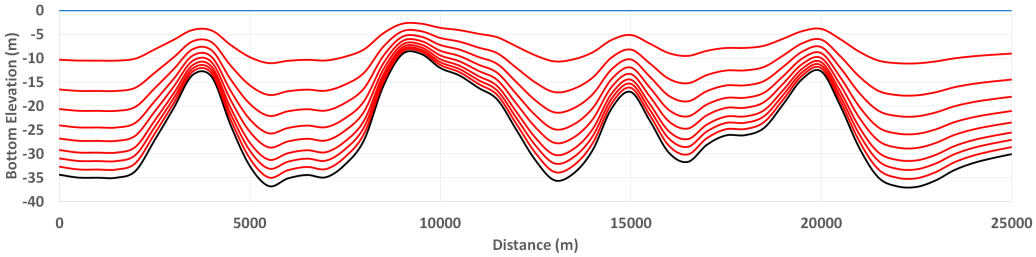

(b) Layers at specified proportions of depth

Figure 3.1: Layer positioning with different transformation methods

3.2.3 SISYPHE

3.2.3.1 Introduction

SISYPHE is the sediment transport and morphodynamic modelling part of the TELEMAC system. Sediment transport is divided into bedload and suspended load which is calculated at each node as functions of flow and sediment parameters. SISYPHE can be applied to cohesive and non-cohesive sediments as well as uniform and mixed sediments. It also takes into account a wide variety of physical processes including bottom slope, rigid beds, secondary currents, slope failure and bed consolidation.

For its calculations, SISYPHE requires the relevant hydrodynamic variables. These can either be imposed in the model itself (via the chaining method) or calculated by a hydrodynamic computation (internal coupling method). In this case SISYPHE will be internally coupled with TELEMAC2D or TELEMAC3D.

3.2.3.2 Sediment Properties

There are four key properties of the sediment which are required by SISYPHE for a morphological simulation: sediment size, sediment density, Shields number and settling velocity. Sediment size and density can be measured in the field and the values assigned to their respective keywords.

The critical Shields number is calculated by the following equation:

$$\Theta_{cr} = \frac{\tau_{cr}}{g(\rho_s - \rho)d_{50}} \tag{3.25}$$

where: τ_{cr} is the critical shear stress for sediment motion, g is the acceleration due to gravity, ρ_s is the sediment density (assumed in this case to be 2650kg/m^3), ρ is the density of water and d_{50} is the mean sediment diameter.

Shields number can be either specified manually or calculated internally by SISYPHE as a function of the non-dimensional grain diameter, D_*.

$$D_* = d_{50}\left[\left(\frac{\rho_s}{\rho - 1}\right)\frac{g}{v^2}\right]^{\frac{1}{3}} \tag{3.26}$$

The Shields Parameter is then given by the following equation:

$$\Theta_{cr} = \begin{cases} 0.24D_*^{-1}, & D_* \leq 4 \\ 0.14D_*^{-0.64}, & 4 < D_* \leq 10 \\ 0.04D_*^{-0.1}, & 10 < D_* \leq 20 \\ 0.013D_*^{-0.29}, & 20 < D_* \leq 150 \\ 0.045, & 150 \leq D_* \end{cases} \tag{3.27}$$

Similarly, SISYPHE presents two methods for the value of the settling velocity. The desired value can be manually assigned to the keyword or calculated internally through a subroutine as a function of the sediment diameter (D_{50}) value

using the following equation:

$$w_s = \begin{cases} \frac{(s-1)g(d_{50})^2}{18\nu}, & d_{50} \leq 1 \times 10^{-4} \\ \frac{10\nu}{d_{50}}(\sqrt{1 + 0.01\frac{(s-1)g(d_{50})^3}{18\nu^2}} - 1), & 1 \times 10^{-4} \leq d_{50} \leq 1 \times 10^{-3} \\ 1.1\sqrt{(s-1)gd_{50}}, & otherwise \end{cases} \tag{3.28}$$

3.2.3.3 Bedload Transport Rate

When the bed shear stress induced by the currents exceeds the critical value, the sediment will be mobilised. Coarser sediment particles are transported via bedload and finer sediment particles are transported in suspension. Bedload describes particles in a fluid transported along the bed by rolling, sliding and/or saltating. Suspended load describes particles transported in a fluid via the turbulence of the fluid. Therefore total sediment transport rate can be described as:

$$Q_{total} = Q_{bed} + Q_{susp} \tag{3.29}$$

SISYPHE solves the Exner equation for sediment mass conservation (see equation 3.30 below):

$$(1 - \lambda)\frac{\partial z_b}{\partial t} + \nabla \cdot Q_{bed} = 0 \tag{3.30}$$

where: λ is the non-cohesive bed porosity, z_b is the bed elevation and Q_{bed} is the solid volume transport per unit width.

This gives the dimensionless current induced sediment transport rate as:

$$\phi_{bed} = \frac{Q_{bed}}{\sqrt{g(s-1)(d_{50})^3}} \tag{3.31}$$

where: s is the relative density (i.e. $\frac{\rho_s}{\rho}$), g is the acceleration due to gravity and d_{50} is the mean sediment diameter.

SISYPHE offers five different options for the formula used to calculate this dimensionless current induced sediment transport rate: Meyer-Peter and Muller, Einstein-Brown, Engelund-Hansen, Engelund Hansen and Chollet et Cunge, and van Rijn. For this research, the van Rijn formula (see equation 3.32) was used as this is the one recommended for finer sediments within the range of 200 to 2000µm.

$$\phi_{bed} = 0.053 D_*^{-0.3} \left(\frac{\Theta - \Theta_{cr}}{\Theta_{cr}} \right)^{2.1} \tag{3.32}$$

In general there are three key aspects that must be considered for computing the magnitude and direction of the bedload: the effects of local bed slope, the effects of secondary flows or helical currents and the effects of skin friction.

When considering these effects on the direction of the bedload transport, the angle, α, between the sediment transport direction and the x-axis deviates from the direction of the shear stress due to the combination of a transverse slope and secondary currents. It is calculated by the following equation:

$$\tan \alpha = \frac{\sin \alpha_{sf} - \frac{1}{f(\theta)} \frac{\partial z_b}{\partial y}}{\cos \alpha_{sf} - \frac{1}{f(\theta)} \frac{\partial z_b}{\partial x}} \tag{3.33}$$

In equation 3.33, the sediment shape function, $f(\theta)$, is a function weighting the influence of the transverse bed slope, expressed as a function of the Shields Parameter using the formulation proposed by Talmon et al. [1995]

$$f(\theta) = \frac{1}{\beta_2 \sqrt{\Theta}} \tag{3.34}$$

The coefficient β_2 is an empirical coefficient that can be defined based on numerical experiments.

In non-linear channels, the direction of sediment transport does not coincide with direction of the shear stress. This is due to the effects of secondary currents (see equation 3.35). The first term in the equation represents the direction of the bed shear stress, which coincides with the direction of the depth averaged velocity flow and the second term represents the direction due to the effects of the secondary spiral currents.

$$\delta^* - \delta_{sc} = \tan^{-1} \frac{v}{u} - \tan^1 \left(\frac{A}{r_s} h \right) \tag{3.35}$$

Similar to the previous equation, the parameter A is modified by the value of another coefficient, α_{SC}, whose value can be selected dependent on the roughness of the bottom. For example, a value of $\alpha_{SC} = 1$ corresponds to $A = 7$.

To correct the magnitude of the bedload transport due to slope effects and secondary currents, the approach used by Koch and Flokstra was chosen. This modified the bedload transport by a factor which acts as a diffusion term in the bed evolution equation.

$$Q^*_{bed} = \left[1 + \beta \left(\frac{\partial z_b}{\partial x} \cos \alpha + \frac{\partial z_b}{\partial y} \sin \alpha \right) \right] \tag{3.36}$$

Similar to the previous two equations, β is an empirical factor accounting for streamwise bed slope effects.

Finally, it is important to consider the effects of skin friction and bedform drag on bedload. The total bed shear stress is due to skin friction and bedform drag but only the component due to skin friction acts on the bedload. Skin friction shear stress is calculated by:

$$\tau_{sf} = \mu \tau_{bed} \tag{3.37}$$

$$\mu = \frac{C_{sf}}{C_f} \tag{3.38}$$

$$\tau_{bed} = 0.5\rho C_f(U^2 + V^2) \tag{3.39}$$

In equation 3.38 the denominator is the friction coefficient due to skin friction and drag, which is computed directly in the hydrodynamics module, and the numerator corresponds to the friction coefficient due to skin friction only, computed by equation 3.40.

$$C_{sf} = 2\left(\frac{\kappa}{log(\frac{12h}{k_s})}\right)^2 \tag{3.40}$$

$$k_s = \alpha_{ks} d_{50} \tag{3.41}$$

Again, the coefficient α_{ks} is an empirical coefficient that is based off numerical experimentation with a suggested value of 3.6 for sandbars.

3.2.3.4 Suspended Sediment Transport Rate

Suspended load is the portion of sediment that is carried by the fluid flow and settles slowly enough that it never really interacts with the bed. It is maintained in suspension by the turbulence of water and usually consists of finer sands, silts and clay. In SISYPHE, suspended sediment transport is solved by a 2D advection-diffusion equation shown below:

$$\frac{\partial hC}{\partial t} + \frac{\partial hUC}{\partial x} + \frac{\partial hVC}{\partial y} = \frac{\partial}{\partial x}\left(h\varepsilon_s \frac{\partial C}{\partial x}\right) + \frac{\partial}{\partial y}\left(h\varepsilon_s \frac{\partial C}{\partial y}\right) + ER - DR \tag{3.42}$$

ER and DR in equation 3.42 above are the non-cohesive erosion and deposition rates respectively and are calculated by equations 3.43 and 3.44.

$$ER = w_s C_{eq} \tag{3.43}$$

$$DR = w_s C_{zref} \tag{3.44}$$

Thus the net sediment flux can be computed by:

$$ER - DR = w_s(C_{eq} - C_{zref}) \tag{3.45}$$

In these equations, the near bed concentration (C_{zref}) is the defined as the concentration at the interface between bedload and suspended load (i.e. where z = z_{ref}) and the equilibrium near bed concentration (C_{eq}) is determined by an empirical formula, in this case the Soulsby and van Rijn formula.

$$C_{eq} = \begin{cases} A_{ss}\left(\sqrt{)}U_c)^2 + \frac{0.018}{C_D}(U_w)^2 - U_{cr}\right)^{2.4}, & if \geq U_{cr} \\ 0, & otherwise \end{cases} \tag{3.46}$$

In the above equation the following constituents are calculated by:

$$A_{ss} = \frac{0.012 h d_{50}\left(\left(\frac{g(s-1)}{v^2}\right)^{\frac{1}{3}} d_{50}\right)^{-0.6}}{((s-1)g d_{50})^{1.2}} \tag{3.47}$$

If considering wave effects the drag coefficient and critical velocity are shown in equations 3.65 and 3.66 (see the following section).

SISYPHE assumes that the vertical concentration distribution is given by a Rouse profile which is valid for uniform steady flow conditions calculated by the equation:

$$C_z = C_{zref}\left(\frac{z-h}{z}\frac{z_{rb}}{z_{rb}-h}\right)^R \tag{3.48}$$

For a Rouse number defined by:

$$R = \frac{w_s}{\kappa u_*} \tag{3.49}$$

In the above equations, the value of z_{rb} is taken as a reference elevation above the bed. Although defined differently by different authors, it tends to be taken as very close to the bed.

The following relationship is established between the depth averaged concentration and the reference concentration by depth integration of the Rouse profile:

$$C_{zref} = FC \tag{3.50}$$

$$F^{-1} = \begin{cases} \frac{1}{(1-Z)}B^R(1-B^{(1-R)}), & if R \neq 1 \\ -B\log B, & if R = 1 \end{cases} \tag{3.51}$$

$$B = \frac{z_{ref}}{h} \tag{3.52}$$

When considering suspended sediment transport the bed evolution equation

becomes:

$$(1-\lambda)\frac{\partial z_b}{\partial t} = DR - ER \tag{3.53}$$

3.2.3.5 Coupling and Chaining

TELEMAC offers two methods for linking the hydrodynamic and morphodynamic models: the chaining method and the internal coupling method.

For the chaining method, both the hydrodynamic and morphodynamic models are running independently. During the hydrodynamic simulation it is assumed that the bed is fixed. The free surface and flow rates from the hydrodynamic simulation are then fed into the subsequent morphodynamic step. Flow velocity is updated at each timestep assuming conservation of flow rate and free surface elevation. Flow velocity is increased locally by deposition and decreased locally by erosion. This method is only suitable for relatively simple flow because there is a difference in the time-scales between the hydrodynamics and the bed evolution. When the bed evolution reaches a critical percentage of the water depth, the hydrodynamic variables will need to be calculated before resuming the morphodynamic simulation. This method can also create further instabilities in the model because it does not always satisfy sediment mass continuity. This is due to the potential losses occurring due to changes in the flow depth as the bed evolves.

The second method is to internally couple the morphodynamic simulation with the hydrodynamic simulation, either TELEMAC2D or TELEMAC3D. This way, the data is exchanged between the memory of the programs, rather than being written to a file. The hydrodynamic simulation calculates the velocity flow field, water depth and shear stress at each time step. These are then sent to the morphodynamic simulation which calculates bed evolution and sends the updated bed profile back to the hydrodynamic simulation. This method is significantly more time consuming than the chaining method but can be sped up by specifying a coupling period. Using a coupling period greater than 1 allows the bedload transport rates and bed evolution not to be calculated at every timestep. For long term simulations, the computational time can be sped up using a morphological

factor which essentially increases the morphological timestep without changing the hydrodynamic timestep.

For the morphological modelling here, the internal coupling method was chosen, mainly due to the large scale domain and complex flow patterns rendering the chaining method too unreliable.

3.2.3.6 Wave Induced Sediment Transport

Calculating the sediment transport rates as a result of wave action requires the variables spectral significant wave height, wave peak period and mean wave direction to be specified. These variables are computed via a wave modelling simulation, either as an input file or by direct coupling with TOMAWAC. Assuming linear theory, the wave orbital velocity is calculated as:

$$U_w = \frac{H_s \omega}{2 \sinh(kh)} \tag{3.54}$$

With the following relationships between the angular frequency, ω, and the wave number, k:

$$\omega = \frac{2\pi}{T_p} \tag{3.55}$$

$$k = \frac{2\pi}{L} \tag{3.56}$$

$$\omega^2 = gk \tanh(kh) \tag{3.57}$$

The maximum shear stress due to waves is calculated at each time step as a

function of the wave orbital velocity and a quadratic friction coefficient.

$$\tau_w = \frac{1}{2}\rho f_w (U_w)^2 \tag{3.58}$$

$$f_w = \begin{cases} \exp\left(-6 + 5.2(\frac{A_0}{k_s})^{-0.19}\right), & if \frac{A_0}{k_s} > 1.59 \\ 0.30, & otherwise \end{cases} \tag{3.59}$$

$$A_0 = \frac{U_w}{\omega} \tag{3.60}$$

The Bijker formulation gives the 'wave induced bottom stress due to combined currents and waves' as a function of the 'bottom shear stress due to currents only' and the 'maximum shear stress due to waves only':

$$\tau_{cw} = \tau_c + \frac{1}{2}\tau_w \tag{3.61}$$

The Soulsby-van Rijn formula can be applied to estimate bedload and suspended load and is suitable for rough beds. The total transport rate due to combined wave action and currents is given as:

$$Q_{bed,susp} = A_{bed,susp} U_c \left[\left((U_c)^2 + \frac{0.018}{C_D} (U_w)^2 \right)^{0.5} - U_{cr} \right]^{2.4} \tag{3.62}$$

The bedload coefficient, suspended load coefficient and critical entrainment

velocity are given by equations 3.63 to 3.66 respectively:

$$A_{bed} = \frac{0.005h(\frac{d_{50}}{h})^{1.2}}{((s-1)gd_{50})^{1.2}} \tag{3.63}$$

$$A_{susp} = \frac{0.012d_{50}D_*^{-0.6}}{((s-1)gd_{50})^{1.2}} \tag{3.64}$$

$$C_D = \left(\frac{0.4}{log(max(h, z_0)/z_0 - 1)}\right)^2 \tag{3.65}$$

$$U_{cr} = \begin{cases} 0.19(d_{50})^{0.1}log_{10}(\frac{4h}{d_{90}}), & if d_{50} \leq 0.0005m \\ 8.5(d_{50})^{0.6}log_{10}(\frac{4h}{d_{90}}), & otherwise \end{cases} \tag{3.66}$$

The parameter d_{90} is characteristic of coarser grains and can be specified manually or assumed to be equal to the mean diameter of the sediment.

3.2.4 TOMAWAC

3.2.4.1 Introduction

TOMAWAC is the part of the TELEMAC software that deals with modelling the power spectrum of waves specifically applied to the oceanic domain, intracontinental seas and the coastal zone. This is achieved through solving the balance equation of the action density directional spectrum which is split into a finite number of propagation frequencies and directions. This is considered to be a third generation model because it does not require any parameterisation on the spectral or directional distribution of power.

3.2.4.2 Wave Theory

The definition of waves is commonly associated with all the wind driven free surface propagations at the surface of the ocean with a time period ranging from 2 seconds to 25 seconds (an equivalent frequency of 0.04Hz to 0.5Hz). Wave modelling is commonly used interchangeably with the term sea state modelling. Common descriptions of the sea state describe their agitation (For example, quiet phase to stormy phase) and the source of the waves (such as wind waves or swell waves). The simplest form of wave modelling is to model monochromatic plane waves, i.e. the wave has one period or frequency and one propagation direction. The free surface elevation at a defined space and time is therefore given as:

$$Z(x, y, t) = a\cos[k(x\sin\theta + y\sin\theta) - \omega t + \varphi] \tag{3.67}$$

The energy per unit area of these waves, consisting of both kinetic and potential energy, is calculated as:

$$E_w = \frac{1}{2}\rho g a^2 \tag{3.68}$$

However, this simplistic representation does not necessarily accurately reflect the position of the actual sea state. Not all waves possess the same physical features: amplitude, period or frequency and propagation direction. These waves are then described as multidirectional random waves i.e. the surface wave energy is distributed over a range of propagation directions and frequencies. Mathematically, this irregularity is expressed by stating that the real sea state is a result of the superposition of an infinite number of elementary monochromatic components as described in equation 3.69.

$$Z(x, y, t) = \sum_{m=1}^{M} a_m \cos[k_m(x\sin\theta_m + y\sin\theta_m) - \omega_m t + \varphi_m] \tag{3.69}$$

When considering the phase distribution of the elementary wave components, TOMAWAC assumes that the phases are randomly distributed over the range between 0 and 2π with a uniform probability density. This means that each component is effectively independent and therefore a phase averaged representation is used. This hypothesis means that the energy per unit area of multidirectional random waves is expressed as:

$$E_w = \sum_{m=1}^{M} \frac{1}{2} \rho g a_m^2 \tag{3.70}$$

This hypothesis cannot be used to model shallow water wave profiles though because the non-linear processes linked to wave propagation and wave interactions with the sea bottom become more significant as water depth decreases. This results in waves becoming steeper and dissymmetrical, no longer following the sinusoidal profile that is modelled here. Modelling these effects involves using non-linear wave theories such as 3rd or 5th order Stokes theory or Cnoidal wave theory. TOMAWAC is not suitable for modelling these non-linear effects directly although it is possible to have them represented through source terms.

So far, the theory has indicated that waves are considered as a discrete sum of elementary components, whereas the sea state power over frequencies and propagation directions is a continuous function. The function known as the wave directional spectrum of energy is denoted by:

$$E(f,\theta)\delta f \delta\theta = \sum_{f}^{f+\delta f} \sum_{\theta}^{f+\delta\theta} \frac{1}{2} \rho g a_m^2 \tag{3.71}$$

The preferred variable for modelling the sea state however, is the variance density directional spectrum which is derived from the directional spectrum energy

via the relationship:

$$F(f,\theta) = \frac{E(f,\theta)}{\rho g} \tag{3.72}$$

Combining equations 3.71 and 3.72 gives:

$$a_m = \sqrt{2F(f,\theta)\delta f \delta\theta} \tag{3.73}$$

Substituting 3.73 into equation 3.69 gives the relationship between the free surface elevation and the variance density directional spectrum denoted below.

$$Z(x,y,t) = \int_{f=0}^{\infty}\int_{\theta=0}^{2\pi} \sqrt{2F(f,\theta)\delta f\delta\theta}\cos[k_m(x\sin\theta_m + y\sin\theta_m) - \omega_m t + \varphi_m] \tag{3.74}$$

The nth order moments of the variance density energy spectrum can then be defined as:

$$m_n = \int_{f=0}^{\infty}\int_{\theta=0}^{2\pi} f^n F(f,\theta)\delta f\delta\theta \tag{3.75}$$

These moments are of particular interest when calculating several important parameters relating to the wave spectrum. For example, the 0-order moment is equal to the variance of the free surface elevation and can be used to calculate significant spectral wave height which is equal to the significant wave height, that is the average height of the highest third of the waves assuming a Rayleigh distributing, by the following relationships:

$$m_0 = \int_{f=0}^{\infty}\int_{\theta=0}^{2\pi} F(f,\theta)\delta f\delta\theta \tag{3.76}$$

$$H_{m0} = 4\sqrt{m_0} \tag{3.77}$$

In the case whereby a wave is propagating in an unsteady medium, such as sea currents and/or levels that vary in space and time, the directional spectrum of the variance density is replaced by a new variable called the directional spectrum of wave action. This variable remains constant even though the medium is neither homogeneous or steady. This variable is related to the directional spectrum of variance by equation 3.78.

$$N(f, \theta) = \frac{F(f, \theta)}{\sigma} \tag{3.78}$$

The relative angular frequency, denoted by σ is the angular frequency observed in a coordinate system moving at the velocity or current and can be related to the absolute angular frequency, denoted by ω in previous equations, through the Doppler effect in the presence of a current as shown below:

$$\omega = \sigma + \vec{k} \cdot \vec{U} \tag{3.79}$$

In summary, the directional spectra of wave energy, variance or action shall generally be considered as functions dependent on five variables: time, a pair of spatial co-ordinates, either Cartesian or spherical, and the pair of variables applied for directional spectrum discretization, for which the following solutions are theoretically possible:

- absolute frequency; propagation direction, (f_a, θ).
- relative frequency; propagation direction, (f_r, θ).
- wave number; propagation direction, (k, θ).
- wave number vector, (k_x, k_y).

3.2.4.3 Solution to the Evolution Equation

The sea state spectral modelling consists of solving the equation of evolution of the directional spectrum of wave action using the kinematic equations. The transport equation formulation is solved by TOMAWAC using the discretisation variables of Cartesian or spherical space and the relative frequency; propagation direction pair for the discretisation of the angular spectrum. It is worth noting that conventionally, the x-axis (in Cartesian space) or the λ axis (in spherical space) is aligned horizontally and the y-axis (in Cartesian space) or the φ axis (in spherical space) is aligned vertically. Then in terms of angular propagation directions, the angle θ is defined with respect to the vertical axis in a clockwise direction.

The directional spectrum of wave action is therefore of the form:

$$N(x, y, k_x.k_y, t) = \tilde{B}\tilde{F}(x, y, f_r, \theta, t) \tag{3.80}$$

$$\tilde{B} = \frac{C_g}{(2\pi)^2 k f_r} \tag{3.81}$$

Whereby the relative group velocity of waves is given by the equations:

$$C_g = n\frac{\sigma}{k} \tag{3.82}$$

$$n = \frac{1}{2}\left(1 + \frac{2kd}{\sinh(2kd)}\right) \tag{3.83}$$

In this form the evolution equation solved becomes:

$$\frac{\partial(\tilde{B}\tilde{F})}{\partial t}+\dot{x}\frac{\partial(\tilde{B}\tilde{F})}{\partial x}+\dot{y}\frac{\partial(\tilde{B}\tilde{F})}{\partial y}+\dot{\theta}\frac{\partial(\tilde{B}\tilde{F})}{\partial \theta}+\dot{f}_r\frac{\partial(\tilde{B}\tilde{F})}{\partial f_r}=\tilde{B}\tilde{S}(x,y,f_r,\theta,t) \quad (3.84)$$

With the transport rates derived from linear theory in equations 3.85 to 3.88:

$$\dot{x}=C_g\sin\theta+U_x \quad (3.85)$$

$$\dot{y}=C_g\cos\theta+U_y \quad (3.86)$$

$$\dot{\theta}=-\frac{1}{k}\frac{\partial\sigma}{\partial d}\tilde{G}_n d-\frac{\vec{k}}{k}\tilde{G}_n(\vec{U}) \quad (3.87)$$

$$\dot{f}_r=\frac{1}{2\pi}\left[\frac{\partial\sigma}{\partial d}\left(\frac{\partial d}{\partial t}+\vec{U}\vec{\nabla}d\right)-C_g\vec{k}\tilde{G}_t(\vec{U})\right] \quad (3.88)$$

where:

$$\tilde{G}_n(g)=\cos\theta\frac{\partial g}{\partial x}-\sin\theta\frac{\partial g}{\partial y} \quad (3.89)$$

$$\tilde{G}_t(g)=\sin\theta\frac{\partial g}{\partial x}+\cos\theta\frac{\partial g}{\partial y} \quad (3.90)$$

The spatial transfer rates (equations 3.85 and 3.86) model the spatial propaga-

tion and shoaling. The directional transfer rate (3.87) models refraction induced changes in propagation direction generated by bathymetric variation (first term) or from current gradients (second term). The relative frequency transfer rate (equation 3.88) models the relative frequency change from sea level variations in both time and space and current variations in space. The operators (equations 3.89 and 3.90) refer to the computation of a function gradient that are respectively normal and tangential to the characteristic curve.

3.2.4.4 Consideration of Source Terms

TOMAWAC considers a variety of physical processes which make up the source and sink terms, composing the right hand term of the evolution equation (3.84).

$$S = S_{in} + S_{ds} + S_{nl} + S_{bf} + S_{br} + S_{tr} + S_{ds,cur} + S_{veg} \tag{3.91}$$

Each of these processes can be numerically modelled in different ways or discounted completely if that process is not to be modelled. They are, respectively from the above equation: wind-driven wave generation, whitecapping induced energy dissipation, non-linear quadruplet interactions, bottom friction induced energy dissipation, bathymetric breaking induced energy dissipation, non-linear triad interactions, enhanced breaking dissipation of waves on a current and dissipation due to vegetation.

Obviously, consideration of more source terms adds additional complexity into the modelling and since the research is not so much focused on the precision of the wave modelling, more the presence of it, it was decided to only consider the effects of bathymetric breaking induced energy dissipation, noting that the large scale of the domain and the complex bathymetry is therefore likely to have a significant effect.

Chapter 4

Model Setup

4.1 Introduction

This chapter deals with the methodology and preliminary setup and construction of the model as well as a description of the site it was applied to.

4.2 Methodology

The methodology used here was disseminated into six stages, briefly described below. Figure 4.1 shows the model development procedure.

1. **Define study site** - First, the domain to which the model would be applied was selected.

2. **Create preliminary model** - With the extents of the domain defined, the preliminary model was created. This involved creating the base mesh and applying the bathymetric data across the domain as well as defining the initial conditions and boundary conditions. The model files were created and initial parameter values were assigned.

3. **Model calibration and validation** - The preliminary model was then calibrated and validated against observation data to ensure that the model is accurately predicting the hydrodynamic conditions.

4. **2D/3D Hydrodynamic Modelling** - Once the model was calibrated and validated, the final model cases were defined: one case for the 2D model and one case for the 3D model. These cases were then simulated and analysed so that the results could be compared.

5. **2D/3D Morphodynamic Modelling** - The morhpodynamic model was created by coupling the hydrodynamic model with sediment transport processes.

6. **Inclusion of normal wave condition** - A wave model was created to simulate a simple normal wave condition to be coupled with the morphodynamic model.

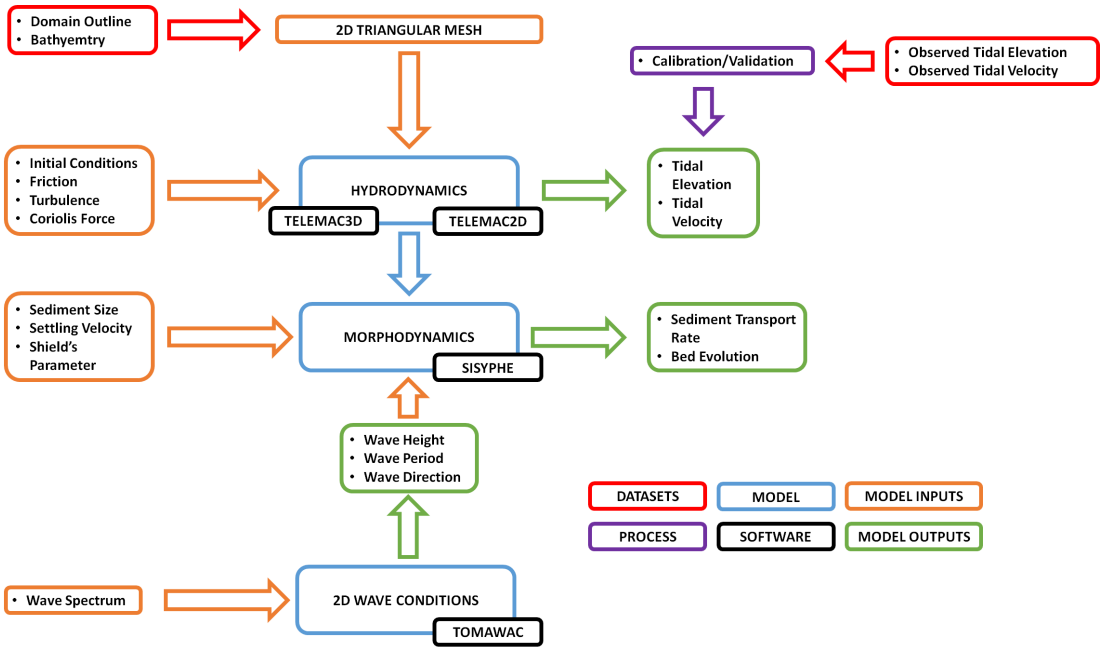

Figure 4.1: Schematic diagram of modelling framework

4.3 Site Description

The study area for this research is the southern region of the North Sea extending from 0.6°E to 6°E and from 50.8°N to 54°N. The model created is a large scale

model but will focus on a smaller area that covers the Norfolk Banks for the detailed analysis of the results. The site covers an area of 85572.022km^2 with a maximum water depth of approximately 90 meters and an average water depth of approximately 26 meters. The Southern North Sea is characterised by semi-diurnal tides [van der Veen et al., 2006]. The flood flow enters from the south and the ebb flow enters from the North [Brooks, 2010]. The tidal range varies from 2.4m in the Dover Strait (near the South) to 3m further North [van der Veen et al., 2006]. Storm surges are common in the region. For example, at Lowestoft the Highest Astronomical Tide (HAT) is 2.98m but during storm surges it has reached levels between 4.1-4.6m. Sea level rise within the region is estimated to be between 2.24 and 2.9mm/year with 0.61mm/year of this being accounted for by geological subsidence. [Brooks, 2010]. Surface velocity at spring tide varies from 1.4m/s in the Western areas to 0.7m/s along the Dutch coast [van der Veen et al., 2006]. The waves are created by dominant South-west winds and secondary North-east winds. The direction of approach of the largest waves (wave height greater than 2.2m) is from the North-east. The waves in the Southern North Sea have relatively low energy [Brooks, 2010].

The seabed consists of fine sand ranging from 125 to 500µm [van der Veen et al., 2006]. Particle size analysis shows that for nearshore sandbanks in the North Sea the mean sediment size was 261.91µm on the flanks, 279.92µm on the crest and 428.70µm in the troughs. For offshore sandbanks the mean sediment size was 305.94µm on the flanks, 275.46µm on the crest and 477.14µm in the troughs. A survey conducted by Jenkins et al. [2015] showed that the sandbanks in the North Sea were characterised by shallower crests and deeper troughs. The sediment which makes up these sandbanks was noted to be finer on the crests and flanks and more heterogeneous in the troughs. The slightly coarser material in the trough was also accompanied by a slightly higher mud content [Jenkins et al., 2015]. Estimates of sediment sources and sinks, more specifically relating to suspended particulate matter (SPM) are given by Gerritsen et al. [2000]:

- Influx through the Dover Strait (20 to 40 $\times$ 10^{9}kg/year).
- Influx from the Atlantic Ocean (10 $\times$ 10^{9}kg/year).
- Influx from rivers (4 $\times$ 10^{9}kg/year).

- Effects of dredging activities (14×10^9kg/year).
- Effects of coastal erosion (2 to 8×10^9kg/year).
- Losses due to sedimentation (32 to 45×10^9kg/year).
- Outflow to the Atlantic Ocean (11 to 14×10^9kg/year).

However, as noted by Gerritsen et al. [2000] these numbers are highly uncertain and therefore qualitative judgements relating to these sources and sinks are potentially misleading.

4.3.1 Norfolk Banks

The Norfolk Banks are a group of offshore sandbanks located 100km seaward from the East Anglian coastline [Collins et al., 1995]. The Norfolk Banks are well established classical examples of tidally controlled sandbanks. The Norfolk Banks system consists of three main groups of sandbanks: the Great Yarmouth Banks, consisting of several sandbanks between Lowestoft and Great Yarmouth out to Smith's Knoll. They all lie within 40km of the present day coastline. The Dudgeon-Dowsing shoal comprises of smaller banks scattered towards the northern Norfolk coastline. Finally the Norfolk Offshore Banks consists of the much larger linear banks which lie between 40-80km offshore from the North-east Norfolk coastline. Specifically they are the Leman, Haddock, Ower, Inner, Well, Broken, Swarte and the Indefatigable banks. These banks will be the main focus for this research. The location of the main banks in the Southern North Sea as well as some physical characteristics is presented in Figure 4.2 and Tables 4.1 and 4.2.

Figure 4.2: North Sea Sandbanks (sourced from Smith [2013])

Table 4.1: Dimensions of major sandbanks in the Norfolk Banks area (sourced from Caston [1972])

Bank	Length (km)	Average Width (km)	Length/Width Ratio	Maximum Height Above Seabed (m)
Broken	32.5	1.1	29:1	30.5
Inner	12.6	1.1	12:1	24.4
Leman	40.8	1.5	28:1	41.2
Ower	39.0	1.7	24:1	32.9
Haisborough Sand	21.5	2.2	10:1	33.5
Hammond Knoll	13.9	0.7	19:1	30.5
Hearty Knoll	12.2	0.9	13:1	32.9
Hewett Ridge	18.2	1.3	14:1	24.4
Smiths Knoll	30.6	0.9	33:1	42.7
Swarte	37.1	1.3	28:1	27.4
Well	51.9	1.7	29:1	38.4
Winterton Ridge	17.6	0.9	19:1	29.3
East Dyck	26.9	2.2	12:1	27.4

Table 4.2: Geometric characteristics of the Norfolk Banks (sourced from Cooper [2008])

Bank	Distance offshore (km)	Spacing (km)	Length (km)	Average Width (km)	Height (m)	Estimated Volume (x $10^6 m^3$)
Indefatigable 3	97	-	31.0	3.0	10.0	310
Indefatigable 2	86	10.3	13.8	1.5	10.0	69
Indefatigable 1	83	3.4	29.3	1.0	10.0	98
Swarte	76	6.9	37.1	1.3	27.4	440
Broken	67	8.6	32.5	1.1	30.5	360
Well	59	8.6	51.9	1.7	38.4	1100
Inner	53	5.2	12.6	1.1	24.4	110
Ower	48	5.2	39.0	1.7	32.9	730
Leman	41	6.9	40.8	1.5	41.2	840

The average water depth is around 31-40m [Caston, 1972]. Some of the banks rise to within 5m of the sea surface, those in deeper waters have submerged crestlines. The Well Bank, Broken Bank and Swarte Bank are asymmetric with

the steep slope facing the north-easterly direction and the gentle slope facing the southwest ([Caston, 1972], [Collins et al., 1995], [Cooper, 2008]). Maximum angle of the steep slope decreases going further offshore from 6° for the Broken Bank to 2° for the Swarte Bank. Tidal range over the Broken Bank ranges from 1.2-2.8m. Maximum velocity occurs towards high and low water with slight asymmetry towards the southeast. Peak surface currents are orientated Northwest to Southeast with a spring current of 1.6m/s and a neap current of 1m/s. Currents are dominated by the semi-diurnal tidal constituents [Collins et al., 1995].

The great majority of the banks consist of superficial accumulations of sand standing upon a surface, which in the interbank channels or swales is exposed on the seabed. The surface material is a thin to discontinuous sheet of gravel and stones. The material beneath ranges from clays to sands and gravel [Caston, 1972]. Loosely consolidated sediment on the Broken Bank is predominately well-sorted, fine-grained sands [Collins et al., 1995]. The two outermost banks in this group, Swarte and Broken Banks, mostly overlie the Eem Formation but their north western ends lie on the Devensian till of the Bolders Bank Formation. The Well, Inner, Ower and Leman Banks overlie Anglian glacial deposits of the Swarte Bank Formation in the west and the Eem Formation in the east. At its south eastern end, Well Bank overlies a formation of well-sorted, fine-grained sands which are associated with the Devensian glacial period. These sands may once have been more extensive and were deposited in the periglacial environment to the south of the glacial ice limit [Cooper, 2008]. Seismic profiles obtained by the British Geographical Survey, particularly over Leman and Well Banks show them to occasionally overlie the early Holocene intertidal deposits.

The Norfolk Banks had smaller elevations compared with the more southern sandbanks and as a whole the banks appear to be migrating in a northerly direction [Jenkins et al., 2015]. However, it remains to be proven whether migration is presently occurring and at what rate, although recent work has shown the potential for north-westerly sand transport and migration. Migration rates vary but are estimated to be somewhere between 0.5-1m per year. This comes from the idea that the banks must have migrated at least their entire width to establish their current observed internal structure. Surveys and charts appear to agree with this rate, showing around 100m of movement in the past century [Cooper,

2008].

Many of the Norfolk Banks are covered in active sand waves, which reflect the pattern of modern sand transport around these banks. Over the lower part of the banks the sand waves have their crests aligned more or less at right angles to the bank crest with their steep faces in opposing directions on either side of the sandbanks. Where visible, the sand waves on the upper part of the flatter slope are seen to be directed more towards the crest, suggesting that the process that gave rise to the internal structure is ongoing and evidence that such features remain as sinks for sand. The Norfolk Offshore Banks systems represent a significant sink for sand-sized sediment in the Southern North Sea. It is difficult to accurately estimate the total amount of sediment involved. The major sediment sources in the area are the eroding cliffs of the Holderness coast and the north east Norfolk coast. The rivers along this coast input relatively little sediment (around $0.1 \times 10^6 m^3$ per year). Estimates for the inputs from cliff erosion vary widely; for the Holderness coast a figure of 3 to $4 \times 10^6 m^3$ per year is generally accepted. The northeast Norfolk cliffs are estimated to provide a total of approximately 0.5 to $0.6 \times 10^6 m^3$per year [Cooper, 2008].

4.4 Preliminary Model Setup

4.4.1 Mesh

The unstructured mesh was generated using the BlueKenue software ([National Research Council Canada, 2019]). To begin with satellite images of the domain were extracted from Google Earth and used to create an approximate outline of the site described above. The outline includes both the UK and European coastlines within the domain area, as well as accounting for some of the larger islands present near the coastline. Permanent offshore structures such as wind farms were not accounted for as hard points within the mesh. The outline of the mesh that forms the boundaries of the model is shown in Figure 4.3.

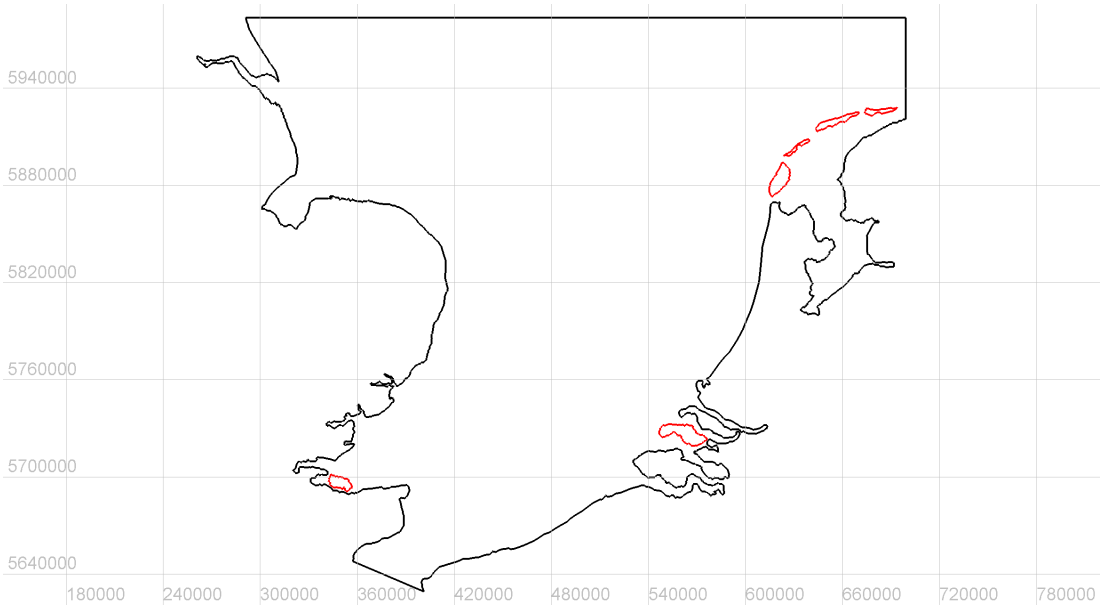

Figure 4.3: Mesh outline (black) showing the islands as hard points (red)

The triangular mesh structure consists of three areas of refinement: a coarse grid, an intermediate grid and a fine grid. The coarse grid has a resolution of 2.5km. The intermediate grid has a resolution of 500m and covers the areas that lie close to the coastlines. The fine grid has a resolution of 100m and covers the area of the Norfolk Banks. This latter area will be focussed on in later chapters. The line boundaries used for each area of the grid refinement are shown in Figure 4.4. The final generated mesh is shown in Figure 4.5 and its geometric properties are shown in Table 4.3.

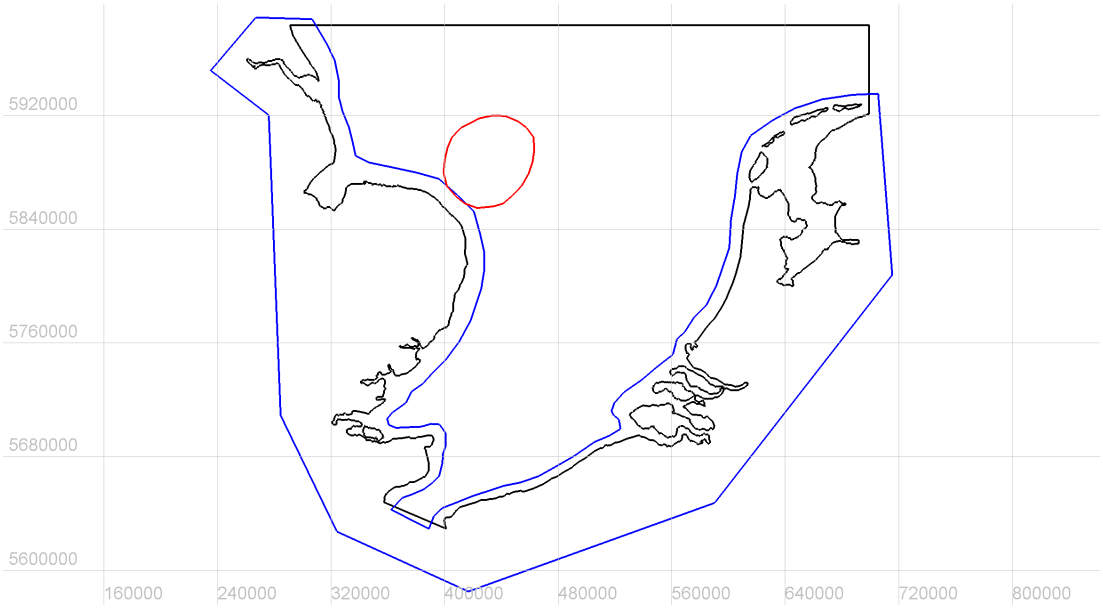

Figure 4.4: Areas of mesh refinement - 500m (blue) and 100m (red)

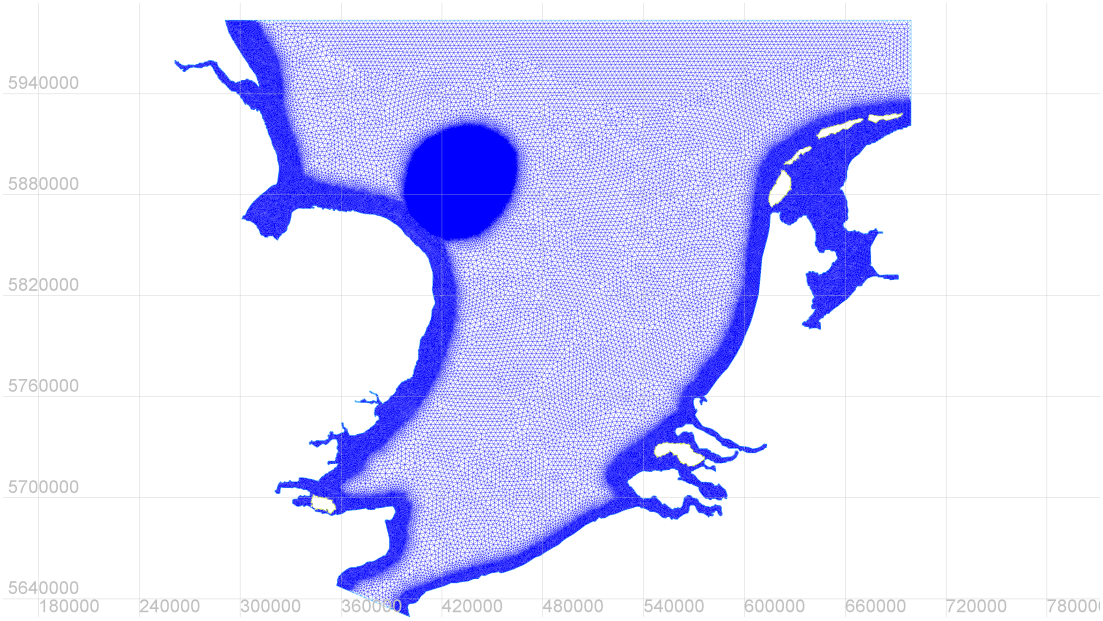

Figure 4.5: Final 2D triangular mesh

Table 4.3: Geometric properties of the final mesh

Mesh Geometry	
Number of Nodes	450344
Number of Elements	895657
Element Area (Min - Max)	2040m^2 - 6.12km^2
Element Area (Mean)	95 541m^2
Edge Length (Min - Max)	58.8m - 4.01km
Edge Length (Mean)	243.2m

4.4.2 Bathymetry

Bathymetry data was obtained from the British Oceanographic Data Centre (BODC) at an interval of 30 seconds across the entire domain. The data was mapped onto the mesh using an inverse interpolation algorithm (see Figure 4.6).

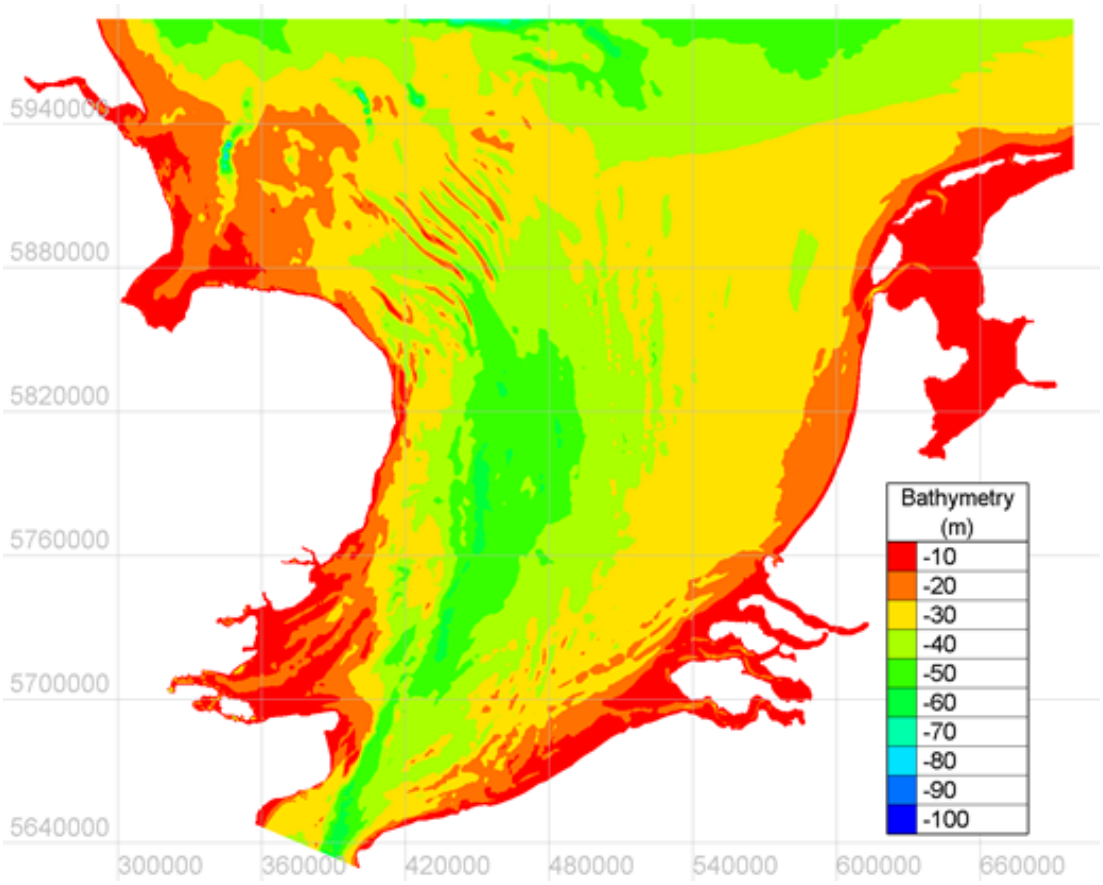

Figure 4.6: Model bathymetry

4.4.3 Boundary Conditions

The model contains four open boundaries; one in the north of the domain, one in the south of the domain and two representing the rivers Humber and Thames. There are two closed boundaries representing the main UK and European coastlines and several large islands located throughout the domain.

Each of the TELEMAC modules requires separate boundary conditions owing to the different types of boundaries that can be prescribed. Each of the boundary segments is the same between the modules (i.e. the North Boundary is always the same nodes) but has a different code for each module. Each of the assigned codes defines a different condition depending on the module. In the TELEMAC2D boundary condition file the codes correspond to prescribing

water depth (H), flowrate (Q) velocity in x and y (UV). The boundary for tracers can also be prescribed with similar values (i.e 2 = closed 4 = free and 5 = prescribed). In SISYPHE the boundaries are either closed (2), free Neumanns type (4) or imposed Drichtler type (5). Evolution (E) or sediment discharge (Q2) for bedload transport and sediment concentration (C) for suspended sediment transport can be imposed. In TOMAWAC there are only two types of boundary; a free boundary and a prescribed boundary. A free boundary fully absorbs all wave energy and can either be liquid (allows propagation beyond the domain) or solid (allows the shore to absorb the energy). The numbering convention is the same as TELEMAC2D but only the first value of the code is used (i.e 2 for a free boundary and 5 for a prescribed boundary). The type of spectrum used is then prescribed in the steering file (in case a parametrised JONSWAP for frequencies and a parametrised angular distribution for directions).

Each of the open boundaries were prescribed as tidal boundaries. This allows for the use of tidal databases to prescribe water levels and velocities at the boundary. Four global tidal databases can be implemented with the TELEMAC software: the JMJ database (from the LNHE Atlantic Coast model), the TPXO database (from Oregon State University), the North-East Atlantic Atlas (from LEGOS) or the PREVIMER atlases. In this research, the TPXO database was used. TPXO is a global set of models of ocean tides that fits the Laplace tidal equations and altimetry data. The tides are provided as complex amplitudes of earth relative sea surface elevations for the 13 harmonic constituents: 8 Primary (M_2, S_2, N_2, K_2, K_1, O_1, P_1 and Q_1), 2 Long Period (M_f and M_m) and 3 Non-linear (M_4, MS_4 and MN_4). Further information about the methods used to create the TPXO database are not described here but can be found at Oregon State University [2010] and the references contained therein.

Table 4.4: Boundary condition codes

Boundary Code	Boundary Type			Colour
	TELEMAC2D	SISYPHE	TOMAWAC	
2 2 2	Closed	Closed	Free	Brown
4 5 5	Open with prescribed Q	Open with prescribed E/Q2/C	N/A	Blue
5 4 4	Open with prescribed H	Open with free E/Q2/C	Prescribed	Green
5 5 5	Open with prescribed H and Q	N/A	Prescribed	Cyan
4 6 6	Open with prescribed UV	N/A	N/A	Red
5 6 6	Open with prescribed H and UV	N/A	Prescribed	Orange

Figure 4.7: Boundary conditions for TELEMAC2D/3D

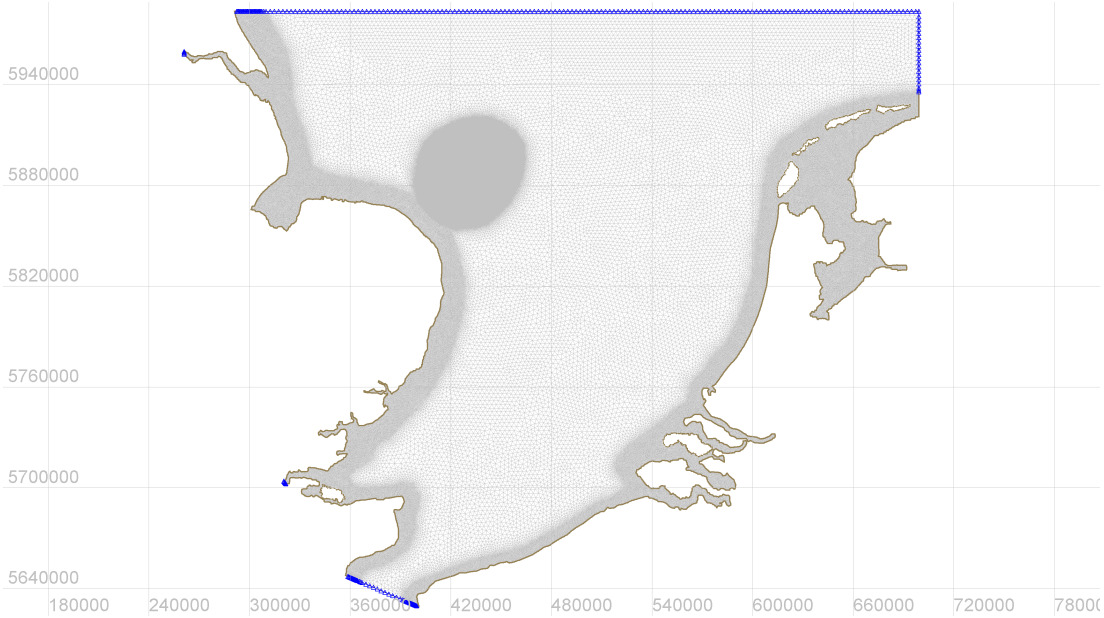

Figure 4.8: Boundary conditions for SISYPHE

Figure 4.9: Boundary conditions for TOMAWAC

4.4.4 Initial Conditions

TELEMAC presents several options for defining the initial conditions across the domain. The first option involves either setting the water depth to zero (i.e the entire domain is dry) or the elevation to zero. The second option requires the water depth or elevation to be set to a specific prescribed value by the user. The third option is to prescribe the initial conditions from a preset database (the same as used for the boundary conditions). The disadvantage of selecting either of the first two options is that it requires simulation time in order for the tidal conditions to reach equilibrium. The modern databases are capable of prescribing the equilibrium conditions with sufficient accuracy. However, calibration of the model to the local conditions is still required. For this research, the initial conditions for the free surface elevation and velocity were defined through the TPXO global database.

Chapter 5

Model Calibration and Validation

5.1 Introduction

This chapter deals with the initial 2D hydrodynamic modelling. This part consists of testing the model created in the previous chapter. First the 2D model is calibrated and validated against observed data to assess the accuracy and reliability of the model. The second stage is to test the 2D model's sensitivity to input parameters by modifying them and comparing the output to that of the calibrated model.

5.2 Model Calibration

It is necessary to prove that the model is capable of accurately simulating the hydrodynamic conditions within the domain. This is achieved through calibrating the model. Calibration is the process of training the model to match the output with the desired real time observational data. Calibration of the model is achieved by modifying input parameters linearly until the model output matches the observational data within an acceptable error boundary.

5.2.1 Calibration Parameters

The model has three coefficients relating to the TPXO database that could be calibrated, namely: the coefficient to calibrate sea level (CSL), the coefficient to calibrate tidal range (CTR) and the coefficient to calibrate tidal velocities (CTV). The behaviour of these coefficients is described in equations 5.1 to 5.3.

$$h = CTR \sum_i h_i - z_b + CSL \tag{5.1}$$

$$u = CTV \sum_i u_i \tag{5.2}$$

$$v = CTV \sum_i v_i \tag{5.3}$$

The CSL is an additive coefficient that controls the initial value of the free surface elevation (i.e. a CSL value of 0.1 will increase the initial elevation at each node by 0.1m) . The CTR is multiplicative and controls the value of the tidal amplitudes (i.e. a CTR value of 1.1 will multiply the tidal amplitudes by 1.1) . The CTV is multiplicative and controls the magnitude of the velocity vectors (i.e. a CTV value of 1.1 will multiply the initial velocity by 1.1).

5.2.2 Observation Data

5.2.2.1 Free Surface Elevation

The model domain encompasses many tidal gauge stations. For the purposes of calibration, 16 stations are selected to ensure coverage of the different areas of the domain including some nearshore stations and some offshore stations. The location of these stations is displayed in Table 5.1 below.

Table 5.1: Locations for free surface calibration

Station		Location (UTM)		
Number	Name	Easting	Northing	Datum (m)
1	Immingham	318419.406	5869120.000	-3.90
2	Cromer	386800.000	5867000.000	-2.75
3	Lowestoft	418000.000	5814268.500	-1.50
4	Harwich	385017.625	5753947.000	-2.02
5	Sheerness	342057.188	5700600.000	-2.90
6	Dover	383011.344	5663415.500	-3.67
7	Calais	454906.563	5657702.000	-3.99
8	Dunkerque	419043.813	5649670.500	-3.14
9	Westhinder	461035.000	5693345.000	0.00
10	Oostende	490030.156	5679014.500	0.00
11	Hoek van Holland	574928.938	5759094.500	0.00
12	Europlatform	519222.000	5761075.000	0.00
13	Ijmuiden	602897.938	5814126.000	0.00
14	K13a	630298.183	5943047.772	0.00
15	J61	496050.080	5963496.747	0.00
16	L91	514689.114	5896766.757	0.00

Free surface elevations at these 16 stations are obtained for a one month period from 23/05/2017 to 23/06/2017. Data is sourced from the British Oceanographic Data Center (BODC) for stations 1 through 6, the (REFMAR) for stations 7 and 8 and the North West Shelf Operational Oceanographic System (NOOS) for stations 9 through 16 ([Natural Environment Research Council, 2018], [Service Hydrographique et Océanographique de la Marine, 2012], [North West Shelf Operational Oceanographic System, 2018]). The data obtained from the BODC and REFMAR is measured with respect to chart datum, whereas the data obtained from the NOOS and the calculations of the TELEMAC model are measured with respect to ordnance datum. In order to convert between the two, a conversion value is added, shown for each station in the final column of Table 5.1.

5.2.2.2 Velocity

Velocity data is extracted from Admiralty Chart 2182A (see Figure 5.1). This provides current magnitudes and directions at hourly intervals at several locations throughout the southern North Sea. The data is relative to the high water level at Dover. The speed of the current is given in knots on the Admiralty Chart so each value is multiplied by 0.514 to convert into metres/second, while the direction of the current is left in decimal degrees in order to match the velocity output of the model. Of the 16 locations on the chart, 9 lie within the computational domain of the model detailed in Table 5.2.

Figure 5.1: Admiralty Chart 2182A

Table 5.2: Locations for velocity calibration

Point	Latitude (N)	Longitude (E)	UTM Northing	UTM Easting
M	53°45′	5°58′	695600.715	5959792
N	53°24′	4°9′24″	576903.518	5917392
P	53°20′	2°44′	482242.054	5909385
Q	53°19′	1°25′24″	394968.896	5908657
R	52°33′9″	4°9′18″	578310.141	5823118
S	52°29′	2°43′	480759.212	5814836
T	51°55′	2°59′	498853.701	5751770
U	51°32′	2°13′	445666.742	5709427
V	51°8′8″	1°57′12″	426770.894	5665420

5.2.3 Model Configuration

The model is configured to run for a duration of 15 days. Since the durations of the spring and neap tidal cycles are both approximately 7 days, this ensured that no matter what initial date and times are chosen, the model would cover a whole spring and neap cycle. This is important for the models capability to accurately simulate different tidal conditions. The initial date and time is chosen to be midnight on the 23rd of May 2017, the same date and time as the start of the observation data period.

5.2.3.1 Cases

In total 21 cases are run which are described in Table 5.3

Table 5.3: Calibration coefficient values for each test case

Case	Baseline	S014	S021	S007	S004	S011	S006	S009	S008
CSL	0.00	0.14	0.21	0.07	0.04	0.11	0.06	0.09	0.08
CTR	1.00	1.00	1.00	1.00	1.00	1.00	1.00	1.00	1.00
CTV	1.00	1.00	1.00	1.00	1.00	1.00	1.00	1.00	1.00
Case	T120	T110	T105	T115	T113	T108			
CSL	0.08	0.08	0.08	0.08	0.08	0.08			
CTR	1.20	1.10	1.05	1.15	1.13	1.08			
CTV	1.00	1.00	1.00	1.00	1.00	1.00			
Case	V110	V090	V080	V070	V075	V085			
CSL	0.08	0.08	0.08	0.08	0.08	0.08			
CTR	1.13	1.13	1.13	1.13	1.13	1.13			
CTV	1.10	0.90	0.80	0.70	0.75	0.85			

5.2.4 Results

5.2.4.1 Methods of Analysis

In order to assess the accuracy of the model, several methods of error calculations are performed.

The Root Mean Square Error (RMSE) is a measure of absolute fit. As such, it is a measure of how close the models calculations are to the observed data and can be interpreted as the standard deviation of the unexplained variance. The RMSE value is calculated in equation 5.4. Lower values of RMSE indicate

a better fit and a value of zero indicates that model has a perfect fit, i.e the model outputs are exactly the same as the observation data. Since there is no distinguishable criteria that specifically states set values for RMSE as acceptable or unacceptable, the training procedure will focus purely on minimising the value of RMSE as much as possible.

$$RMSE = \sqrt{\frac{\sum_{t=1}^{t} \left(Z_{mod}^{t} - Z_{obs}^{t}\right)^2}{t}} \tag{5.4}$$

The Nash-Sutcliffe Efficiency (NSE) is a measure of goodness of fit in hydrological or hydrodynamic models. The equation to calculate the NSE is shown in equation 5.5.

$$NSE = 1 - \frac{\sum_{t=1}^{t} \left(Z_{mod}^{t} - Z_{obs}^{t}\right)^2}{\sum_{t=1}^{t} \left(Z_{obs}^{t} - \bar{Z}_{obs}\right)^2} \tag{5.5}$$

The value of the NSE coefficient ranges from -infinity to 1. A value of 1 indicates that there is a perfect match between the observation data and the model calculation. A value of 0 indicates that the model predictions are as accurate as the observational mean. A negative value indicates that the observational mean is more accurate than the model predictions (i.e residual variance in the model is greater than observational variance in the data).

$$Bias = \frac{\sum_{t=1}^{t} \left(Z_{mod}^{t} - Z_{obs}^{t}\right)}{t} \tag{5.6}$$

Bias is a simple measure of the magnitude of the error between the model calculation and the observed data. High values of bias result from a large difference between the model calculation and the observation. The bias values can be positive (model is over-predicting) or negative (model is under-predicting). However, average bias alone can be a poor indicator of model accuracy because the positive and negative values can cancel each other out. A specific example

of this is shown in Figure 5.2 below. Here, Figure 5.2a has a lower average bias than Figure 5.2b but it can be seen both visually and from the RMSE and NSE values that Figure 5.2b has a better fit to the observational data. Therefore it can be concluded that although bias values can be a good indicator of whether the model has a tendency to over or under predict, it is better to rely on the RMSE and NSE values when making the judgement of whether one simulation is more accurate than another.

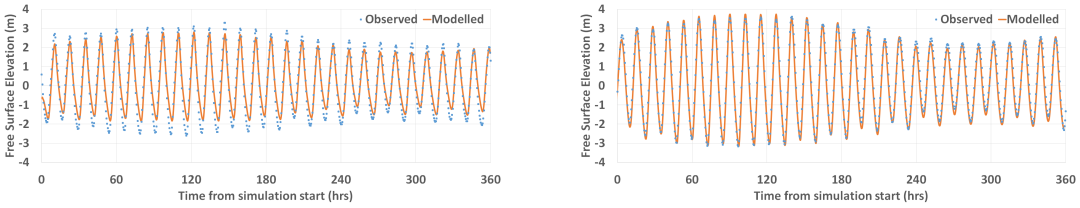

(a) Station with low bias value

(b) Station with high bias value

Figure 5.2: Comparison of stations with a high and low bias

5.2.4.2 Free Surface Elevations

The free surface elevations corresponding to the final calibration case (V085) for the stations at Cromer, Dover, Ijmuiden and J61 are shown in Figures 5.3 to 5.6.

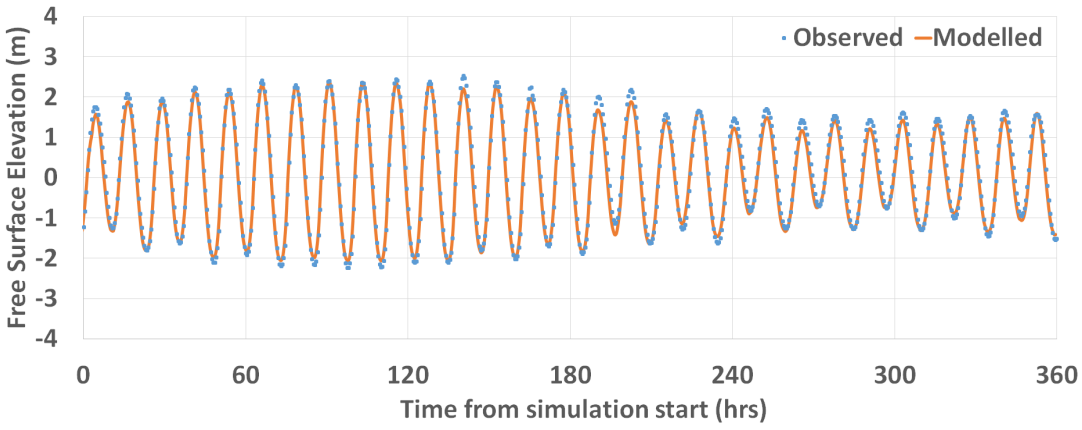

Figure 5.3: Observed against calculated free surface elevation at Cromer

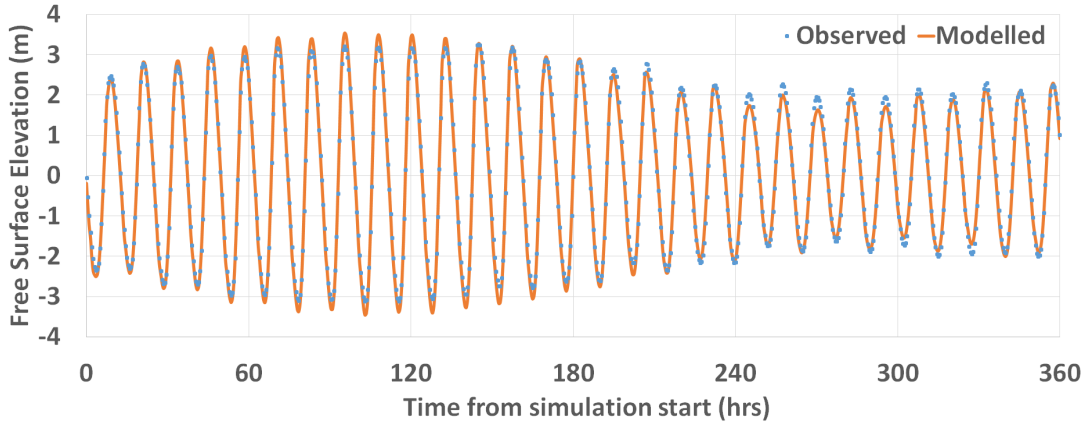

Figure 5.4: Observed against calculated free surface elevation at Dover

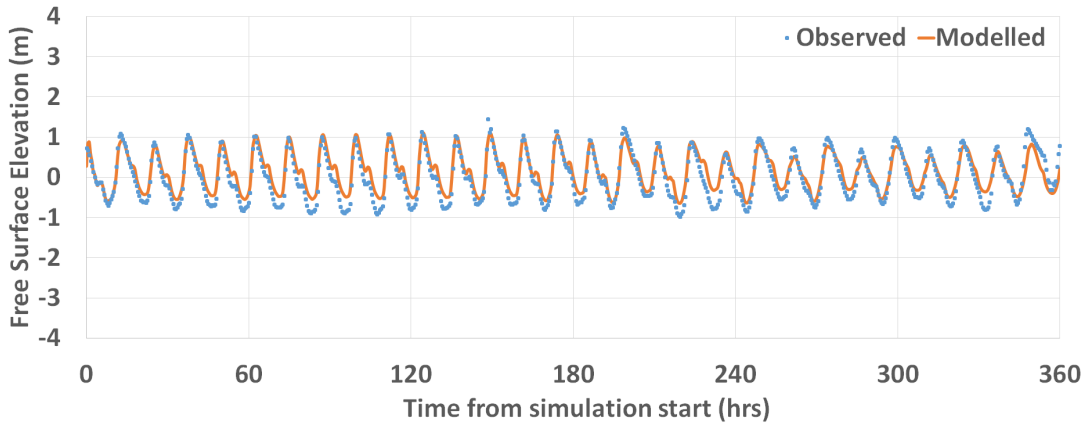

Figure 5.5: Observed against calculated free surface elevation at Ijmuiden

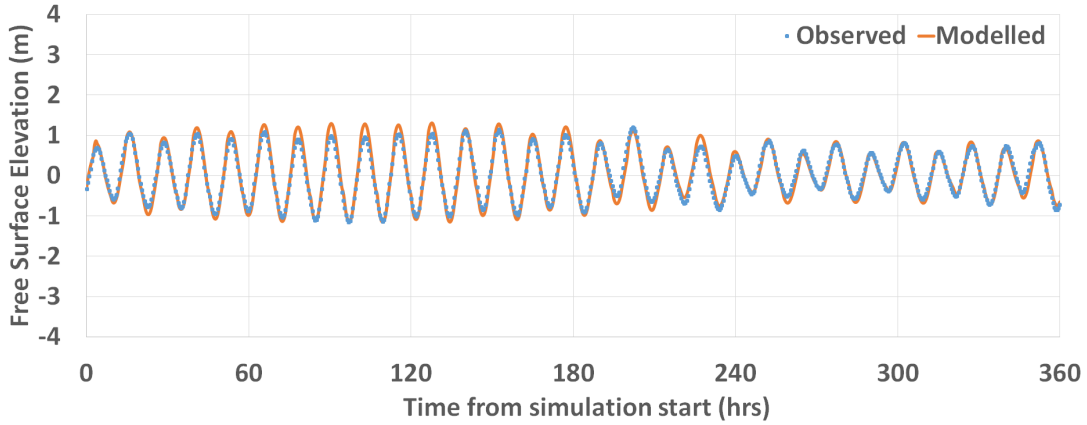

Figure 5.6: Observed against calculated free surface elevation at J61

Figures 5.3 to 5.6 show that there is good agreement between the models calculated free surface elevations and the observation data. The average RMSE and NSE values across all stations for each test case are shown in Table 5.4.

Table 5.4: Average RMSE and NSE values across all stations for each test case

Case	Baseline	S014	S021	S007	S004	S011	S006	S009	S008
RMSE	0.264	0.267	0.294	0.256	0.271	0.260	0.256	0.258	0.257
NSE	0.928	0.904	0.876	0.926	0.928	0.917	0.926	0.922	0.924
Case	T120	T110	T105	T115	T113	T108			
RMSE	0.248	0.242	0.246	0.245	0.242	0.243			
NSE	0.921	0.927	0.926	0.924	0.926	0.926			
Case	V110	V090	V080	V070	V075	V085			
RMSE	0.245	0.240	0.240	0.240	0.240	0.240			
NSE	0.925	0.929	0.929	0.929	0.925	0.929			

In general the results show that the average RMSE value is low for each of the test cases. The average NSE values are in a good range of acceptable values. In general the UK stations (Stations 1-6) showed higher average RMSE values but also higher NSE values. The worst NSE values came from the offshore stations (Stations 14-16) but these stations tended to have the best RMSE values. The average RMSE error value calculated for the best case is 0.24m and the corresponding NSE value is 0.929.

Looking at the tendency of the model to over or under-predict, it is seen that in the best case the model tended to under-predicted the free surface elevation for stations 1-8 and over-predict for stations 9-16. This trend is observed throughout each of the test cases.

Another interesting point is that when increasing the value of the CTV, the average RMSE values became noticeably worse. However when decreasing the value of the CTV there is no noticeable change. The difference in the values is only distinguishable at the 4th decimal place. However, it is important to note that the CTV value is controlling the initial velocity not the initial elevation. It is interesting to see that a 10% increase in the value of this coefficient had a greater effect on the model accuracy than a 30% decrease. Therefore, it could be reasonable to assume that the model is accurate and calibrated at case V090 - since there is no improvement in the RMSE or NSE value between case V090 and V080. However, it is uncertain which coefficient value is producing a more accurate representation of the observed velocity. This highlights the need for multiple datasets covering different model outputs to more accurately calibrate numerical models.

5.2.4.3 Velocity

Figures 5.7 to 5.9 show the velocity calibration in terms of both magnitude and direction. It can be seen that at each of the points the modelled results are in agreement with the observations. However, it is important to note that the observation results are taken from the Admiralty chart and not from direct field measurements and therefore the time series variations may not be as accurately calibrated as the Figures imply. Moving forward, the setup of case V085 was used

as the most calibrated case, as this case produced the best fit for the flow fields and the free surface elevations

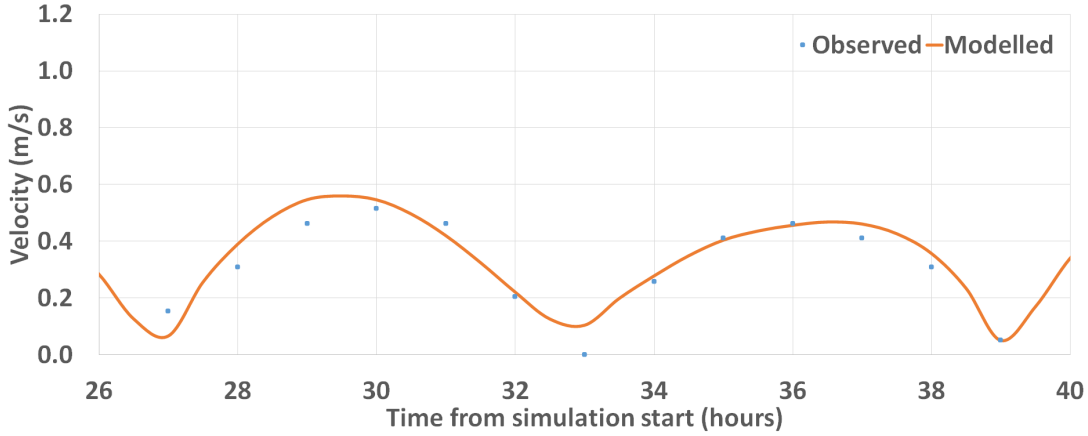

(a) Magnitude

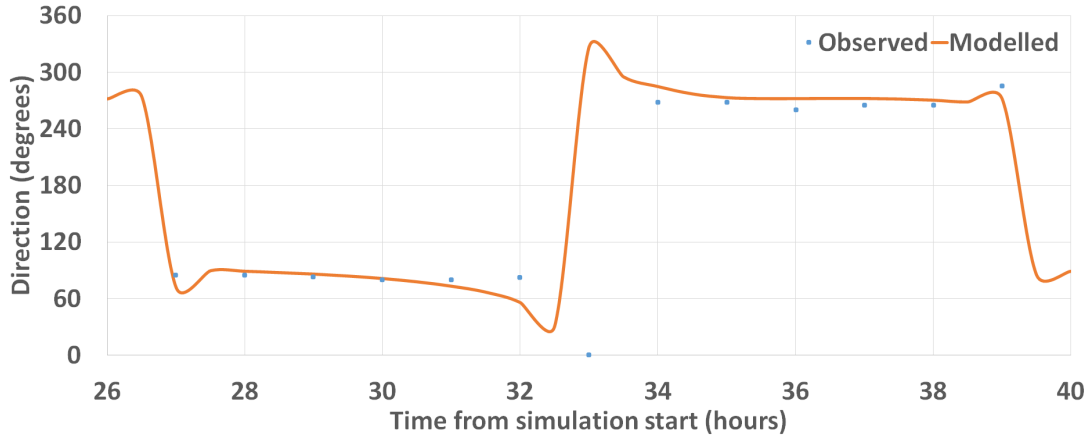

(b) Direction

Figure 5.7: Velocity magnitude and direction at Point M

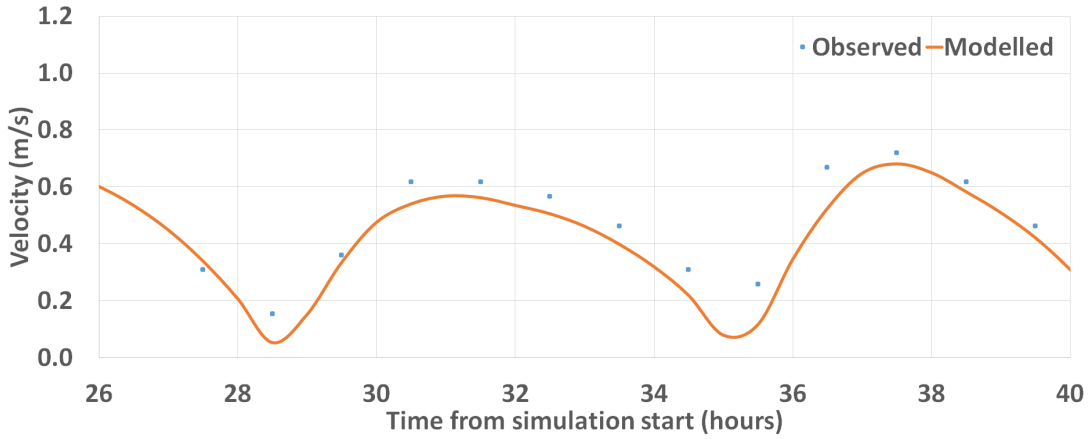

(a) Magnitude

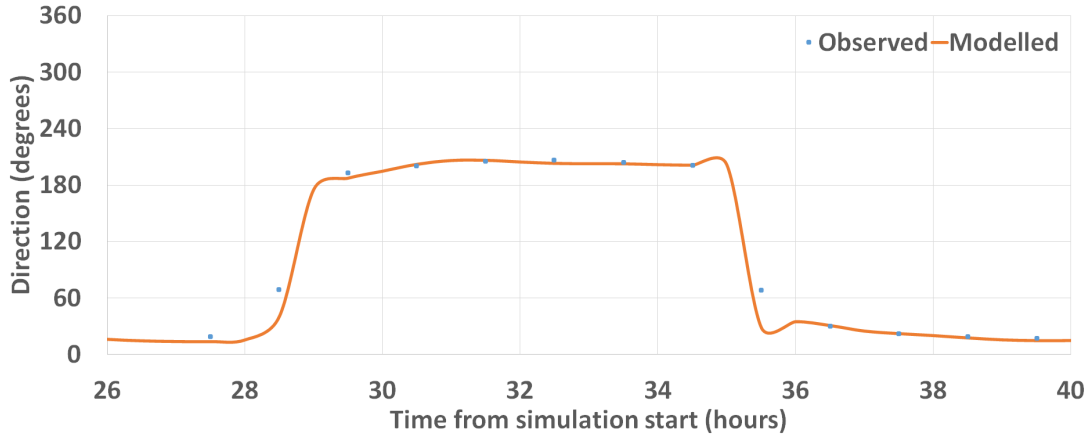

(b) Direction

Figure 5.8: Velocity magnitude and direction at Point R

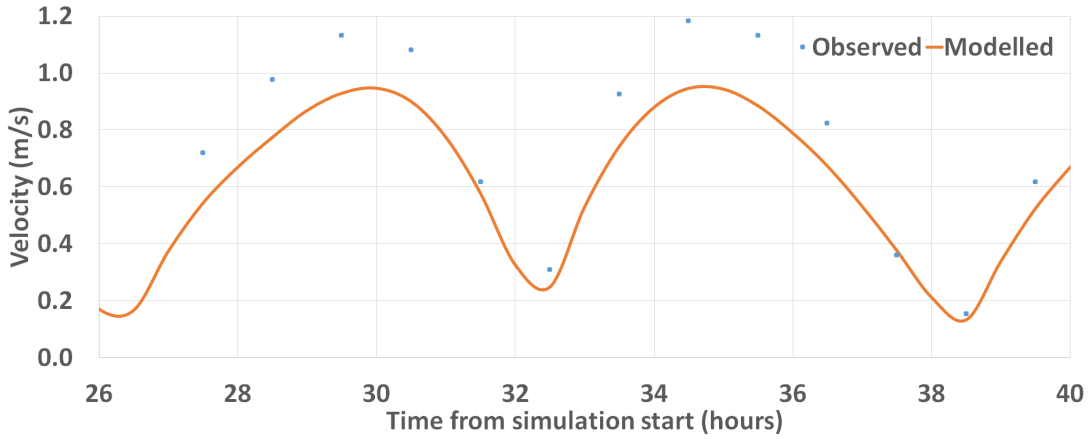

(a) Magnitude

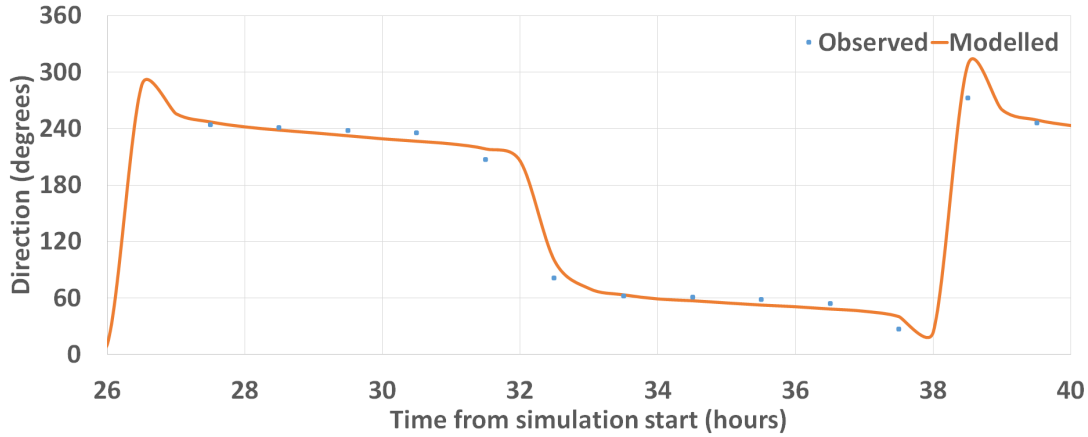

(b) Direction

Figure 5.9: Velocity magnitude and direction at Point V

5.3 Model Validation

Model validation is the confirmation that a calibrated model's outputs are acceptable to the outputs of a set of observation data. Validation data is usually different to the data used to calibrate the model and therefore is testing that the model's predictive capability does not negligibly decrease when applied to relevant observation data sets. Although it is possible to validate a simulation model from the same dataset that it is trained with, it is commonly accepted that this method is inadequate as it relies on "goodness of fit" rather than residual

variance. Goodness of fit by itself can be a poor indicator of accuracy as two models with the same goodness of fit can have poor residual variance and vice versa.

5.3.1 Model Configuration and Observation Data

New observation data is obtained from the same sources used for the calibration data (see section 5.2.2). For the validation, 5 months of observation data is obtained covering a period starting on 01/03/2016 and ending on 31/07/2016. The validation process would only cover the free surface elevation, as the only available dataset for the velocity is used in the calibration. In total, five validation cases are set up, each starting one month later than the previous one. The model configuration is identical to the final calibration case, V085, with the exception of the initial date and initial time keywords whose values are changed to match those of the desired cases.

5.3.2 Results

The average RMSE, NSE and bias values are calculated for each of the 5 cases as shown in Table 5.5. Theses values compared to the values from the final calibration case, which are 0.240, 0.929 and 0.011 respectively.

Table 5.5: Results for the validation test cases

Case	Start Date	Average RMSE (m)	Average NSE	Average Bias (m)
VAL1	01/03/2016	0.337	0.833	-0.007
VAL2	01/04/2016	0.255	0.911	-0.006
VAL3	01/05/2016	0.265	0.909	-0.011
VAL4	01/06/2016	0.236	0.926	0.013
VAL5	01/07/2016	0.221	0.934	0.011

The first validation case (VAL1) shows a significantly larger RMSE value and a significantly worse NSE value compared to the values calculated at the end of the calibration process. The remaining four cases show similar values when compared to the calibration case. This shows that for the examined cases the model is fairly well validated and retains its predictive capabilities when applied to new datasets.

5.4 Sensitivity Testing

Sensitivity testing is performed on the model to test the model's robustness and response to changes in the input parameters. Four parameters are chosen for the sensitivity testing: namely timestep, friction coefficient, Coriolis parameter and velocity diffusitivity. The first case is run with parameter values equal to that of the final calibration case for a duration of 24 hours in order to establish the baseline scenario. Each of the parameters for the sensitivity analysis are then changed individually ensuring all other parameters remained constant. Five points are chosen for analysis in the testing: the crest, left and right flanks and the nearshore and offshore faces of the sandbank. The differences in free surface elevation, velocity magnitude and velocity direction between each case and the base case are calculated at each of these five points. The average values calculated took into account the absolute value of the difference to cancel out the impact of sign on the average values. For these cases the model outputs are not being measured against real-time observations but against the established baseline case.

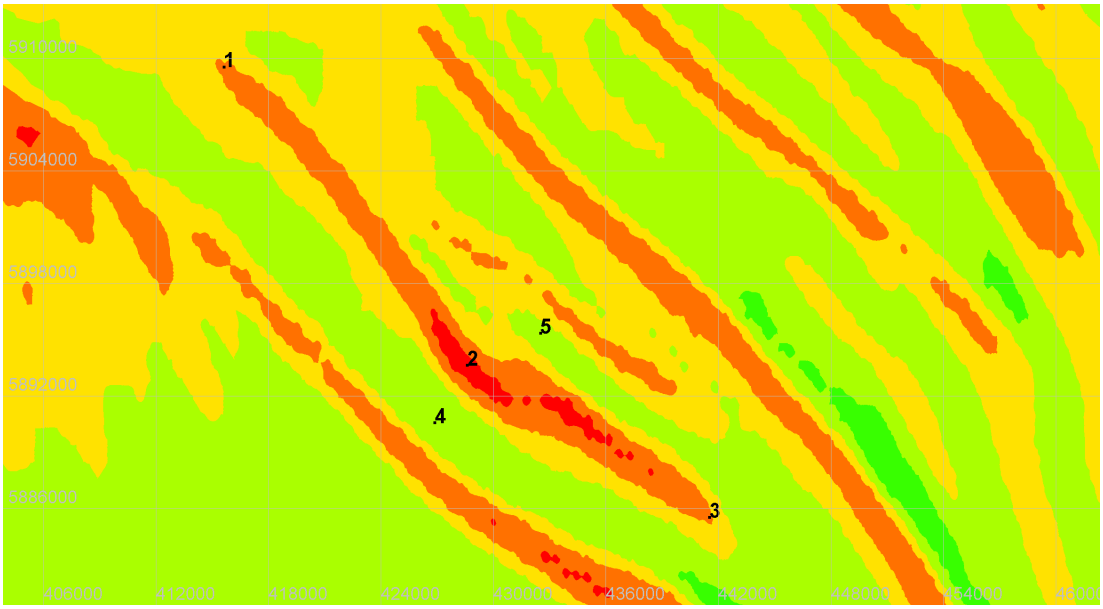

Figure 5.10: Location of the five points used for sensitivity testing

5.4.1 Timestep

The model timestep is a vital parameter in computational modelling. Smaller timesteps have the advantage of improving model stability but the disadvantage of increasing computational time and resources. The default model is run with a timestep of 60 seconds. For the sensitivity analysis, timesteps of 10 seconds, 30 seconds, 150 seconds and 300 seconds are chosen. Figure 5.11 displays the sensitivity of the velocity magnitude to the model timestep and Table 5.6 shows the percentage change between the baseline cases and each of the cases for free surface elevation and velocity.

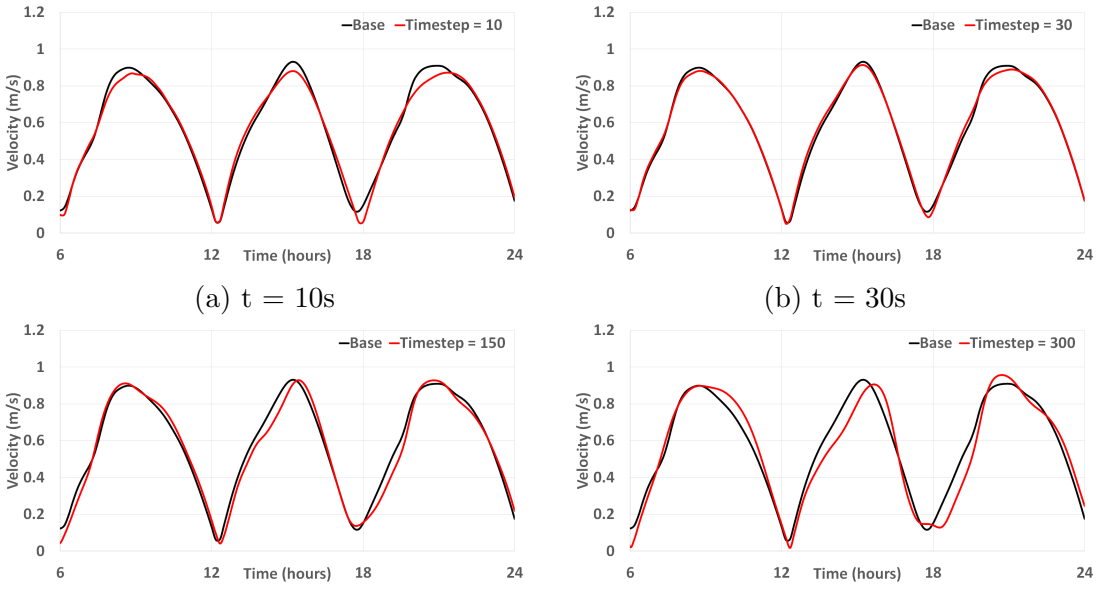

(a) t = 10s (b) t = 30s

(c) t = 150s (d) t = 300s

Figure 5.11: Sensitivity of velocity magnitude to timestep at the offshore trough

Table 5.6: Sensitivity of model to timestep

Case	Point 1 (Flank)	Point 2 (Crest)	Point 3 (Flank)	Point 4 (NS Trough)	Point 5 (OS Trough)
	Percentage change in free surface elevation compared to baseline case				
Timestep10	3.01%	1.41%	-2.11%	0.62%	0.12%
Timestep30	-1.49%	5.56%	-2.34%	-0.03%	2.84%
Timestep150	15.55%	-26.01%	10.38%	2.91%	-13.33%
Timestep300	33.32%	-48.75%	24.49%	11.19%	-25.38%
	Percentage change in velocity magnitude compared to baseline case				
Timestep10	2.10%	-0.07%	2.40%	3.68%	2.79%
Timestep30	2.04%	0.92%	1.39%	2.18%	2.06%
Timestep150	-7.03%	-1.78%	0.13%	-1.61%	-4.38%
Timestep300	-10.93%	2.64%	0.65%	-0.31%	-7.59%

It can be seen from Figures 5.11c and 5.11d that the small variations in the velocity near the beginning of the timestep are not captured with the larger timesteps. There is little difference when the timestep is reduced to 30 seconds and further to 10 seconds compared to the baseline case although the simulation took significantly longer to run. The free surface elevations are more sensitive to

the increase timestep compared to the velocity. The changes are more noticeable at the crest of the sandbank compared to the troughs and flanks for most cases.

5.4.2 Friction Coefficient

The values chosen for the sensitivity testing of the Chezy coefficient are 50, 55, 65 and 70. Figure 5.12 and Table 5.7 show the sensitivity of the velocity to changes in the value of the friction coefficient.

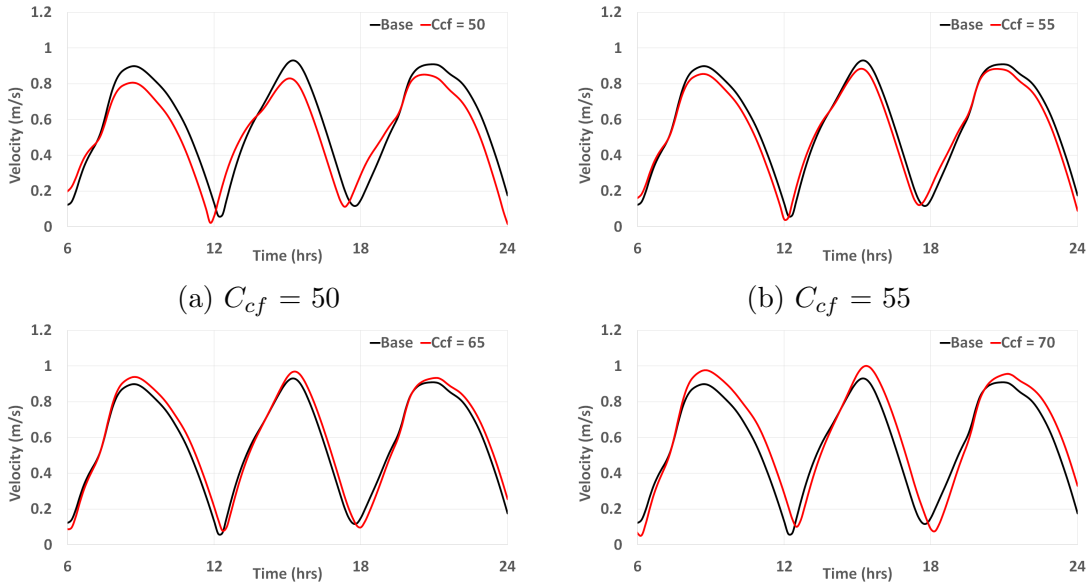

(a) $C_{cf} = 50$ (b) $C_{cf} = 55$

(c) $C_{cf} = 65$ (d) $C_{cf} = 70$

Figure 5.12: Sensitivity of velocity magnitude to friction coefficient at the offshore trough

Table 5.7: Sensitivity of model to friction coefficient

Case	Point 1 (Flank)	Point 2 (Crest)	Point 3 (Flank)	Point 4 (NS Trough)	Point 5 (OS Trough)
	Percentage change in free surface elevation compared to baseline case				
Friction50	14.32%	-21.83%	-2.39%	1.37%	-7.70%
Friction55	7.51%	-11.06%	-1.02%	0.82%	-3.71%
Friction65	-8.02%	11.21%	0.66%	-0.99%	3.50%
Friction70	-16.30%	22.44%	1.05%	-2.09%	6.81%
	Percentage change in velocity magnitude compared to baseline case				
Friction50	-2.37%	-2.21%	-6.75%	-6.68%	-6.19%
Friction55	-1.30%	-2.68%	-4.71%	-3.15%	-3.04%
Friction65	1.62%	5.92%	8.08%	2.93%	3.08%
Friction70	3.57%	13.11%	16.54%	5.73%	6.67%

The crest of the sandbank is much more sensitive to increases in friction coefficient compared to other locations. However, the troughs are more sensitive to decreases in friction coefficient.

5.4.3 Coriolis Parameter

The Coriolis Parameter is assumed to be constant throughout the entire domain. However, in reality the Coriolis parameter is dependent on the latitude so varies spatially. TELEMAC has the option to vary the Coriolis coefficient at each node, calculating the value dependent on the node location. However, this adds another layer of complexity into the model and thus increases the computational resources. Four cases are run: the first neglecting the Coriolis parameter altogether and three with varying values based off different positions throughout the domain. The values of the Coriolis Parameter are tested corresponding to the southernmost latitude (50.8°N, CP $= 1.127 \times 10^{-4}$ rad/s), average latitude (52.4°N, CP $= 1.155 \times 10^{-4}$ rad/s) and northernmost latitude (54.0°N, CP $= 1.177 \times 10^{-4}$ rad/s) of the domain. The sensitivity of the velocity to the Coriolis parameter is displayed in Figure 5.13 and Table 5.8.

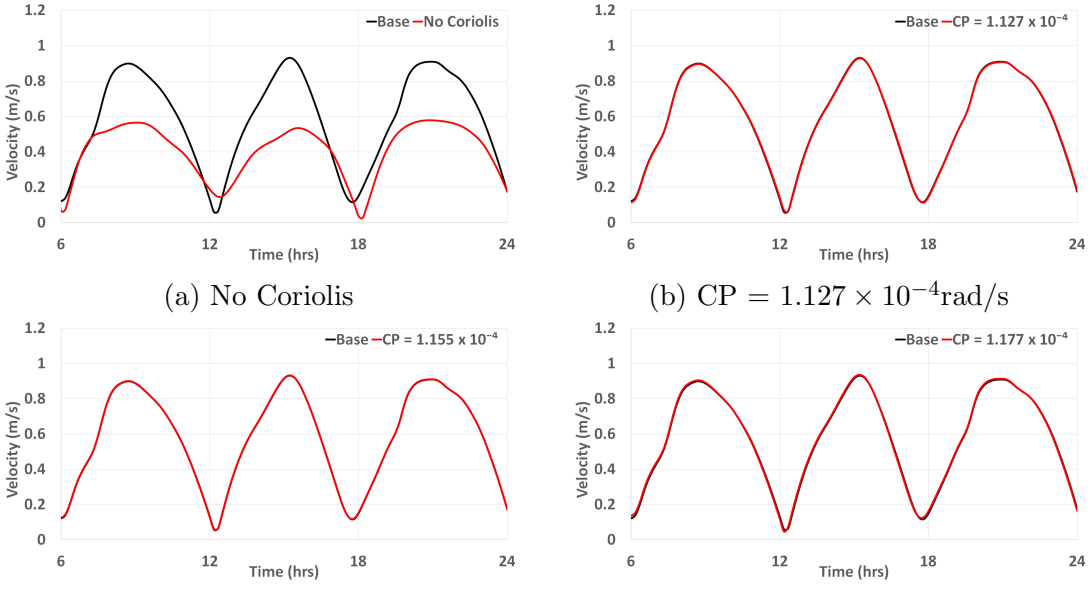

(a) No Coriolis

(b) CP $= 1.127 \times 10^{-4}$rad/s

(c) CP $= 1.155 \times 10^{-4}$rad/s

(d) CP $= 1.177 \times 10^{-4}$rad/s

Figure 5.13: Sensitivity of velocity magnitude to Coriolis parameter at the offshore trough

Table 5.8: Sensitivity of model to Coriolis parameter

Case	Point 1 (Flank)	Point 2 (Crest)	Point 3 (Flank)	Point 4 (NS Trough)	Point 5 (OS Trough)
	Percentage change in free surface elevation compared to baseline case				
Coriolisnone	-271.03%	340.12%	-101.99%	-112.33%	131.49%
Coriolis127	-3.62%	3.72%	-1.12%	-1.35%	1.39%
Coriolis155	1.69%	-1.73%	0.50%	0.63%	-0.64%
Coriolis177	5.75%	-5.85%	1.74%	2.15%	-2.18%
	Percentage change in velocity magnitude compared to baseline case				
Coriolisnone	9.19%	-1.16%	10.36%	14.38%	19.15%
Coriolis127	0.00%	-0.01%	0.63%	0.30%	0.48%
Coriolis155	0.00%	0.02%	-0.30%	-0.14%	-0.22%
Coriolis177	0.01%	0.08%	-1.05%	-0.46%	-0.76%

Changing the numerical value of the Coriolis parameter has very little effect on the values of the free surface elevation and velocity. However, neglecting the Coriolis parameter altogether has a marked effect on the current magnitude and direction (especially on the crest) of the sandbank. This effect is also observed by [Stansby et al., 2006] which suggests the Coriolis parameter is vital to calculating the recirculation of the flow. Differences of 40cm/s are calculated when ignoring

the Coriolis parameter. The changes in free surface elevation are large when compared to the baseline value with all locations show changes of greater than 100%. At the left flank and crest, the model calculates virtually no change for any of the different parameter values. The largest differences in free surface elevation occurred over the crest of the sandbank compared to the other points. Accurate parametrisation of the Coriolis coefficient is not necessarily important. The suggestion of having the Coriolis coefficient varying at each node due to its location appears to be an unnecessary complexity to add into the model. The minor changes in the output variables justify the assumption of a constant Coriolis parameter in the model.

5.4.4 Turbulence Coefficient

The turbulence model used here is a constant eddy viscosity model. The value of the turbulence coefficient controls the size of the eddies that will be dissipated by the model. The value of 1×10^{-6} (the value of the kinematic viscosity of water) represents the case where there is no turbulent diffusion. The results are displayed in Figure 5.14 and Table 5.9.

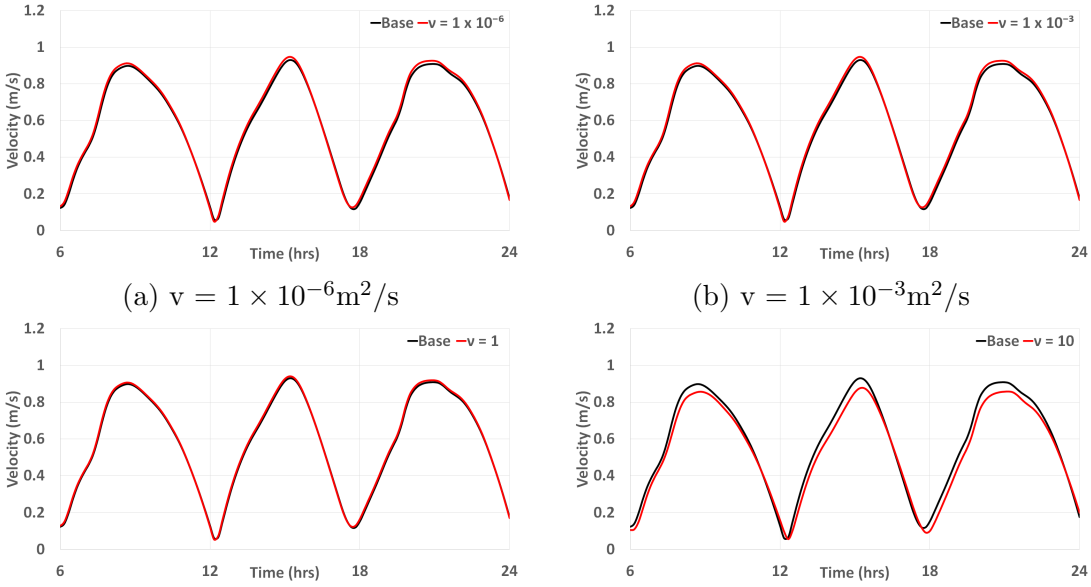

(a) v = $1 \times 10^{-6} \mathrm{m}^2/\mathrm{s}$

(b) v = $1 \times 10^{-3} \mathrm{m}^2/\mathrm{s}$

(c) v = $1 \mathrm{m}^2/\mathrm{s}$

(d) v = $10 \mathrm{m}^2/\mathrm{s}$

Figure 5.14: Sensitivity of velocity magnitude to turbulence coefficient at the offshore trough

Table 5.9: Sensitivity of model to turbulence coefficient

Case	Point 1 (Flank)	Point 2 (Crest)	Point 3 (Flank)	Point 4 (NS Trough)	Point 5 (OS Trough)
	Percentage change in free surface elevation compared to baseline case				
Diffusivity1en6	2.36%	-1.44%	-0.54%	-0.34%	-0.58%
Diffusivity1en3	2.36%	-1.45%	-0.54%	-0.33%	-0.58%
Diffusivity1	1.40%	-0.85%	-0.32%	-0.20%	-0.35%
Diffusivity10	-6.32%	4.49%	1.71%	0.98%	1.73%
	Percentage change in velocity magnitude compared to baseline case				
Diffusivity1en6	2.19%	2.10%	1.31%	3.38%	1.05%
Diffusivity1en3	2.19%	2.10%	1.31%	3.38%	1.05%
Diffusivity1	1.30%	1.10%	0.70%	1.52%	0.62%
Diffusivity10	-5.82%	-2.93%	-2.11%	3.06%	-2.43%

The model seems to be insensitive to the value of the turbulence coefficient. It can be seen that there is no difference in the changes of free surface elevation and velocity between the first two cases where the diffusivity coefficient is small. However, the changes are larger when the value of the coefficient increases. This due to the changes in the recirculation of the flow around sandbanks.

5.5 Discussion

The limitations of the calibration and validation process are discussed as follows:

Firstly, the calibration coefficients are calibrated in series; starting with the CSL and then moving on to the CTR and the CTV once the preceding coefficients are calibrated. This method did not consider how the coefficients might behave in parallel. For example, case S007, where the value of the CSL is 0.07 produced a lower RMSE error value compared to case S011 where the value of the CSL is 0.11 (noting that in both cases the values of the CTR and CTV are both 1). Therefore it is concluded that a CSL value of 0.07 is better. However, a CSL value of 0.11 might produce a lower value of RMSE when different values of the other coefficients are used. Also the model is only calibrated with the three described coefficients. Other coefficients such as friction coefficient or turbulence model coefficients could also be calibrated. However, the effects of these coefficients was considered as part of the sensitivity analysis.

Secondly the observation data itself could affect the calibration results. The observations of the velocity are hindered by the lack of availability of long term velocity time series data. The observation data used is extracted from an Admiralty chart which does not necessarily reflect real time current variations over small time intervals. Some of the calibration stations did not have complete datasets over the time periods concerned. This could cause skew in the calculation of the RMSE values due to the missing data points.

Thirdly the calibration results can be affected by extreme events. For example storm surge events or significantly larger waves could cause sudden increases in the observed free surface elevations which the model would not be anticipating. This would then correlate to a perceived increase in the error values. There are some periods in the observation data where these effects are clearly visible and the negative impact of this on the results is limited by the selection of the initial time of the model.

In terms of the validation process the main limitation is the fact that only the free surface elevation is compared as a model output and not the velocity. This is due to the fact that no validation data is available for the velocity. Another limitation is the small test case sample size. Additional test cases could have

been used to validate the model using data available from other sites. This would add weight to the model's overall versatility as it would demonstrate whether or not the same model could be easily applied to other study areas.

The sensitivity analysis conducted had some limitations. The turbulence and friction coefficient sensitivities only considered the values of the parameter for the already chosen law. It did not consider the sensitivity of the model to different friction laws (e.g. Manning's Law) or turbulence models (e.g. Elder model or the k-ϵ model). The sensitivity analysis has only considered the sensitivity of the free surface elevation and the velocity. Further analysis could include the sensitivity of other model outputs such as bed shear stress. It could also include the sensitivity at more locations rather than just purely focussing on a single sandbank.

Chapter 6

3D Hydrodynamics

6.1 Introduction

This chapter introduces the 3D hydrodynamic model and compares the 2D and 3D model with respect to hydrodynamics. First, the differences between different vertical mesh structures are described and evaluated. Then the differences between the 2D model and the 3D model are discussed in relation to hydrodynamics.

6.2 Vertical Layer Structure

Now that the 2D model has been calibrated and validated, the 2D model can be developed into a 3D model for TELEMAC3D. One important factor to test when developing the 3D model is the number and the arrangement of the vertical layers. Having too few layers in the model could result in less overall accuracy of the flow conditions. Having too many layers would increase the computational effort required and could result in the model becoming unstable, especially in shallower areas, for example at the crests of sandbanks, where the layers would become too compact. This latter point also extends into the structure of the layers; by refining the layers too close together the model can also become unstable. For example, if the water depth is 10m (as is the case near the sandbank crest) then layers that

are spaced at 5% intervals are physically only 50cm apart. However, having the layers spread too far apart means that the model could be unable to capture some of the differences in the vertical flow structure, which is highlighted as important when studying the long term morphodynamic behaviour of sandbanks.

Due to this, three different layer structures are tested to determine whether: firstly the differences in the number of layers or the structure of the layers impacts the overall hydrodynamic conditions and secondly whether there are significant differences in the observed velocity profiles.

6.2.1 Model Configuration

The first case (referred to as HYD1) consists of 5 equally spaced layers. Remembering that the first layer is located at the bed level and the top layer is at the free surface, this equates to layers positioned at intervals of 25% of the water depth. The second case (referred to as HYD2) consists of 11 equally spaced layers, i.e. at intervals of 10% of the water depth. The final case (referred to as HYD3) used the option to manually specify the location of the layers. It is decided to have 10 layers which are more closely refined nearer the bed. Villaret et al. [2013] suggests that unevenly spaced layers with refinement near the bed enables a more accurate representation of the flow field. It also allows better representation of the turbulence models which in turn leads to a more precise prediction of the bed shear stress. The proportions of the water depth followed a logarithmic profile shown in equation 6.1. Table 6.1 and Figure 6.1 present a visualisation of the layer structure of each of the models.

$$\frac{h_l}{h} = 1 - \log(11 - l) \tag{6.1}$$

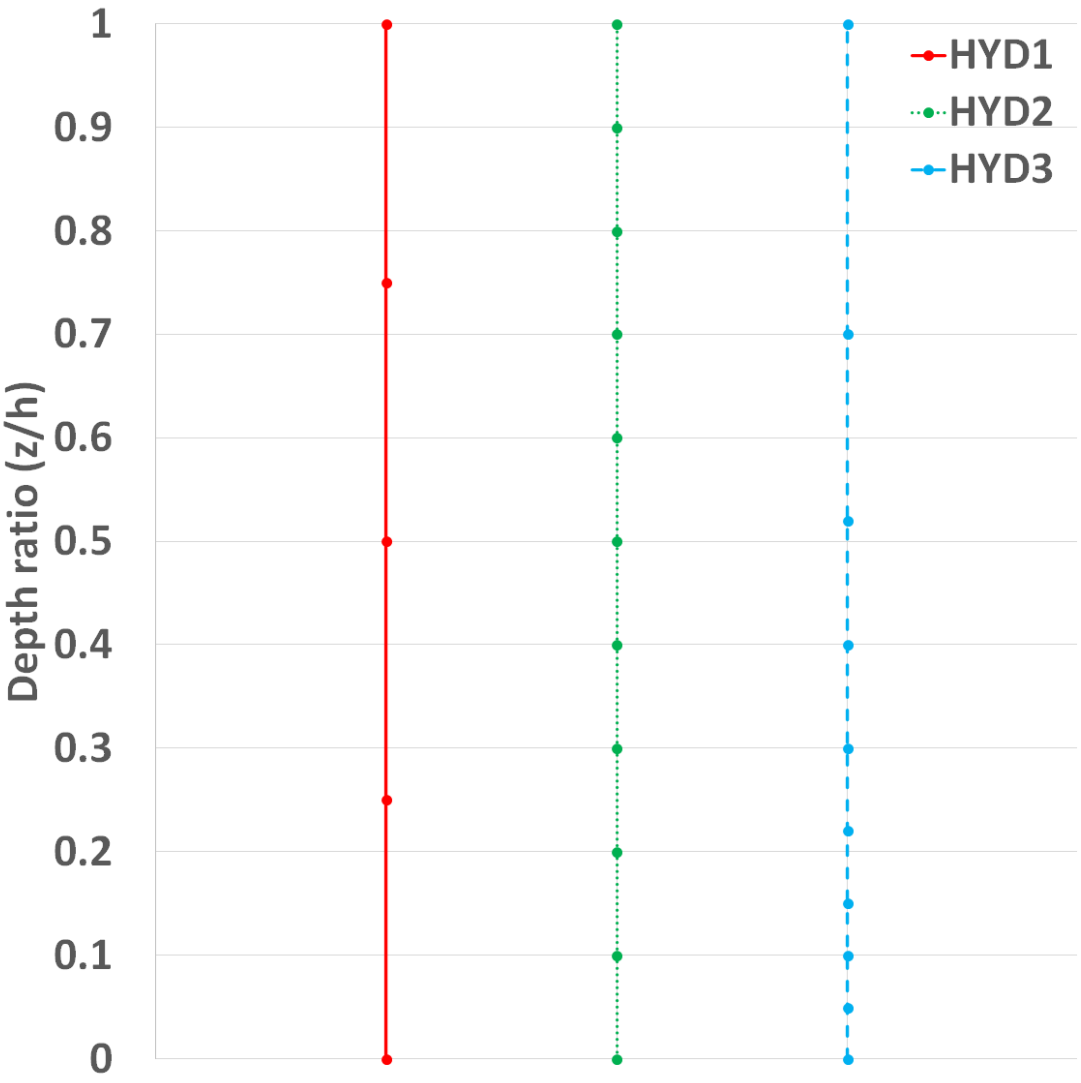

Figure 6.1: Layer structure for each model

Table 6.1: Depth ratio (z/h) at each layer for the layer structure models

	Layer										
Model	1	2	3	4	5	6	7	8	9	10	11
HYD1	0	0.25	0.5	0.75	1						
HYD2	0	0.10	0.20	0.30	0.40	0.50	0.60	0.70	0.80	0.90	1
HYD3	0	0.05	0.10	0.15	0.22	0.30	0.40	0.52	0.70	1	

6.2.2 Results

In order to investigate the best configuration of the vertical layers used in the modelling system, the velocity profiles and vectors at specific points and times are analysed. In addition, time series of the depth averaged velocity, surface velocity and near bed velocity are also analysed. The near bed velocity is defined here as the velocity at a depth ratio of 0.1 from the bed. This corresponds to the second and third layers in the HYD2 and HYD3 models respectively. Since HYD1 does not have a layer located at this depth ratio, the velocity is calculated by linearly interpolating between the depth ratios 0.0 and 0.25 as indicated in Figure 6.1. This in itself may not be an accurate representation of the velocity at that depth, since it can be seen by the vertical profiles from all the models that the velocity does not vary linearly between adjacent layers. However, it provides an indication of what the velocity at that depth could be for a comparison between the three models.

6.2.2.1 Vertical Velocity Profiles at the Sandbank Crest

Figure 6.2 shows the velocity magnitude profiles at the sandbank crest during flood and ebb tides. It can be seen that the shape of the profiles for all three models show similar patterns. However, the peak flood flow values are signif-

icantly smaller for the HYD1 model when compared to the HYD2 and HYD3 models. During the minimum flood flow there is a significant difference in the vertical profile in the mid-depth (between 0.1 and 0.9 of the water depth) between the HYD2 and HYD3 profiles. Similar patterns over other tidal cycles are observed. This suggests that at the crest location, the peak flows are more accurately modelled by the more refined layer structures. Here, the shallower depths mean that the layers are spaced closer together. Therefore, having more layers or closer spaced layers does not necessarily have an impact on the velocity profiles. The ebb flow seems to indicate the opposite effect. The minimum ebb flow shows consistent profiles for all three models. At the maximum ebb flow, the near bed profiles are consistent (below a depth ratio of 0.1 from the bed) but the surface profiles (above a depth ratio of 0.5 from the bed) show consistency between the HYD2 and HYD3 models but a much lower velocity for the HYD1 model.

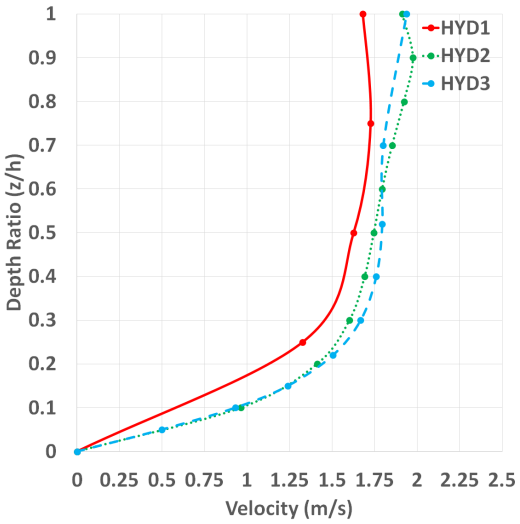

(a) Peak Flood Flow

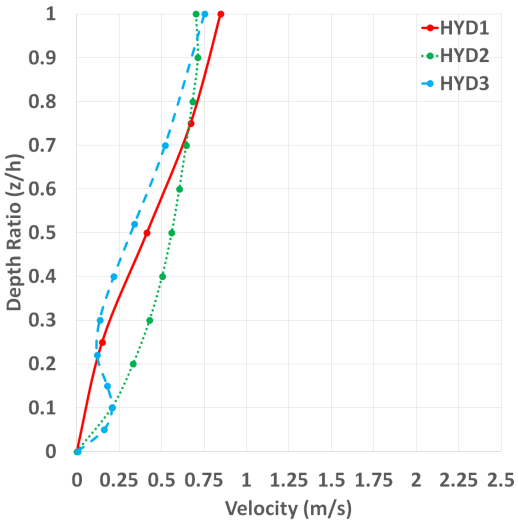

(b) Minimum Flood Flow

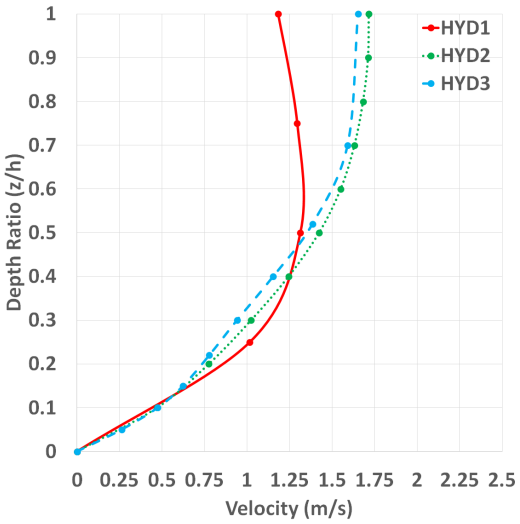

(c) Peak Ebb Flow

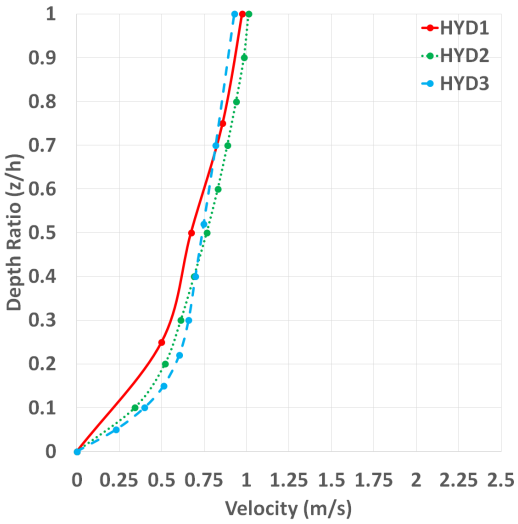

(d) Minimum Ebb Flow

Figure 6.2: Comparison of velocity magnitude profiles for different layer structures at the sandbank crest at different tidal stages

Figure 6.3 shows the depth averaged velocity vectors for the corresponding profiles shown in Figure 6.2. Interestingly here it can be seen that at the peak flood and ebb tides, the vectors are all relatively similar for each model. The differences in the vectors are a result of the difference in the magnitude of the velocity itself (represented by the size of the arrows). The differences become

more pronounced at the minimum flood and ebb flows. Here it can be seen that although the magnitudes and profiles are similar, the direction of the vector is different in the HYD3 model. It suggests that the tidal phases are all slightly out of sync with each other. The tide in HYD3 is rotating quicker compared to the other 2 models.

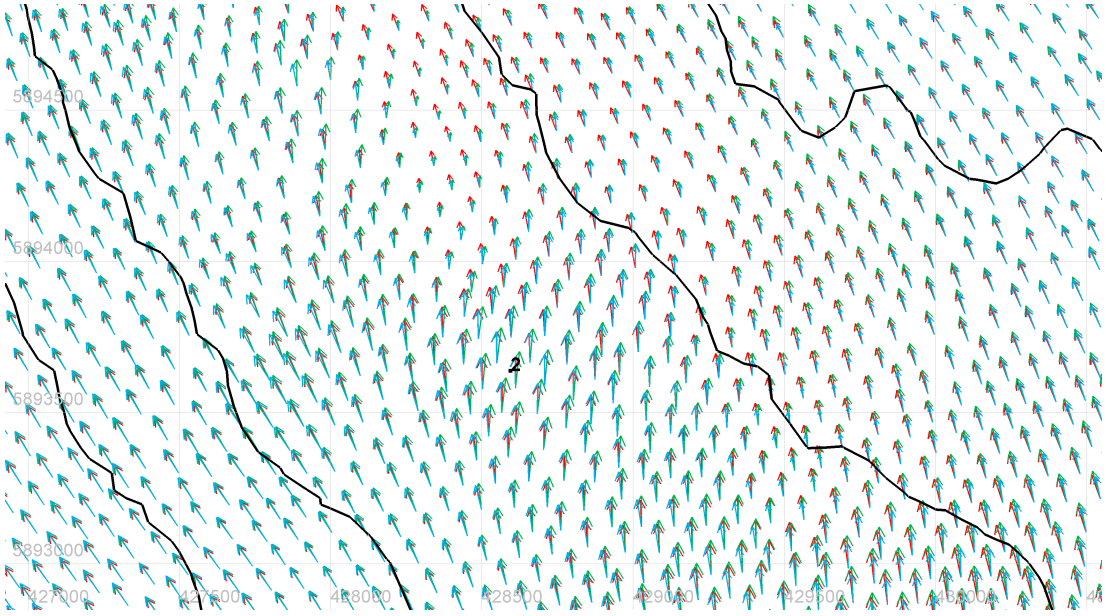

(a) Peak Flood Flow

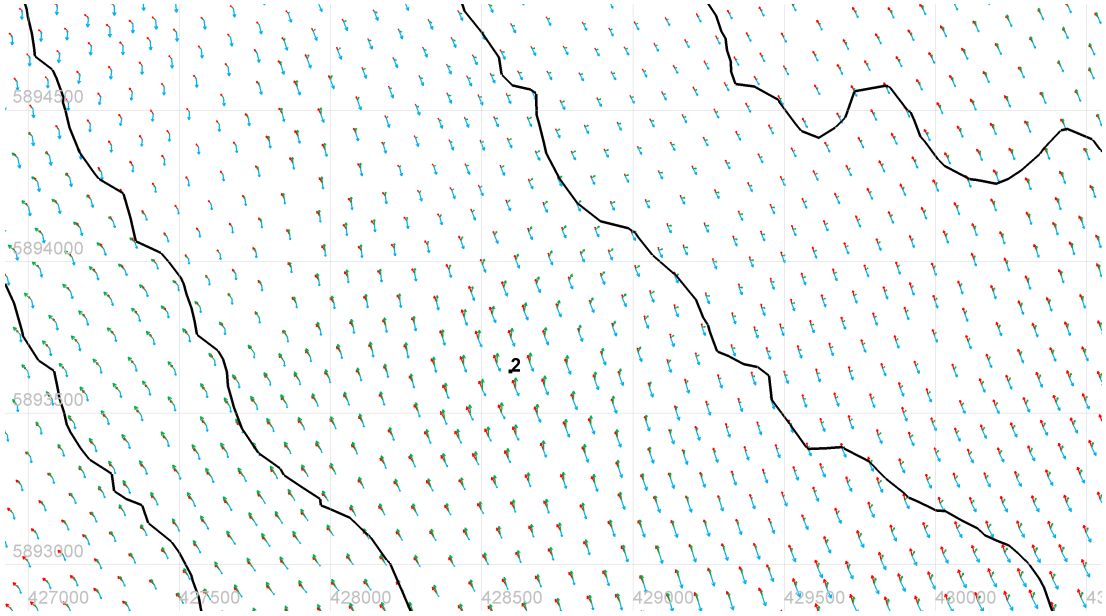

(b) Minimum Flood Flow

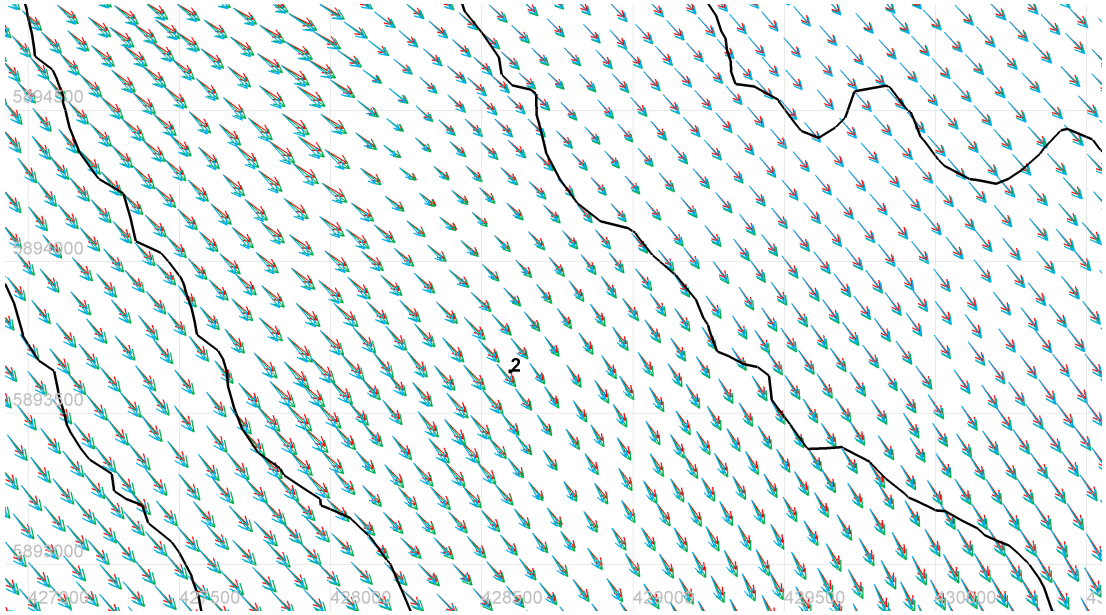

(c) Peak Ebb Flow

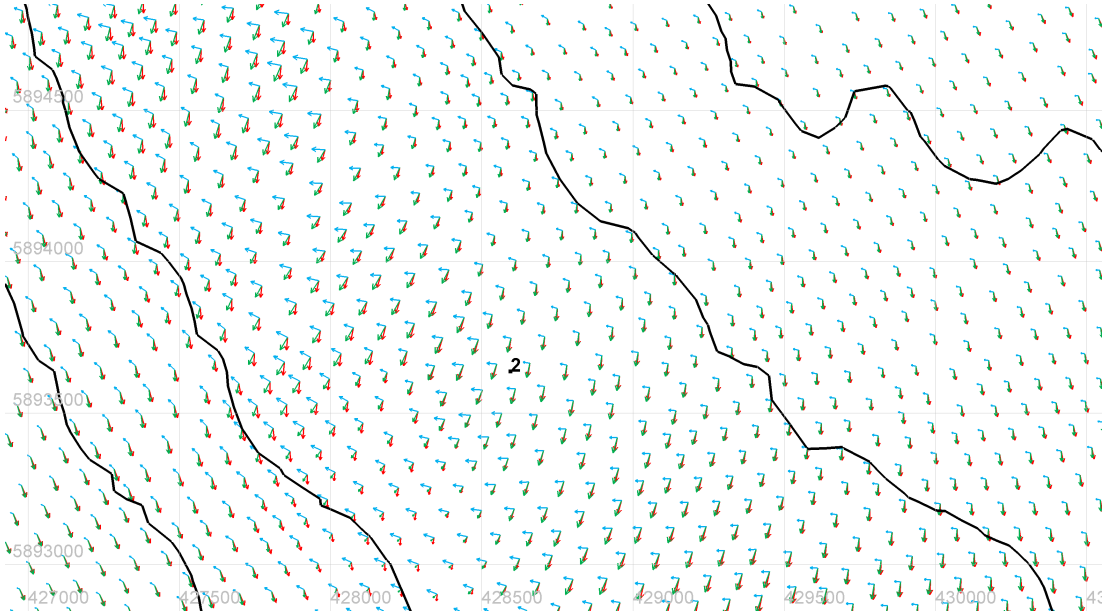

(d) Minimum Ebb Flow

Figure 6.3: Comparison of velocity vectors for different layer structures at the sandbank crest at different tidal stages

Figure 6.4 shows the time series variations in the depth averaged, near bed and surface velocities over two tidal cycles. It can be seen from this figure that

again the HYD2 and HYD3 models output similar results especially in the times around the peak flows. For this location the results of the HYD1 model are different from the other two configurations.

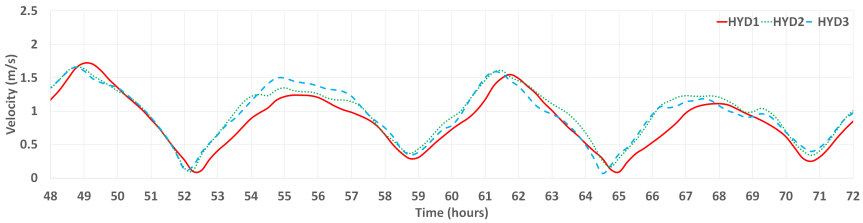

(a) Depth Averaged Velocity

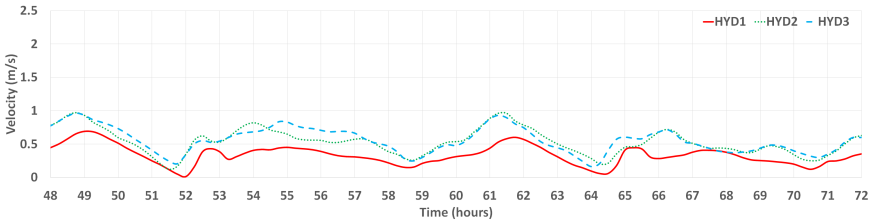

(b) Near bed Velocity

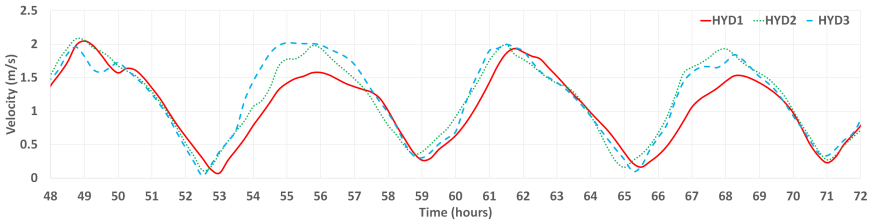

(c) Surface Velocity

Figure 6.4: Comparison of velocity time series for different of layer structure at the sandbank crest

6.2.2.2 Vertical Velocity Profiles at the Sandbank Flanks

Figure 6.5 shows the velocity magnitude profiles at the sandbank flank. Here it can be seen that for the flood tide, all three models have fairly similar profiles in the top 70% of the water depth. However, the HYD1 model does not accurately predict the variations in the flow for the bottom 30% when compared to the other two models. At peak ebb flow, the profiles are all similar until the top 30% of the water depth. At minimum ebb flow, the HYD1 and HYD2 models are both similar but the HYD3 model profiles is markedly different.

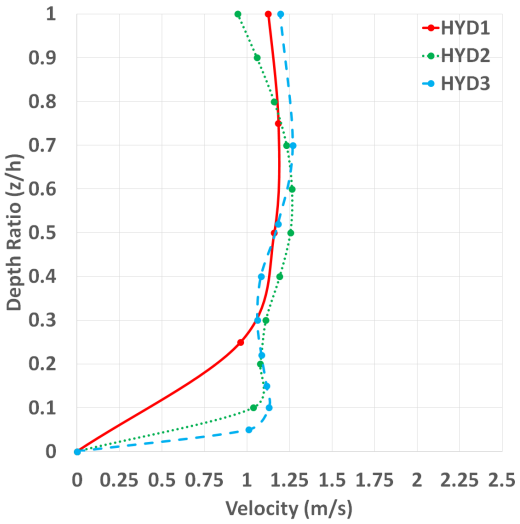

(a) Peak Flood Flow

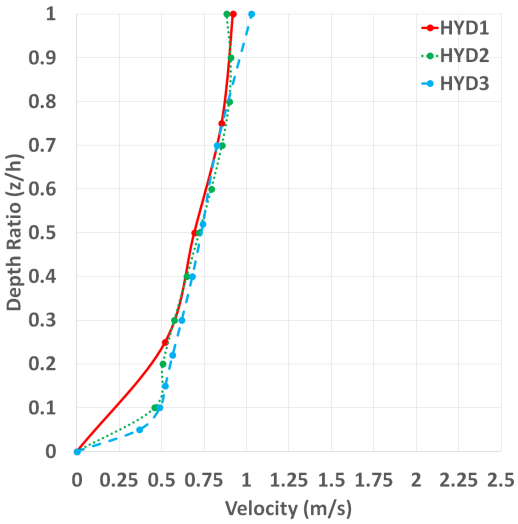

(b) Minimum Flood Flow

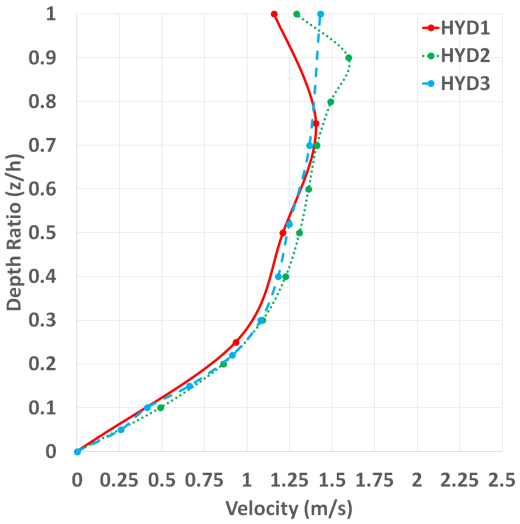

(c) Peak Ebb Flow

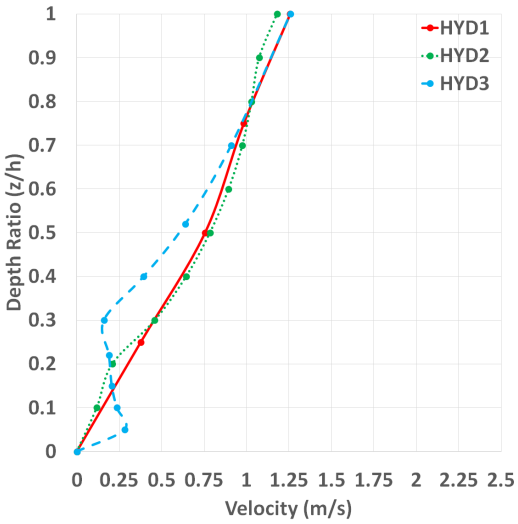

(d) Minimum Ebb Flow

Figure 6.5: Comparison of velocity magnitude profiles for different layer structures at the sandbank flank at different tidal stages

Figure 6.6 shows the velocity vectors at the corresponding timesteps. Again it can be seen that at the peak flows, the vectors are all similar. At the minimum flows although the vectors are all roughly in the same direction, the magnitude of the HYD3 model vectors is much smaller than the other two.

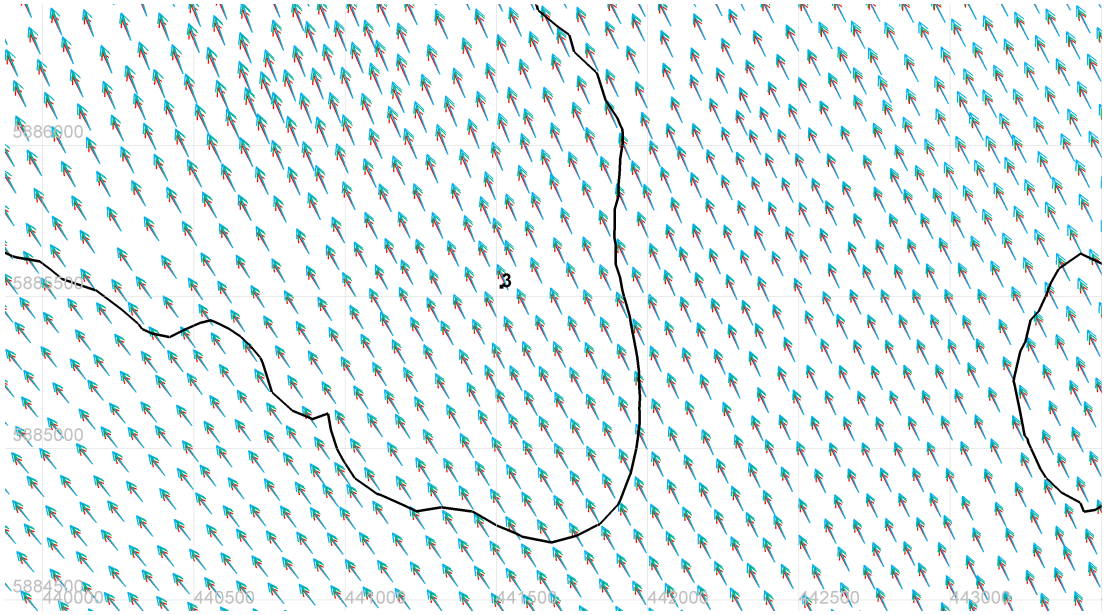

(a) Peak Flood Flow

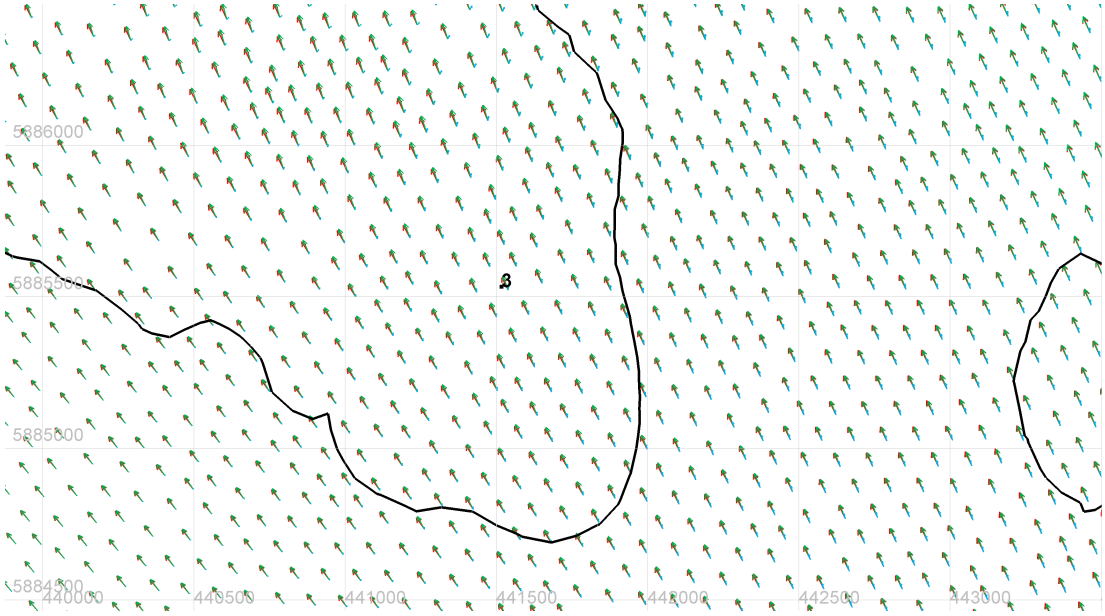

(b) Minimum Flood Flow

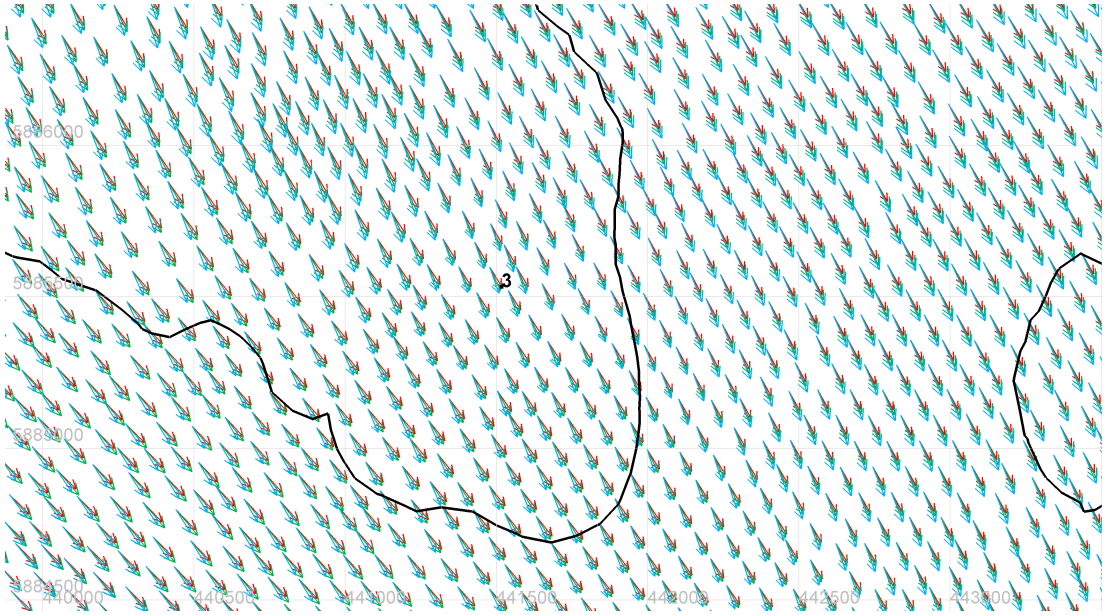

(c) Peak Ebb Flow

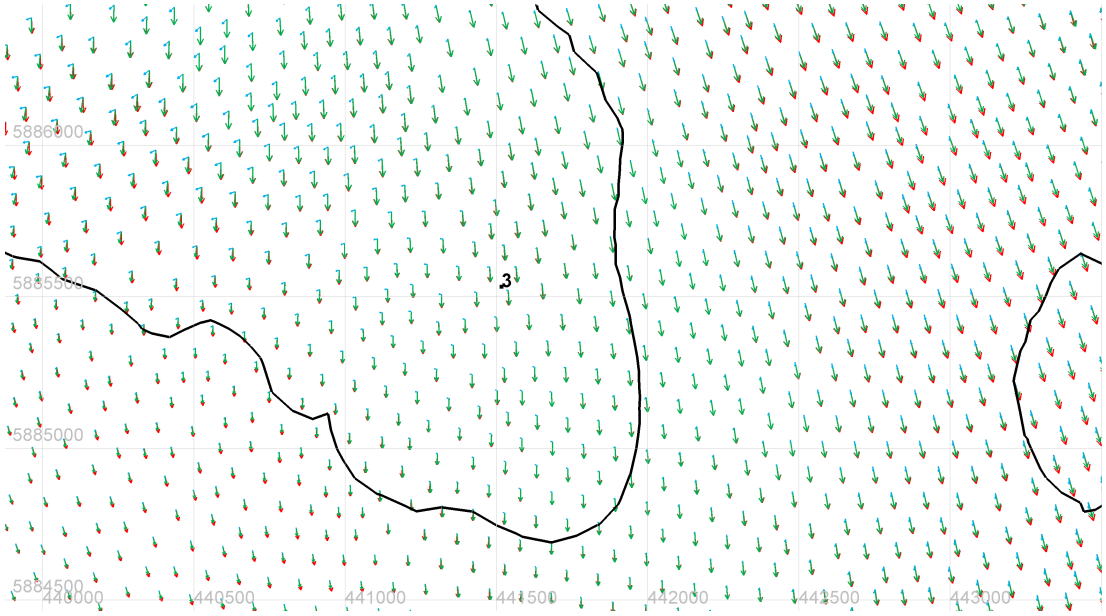

(d) Minimum Ebb Flow

Figure 6.6: Comparison of velocity vectors for different layer structures at the sandbank flank at different tidal stages

Figure 6.7 shows the time series of the depth averaged, near bed and surface velocities. Similar to the crest location, the HYD2 and HYD3 models show similar

results. There are noticeablely larger velocities at the peak flows when compared to the HYD1 model especially nearer the bed.

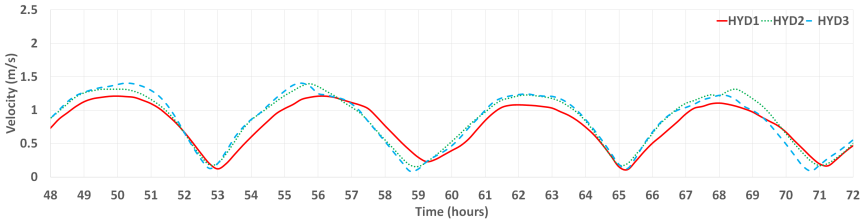

(a) Depth Averaged Velocity

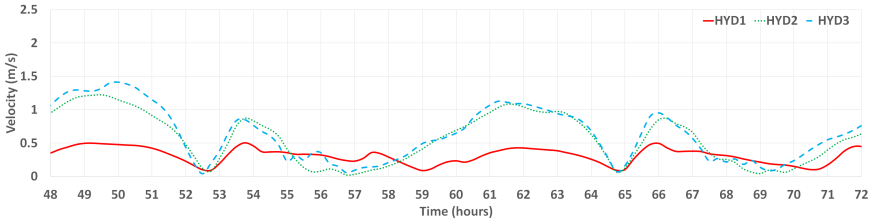

(b) Near bed Velocity

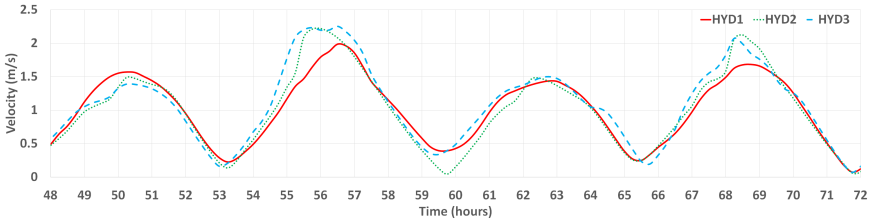

(c) Surface Velocity

Figure 6.7: Comparison of velocity time series for different layer structure at the sandbank flank

6.2.2.3 Vertical Velocity Profiles in the Sandbank Troughs

Figure 6.8 shows the velocity magnitude profiles at the same timesteps used previously at the nearshore trough. At peak flood flow, the HYD1 model shows an almost constant velocity for the top 70% of the water depth. The HYD3 model shows a completely different profile. The HYD2 model shows a mix of both, replicating the HYD3 profile near the bed and surface but replicating the HYD1 model at the mid-depth section. At minimum flood the profiles are all similar with the main differences being in the magnitude of the velocity for each model. At peak ebb flow all three models show a similar profile above 30% of

the depth but again the HYD1 model is not showing the same profile nearer the bed. At minimum ebb flow, the profiles are similar for the HYD1 and HYD3 models. The HYD2 model has similar patterns near the bed and at the surface but a noticeably different profile at mid-depth.

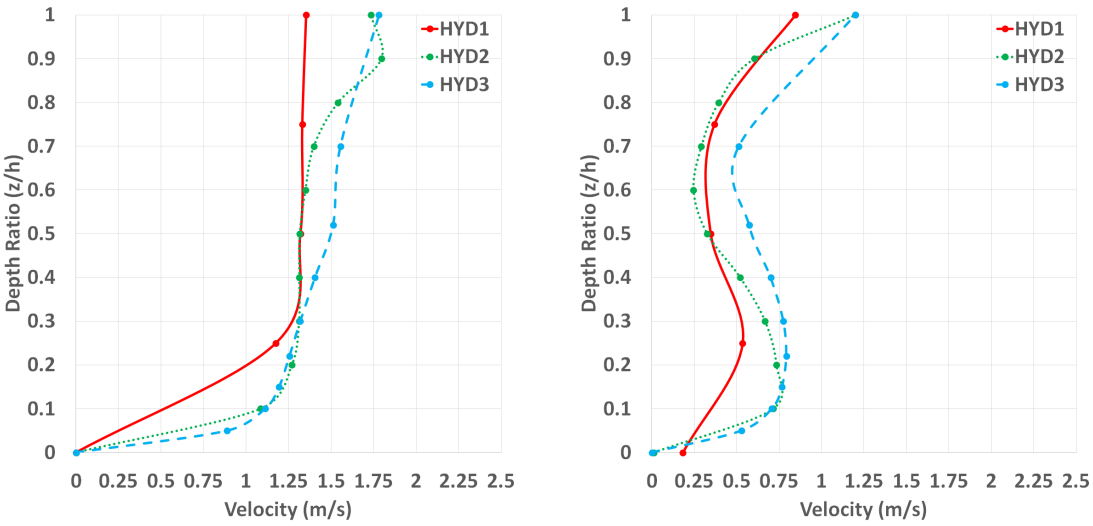

(a) Peak Flood Flow

(b) Minimum Flood Flow

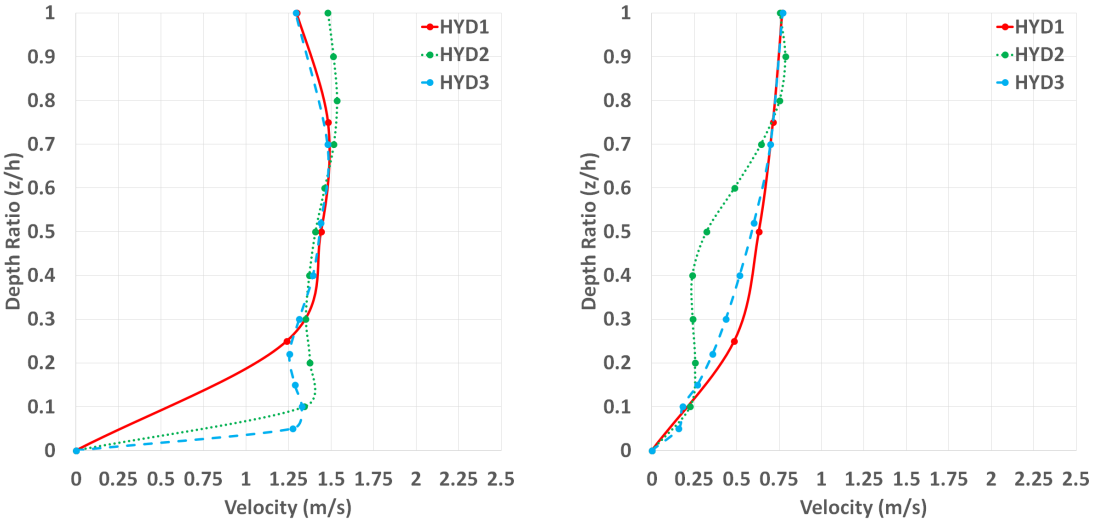

(c) Peak Ebb Flow

(d) Minimum Ebb Flow

Figure 6.8: Comparison of velocity magnitude profiles for different layer structures at the nearshore trough at different tidal stages

Figure 6.9 shows the velocity vectors at the corresponding timesteps. Similar to the other locations, the different models are all in agreement at the peak flows. At the minimum flows, the HYD3 model vectors are all in the opposite direction suggesting that tide is out of phase when compared to the other two models.

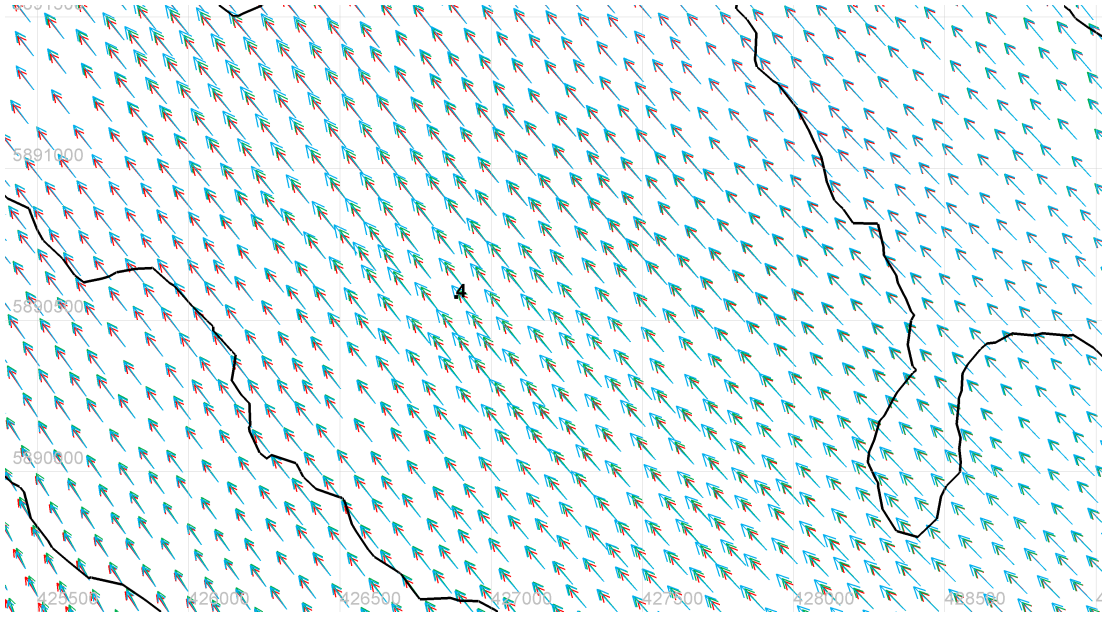

(a) Peak Flood Flow

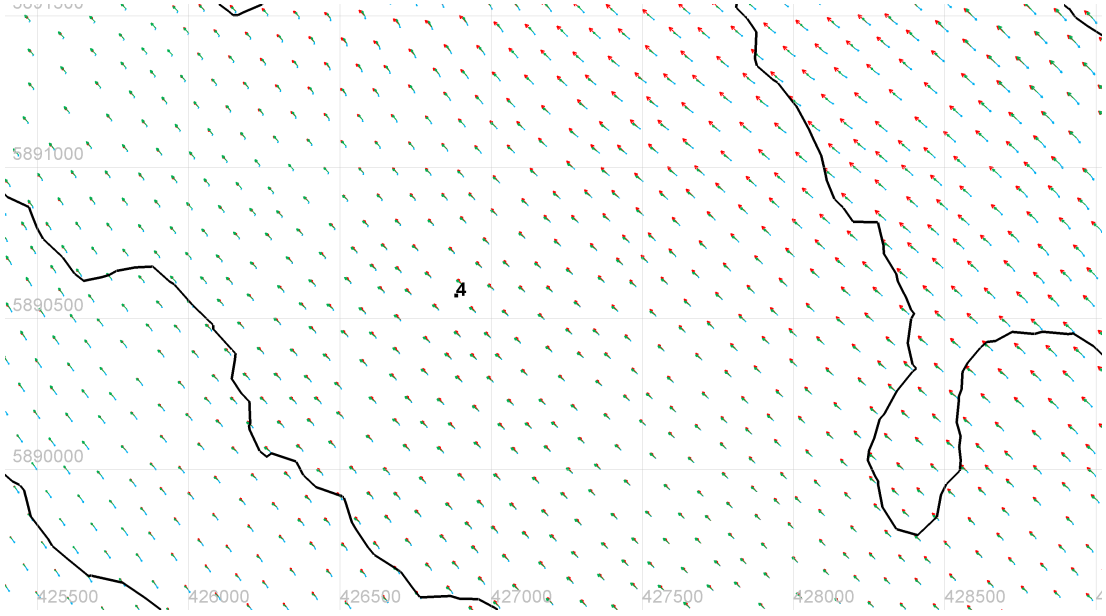

(b) Minimum Flood Flow

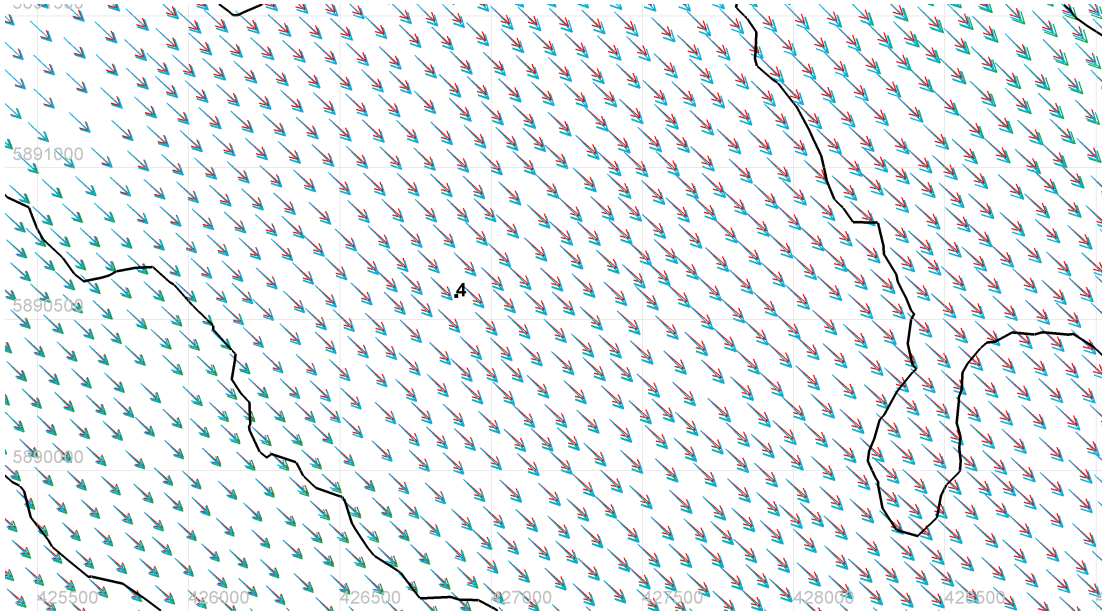

(c) Peak Ebb Flow

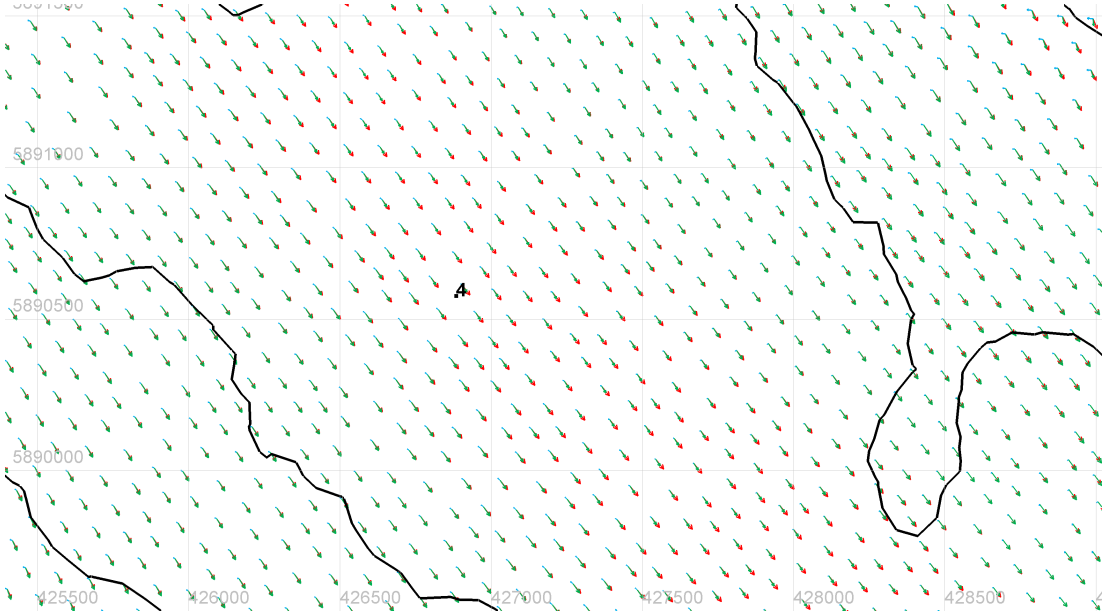

(d) Minimum Ebb Flow

Figure 6.9: Comparison of velocity vectors for different layer structures at the nearshore trough at different tidal stages

Figure 6.10 shows the time series of the depth averaged, near bed and surface velocities at the nearshore trough. Similar to the crest and the flanks, the HYD2

and HYD3 models are in good agreement but the HYD1 model shows smaller velocities especially at peak flows.

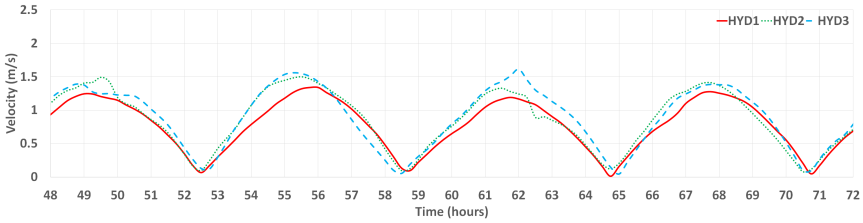

(a) Depth Averaged Velocity

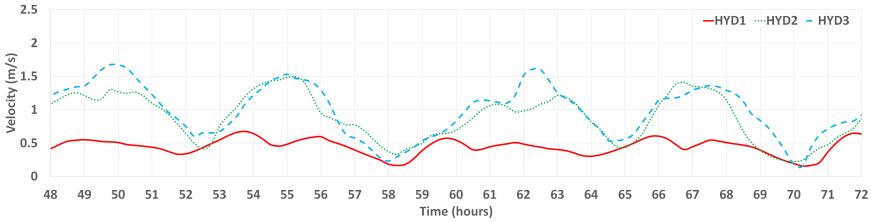

(b) Near bed Velocity

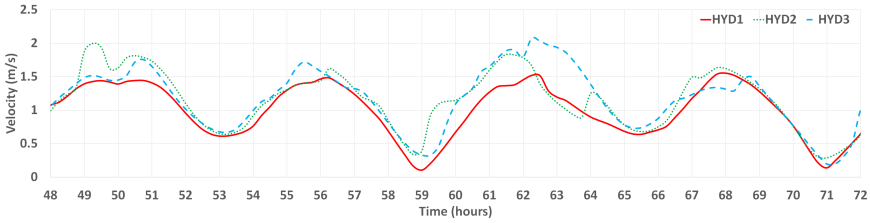

(c) Surface Velocity

Figure 6.10: Comparison of velocity time series for different layer structure at the nearshore trough

6.2.2.4 Effect of the Vertical Layer Structure

In most instances, the profiles and time series for the HYD2 and HYD3 models are in good agreement. They both showed some significant differences compared to the HYD1 model. The HYD1 model does not capture the velocity profile nearer the bed (below 25% of the water depth) as accurately as the HYD2 and HYD3 models. This is especially the case in areas of deeper water. The most likely cause is that the actual distance between adjacent layers is too large in the HYD1 model. The additional refinement nearer the bed provided by the HYD2 and HYD3 models allows the variations in velocity to be captured. This is

especially the case during periods of peak flow. The surface velocities are similar for the HYD2 and HYD3 models. However, there is often a significant difference between the surface velocity in the HYD1 model compared to the other two. The highlighted differences between the HYD2 and HYD3 model tended to occur in the mid-depth section of the profile (between approximately 30% and 70% of the water depth).

When looking at the depth averaged velocity, all the models are in fairly good agreement. Noted differences are larger at times of peak velocity but results are similar at times of low velocity. The models all showed similar vectors, but appeared to be slightly out of phase with each other at time of slack tide. This is more noticeable near the areas of shallower water and could indicate that the sandbanks interacting with the near bed currents is causing this behaviour.

In terms of computational time and efficiency, the HYD1 model performed significantly better than the HYD2 and HYD3 models. It would take around 24 hours to simulate the 5 day period for HYD1 but approximately 72 hours to simulate the same 5 day period for HYD2 and HYD3. These simulations were run on a standard computer using 6 processor cores rather than on high performance computing. For the final 3D model, the configuration of the HYD3 model was chosen. The HYD1 does not reflect the near bed flow field as accurately as the HYD2 and HYD3 models despite being more computationally efficient. The similarity between the results shows that both the HYD2 and HYD3 models are more accurately representing the hydrodynamic conditions at least in terms of the near bed and depth averaged velocities. Since sediment transport occurs in the near bed layers, accurately representing the hydrodynamic conditions near the bed is more important when it comes to modelling the morphodynamic behaviour of sandbanks. The HYD3 model is selected over the HYD2 model purely down to the greater refinement near the bed. Maintaining the level of refinement near the bed that is offered by the HYD3 model but using the equally spaced layers configuration offered by the HYD2 model is simply not feasible. The configuration would be looking at around twenty or more layers which, given the scale of the model domain, is too computationally intensive. More layers could further increase the accuracy of the flow field but given the similarity between the results of the two models, this does not seem an efficient trade off. However,

validation of the velocity results could further justify which layer structure is the most accurate.

6.3 Comparison with 2D Model

6.3.1 Model Configuration

In the previous sections the preliminary hydrodynamic models have been described and tested in both 2D and 3D. The finalised models that will be used for the main results and discussion are configured as follows: the 2D model is configured the same as the model used in case V085 (see chapter 5) and the 3D model is configured the same as the model used in case HYD3 (see previous section). The models are run using the same hot-starting procedure previously described, for a duration of 30 days. In order to analyse the results a line is drawn transecting the Norfolk Offshore Banks. The total line length is 25km and the line is divided into 51 analysis points each at a distance of 0.5km along the line. The position and bed profile of the line is shown in Figure 6.11.

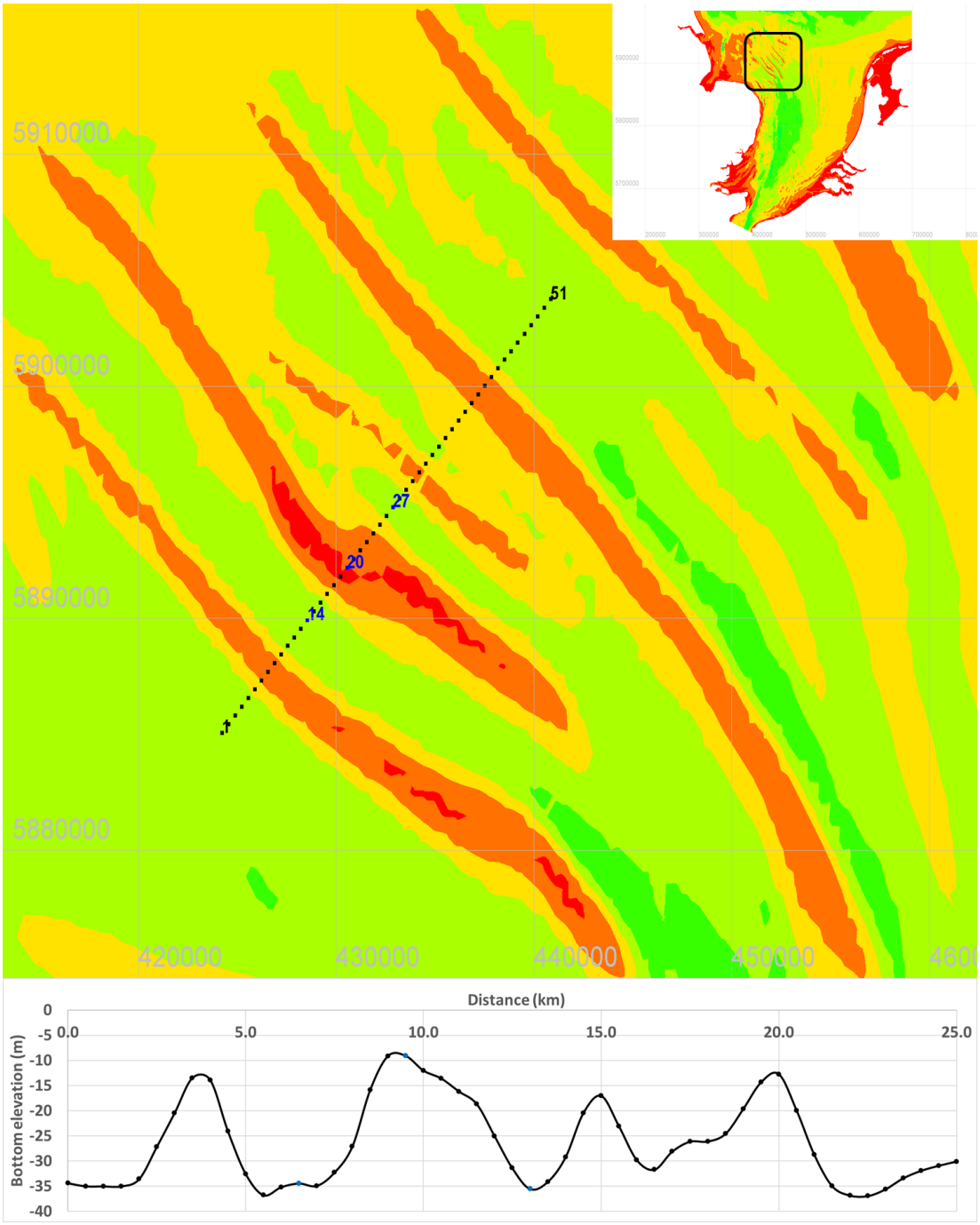

Figure 6.11: The location of a selected transect (top) and its bathymetry (bottom)

In the following sections the results will be presented and discussed. For the

sake of brevity, continuity and ease of comparison, the main discussion in this chapter will focus on three select points: Point 14, Point 20 and Point 27. These points represent the nearshore trough, crest and offshore trough of a sandbank respectively. From a terminological point of view, the nearshore trough refers to the sandbank trough that faces towards the shore and the offshore trough refers to the trough that faces away from the shore.

6.3.2 Results

6.3.2.1 Velocity at the Nearshore Trough

Figures 6.12 and 6.13 show the velocity magnitude profiles at the nearshore trough for neap and spring tides. The neap and spring profiles are consistent with others in terms of shape with the exception of the peak ebb flow. This profile shows a decrease in velocity between the near bed and the middle portion of the water column followed by an increase as it approaches the surface. The equivalent spring tide profile does not show this decrease. During the flood tides, the maximum velocity in the profile is at the surface, except during the peak flood neap flow. During the ebb flow however, the maximum velocity occurs within the middle portion of the water column, usually at somewhere between 50% and 70% of the water depth.

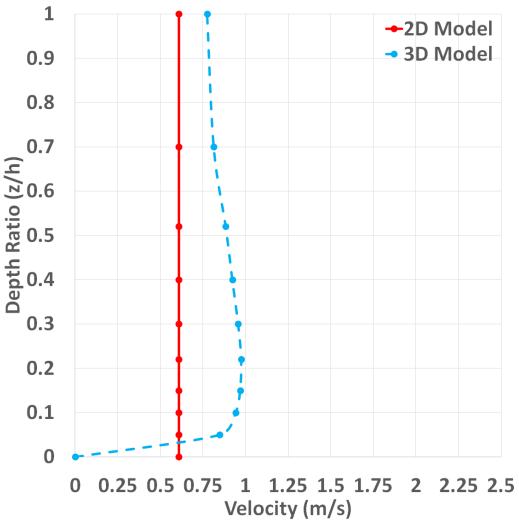

(a) Peak Flood Flow

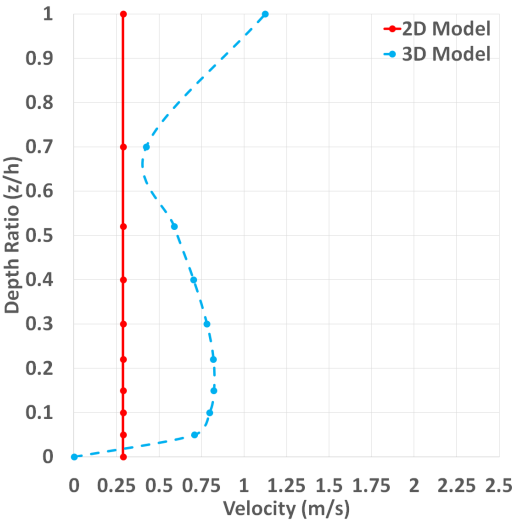

(b) Minimum Flood Flow

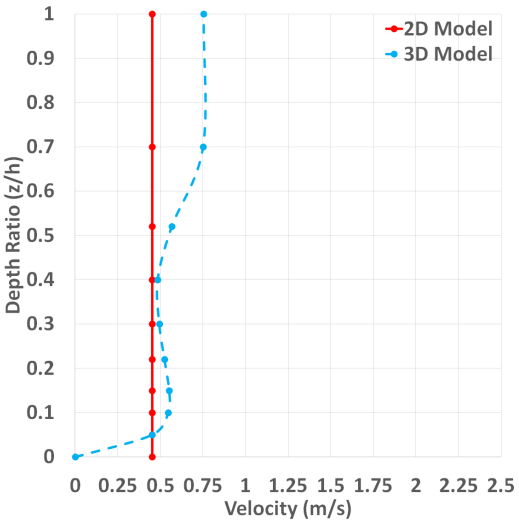

(c) Peak Ebb Flow

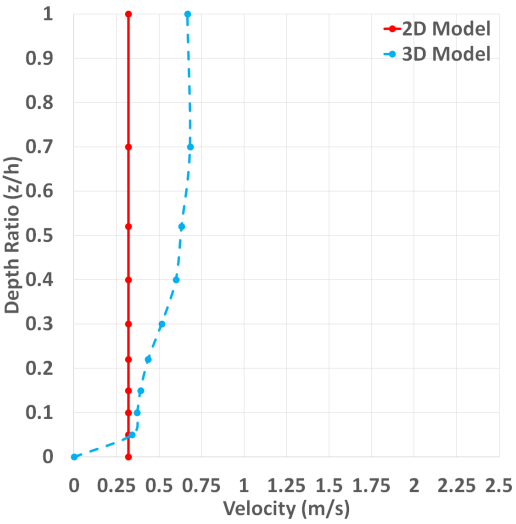

(d) Minimum Ebb Flow

Figure 6.12: 2D and 3D velocity magnitude profiles during neap tides at the nearshore trough

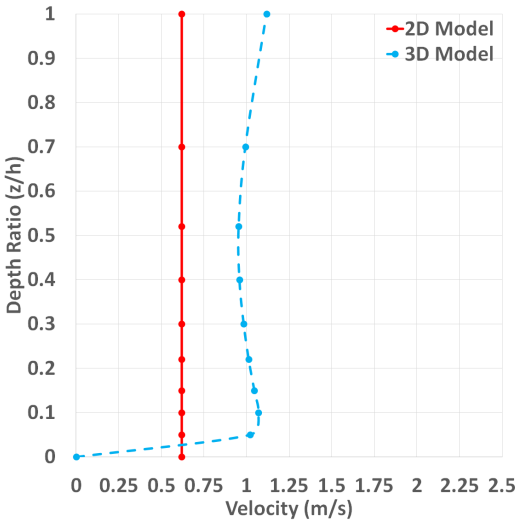

(a) Peak Flood Flow

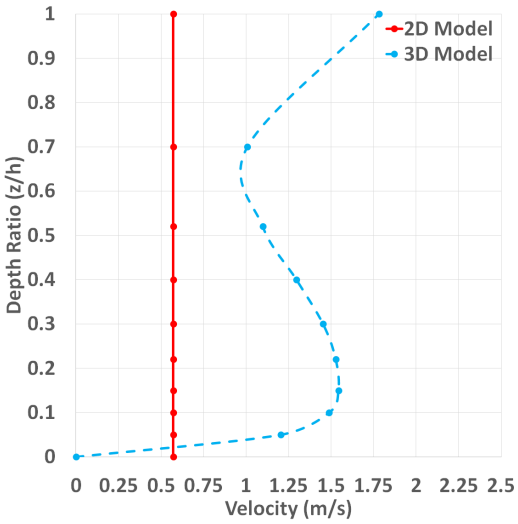

(b) Minimum Flood Flow

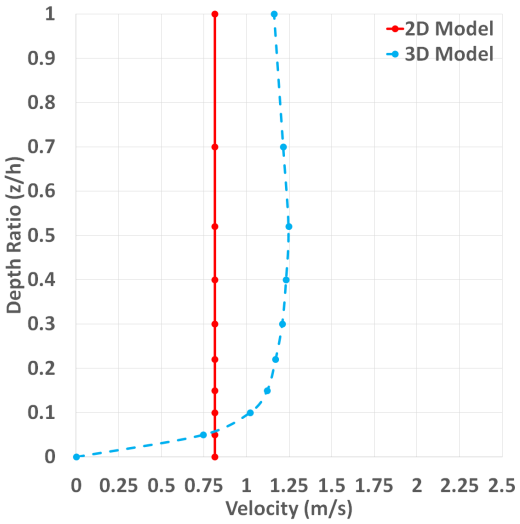

(c) Peak Ebb Flow

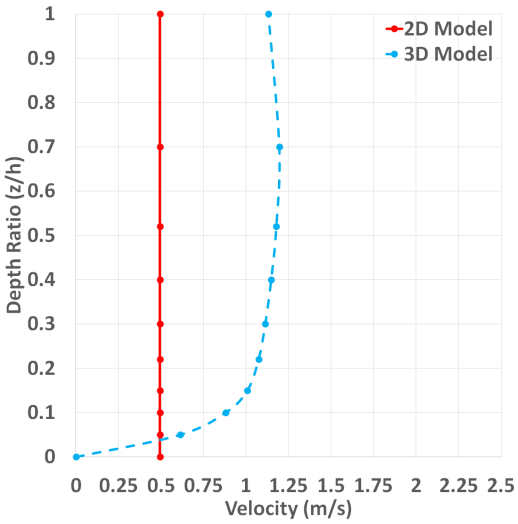

(d) Minimum Ebb Flow

Figure 6.13: 2D and 3D velocity magnitude profiles during spring tides at the nearshore trough

Figure 6.14 shows the peak flow depth averaged, near bed and surface velocity vectors during spring tides (the same timesteps as Figures 6.13c and 6.13a). It can be seen that although the vectors of the depth averaged velocity are different in terms of magnitude they are similar in terms of direction. The 3D near bed velocity vectors differ in both magnitude and direction for the peak ebb flow

compared to the 2D vectors. The implication of this is that, since sediment transport is influenced more by the near bed velocity, the direction of the sediment transport vectors may differ between the 2D and the 3D model. However, for the peak flood flow the direction is more aligned with the 2D model although there is still a noticeable difference in the magnitude of the velocity. The surface velocity vectors show a large difference in the direction of the vector between the 2D and the 3D models. The 3D surface velocities are also much larger in magnitude when compared to the 2D model.

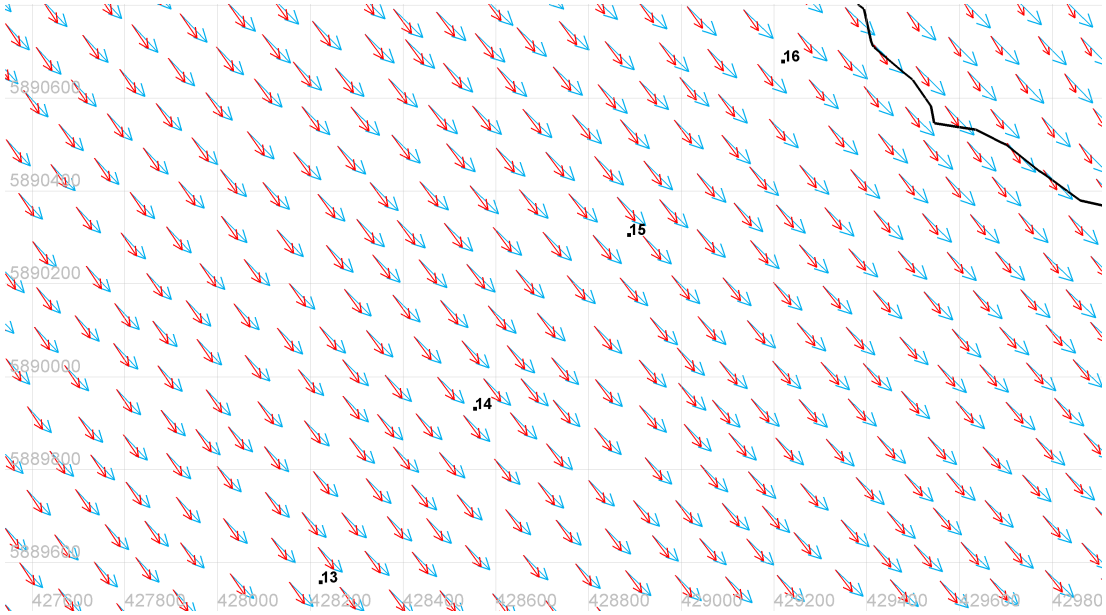

(a) Peak Ebb Flow

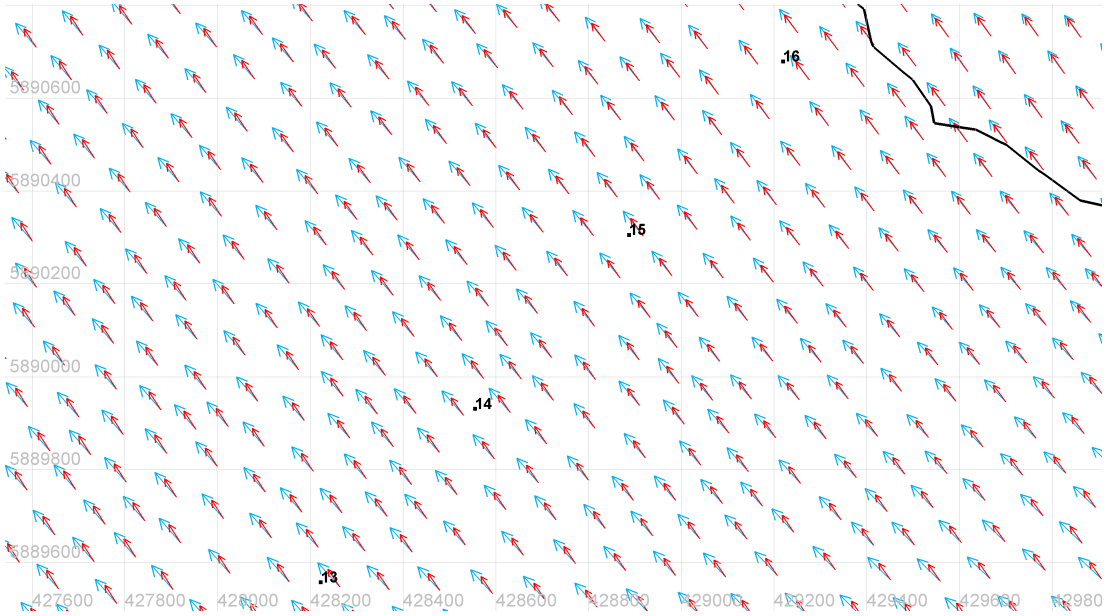

(b) Peak Flood Flow

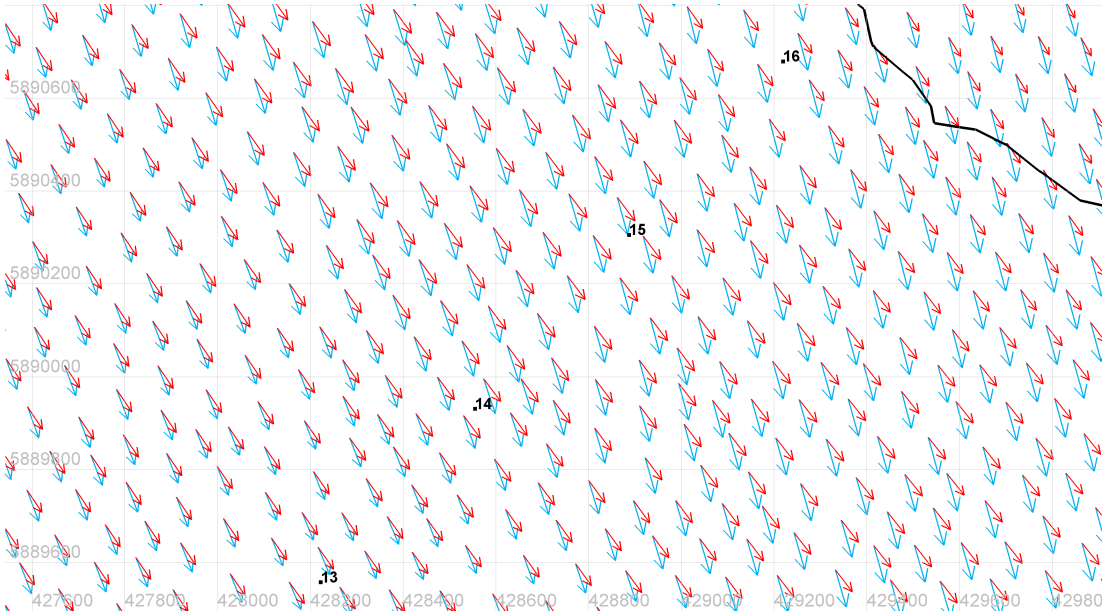

(c) Peak Ebb Flow

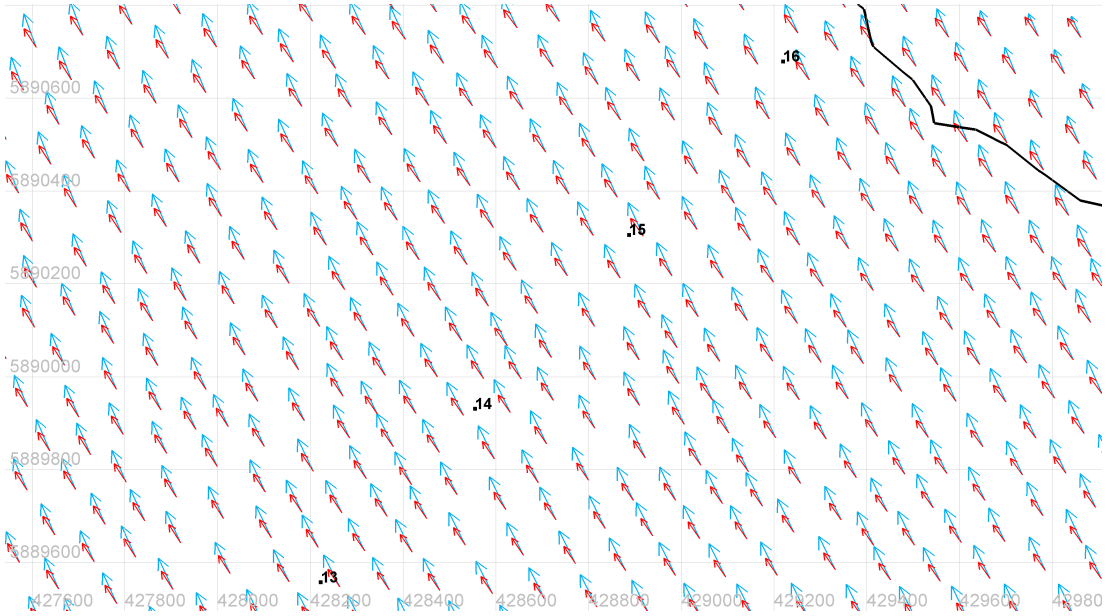

(d) Peak Flood Flow

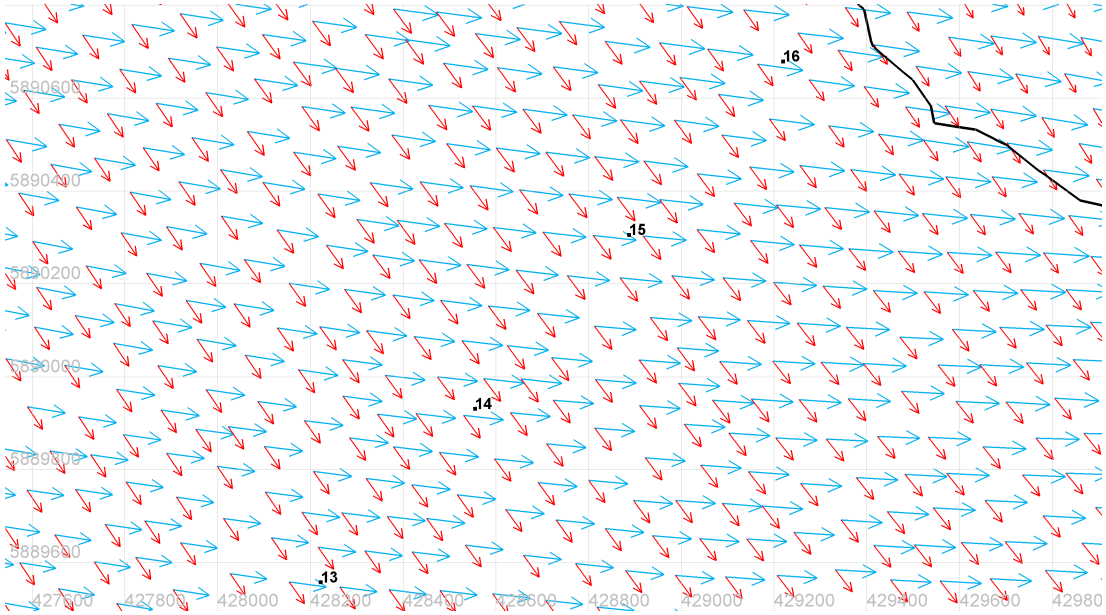

(e) Peak Ebb Flow

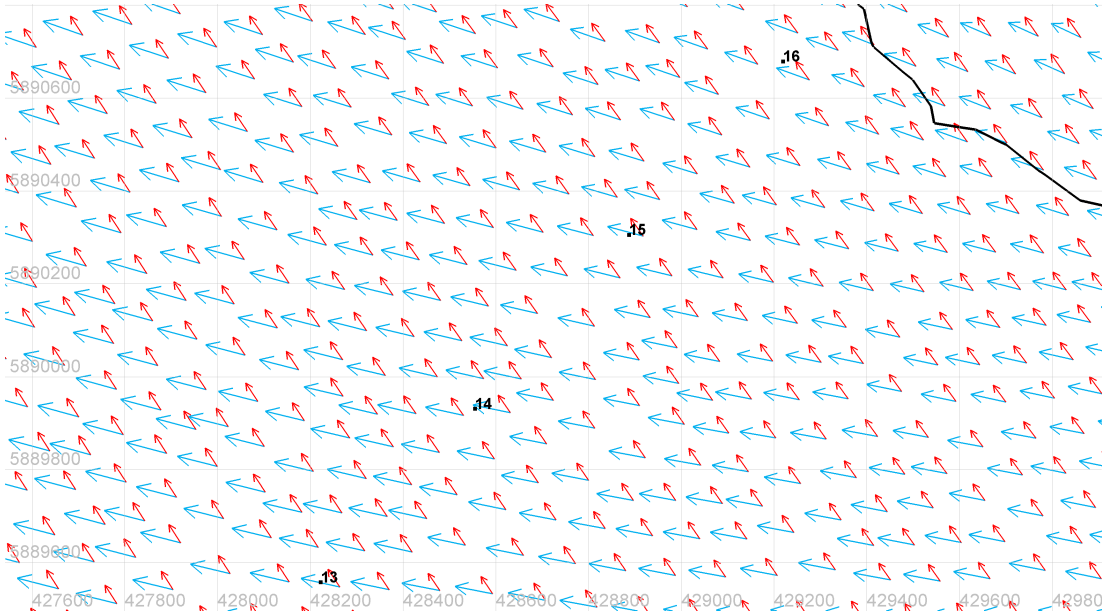

(f) Peak Flood Flow

Figure 6.14: 2D (red) vs 3D (blue) Depth averaged (a,b), Near bed (c,d) and Surface (e,f) velocity vectors at the Nearshore Trough during spring tide

Figures 6.15 and 6.16 show the time series variations in the velocities for three neap and spring tidal cycles (with the numbered points referring to the

location along the transect in Figure 6.11). During neap tides it shows a repeating pattern where the depth averaged and near bed velocities are comparable between the 2D and the 3D model for periods of low velocity. As the velocity increases and approaches peak flows, the differences become more pronounced. This is especially the case for flood tides. The near bed velocity time series seems to follow a pattern whereby alternating tidal cycles show a flood tide with a large difference followed by a similar ebb tide, then a similar flood tide and a similar ebb tide. During the spring tide the 3D depth average velocity is significantly larger than the 2D model velocity during the peak flows. However, the figure shows that as the velocity increases from the minimum flow towards the peak flow then for a short time the models are in agreement. The minimum near bed velocity is much greater than the 2D velocity at spring flood tides but shows similar values at spring ebb tides. Since the regional sediment transport is dominated by the flood tide and more influenced by the near bed velocities, greater levels of erosion would be expected in the nearshore troughs of the sandbank when considering 3D hydrodynamics compared to 2D hydrodynamics.

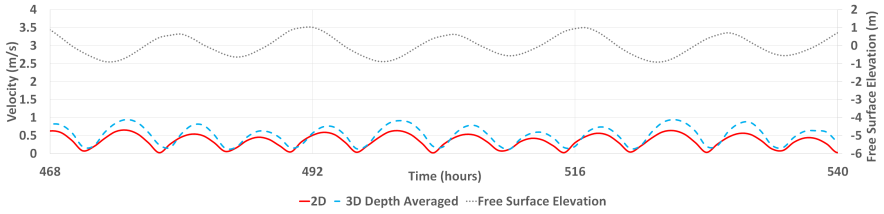

(a) 2D Depth Averaged vs 3D Depth Averaged velocity

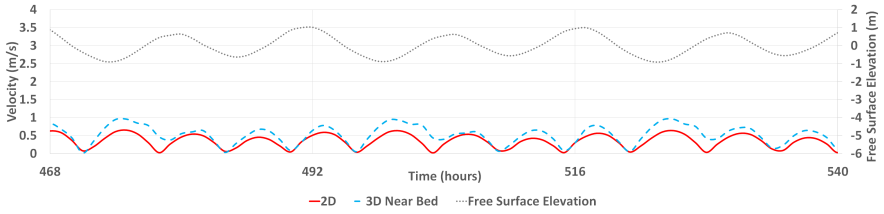

(b) 2D Depth Averaged vs 3D Near bed velocity

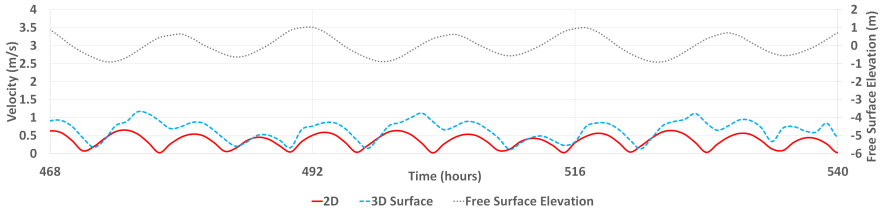

(c) 2D Depth Averaged vs 3D Surface velocity

Figure 6.15: Comparison of 2D and 3D velocity at the nearshore trough for neap tides

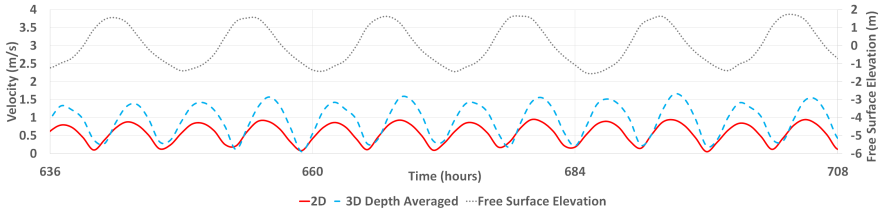

(a) 2D Depth Averaged vs 3D Depth Averaged velocity

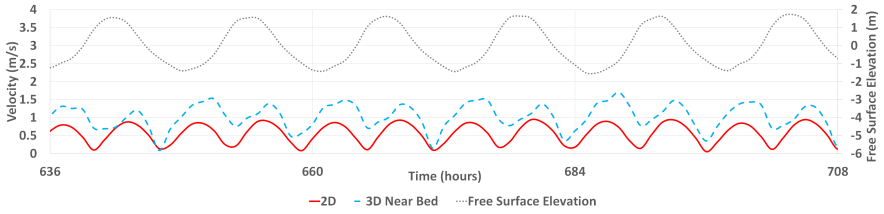

(b) 2D Depth Averaged vs 3D Near bed velocity

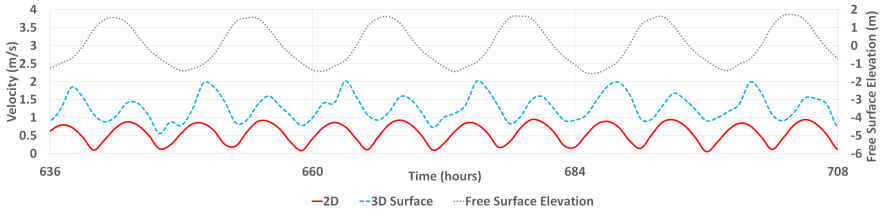

(c) 2D Depth Averaged vs 3D Surface velocity

Figure 6.16: Comparison of 2D and 3D velocity at the nearshore trough for spring tides

6.3.2.2 Velocity at the Crest

Figures 6.17 and 6.18 show the velocity magnitude profiles at the crest location. The profiles here show a similar pattern whereby the upper portion of the water column has a higher velocity in the 3D model compared to the 2D model. During the flood periods it can be seen that the 2D depth averaged velocity is greater than the near bed velocities whereas the opposite is true during ebb periods. The minimum flood profiles for both spring and neap tides show very small near bed velocities but also significant differences in the surface velocity compared to the 2D profiles. The shape of the profiles is consistent between neap and spring tides for both peak and minimum flows.

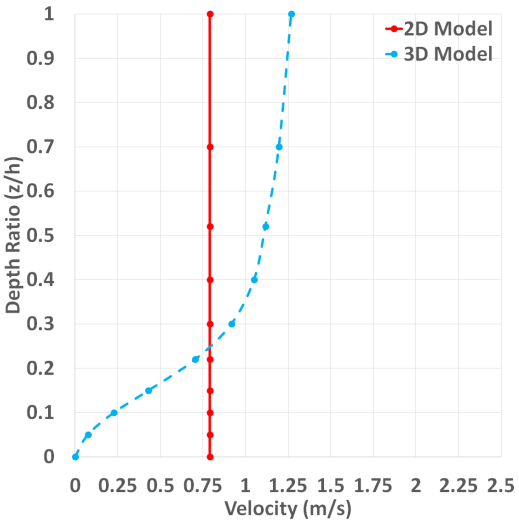

(a) Peak Flood Flow

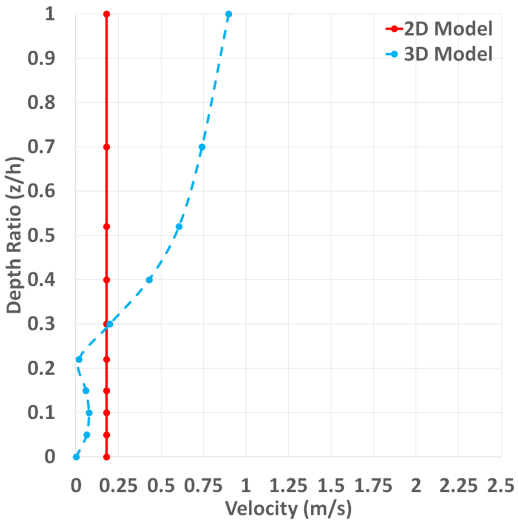

(b) Minimum Flood Flow

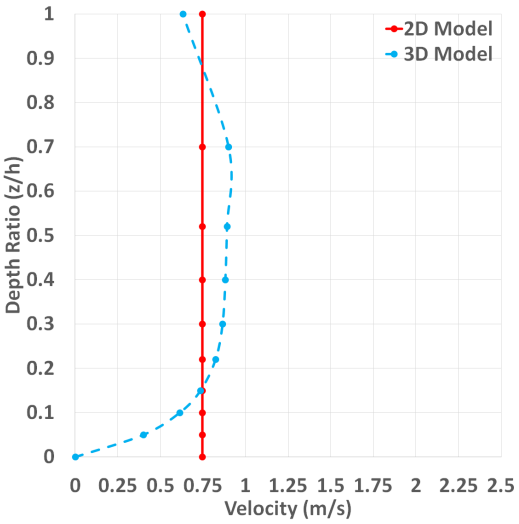

(c) Peak Ebb Flow

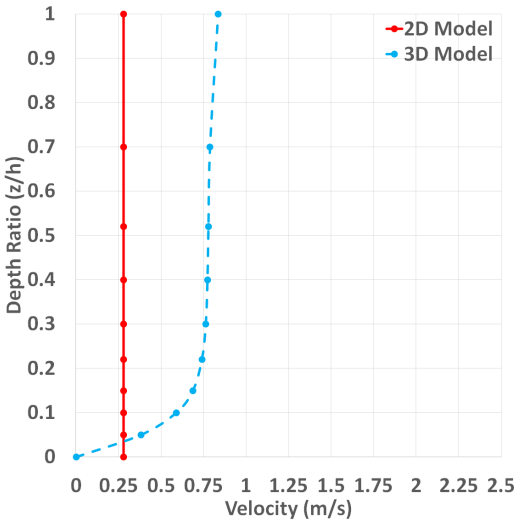

(d) Minimum Ebb Flow

Figure 6.17: 2D and 3D velocity profiles during neap tides at the crest

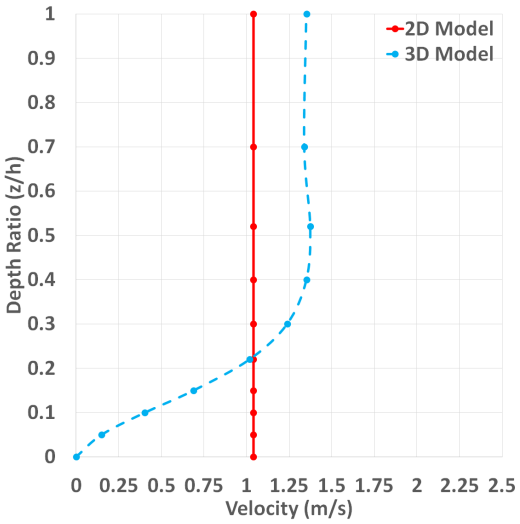

(a) Peak Flood Flow

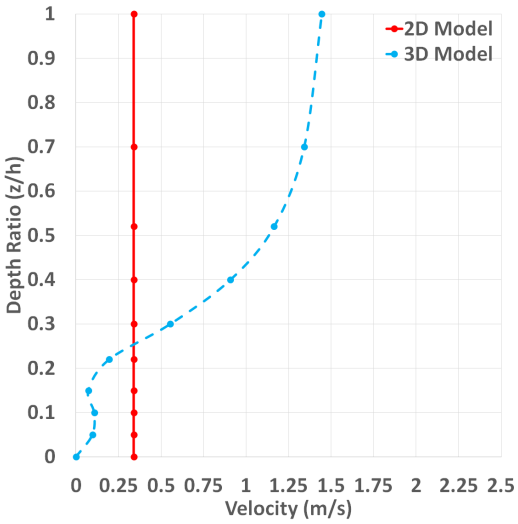

(b) Minimum Flood Flow

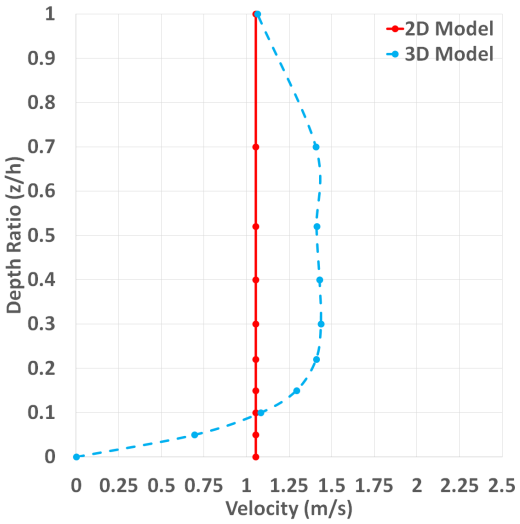

(c) Peak Ebb Flow

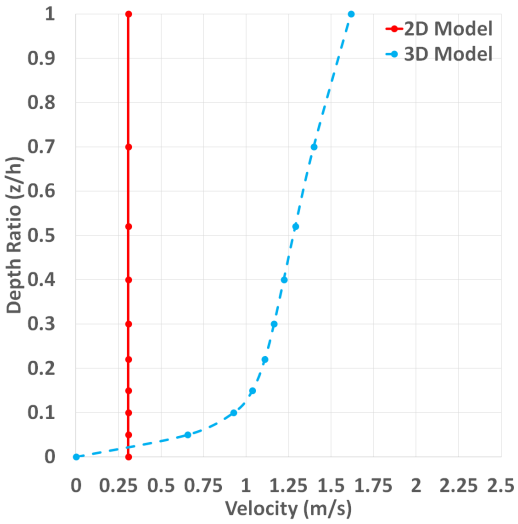

(d) Minimum Ebb Flow

Figure 6.18: 2D and 3D velocity profiles during spring tides at the crest

Figure 6.19 shows the velocity vectors for the depth averaged, near bed and surface velocities at the same timesteps as Figures 6.18c and 6.18a. At this location, it can be seen that during peak flood flow the depth averaged velocity vectors are consistent between the 2D and the 3D models. However, at peak ebb flow the vectors are fairly consistent in terms of magnitude but significantly

different in terms of direction. This same pattern is repeated for the near bed velocity. At the surface the magnitude is fairly consistent between the two models, but the direction is significantly different at both peak ebb and peak flood flows.

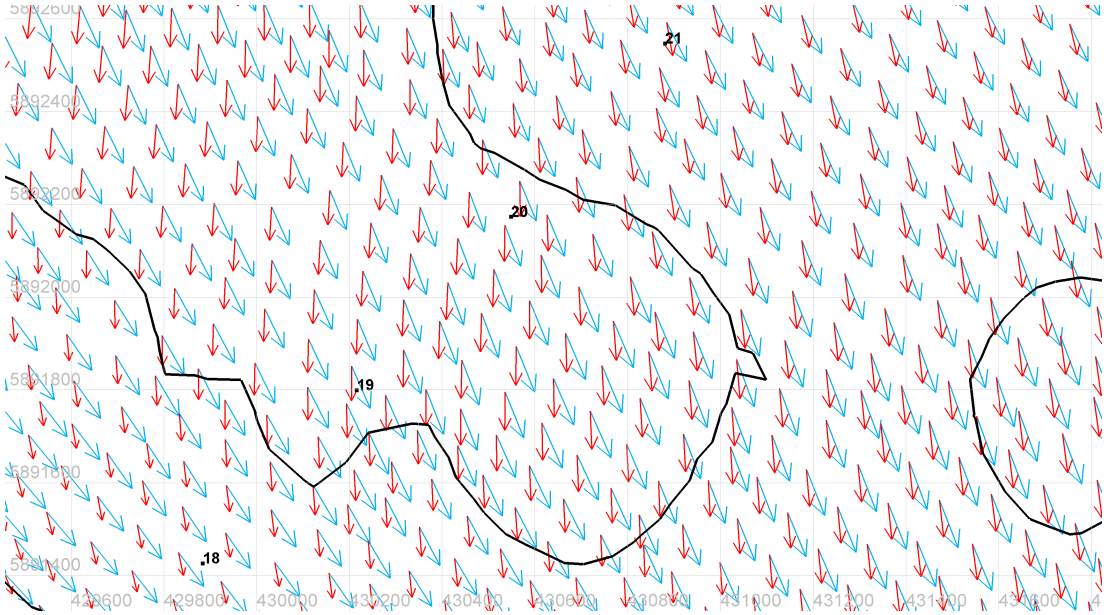

(a) Peak Ebb Flow

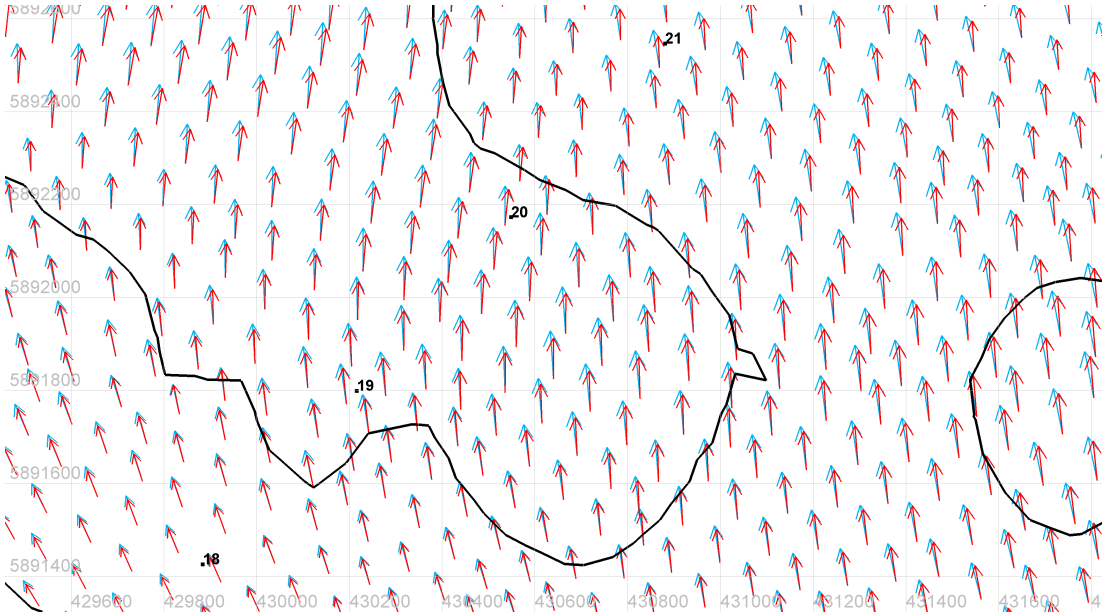

(b) Peak Flood Flow

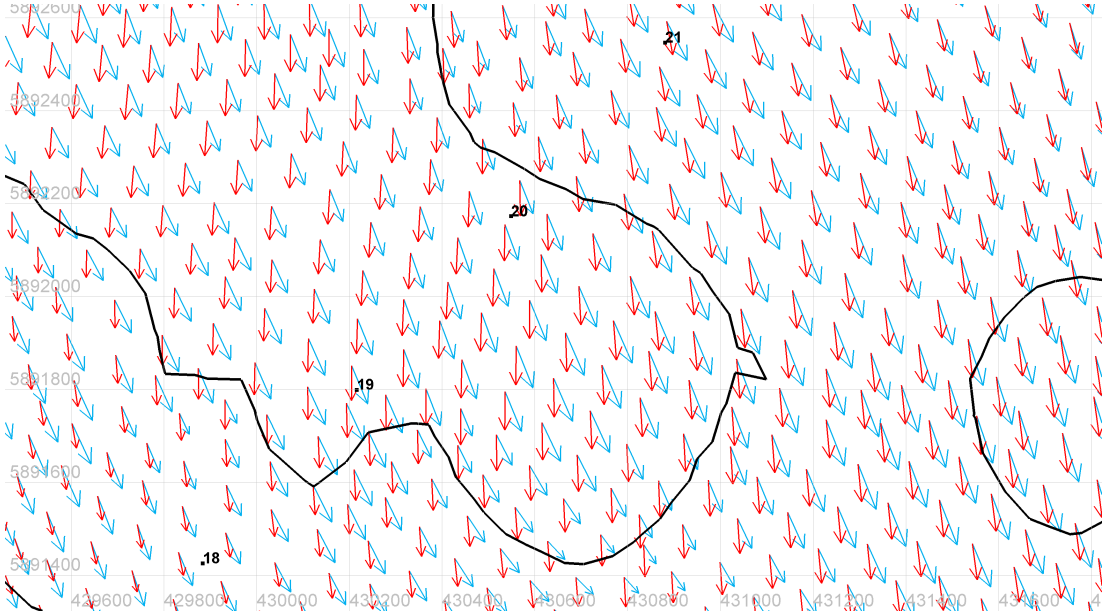

(c) Peak Ebb Flow

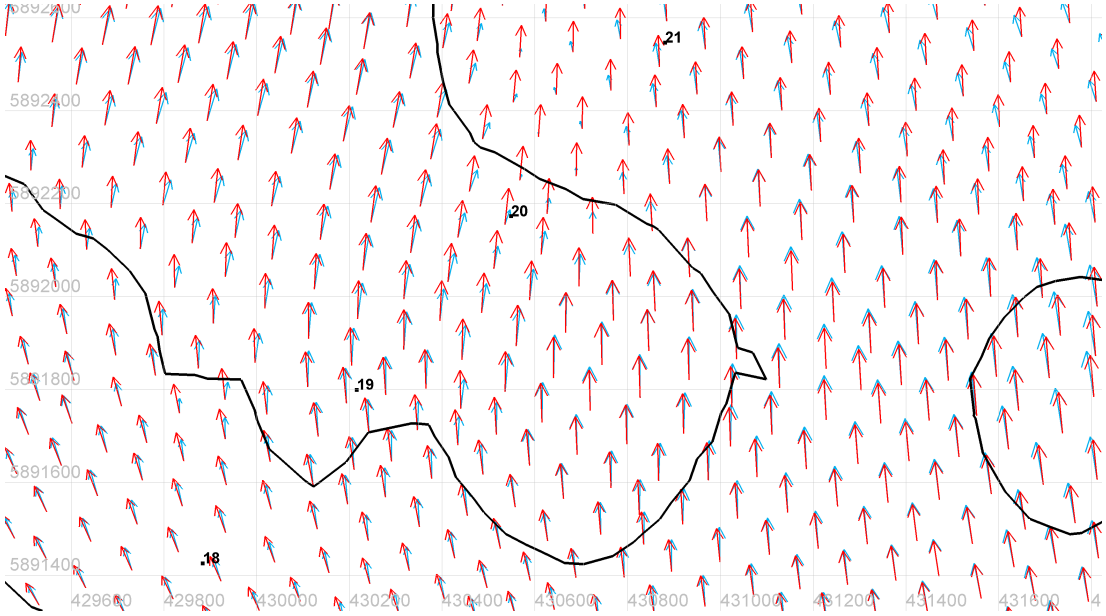

(d) Peak Flood Flow

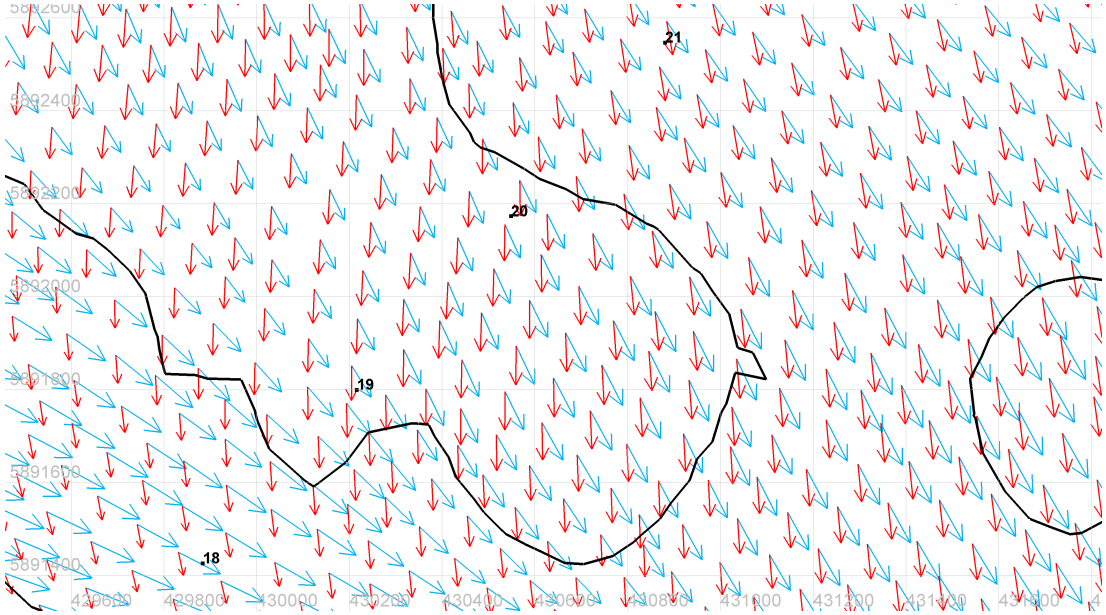

(e) Peak Ebb Flow

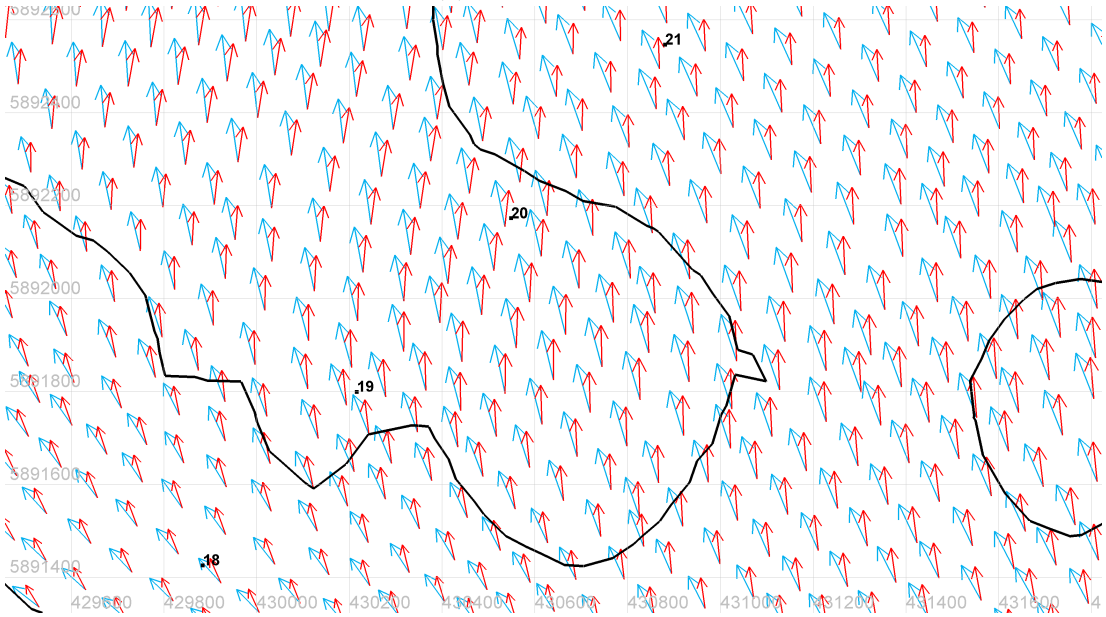

(f) Peak Flood Flow

Figure 6.19: 2D vs 3D Depth averaged (a,b), Near bed (c,d) and Surface (e,f) velocity vectors at the Crest during spring tide

Figures 6.20 and 6.21 show the time series differences between the 2D and the 3D models for several neap and spring tidal cycles. In terms of the depth

averaged velocity, the 3D model predictions are higher than the 2D model and that difference is larger during the spring tides. It is interesting to note that there is also a phase difference between the two models, in that the minimum depth averaged velocity for the 3D model appears to occur a few hours after the minimum depth averaged velocity predicted by the 2D model. This could account for some of the observed differences in the velocity vectors. The near bed velocity time series are similar and since sediment transport is influenced more by near bed currents, at this particular location it can be concluded that both models are likely to accurately predict sediment transport rates over time. During the spring tide however, there is a significant difference in the time series between the 2D and the 3D time series. By following the time series through a tidal cycle it can be seen that the first velocity cycle is fairly consistent between two models but during the successive velocity cycle the 3D model does not appear to have a peak. This is consistent with the profiles shown earlier whereby it is noted that the velocity in the bottom quarter of the water column is significantly less than simulated by the 2D model.

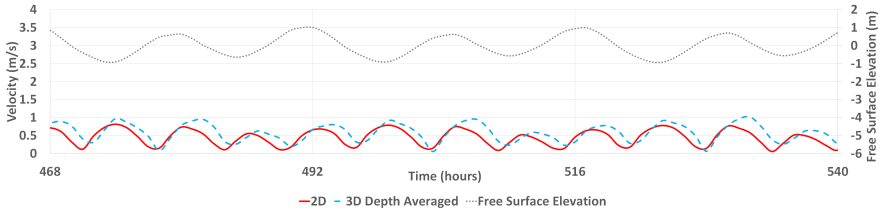

(a) 2D Depth Averaged vs 3D Depth Averaged velocity

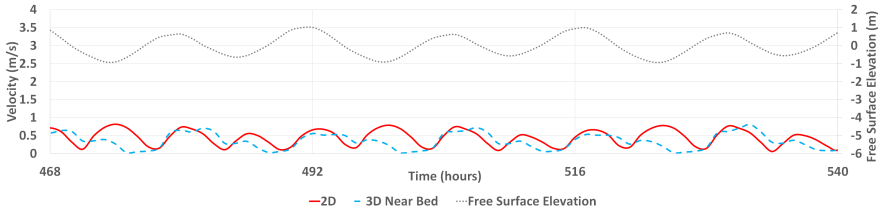

(b) 2D Depth Averaged vs 3D Near bed velocity

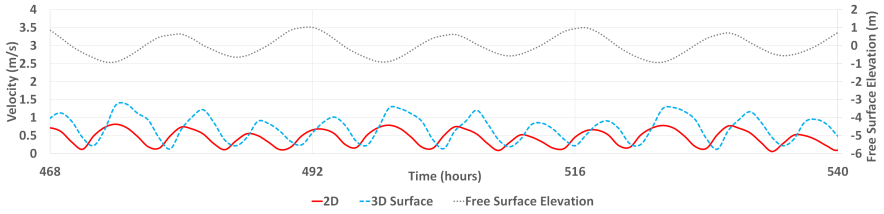

(c) 2D Depth Averaged vs 3D Surface velocity

Figure 6.20: Comparison of 2D and 3D velocity at the crest for neap tides

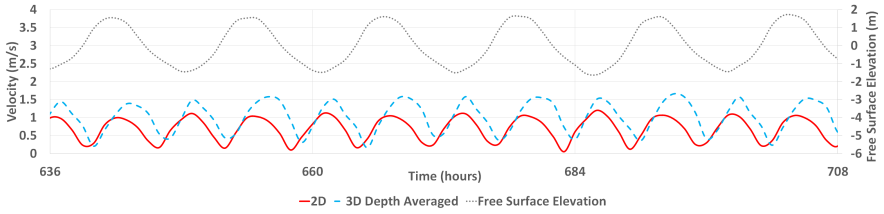

(a) 2D Depth Averaged vs 3D Depth Averaged velocity

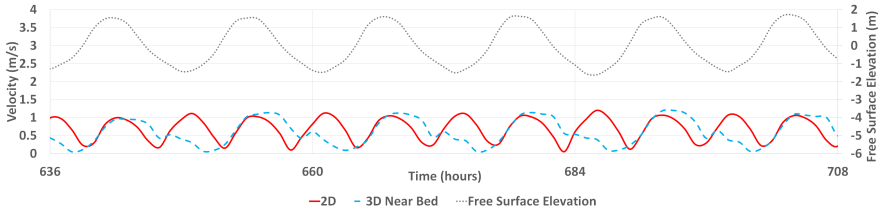

(b) 2D Depth Averaged vs 3D Near bed velocity

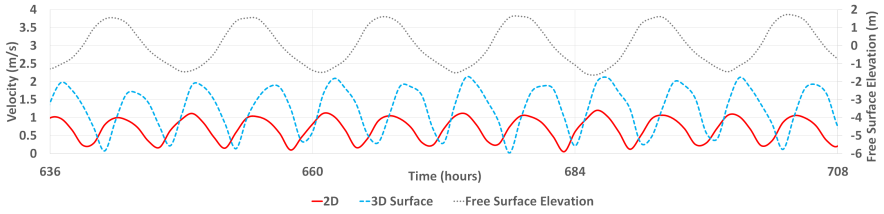

(c) 2D Depth Averaged vs 3D Surface velocity

Figure 6.21: Comparison of 2D and 3D velocity at the crest for spring tides

6.3.2.3 Velocity at the Offshore Trough

Figures 6.22 and 6.23 show the velocity magnitude profiles at the offshore trough location for the same timesteps used in the previous sections. During the neap tides the profiles are all consistent in shape with the exception of the peak flood flow. During the spring tides all the profiles show a similar kink at a depth of between 40% and 70% of the water column with the exception of the minimum ebb flow which has a kink nearer to the bed.

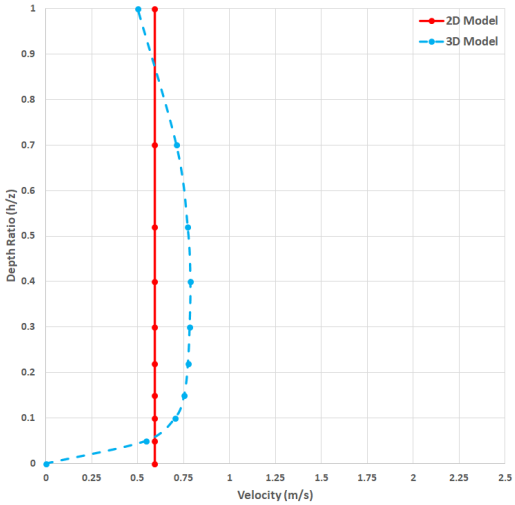

(a) Peak Flood Flow

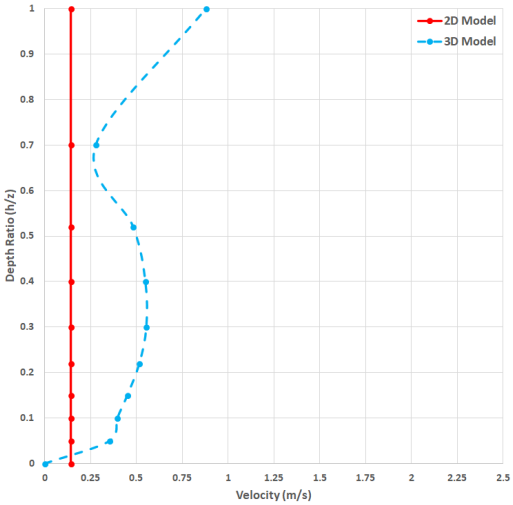

(b) Minimum Flood Flow

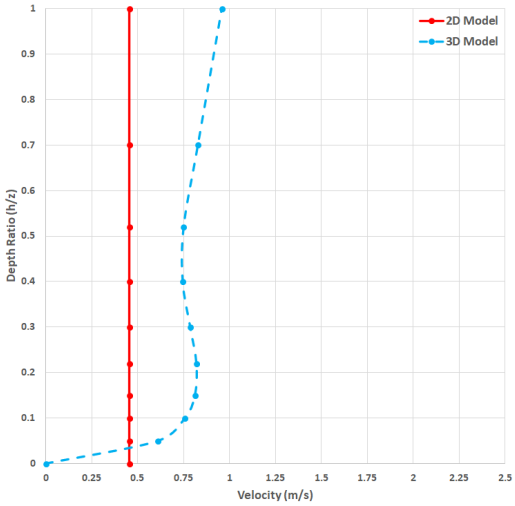

(c) Peak Ebb Flow

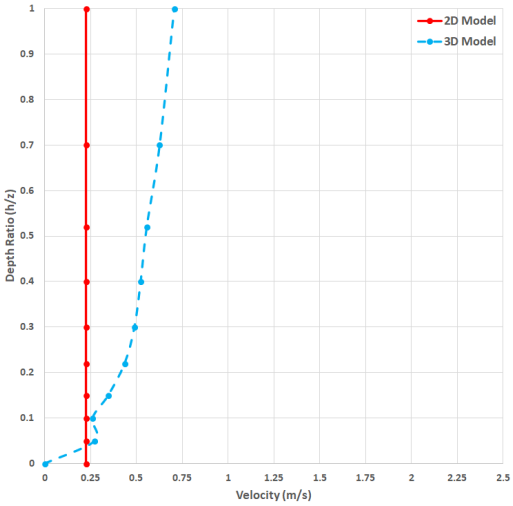

(d) Minimum Ebb Flow

Figure 6.22: 2D and 3D velocity magnitude profiles during neap tides at the offshore trough

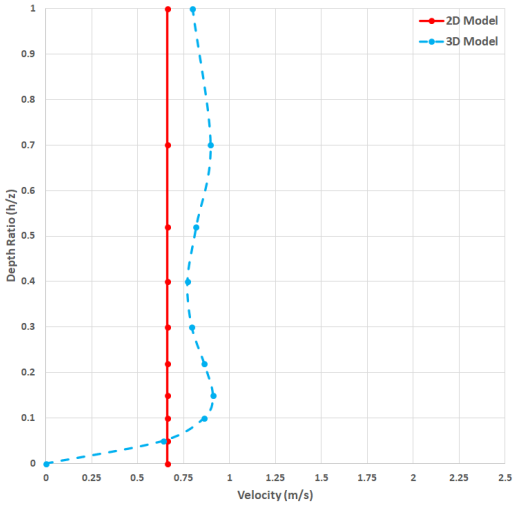

(a) Peak Flood Flow

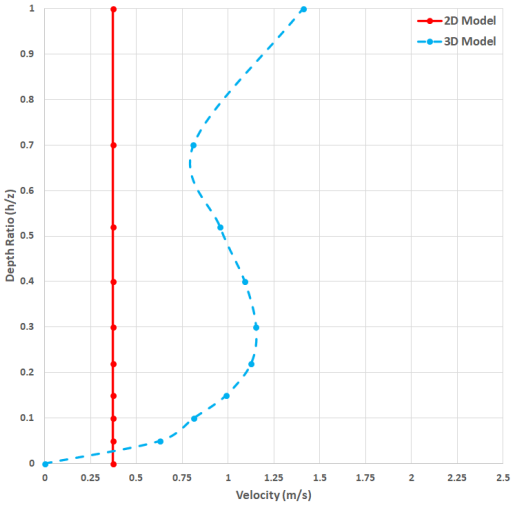

(b) Minimum Flood Flow

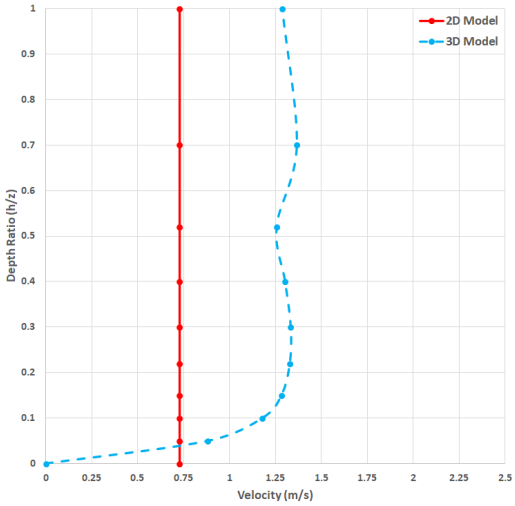

(c) Peak Ebb Flow

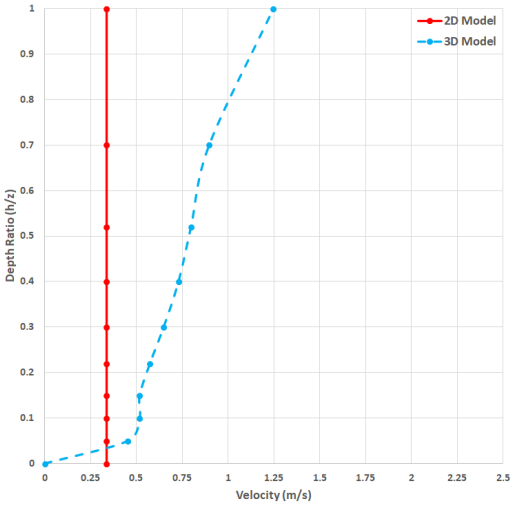

(d) Minimum Ebb Flow

Figure 6.23: 2D (red) and 3D (blue) velocity magnitude profiles during spring tides at the offshore trough

Figure 6.24 shows a comparison between the 2D depth averaged and the 3D depth averaged, near bed and surface velocity vectors at the peak flood and ebb spring tide. Similar to the nearshore trough, the depth averaged velocity is consistent in terms of direction but not magnitude. The near bed velocity is fairly consistent in terms of magnitude but not direction. The surface velocity

vectors are significantly different in terms of direction but similar in magnitude.

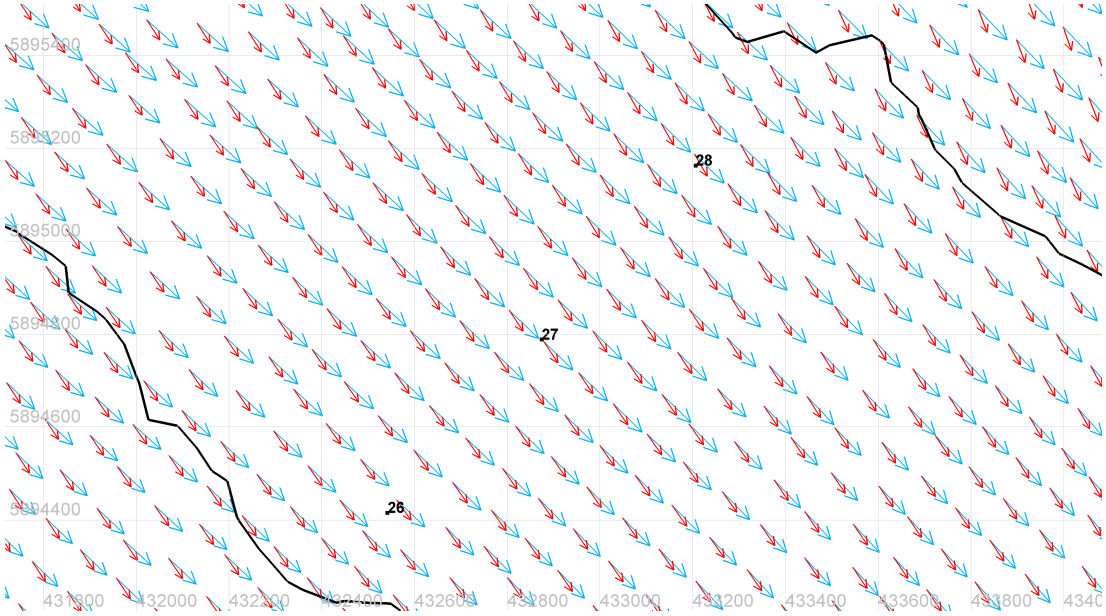

(a) Peak Ebb Flow

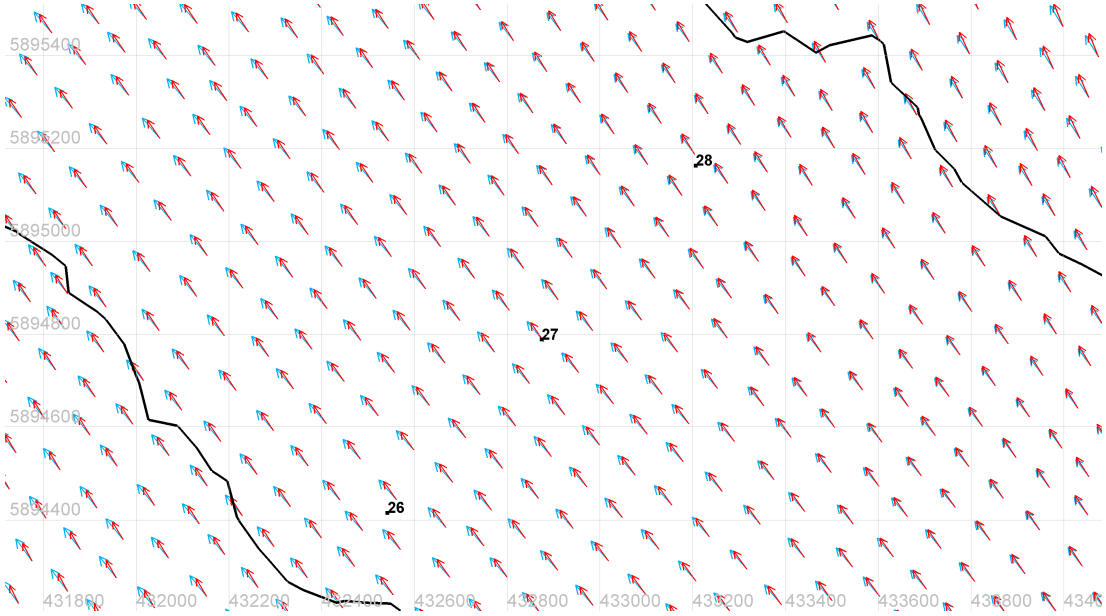

(b) Peak Flood Flow

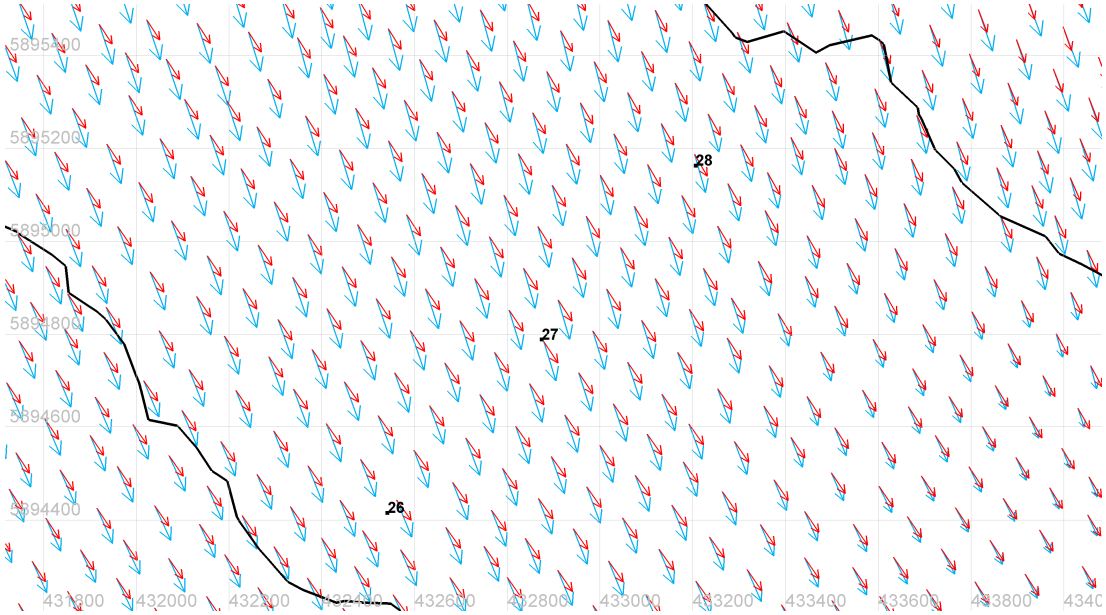

(c) Peak Ebb Flow

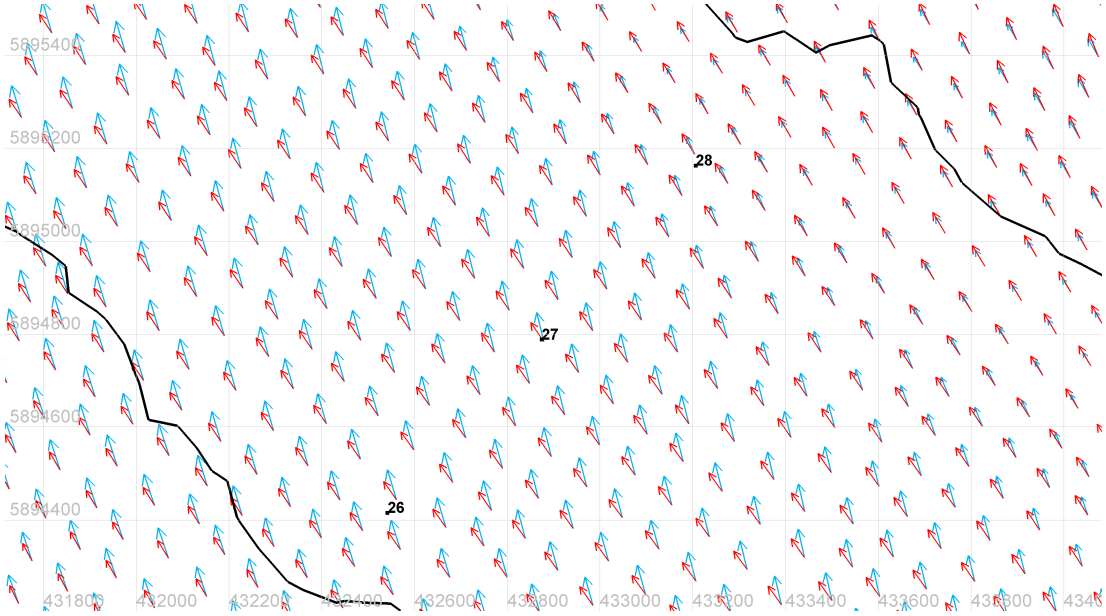

(d) Peak Flood Flow

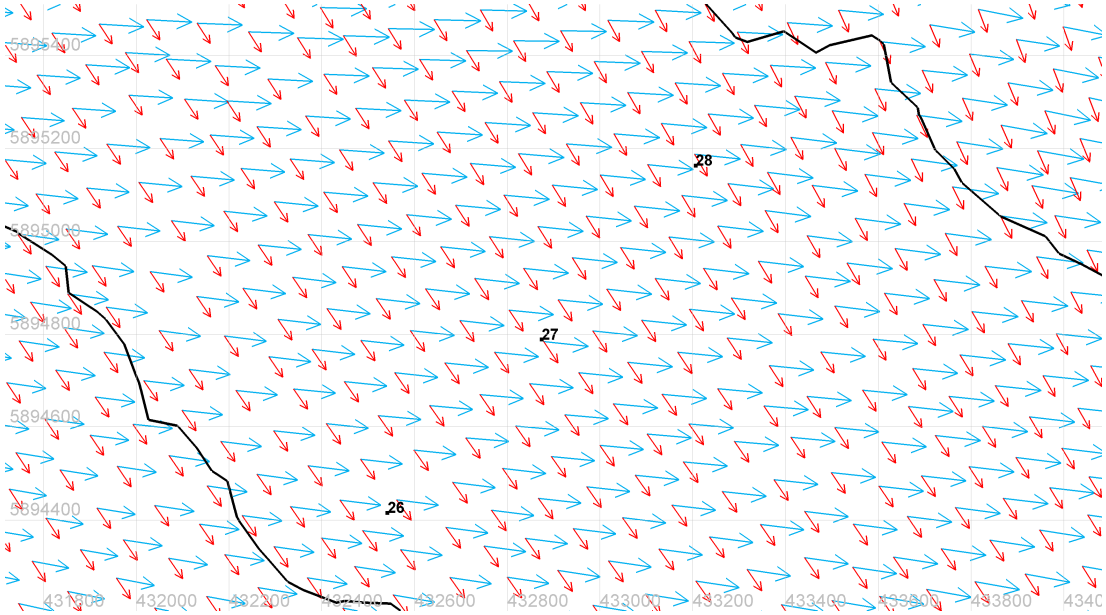

(e) Peak Ebb Flow

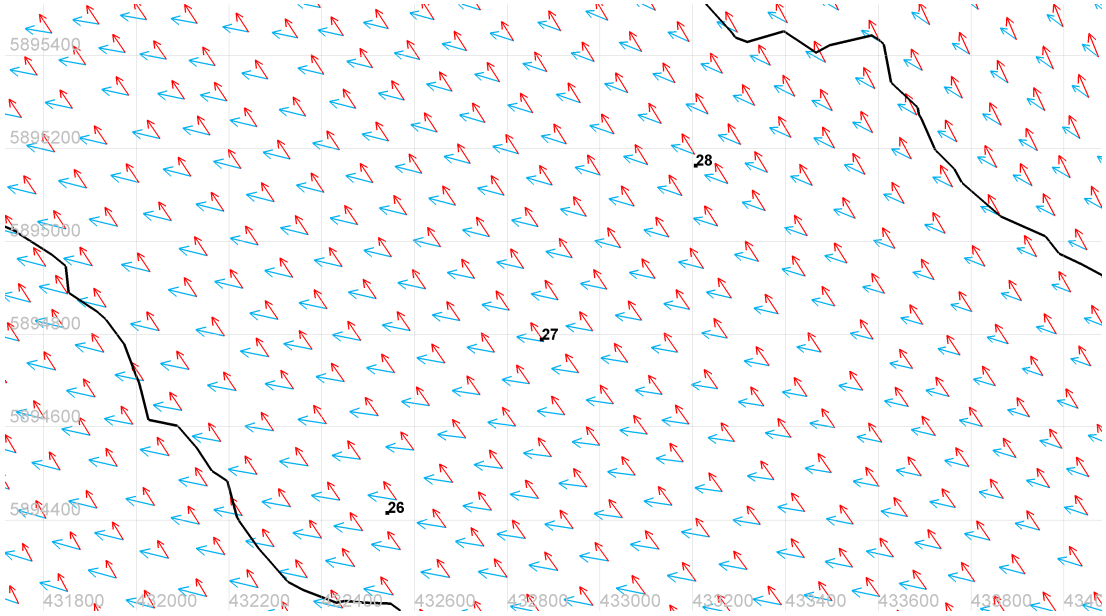

(f) Peak Flood Flow

Figure 6.24: 2D (red) vs 3D (blue) Depth averaged (a,b), Near bed (c,d) and Surface (e,f) velocity vectors at the offshore trough during spring tide

Figures 6.25 and 6.26 show the time series, similar to the previous locations. It describes similar patterns to those previously described at other locations. More

noticeable here is that the near bed velocities are much smaller than at the other locations and thus the time series appears to be more consistent with the 2D model.

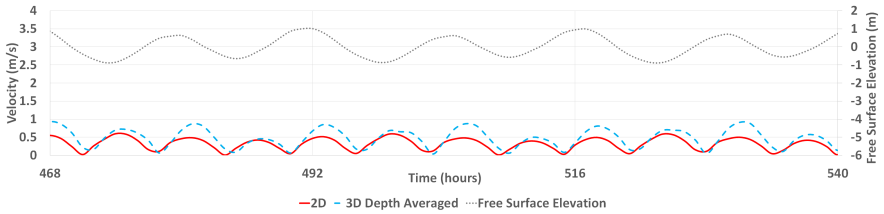

(a) 2D Depth Averaged vs 3D Depth Averaged velocity

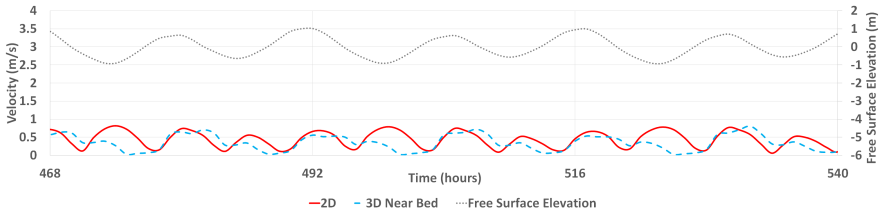

(b) 2D Depth Averaged vs 3D Near bed velocity

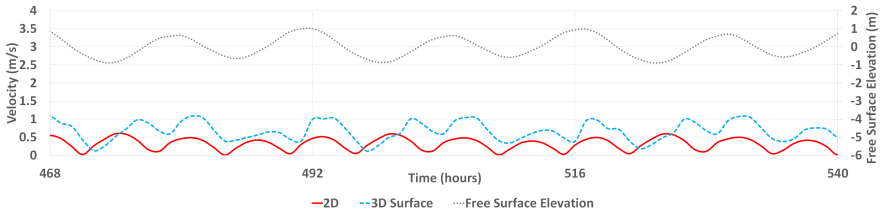

(c) 2D Depth Averaged vs 3D Surface velocity

Figure 6.25: Comparison of 2D and 3D velocity at the offshore trough for neap tides

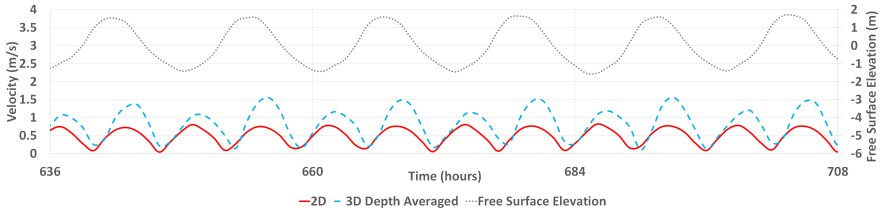

(a) 2D Depth Averaged vs 3D Depth Averaged velocity

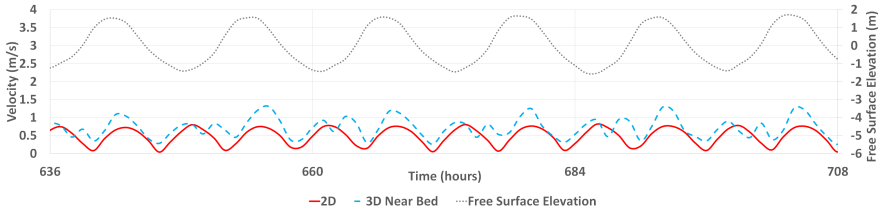

(b) 2D Depth Averaged vs 3D Near bed velocity

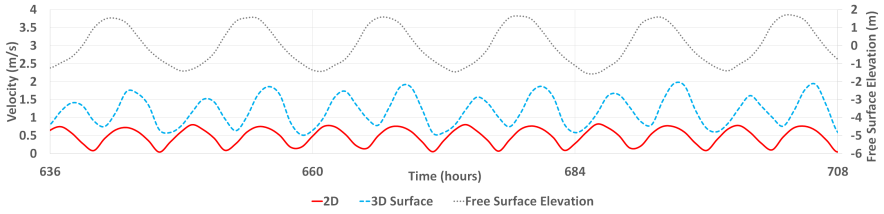

(c) 2D Depth Averaged vs 3D Surface velocity

Figure 6.26: Comparison of 2D and 3D velocity at the offshore trough for spring tides

6.3.3 Discussion

6.3.3.1 Differences in Free Surface Elevation

Figure 6.27 shows the free surface elevation at the nearshore trough. It shows that the 3D model is in good agreement with the 2D model. The RMSE value at this point is 21.8cm and the Mean Absolute Difference (MAD) is 17cm. The corresponding values for the crest are 22.4cm and 17.4cm and for the offshore trough are 21.5cm and 16.8cm. Figure 6.27 shows that the largest differences in the free surface elevation between the two models tend to occur during the peak spring tidal phases (For example, 0-72 hours and 672-708 hours from the simulation start). This trend is observed at the majority of the analysis points. This suggests that in terms of the free surface elevation the 2D and the 3D model

are in good agreement, noting that the 3D model has a tendency to predict higher elevations compared against the 2D model. Since the calibration coefficients are kept constant, it is possible that the differences are a result of the vertical velocity components. Given the highlighted phase differences in the previous section, another explanation could be that the differences are a result of changes in the modelling of bed friction.

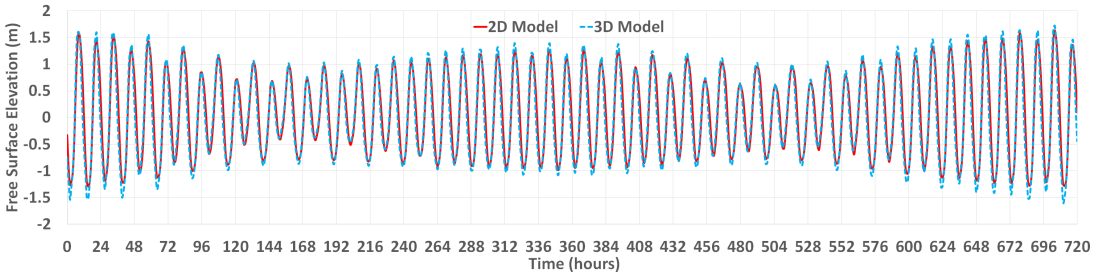

Figure 6.27: Comparison of free surface elevations between the 2D and 3D models at the nearshore trough

This reasoning is used as a validation for the 3D model; the logic being that since the 2D model is calibrated to observation data and deemed accurate and the 3D model is outputting similar results then by progression the 3D model is producing results of a similar confidence. However, it is worth bearing in mind that this does not necessarily hold true in all cases. For example, the next section will highlight the differences between the velocity outputs of both of these models. Whilst these differences can be accounted for as due to the consideration of the vertical components in the 3D model, it does not definitely prove which is more accurate; the 2D model velocity or the 3D model velocity. This conclusion would require further validation from field measurements.

6.3.3.2 Differences in Depth Averaged Velocity

A positive difference indicates that the 3D model is predicting a higher velocity than the 2D model. A negative difference indicates that the 3D model is predicting a lower velocity than the 2D model. Again the velocity is analysed in terms of the depth averaged near bed and surface velocities. Since in 2D the velocity

profile is constant with depth, the near bed and surface velocities are equal to the depth averaged velocity and are therefore referred to as such.

Figure 6.28b shows the differences between the 2D and the 3D velocities at each of the three points over six spring tide periods. Table 6.2 shows the maximum, minimum and mean absolute differences calculation across the whole simulation at each location.

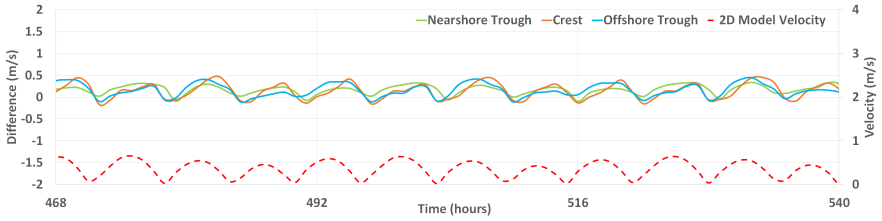

(a) Neap tides

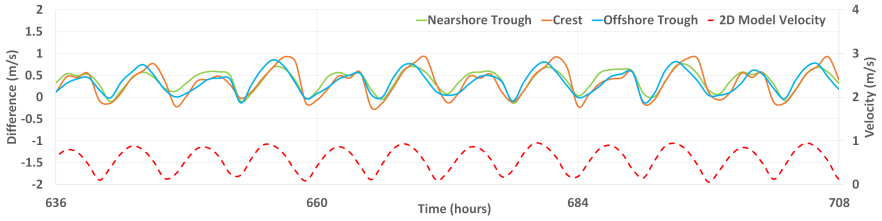

(b) Difference between 2D and 3D Depth Velocity at each location

Figure 6.28: Spring tides

Table 6.2: Difference between 2D and 3D Depth Averaged Velocity

	Velocity Difference		
	Maximum (m/s)	Minimum (m/s)	Mean Absolute (m/s)
Nearshore Trough	0.75	-0.20	0.26
Crest	0.94	-0.27	0.27
Offshore Trough	0.85	-0.23	0.25

From Table 6.2 it can be seen that the mean absolute difference is consistent across all three locations. The same can be said for the minimum difference.

However, the maximum differences are more varied. Figure 6.28 shows that in terms of depth averaged velocity, the time series of the differences is also fairly consistent by location. The magnitude of the differences is much larger for spring tides compared to neap tides. The differences are also larger for ebb tides compared to flood tides. The larger differences also occur just prior and after the peak flow. At times of minimum flow, the differences are either small or negative. During both spring and neap tides, at the troughs the difference is almost always positive indicating that the 3D model is always predicting a higher depth averaged velocity compared to the 2D model. Most sediment transport models use a depth averaged velocity, whether derived from a 2D or a 3D hydrodynamic model. Therefore in this instance, using the depth averaged velocity from the 2D model could result in an underestimation of the sediment transport rates (assuming that it is the 3D model that is more accurately representing the flow). Given that it is concluded that in the North Sea the sediment transport is dominated by the flood tide, it is important to note that the flood differences tended to be lower than the ebb differences. If this is an accurate representation of the flow field, it is possible to some extent that the sediment transport rate during the ebb periods could be underestimated. It highlights that one of the key requirements of a numerical modelling study is to have concurrent field data to validate the results of the simulation.

6.3.3.3 Differences in Near Bed Velocity

Figure 6.29 and Table 6.3 show the differences between the 2D depth averaged and the 3D near bed velocity (defined as the velocity at a depth ratio of 0.1). At the crest during the spring tide (Figure 6.29b) there appears to be a repeating pattern. A large negative difference occurs at peak flow which increases to a small positive or almost zero difference by the successive minimum to peak flow. The difference remains fairly constant until it increases into a large positive difference at the next minimum flow. The magnitude of the negative differences is larger than the positive differences which correlates to the 3D model estimating a smaller velocity at these times. The magnitude of the larger is approximately twice that of the differences at neap tide and roughly equal to the value of the velocity at

peak flow. At the trough locations the difference is almost always positive and the differences tended to be larger in the nearshore trough compared to the offshore trough. In terms of the Mean Absolute Difference between the models, the values are fairly consistent with the differences in the depth averaged velocity.

Sediment transport is largely related to the near bed currents. The 2D depth averaged velocity is often used for near bed shear stress calculations using a logarithmic profile for example. In a way this means that the differences between the 2D depth averaged velocity and the 3D near bed velocity are more significant than those between the 3D depth averaged and the 3D surface velocity. The large fluctuations at the crest location could result in significant changes to bedload and suspended load sediment transport with 3D hydrodynamics compared to 2D hydrodynamics. For example, from Figure 6.29b there are periods where there is a negative difference almost equal to the value of the 2D velocity. This results in the near bed velocity in 3D being almost equal to zero at a point where the 2D velocity is at its peak. At these times, the corresponding difference in the depth averaged velocity tends to be smaller. This suggests that the overall magnitudes in the profile are accurate, but the resulting sediment transport pattern resulting from the velocity would be markedly different.

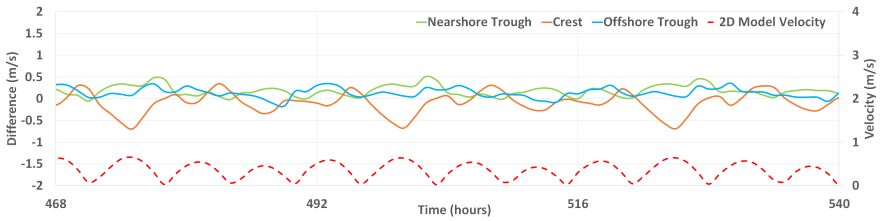

(a) Neap tides

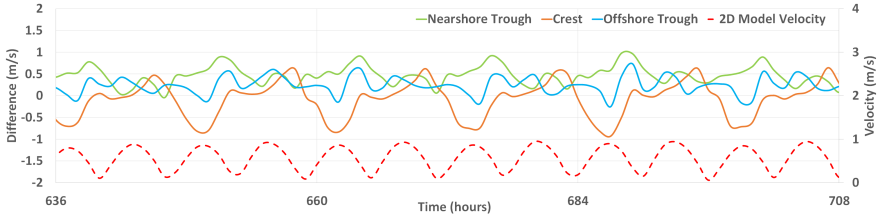

(b) Spring tides

Figure 6.29: Difference between 2D and 3D Near Bed Velocity

Table 6.3: Difference between 2D and 3D Near Bed Velocity

	Velocity Difference		
	Maximum (m/s)	Minimum (m/s)	Mean Absolute (m/s)
Nearshore Trough	0.97	-0.07	0.29
Crest	0.66	-0.92	0.24
Offshore Trough	0.75	-0.32	0.21

6.3.3.4 Differences in Surface Velocity

Figure 6.30 shows the difference in the magnitude of the 2D depth averaged and the 3D surface velocity. The differences between the 2D depth averaged and the 3D surface velocity are much larger than the differences between the 3D near bed and 3D depth averaged velocities. On average the surface velocity differences are approximately twice the depth averaged and near bed velocity differences at each location. The largest differences are observed at the crest location (see Table 6.4). At the crest it can be seen that the largest positive differences occur just after the peak flow and the largest negative differences occur just prior to the peak flow. The differences are roughly twice as large for the spring tides compared to the neap tides. During spring tides these differences are sometimes exceeding the 2D model velocity (i.e. the 3D model is showing doubling the 2D depth averaged velocity at the surface). At the troughs, the differences are always positive with the largest differences roughly coinciding with the times of the largest differences at the crest. This means that the 2D model is always underpredicting the surface velocity in the sandbank troughs compared to the 3D model. These differences could have an impact of the wave modelling. According to Viitak et al. [2016] there is a relationship between the surface currents and the evolution of the wave field. This could result in an increase or decrease in significant wave heights by up to 20%. This effect is observed more in shallower waters (such as the sandbanks crests) or areas where the currents and waves are

propagating in opposite directions [Viitak et al., 2016]. The crest is where the largest differences are modelled and the crest is also where the shallowest depths are. Since wave induced sediment transport has a greater influence in shallower areas, consideration of 3D hydrodynamics over 2D hydrodynamics could have a significant impact when also considering wave conditions.

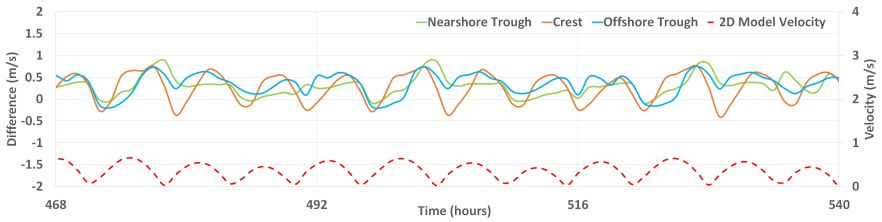

(a) Neap tides

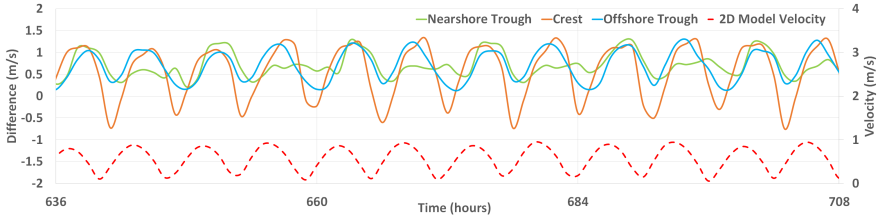

(b) Spring tides

Figure 6.30: Difference between 2D and 3D Surface Velocity

Table 6.4: Difference between 2D and 3D Surface Velocity

	Velocity Difference		
	Maximum (m/s)	Minimum (m/s)	Mean Absolute (m/s)
Nearshore Trough	1.34	-0.25	0.48
Crest	1.33	-0.75	0.51
Offshore Trough	1.29	-0.32	0.50

This section has highlighted the difference between the 2D and the 3D hydrodynamic models. However, the models are not without their limitations. In terms

of the free surface elevations, the models are assumed to be comparable which is a reasonable assumption. Following from this, if the 3D profile is a comparable match to the 2D model, then it would be expected that the depth averaged velocities would be similar which is not the case. Without further investigation and comparison of the 3D profile in respect to either observational data or other calibrated 3D models it is not possible to categorically state whether the 3D profiles are an accurate representation of the flow field. The results presented here highlight that there are significant differences between the 2D current patterns and the 3D current patterns and this is an important factor when considering morphological behaviour through the use of numerical models.

Chapter 7

Morphodynamic Modelling

7.1 Introduction

This chapter deals with the morphodynamic modelling and the application to the study site in 2D and 3D. First the sediment transport model is assessed for its sensitivity to the uncertainty in the input parameters in the 2D model. Next, the case scenarios are defined and the model is run to analyse the evolution in the Norfolk Banks area. Then, a simple wave condition is applied to the model to determine how this impacts the sediment transport and overall evolution. Finally the morphodynamic model is run with the 3D hydrodynamic conditions and the results compared with those of the 2D model.

7.2 Morphodynamic Modelling with 2D Hydrodynamics

7.2.1 Model Configurations

The model is run using TELEMAC2D coupled with SISYPHE for sediment transport processes. The internal coupling method means that at each timestep the hydrodynamic variables such as velocity, water depth and bed shear stress are

directly transferred into the morphodynamic model. The morphodynamic model then calculates sediment transport and bed elevation and sends the updated bed elevation value back into the hydrodynamic model. The configuration of the hydrodynamic model is consistent with the final calibrated model in the previous section.

In order to reduce instability, the model is run using a hotstarting procedure; an uncoupled TELEMAC2D model is run for a period of 5 days to develop the hydrodynamic conditions. TELEMAC then uses the final timestep of this simulation as the initial conditions for the coupled model. This method ensures that instability in the hydrodynamic conditions does not directly impact the morphodynamic conditions and bathymetric changes before the model has stabilized.

The first stage of the morphodynamic modelling was to determine the model's sensitivity to specific input parameters. Since sediment transport processes are highly complex and there is a lot of uncertainty over the model parameterisation, it is important to gain insight into how the model parameters can affect the model results. Six case scenarios are developed in order to test the sensitivity of the model output with particular focus on the bottom evolution. Two main parameters, sediment size and initial sediment concentration are chosen to be tested. It is worth noting also, that other parameters within the SISYPHE code, for example, settling velocity and shields parameter, are functions of the sediment size. As such the sensitivity of these parameters is tested in tandem. The values of these parameters are assigned according to the requirements set out in Chapter 3. Specifically as an example, the different values produced by the formulae used by SISYPHE to calculate the settling velocity for a particle size are not being tested.

The initial test case (referred to as INIT) simulates a baseline case using an initial sediment concentration throughout the domain of 0 and sediment size of 250µm. The Centre for Environment Fisheries and Aquaculture Science [2017] suggests a median grain size of 250µm is representative of the sediment in the domain as a whole.

The next two cases (referred to as D350 and D450) involves testing the impact of the sediment size. Jenkins et al. [2015] suggests that sediment size varies between offshore and nearshore sandbanks and also varies locally between the

crest, flanks and trough of sandbanks. The mean particle size measured here gives the average between nearshore and offshore sandbanks. For offshore sandbanks the mean particle size is 277.69µm on the crests, 283.93µm on the flanks and 452.92µm in the troughs. The average size across all locations is 338.18µm. Using the data from the Centre for Environment Fisheries and Aquaculture Science [2017], but analysing the points within the Norfolk banks area gives an average size of 450µm. The average size of the sand portion of the sediment across the whole domain is 343µm. This gave rise to testing two coarser sediment sizes: 350µm and 450µm.

Consideration is then given to model the sediment as a non-uniform sediment composing of three different classes based on the available sediment data within the region. These are gravel, sand and silt. However the sample data (from the Centre for Environment Fisheries and Aquaculture Science [2017]) suggests that across the domain as a whole, 3.36% of the sediment is gravel, 86.45% is sand and 10.18% is silt-clay. Within the region of the Norfolk Banks, this is even more uniformly distributed with 0.96% of the sediment being gravel and 99.04% being sand. Therefore the assumption of using a uniform sediment within the model is justified for this research.

The next two cases (referred to as SSC4 and SSC15) test the effects of different initial suspended sediment concentrations.Visser et al. [1991] suggests that measured surface concentrations at 10km offshore of the Dutch coast are 10mg/L and decreases further to approximately 3-4mg/L at a distance of 30km offshore. Silva et al. [2016] suggests average sediment concentrations in the Southern North Sea are in the region of 10-15mg/L (see Figure 7.1). As such two test cases are established with varying initial concentrations. The first has an initial concentration of 4mg/L and the second has an initial concentration of 15mg/L corresponding to each of the two previously discussed references respectively. Although the outputs of the SISYPHE model can be expressed in terms of a mass concentration, in the steering file the associated keywords are required to be in the form of a volume concentration. Therefore, the desired mass concentrations are divided by the density of the sediment (in this case 2650kg/m^3).

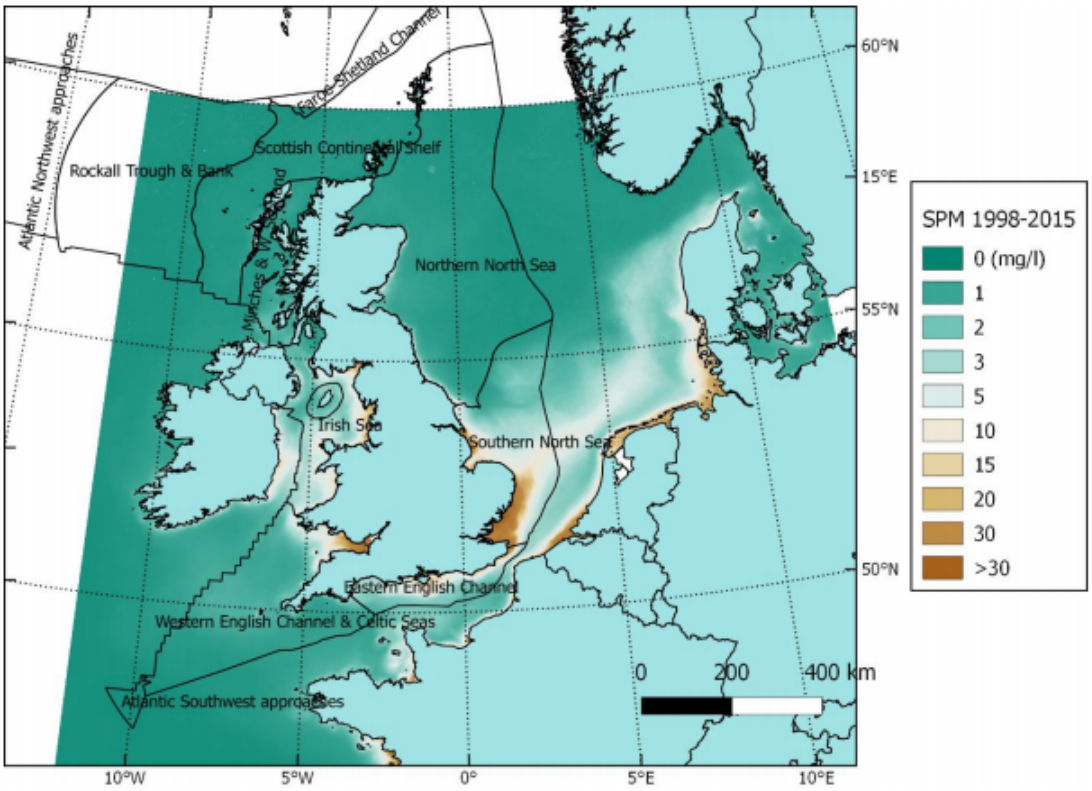

Figure 7.1: Average Suspended sediment concentrations in the North Sea (from Silva et al. [2016])

The final test case (referred to as D350SSC15) combined the effects of an initial suspended sediment concentration and a coarser sediment size; testing an initial concentration of 15mg/L and a sediment size of 350µm.

A summary of the variable parameters for each case is shown in Table 7.1 below. Other parameters such as particle and fluid density, transport formulae et cetera, are kept constant throughout.

Table 7.1: Case test parameters

Test Case	Sediment size (μm)	Initial Concentration (mg/L)	Settling Velocity (m/s)	Shields Parameter (-)
INIT	250	0	0.054	0.0247
D350	350	0	0.105	0.0606
D450	450	0	0.178	0.0663
SSC4	250	4	0.054	0.0247
SSC15	250	15	0.054	0.0247
D350SSC15	350	15	0.105	0.0606

The location of the points used for the analysis of the sensitivity cases are the same as those used in the hydrodynamic only sensitivity analysis (see Figure 5.10).

7.2.2 Sediment Size

Figures 7.2 to 7.4 show the bed evolution results for the D350 and the D450 cases compared to the initial case. It can be seen that an increase in sediment size results in a decrease in the overall evolution after five days. This is the expected result due to the fact that the settling velocity is proportional to the sediment size. The larger sediment size requires larger currents to mobilise and deposit the sediment resulting in a decrease in the overall growth across the sandbanks. The areas of deposition remain consistent between the tested models concentrated around the flanks and crests of the sandbanks although the magnitude of the overall evolution is significantly reduced. On average the final evolution compared to the initial case is reduced by 84.35% for the D350 case and by 91.39% for the D450 case. A similar consistency is noted for the areas of erosion in the domain, whereby compared to the initial case there is a reduction in the final evolution of 73.11% for the D350 case and 84.20% for the D450 case. It can also be noted from Figures 7.2 to 7.4 that there is a much greater similarity in the pattern of the evolution for the first two days of the simulation, after which the evolution patterns diverge into more distinctive patterns for the remaining three. This

occurs at the transition between the weaker neap tides and the more dominant spring tides. This means that the model suggests that the weaker tidal currents have very little impact on sediment transport and sandbank growth regardless of the sediment size used, but the stronger tidal currents are able to mobilise smaller sediments causing accelerated growth and migration. It can be concluded that in order to accurately study the impact of tidal currents on morphology, whether we are considering 2D or 3D hydrodynamics, that accurate validation data of the sediment size is highly important. The majority of previous studies that are analysed (see Chapter 2) have often used historical bathymetric charts spanning long time periods as validations for their theories and results of changing coastal morphology. However, this would prove ineffective in this case where the sensitivity and final modelling (to be discussed later) are taken over much shorter time scales.

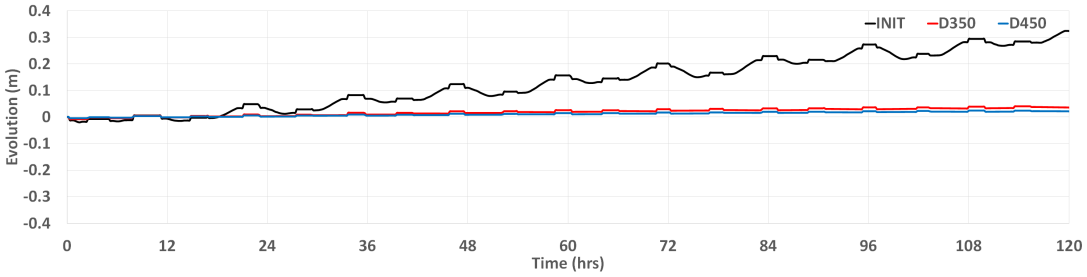

Figure 7.2: Sensitivity of the bottom evolution to sediment size at the crest

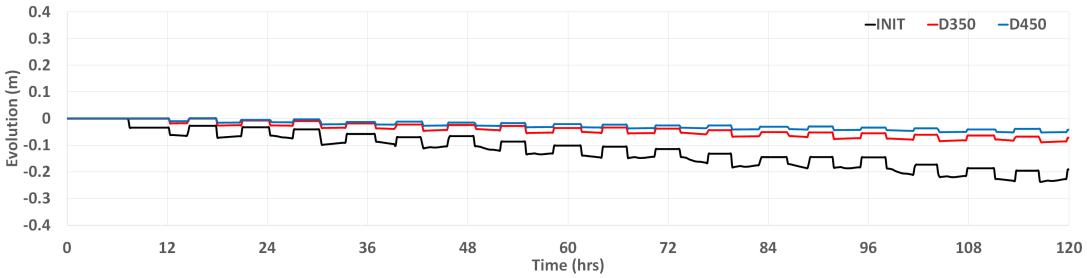

Figure 7.3: Sensitivity of the bottom evolution to sediment size in the troughs

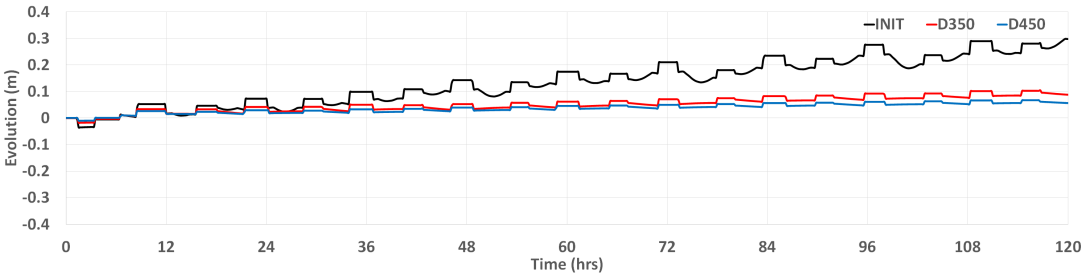

Figure 7.4: Sensitivity of the bottom evolution to sediment size at the flanks

7.2.3 Suspended Sediment Concentration

Figures 7.5 to 7.7 show the bed evolution for the SSC4 and SSC15 cases compared to the initial case. They show that the initial suspended sediment concentrations have very little impact on overall evolution. However, it is worth noting that the tested values of initial concentration are small. It is also important to consider that depth averaged concentrations do not necessary account for the fact that observed larger concentrations nearer the bed could have a greater impact on whether sediment is eroded from or deposited on sandbanks. Also the model is tested under normal tidal conditions and therefore does not account for storm conditions where larger amount of suspended sediment would be present.

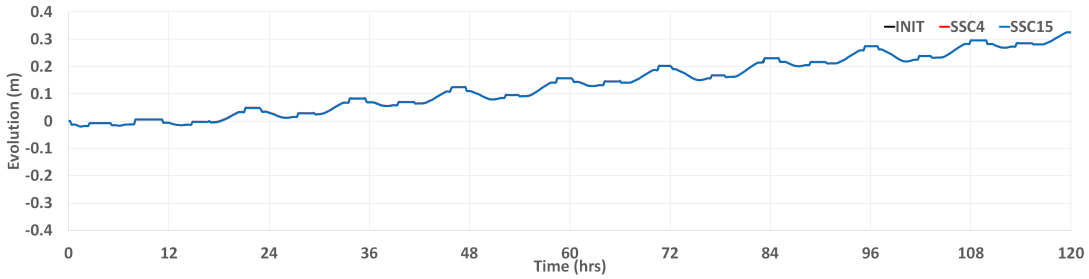

Figure 7.5: Sensitivity of the bottom evolution to initial concentration at the crest

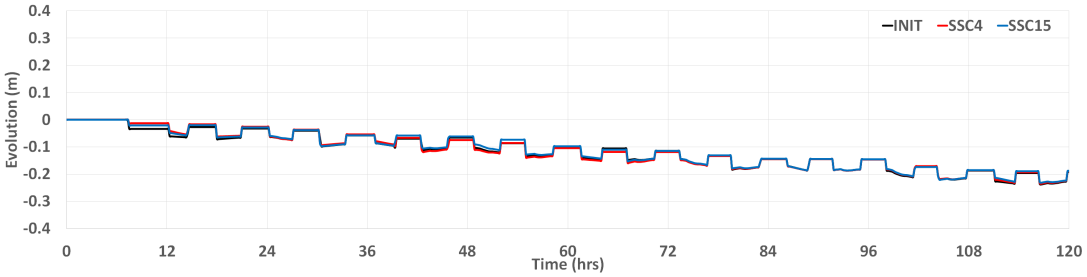

Figure 7.6: Sensitivity of the bottom evolution to initial concentration in the troughs

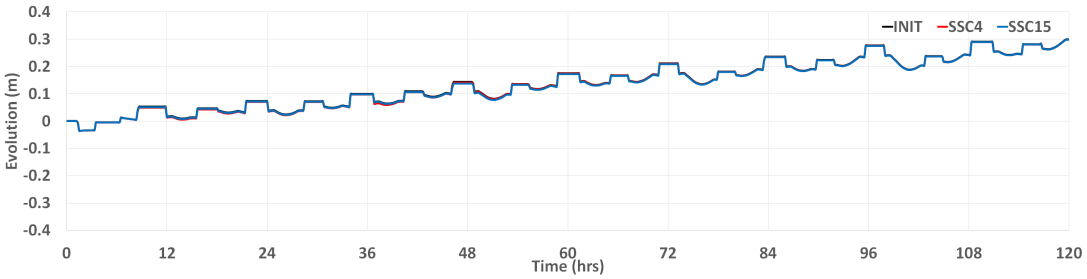

Figure 7.7: Sensitivity of the bottom evolution to initial concentration at the flanks

Figures 7.8 to 7.10 show the bed evolution time series for the D350SSC15 case. Here, there seem to be larger changes in the evolution when accounting for the initial concentration with a sediment size of 350µm than there is for a size of 250µm. For example, at the crest when there is an initial concentration at the end of the simulation the bed level has decreased whereas without an initial concentration it increased. This could be because the higher settling velocity that results from the increased sediment size means that the suspended sediment is not being deposited. Therefore the overall bed evolution is reduced.

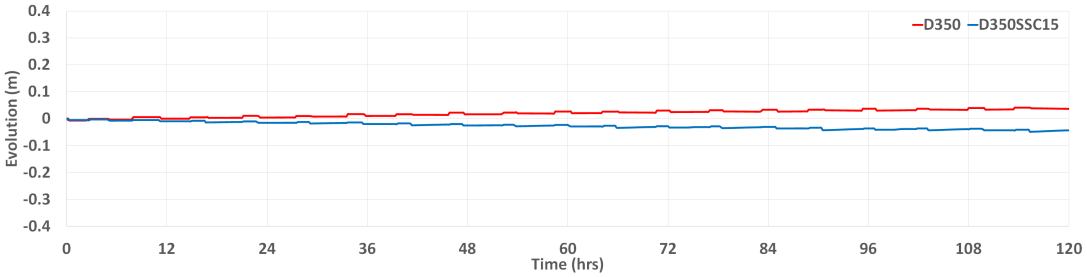

Figure 7.8: Sensitivity of the bottom evolution to sediment size and concentration at the crest

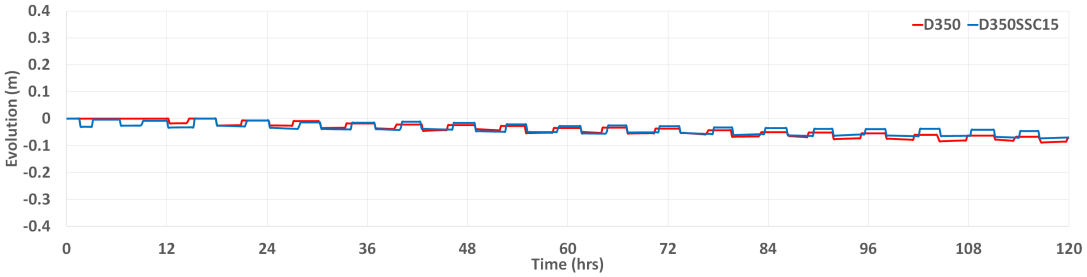

Figure 7.9: Sensitivity of the bottom evolution to sediment size and concentration in the troughs

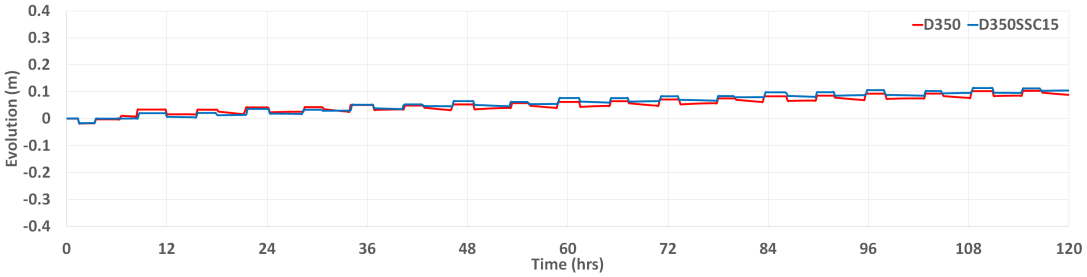

Figure 7.10: Sensitivity of the bottom evolution to sediment size and concentration at the flanks

7.2.4 Waves

The next phase of the morphodynamic modelling is to determine the influence of waves on the sediment transport rates and bed level changes. Normal wave conditions and storm wave conditions can have a significant impact on the morphological behaviour of sandbanks that cannot be accounted for by considering just

tidal conditions in the model. The wave models are set up using TELEMAC2D coupled with both SISYPHE and TOMAWAC. The 2D hydrodynamic setup is the same as previously described in Chapter 5, and the morphodynamic setup is the same as the D350SSC15 case in the previous section. The wave data used for the input into TOMAWAC is sourced from BOC MetOcean [BOC Metocean B.V., 2020] which provides the wave height and direction in addition to peak period at a specified location. Data covering the period of a year is taken at 54°N, 2°E. The wave data is analysed to give the values of the wave parameters such as initial direction, significant wave heights and wave periods which are directly fed into the model. The results of this analysis are shown in Figures 7.11 to 7.13.

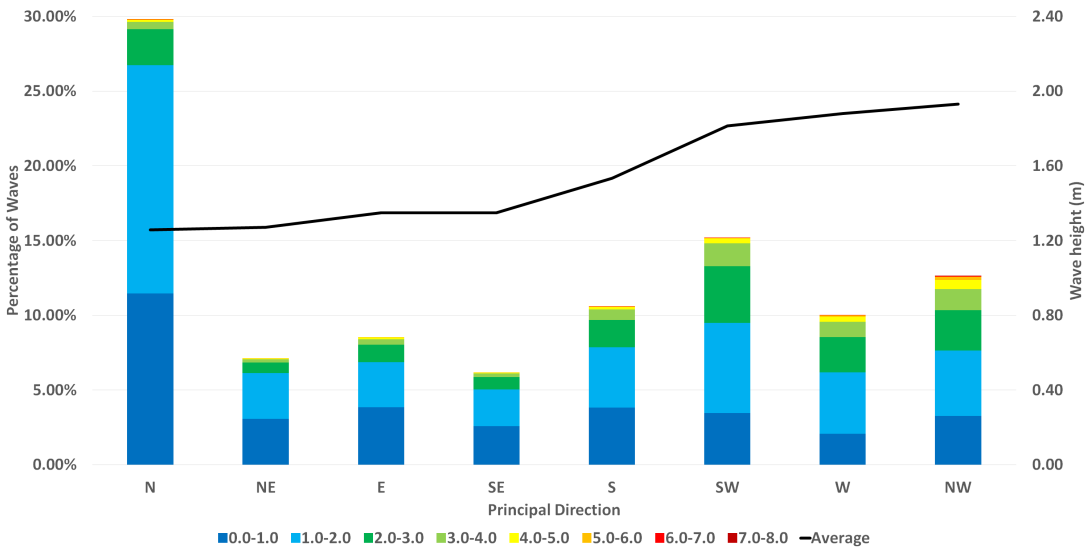

Figure 7.11: Wave heights by principal direction

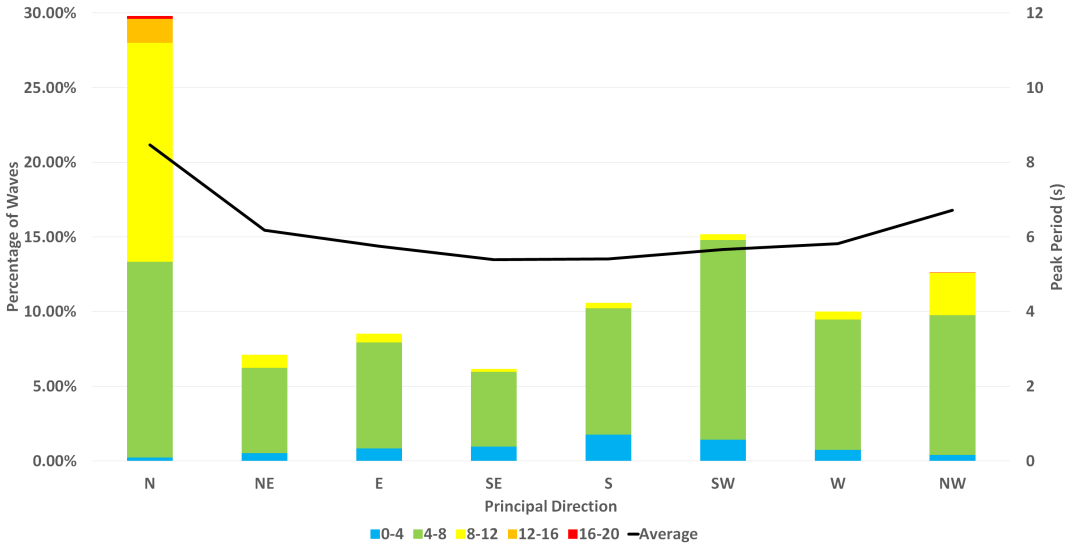

Figure 7.12: Wave period by principal direction

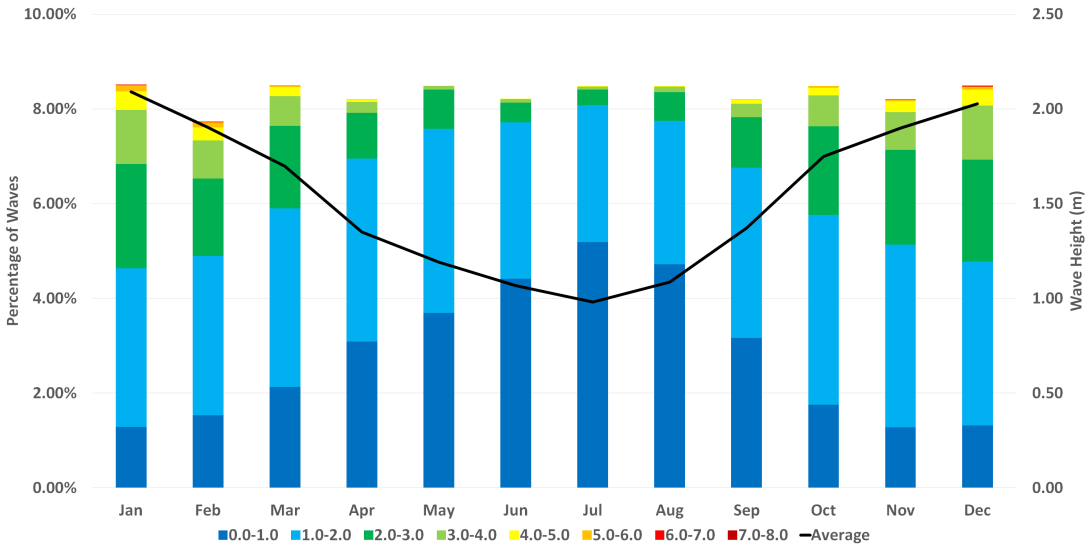

Figure 7.13: Wave heights by month

It can be seen that the majority of waves are coming from the North, which is similar to the conclusions in the literature. As such, that the wave conditions are applied at the northern boundary with the waves travelling south across the domain. The initial significant wave height is taken as 1.5m, representative of the average of the data as a whole. The assigned principal direction was 180 degrees

(i.e. the waves are travel from the North boundary and towards the South of the domain). The minimum period of the waves is 2s up to a maximum of 20s. The wave modelling in this research uses the JONSWAP spectrum [Hasselmann et al., 1973]. The wave model was run for a period of 15 days with the wave parameters being directly fed into the equations used by SISYPHE to calculate the wave induced sediment transport (see section 3.2.3.6).

Figures 7.14 and 7.15 show the wave height distribution across the whole domain for a typical flood and ebb tide. It can be seen that the larger wave heights, in the region of 1.5-2m, are present in the Northwest of the domain. The large waves travel south across the domain as the tide changes from flood to ebb. During the ebb tides, the larger wave heights are more towards the centre of the domain.

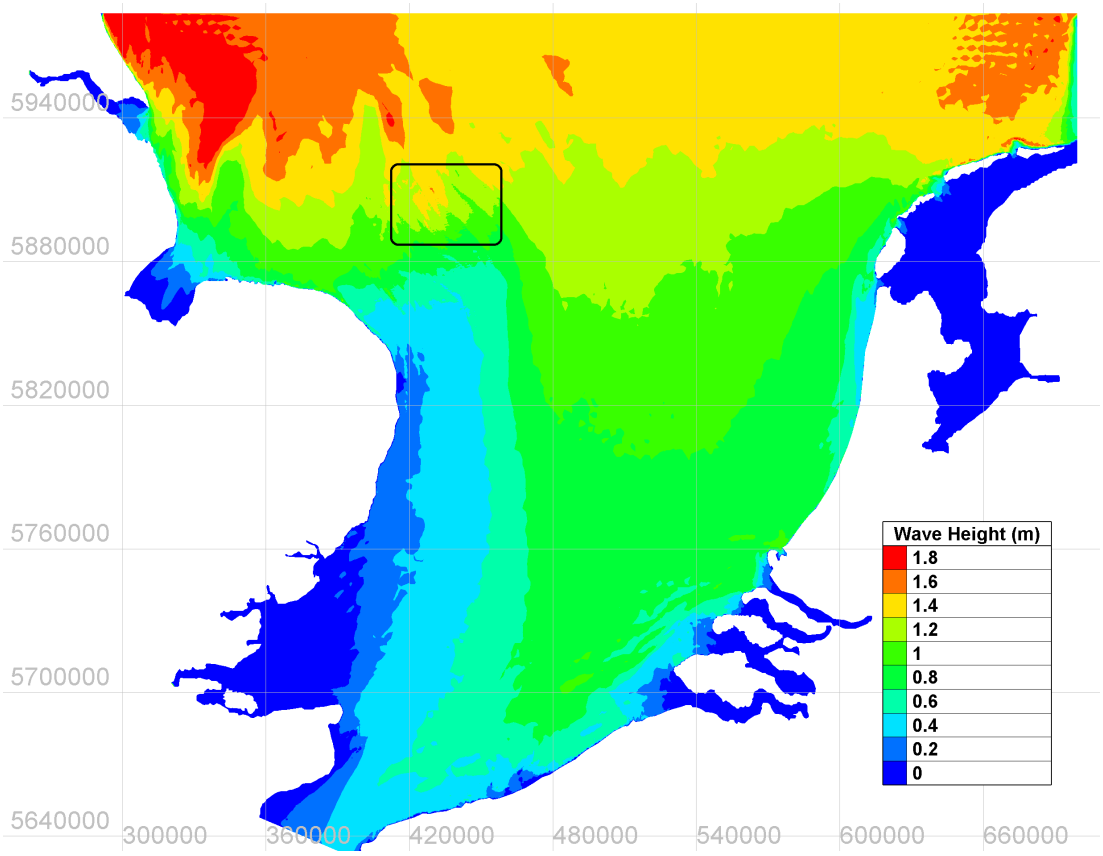

Figure 7.14: Wave height distribution across the whole domain during flood tides

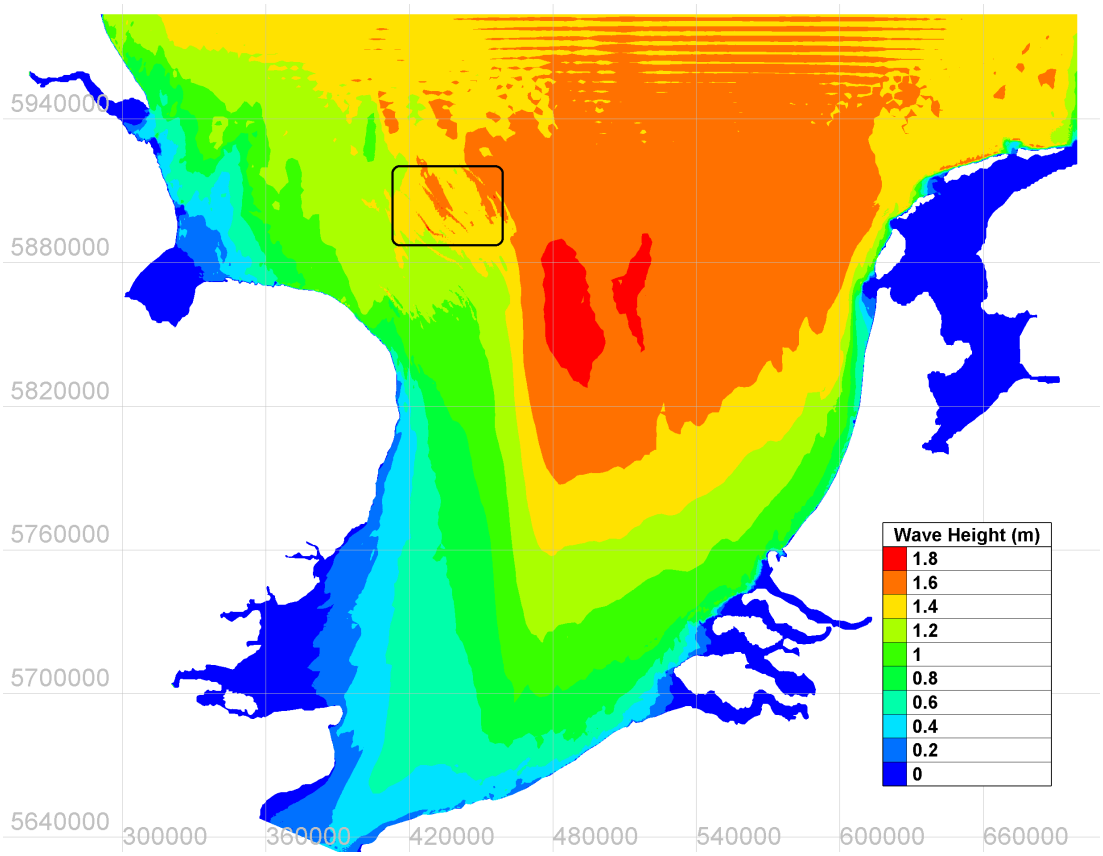

Figure 7.15: Wave height distribution across the whole domain during ebb tides

Figures 7.16 and 7.17 show the wave height distribution in the region of the Norfolk banks (highlighted by the black boxes in Figures 7.14 and 7.15). The wave heights are roughly 20-40cm larger during the ebb tides compared to the flood tide. Therefore it would be expected that the influence of the wave conditions on the morphological changes would be greater during the ebb tides compared to the flood tides. The larger wave heights are seen over the crests of the sandbanks with smaller wave heights in the troughs. This would suggest that the influence of waves would have a greater impact on the sediment transport rates on the sandbank crests. There appears to be no significant difference between the wave heights between the nearshore and offshore troughs of an individual sandbank. However, the sandbanks closer to the shore experience smaller waves compared to those further offshore. This would suggest that the influence of waves on sediment transport rates is greater in offshore regions and could support the idea that the

sandbanks are migrating further offshore.

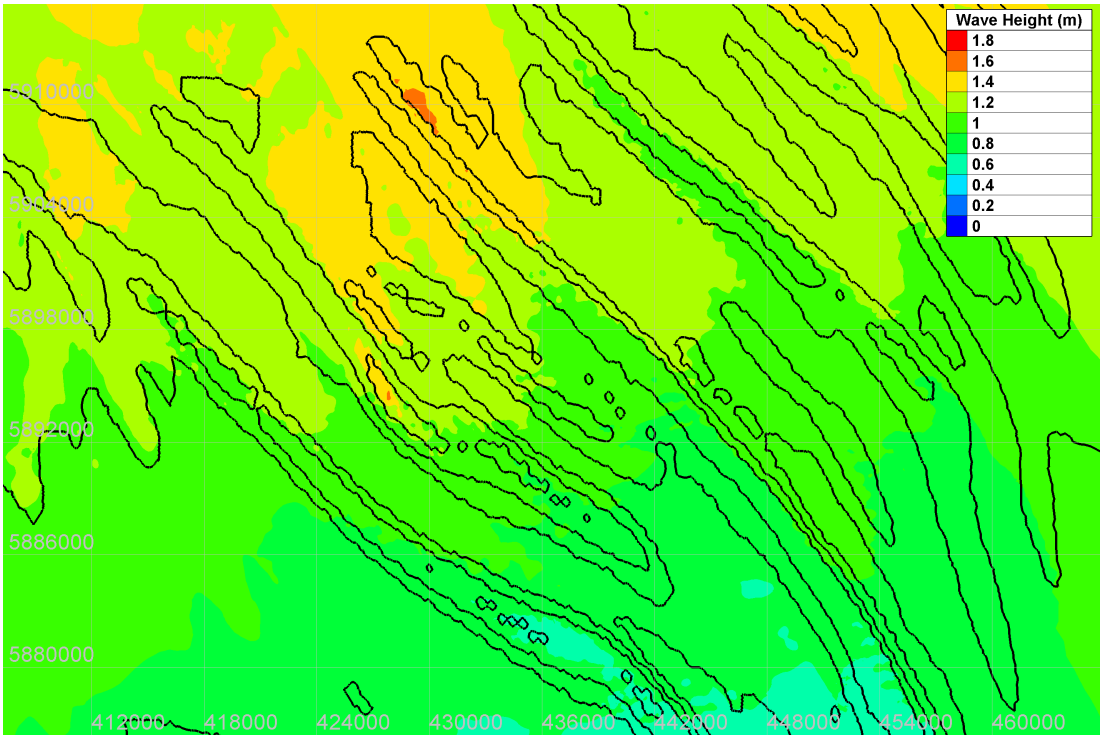

Figure 7.16: Wave height distribution in the sandbank region during flood tides

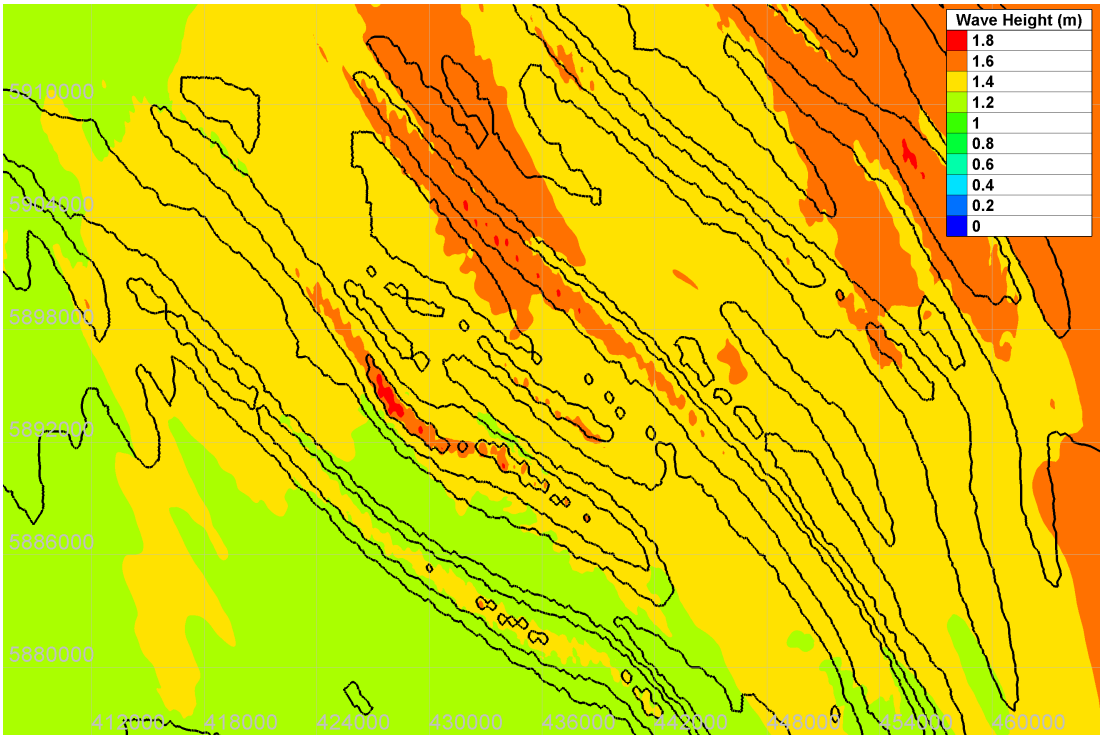

Figure 7.17: Wave height distribution in the sandbank region during ebb tides

Figures 7.18 and 7.19 show the evolution after 30 days of simulation in the region of the Norfolk Offshore banks with the imposed wave conditions. Figure 7.20 shows the bed evolution of the analysis line. The green line represents the original profile and the red and black lines represent the profile after 30 days of simulation with and without imposed wave conditions respectively. These figures show that the bed is eroding in the trough areas and depositing on the slopes and crest. The amount of deposition is greater on the nearshore slopes compared to the offshore slopes, a result that agrees with previous understanding of the morphodynamic behaviour of sandbanks.

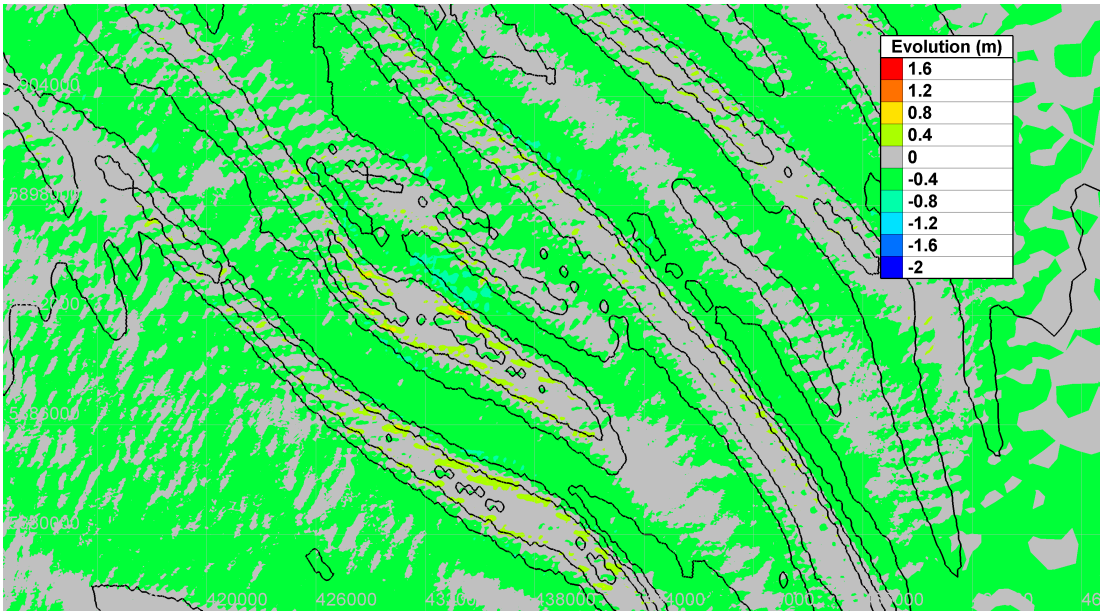

(a) t = 7.5 days

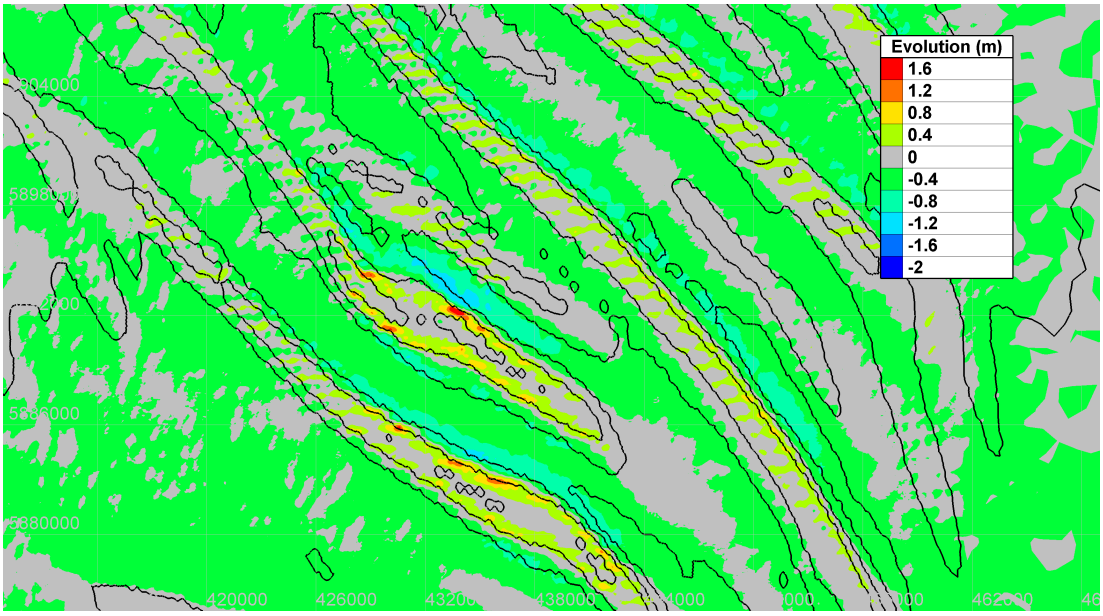

(b) t = 15 days

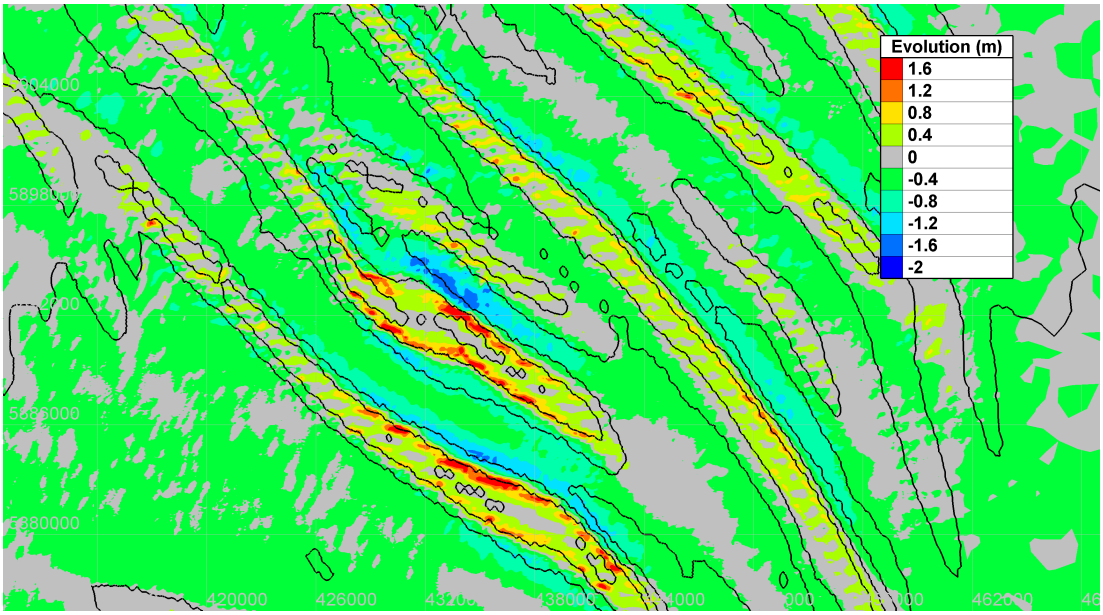

(c) t = 22.5 days

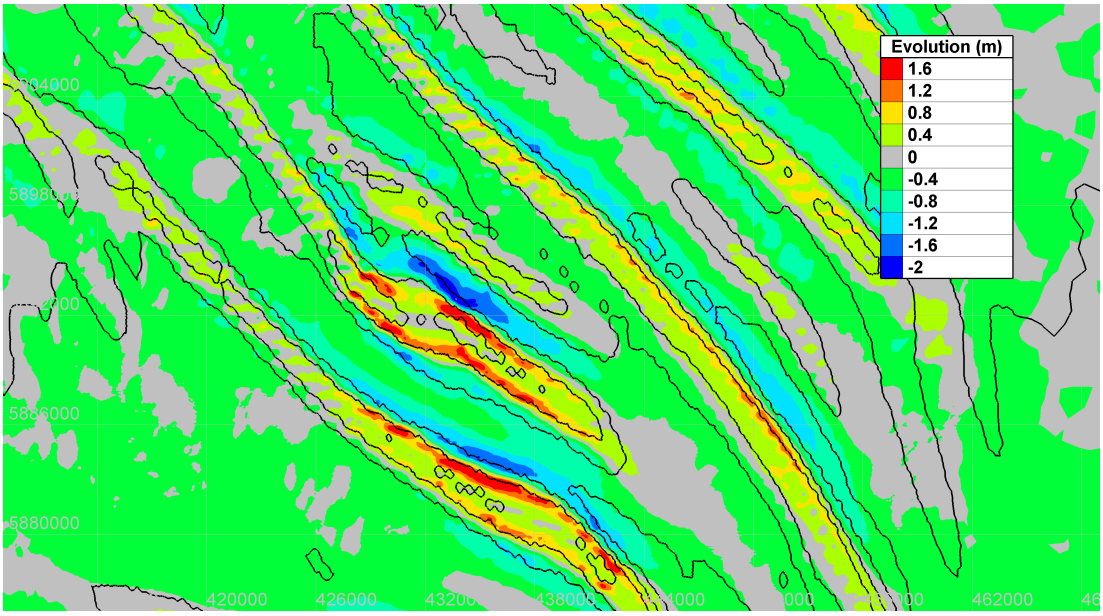

(d) t = 30 days

Figure 7.18: Bed evolution of the Norfolk Banks throughout the simulation without wave conditions

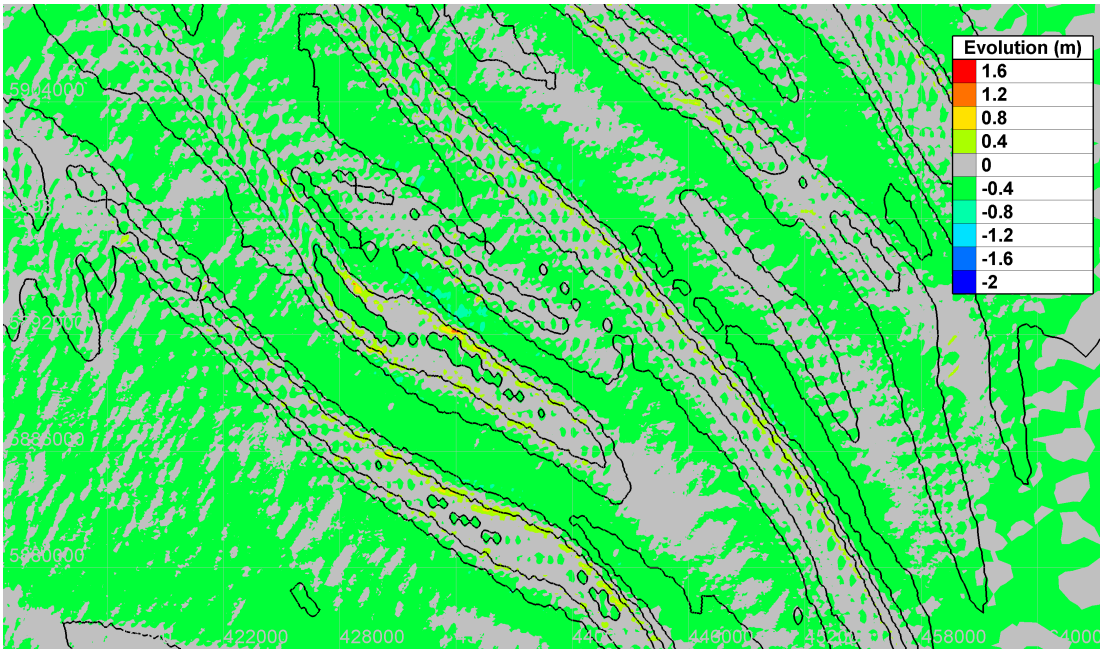

(a) t = 7.5 days

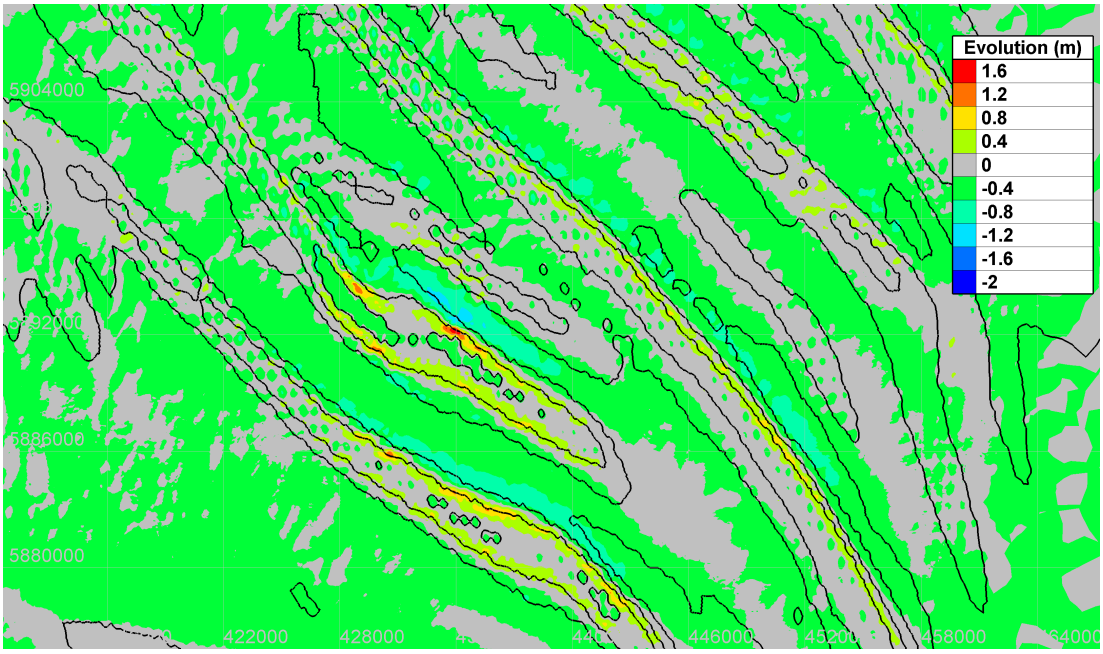

(b) t = 15 days

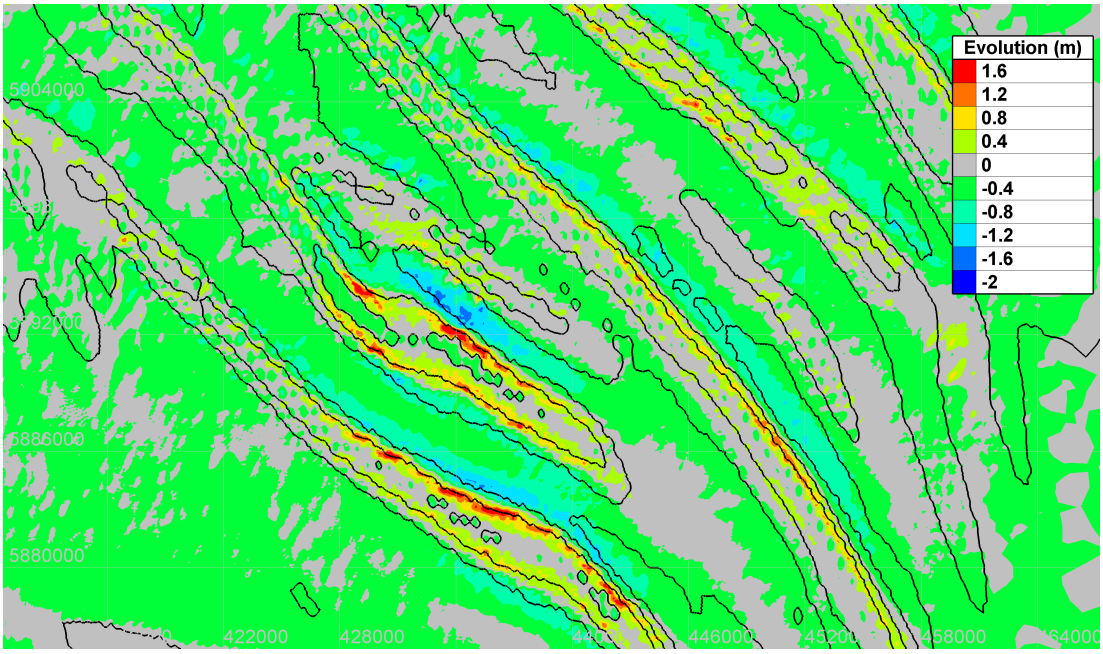

(c) t = 22.5 days

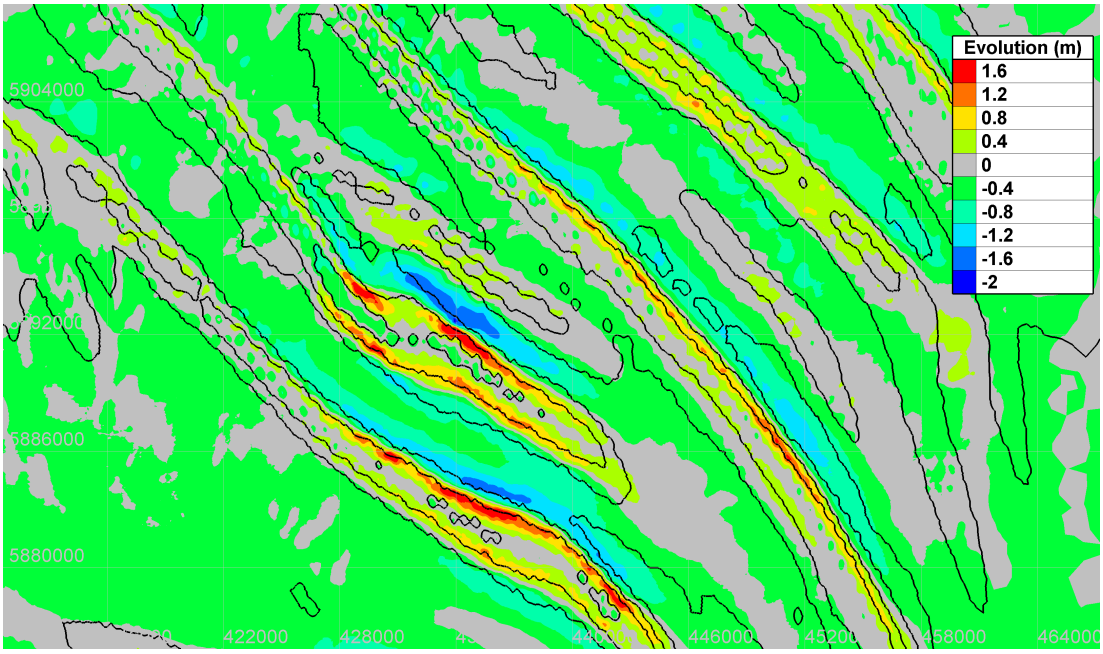

(d) t = 30 days

Figure 7.19: Bed evolution of the Norfolk Banks throughout the simulation with wave conditions

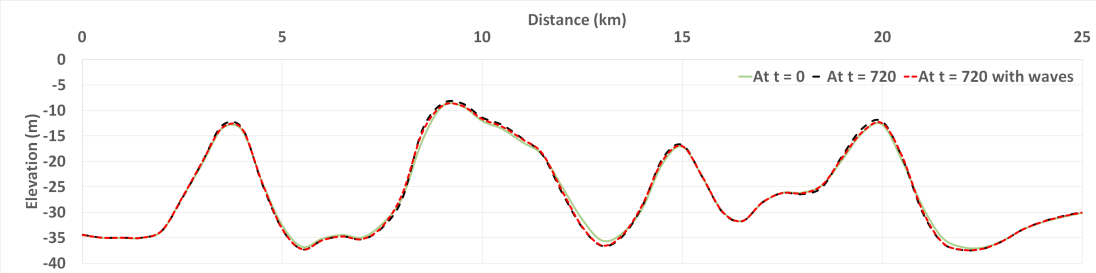

Figure 7.20: Bed profile after 30 days with and without wave conditions

Figure 7.21 shows the evolution at the three chosen points. It can be seen that in the nearshore trough, the consideration of the wave conditions does not seem to impact the evolution whilst in the offshore trough there is a small decrease in the bed evolution (i.e there is more erosion). At the crest it can be seen that without considering the wave condition, sediment is deposited on the crest for the length of the simulation. However, when the wave condition is considered this reverts to erosion at this point. The trend of the wave condition reducing the level of deposition is repeated at other crest locations, but this is the only point along the line where the wave condition reverts the state from deposition to erosion (or vice versa). This crest point is the shallowest crest along the profile suggesting there is a critical depth at which this behaviour occurs. Consideration of the wave condition is therefore vital for studying sandbank growth as otherwise it would imply that the crest heights would continue to increase indefinitely (or at least until they reached the surface). Therefore, artificially increasing the heights of sandbanks may prove beneficial to the protection of nearby coastlines to a degree. However, it should be considered that for the sandbank where the crest is actually eroding, this would prove wasteful as the material would be washed away. The bed level changes rapidly increase for spring tides compared to neap tides. The 15 day simulation covers one full neap followed by one full spring cycle, so continuation of the simulation beyond this time would be expected to show similar cyclical behaviour until an equilibrium point is reached.

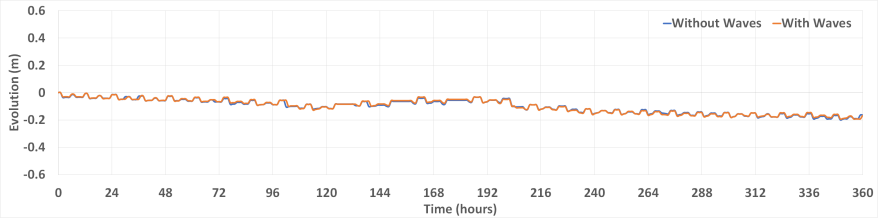

(a) Nearshore trough

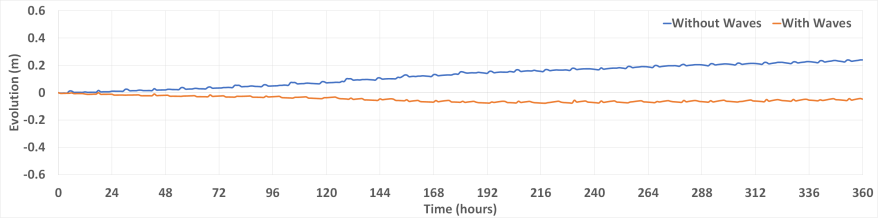

(b) Crest

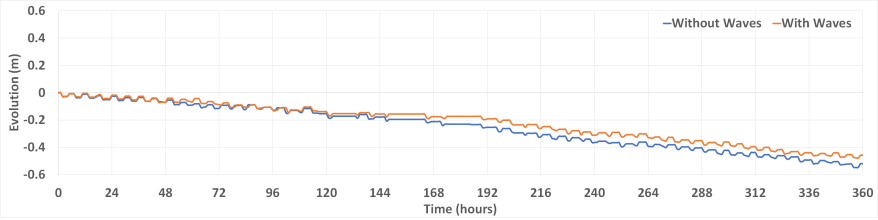

(c) Offshore trough

Figure 7.21: Time series of evolution with and without waves at the nearshore trough, crest and offshore trough

7.2.5 Discussion

The sensitivity testing of the morphodynamic model highlights the importance of ensuring the parameter values used accurately reflect the site conditions and the need for validation data when assessing morphological models. It is important to highlight that the results can also be affected by the simplicity of the case scenarios. The assumptions made here (about sediment sizes and concentrations) are justifiable but do not necessarily reflect an accurate representation of the underlying complex processes that govern sandbank growth. For example, sediment sizes here are tested as a uniform sediment but as discussed previously, the observation data suggests that the sediment in the domain is widely non-uniform and highly variant in its non-uniformity. Modelling the sediment as a non-uniform

distribution would add another layer of complexity into the model but could potentially give more reliable results. The question then becomes whether or not the increased reliability of the results is balanced against other factors such as computational time.

The wave model considered here was simple in terms of the wave processes that were included in the source terms (see section 3.2.4.4 and equation 3.91). Further improvement of the wave model would include better accuracy in the way that the source terms considered are modelled but also modelling more of the available source terms. It appears from the results that the effects of the wave model on morphological change are more significant in areas of shallower depth. This therefore may not have a significant effect on the results in the troughs or out in the deep water regions but would on the slopes and nearer the crests. Storm waves were not considered here as part of the wave modelling but the effects of storm waves are known to play a significant role in the short term morphological behaviour of sandbanks and the model could be extended to include such scenarios.

7.3 Morphodynamic Modelling with 3D Hydrodynamics

7.3.1 Model Configuration

The morphodynamic model is next developed to consider the effects of 3D hydrodynamics. The 3D hydrodynamics aspect (modelled by TELEMAC3D) is the same as described in the previous chapter and the 2D model for comparison is the same as described earlier in this chapter. The only difference in the configuration of the models is the initial setup. During preliminary testing (which is not described here), the 3D model appeared to become unstable with the applied wave conditions and morphodynamics. In order that this instability would not affect the bed level changes, the model is run with a double hotstart: first the TELEMAC3D is run by itself for a period of 5 days, then the wave conditions are applied (by coupling with TOMAWAC) and run for 15 days and then the mor-

phodynamic conditions are applied (by coupling with SISYPHE) for a period of 30 days. This procedure is also repeated for the 2D model to ensure consistency.

7.3.2 Comparison of Morphological Changes with 2D/3D Hydrodynamics

Figures 7.22 and 7.23 show the progressive evolution throughout the simulation. It can be seen that the 3D model is predicting a much greater scale of erosion in the region highlighted.

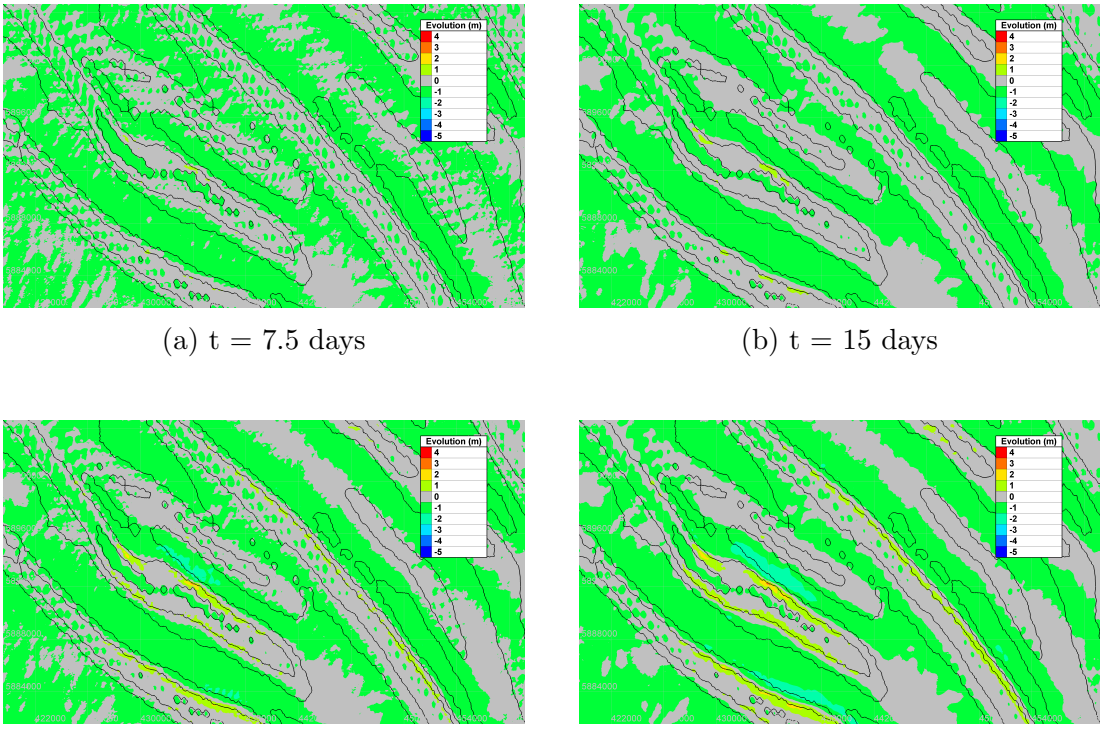

(a) t = 7.5 days

(b) t = 15 days

(c) t = 22.5 days

(d) t = 30 days

Figure 7.22: 2D model evolution of the Norfolk Banks throughout the simulation

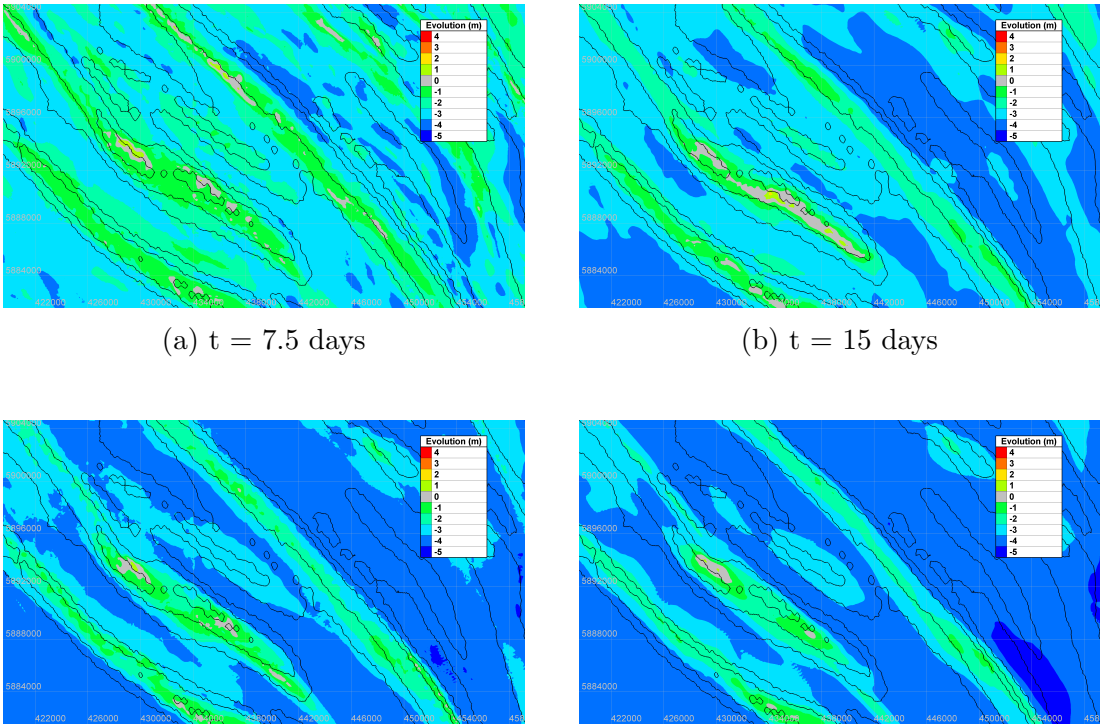

(a) t = 7.5 days

(b) t = 15 days

(c) t = 22.5 days

(d) t = 30 days

Figure 7.23: 3D model evolution of the Norfolk Banks throughout the simulation

Figure 7.24 shows the comparison between the 2D and 3D models at the nearshore trough. The evolution trends are similar between the models in that they both follow a sort of linear progression and both exhibit erosion. However there is a large discrepancy between the models in terms of the magnitude of the evolution. This could be a result of the large difference in the magnitude of both the bedload and the suspended transport rates. The 2D model shows bedload transport rates of the orders of 10^{-7} to 10^{-6} whereas the 3D model shows are of the order of 10^{-6} to 10^{-5}. Figure 7.24b is showing the times where the largest bedload transport rate occurred. The suspended transport rate shows a similar trend whereby the 3D model transport rate is a rough factor of 10 times larger than the 2D model.

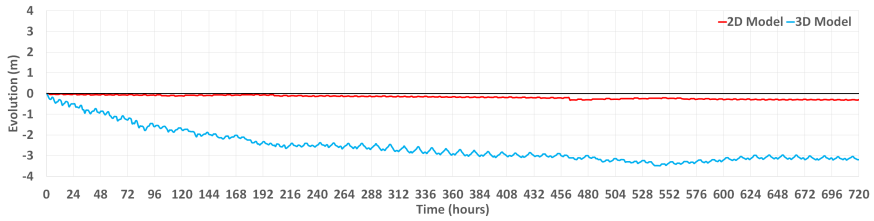

(a) Evolution

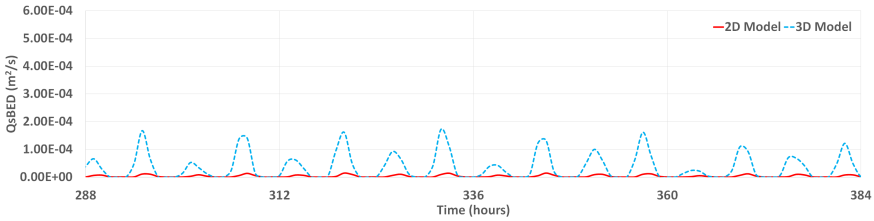

(b) Bedload Transport Rate

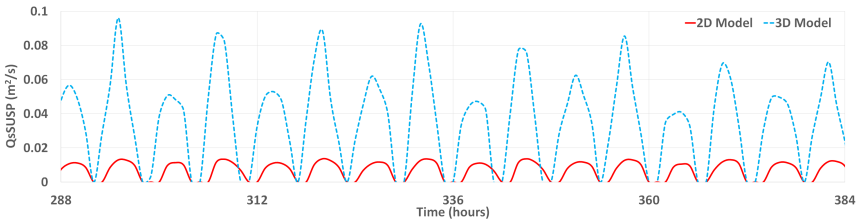

(c) Suspended Sediment Transport Rate

Figure 7.24: Comparison of 2D and 3D evolution, bedload and suspended sediment transport rates at the nearshore trough (Point 14)

Figure 7.25 shows a comparison between the 2D and 3D models with respect to the evolution and the sediment transport rates at the crest location. The pattern of evolution is markedly different for the 3D model compared to the troughs. At this location the 2D model shows a stable equilibrium whereby throughout the simulation there are only small changes in the bed level. However, the 3D model shows a cyclical behaviour where during the spring tides there is overall erosion and during the neap tides there is growth. This can be interpreted to conclude that both models are suggesting that the sandbanks are in a dynamic equilibrium but the 3D model is showing larger scale variations in the bed level with the tidal cycles and wave conditions.

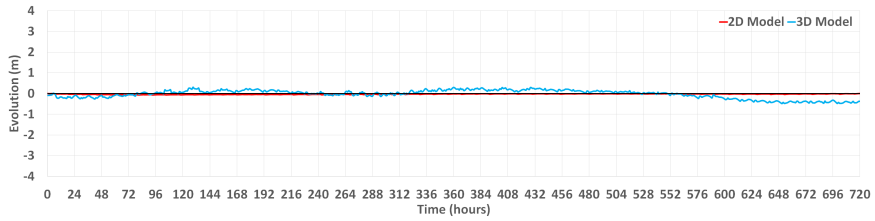

(a) Evolution

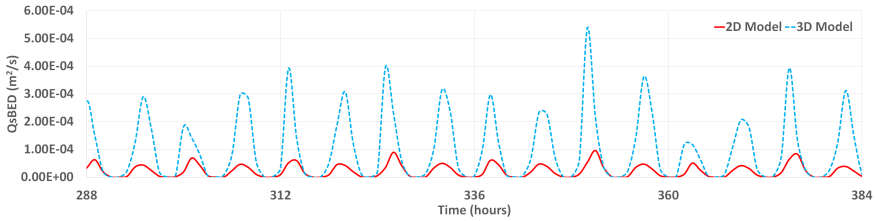

(b) Bedload Transport Rate

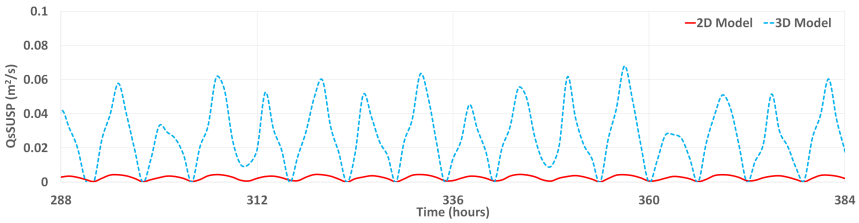

(c) Suspended Sediment Transport Rate

Figure 7.25: Comparison of 2D and 3D evolution, bedload and suspended sediment transport rates at the crest (Point 20)

Figure 7.26 shows a comparison between the 2D and 3D models with respect to the evolution and the sediment transport rates at the offshore trough location. The pattern of evolution is similar to that of the nearshore trough with the exception of the scale of the erosion. Again at this location the 2D model shows a much smaller scale of erosion compared to the 3D model. In terms of sediment transport rate, again the results and patterns are comparable to the nearshore trough location albeit the magnitudes are slightly different (between the two locations). There is still the discrepancy in the scale of the magnitude between the 2D and 3D models.

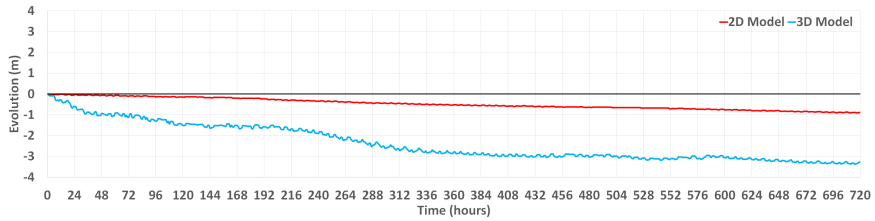

(a) Evolution

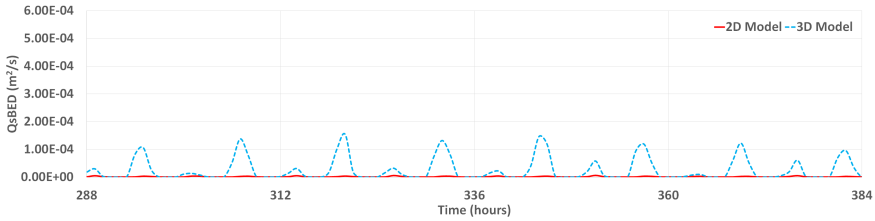

(b) Bedload Transport Rate

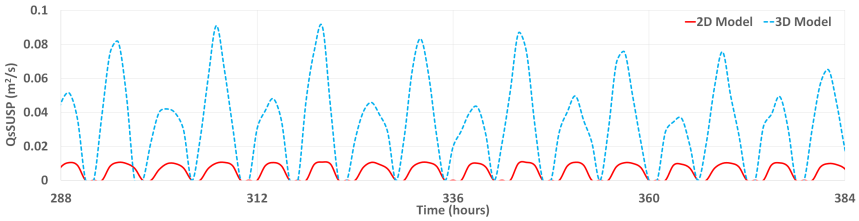

(c) Suspended Sediment Transport Rate

Figure 7.26: Comparison of 2D and 3D evolution, bedload and suspended sediment transport rates at the offshore trough (Point 27)

Analysis of the whole profile shows that some points display similar final evolution values (i.e. after the 30 days of simulation) but display a different pattern of how they reach this value. The vast majority of points show a large difference though, with the 3D model predicting much greater levels of erosion and very little deposition. Figure 7.27 and Table 7.2 show the amount of evolution that occurs in each quarter of the simulation (roughly approximately equal to the individual spring and neap tidal cycles). Here it can be seen that as the simulation progresses, the differences between the 2D and 3D models tends to decrease. Comparison of each quarter shows that the first quarter always exhibits a large difference between the 2D and 3D models. By the final quarter the models are comparable at most points. This could suggest that during the first quarter of the simulation there is still some instability in either the sediment transport model or in the application of the wave conditions. This instability is observed during

testing and could potentially be solved by running the wave conditions for longer before starting the sediment transport module or alternatively by increasing the length of the simulation to determine if the excess erosion corrects itself. However, since the bed level change appears to have reached an equilibrium it is less likely that this second approach would yield such a significant change. In a way it can be considered that the results are accurate to an extent, just offset by a fixed value for each point.

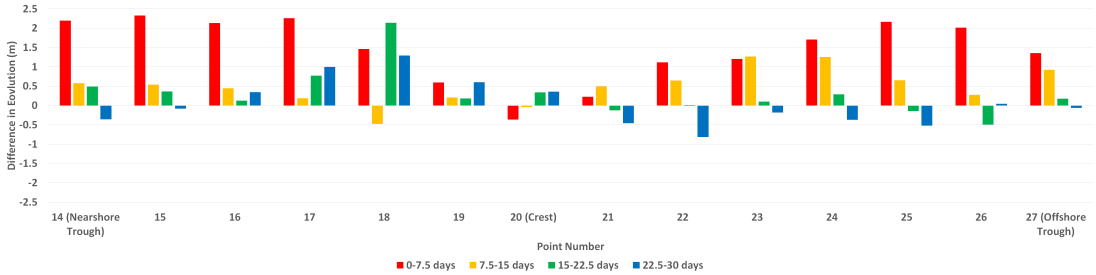

Figure 7.27: Difference in the amount of evolution between the 2D and 3D models that occurs between each spring and neap cycle

Table 7.2: Evolution occurring between two timesteps at each location

Evolution (m) occuring	Nearshore Trough		Crest		Offshore Trough	
between:	2D Model	3D Model	2D Model	3D Model	2D Model	3D Model
0 - 30 days	-0.299	-3.196	-0.001	-0.379	-0.890	-3.275
0 - 7.5 days	-0.052	-2.245	-0.056	0.212	-0.201	-1.556
7.5 - 15 days	-0.100	-0.676	0.038	-0.081	-0.315	-1.232
15 - 22.5 days	-0.077	-0.562	0.000	-0.334	-0.159	-0.329
22.5 - 30 days	-0.070	0.287	0.017	-0.338	-0.216	-0.158

7.3.3 Discussion

The effects of the 3D hydrodynamics on the short and long term evolution of sandbanks are significant. The 3D model shows a larger scale of evolution over the 30 day period which is likely to be as a result of hydrodynamic processes

that are not accounted for when using a 2D model. These include vertical mixing and sediment transport at various locations around the bank, the influence of bed shear stress and friction in 3D to the vertical flow and the influences of turbulence and secondary circulations around the sandbanks. The models developed here considered these issues qualitatively rather than quantitatively. The development of research into 3D morphological models is somewhat limited by the difficulty in establishing these quantities (i.e. through laboratory experiments or through field experiments). When it comes to using numerical models as evidence for coastal engineering projects, (such as schemes to develop natural or artificial sandbanks to provide protection against coastal erosion), using a 3D model has several advantages over a 2D model but also requires greater development of the current understanding.

The model described here is neither calibrated nor validated against field measurements (such as bathymetric surveys). Therefore the specific results have a fairly large degree of uncertainty and are not necessarily a precise picture of the morphodynamic behaviour. However, since the main aim of this research is to determine the differences between the 2D and 3D hydrodynamic modelling and the impact this could have on sediment transport on morphodynamics it is important to establish some idea of what the potential morphodynamic behaviour looks like. However, the results of both the morphodynamic model and the model with the wave conditions are supported to some extent by results from other studies in that the morphodynamic behaviour observed is similar. As such the real limitation of the morphodynamic model is not that it is not accurate in predicting the pattern of the morphodynamic behaviour, more that it is the magnitude of the numerical values that is in doubt.

Chapter 8

Conclusions and Recommendations

8.1 Conclusions

The aim of this research is to use a numerical modelling system to study the effects of 3D hydrodynamics on the morphological evolution of the offshore sandbanks Norfolk coast of the southern North Sea. The modelling system is built using the TELEMAC suite: specifically TELEMAC2D and TELEMAC3D for the 2D/3D hydrodynamics, SISYPHE for the morphodynamics and TOMAWAC for the wave modelling. The system is calibrated and validated through the 2D hydrodynamic modelling. Model sensitivity tests are carried out by varying numerical and physical parameters and measuring the effect on the hydrodynamic outputs. Established models are applied to simulate the morphological evolution around the sandbanks with both 2D and 3D hydrodynamics including the effects of waves. The results from this study can be concluded as follows:

- The 2D hydrodynamic model is calibrated and validated against observation data from the North Sea. In terms of free surface calibration the model output is in good agreement with the observation data at all measurement stations. When validated against a different data set the RMSE value increased for one validation case but showed similar values for the remainder of the test cases. In terms of velocity, the model also showed good agreement with data extracted from the Admiralty chart, but this is a limitation

in that it only provided short term measurements and therefore does not necessarily represent good accuracy compared to time series data.

- The 2D hydrodynamic model is tested to determine its sensitivity to model input parameters. The model is insensitive to the prescribed value of the Coriolis parameter (within reasonably assumed ranges) but showed large sensitivity to the inclusion of the Coriolis force. The model is also fairly insensitive to the turbulence parameter values. In terms of the friction coefficient the model showed more sensitivity to changes in the value of the friction coefficient, but sensitivity to different friction laws is not tested. The model is insensitive to small changes in timestep but there is significant changes in the flow pattern for large increases in timestep.

- The development of the 3D hydrodynamic model sought to determine how the vertical layer structure impacted the overall results and velocity profiles. Three vertical layerings are tested: 5 equally spaced layers, 11 equally spaced layers and a logarithmic profiles. The results showed that the near bed variations in velocity could not be accurately modelled with 5 equally spaced layers. The other two vertical layer structures produced largely similar results.

- Comparison between the 2D model and 3D model in terms of free surface elevation revealed a slight increase in elevation predicted by the 3D model. The differences are slightly larger at the crest compared to in the troughs and appeared to be associated with the spring tides.

- Comparison between the 2D depth averaged velocity and the 3D depth averaged velocity showed that in general the 3D model is predicting higher velocity compared to the 2D model. The difference between the 2D and 3D velocity tended to be larger at the crest compared to the troughs and tended to occur a few hours either side of the peak flow. In the troughs the difference is almost always positive suggesting that the 3D model velocity is almost always higher than the 2D model. Since morphodynamic models often used depth averaged velocities derived from a hydrodynamic model, using a 2D model could result in the velocity values being underestimated

for sediment transport processes. This is especially the case at times of peak flow where sediment transport is greater. Therefore it is possible that sediment transport rates are underestimated by the 2D model.

- Comparison between the 2D depth averaged velocity and the 3D near bed velocity showed significant differences. The average absolute difference is comparable to that of the depth averaged velocity comparison. In the trough, the differences are almost always positive which means that the 3D near bed velocity is greater than the 2D depth averaged velocity. At the crest location, the difference fluctuated between periods of a large negative difference followed by a period of small almost zero difference to a period of a large positive difference. The magnitude of the negative differences are usually greater than the positive differences. Since sediment transport is influenced more by near bed currents it suggests that at times the 3D will be overestimating the velocity and at times underestimating it when compared to the 2D model. This would result in a largely different, but potentially more accurate, sediment transport pattern.

- Comparison between the 2D depth averaged velocity and the 3D surface velocity revealed much larger differences than before. In some cases, the 3D surface velocity is greater than twice the 2D depth averaged velocity. This tended to occur during spring tides at times of peak flow. Surface velocity has an impact on the evolution of the wave field. In shallower waters, increases in surface currents can cause large increases in significant wave height. This in turn impacts the level of erosion and the amount of sediment transport induced by wave currents.

- Both the 2D and 3D models showed a similar expected pattern of sediment transport in that there is a level of erosion in troughs and sediment is transported towards the crest. Where the main differences arose between the two models is in terms of the scale and magnitude of the bed level changes. The 3D model exhibited much larger values of bed level change compared to the 2D model. However, in the latter portions of the simulation the amount of bed level change appeared to be consistent between the two

models. Nevertheless, changes in the patterns at the detailed level are an important factor in coastal management as well as the final outcome.

- The difference in the scale and magnitude of the bed level change initially could be a result of instability in the applied wave conditions causing excessive erosion which then reduces over time. In a way the models are at least similar in terms of results even though there appears to be a significant difference in the final bed level change.

8.2 Recommendations for Future Work

The research presented here by no means offers an exhaustive study in the areas of sandbanks and numerical modelling. The author believes that the following points highlight potential areas where the work here could be improved or expanded to address some of the assumptions and limitations previously described and provide further knowledge and understanding in this area:

- The 2D morphodynamic model requires calibration and validation. This could be done by a combination of laboratory and field experiments. For example, fluorescent sand tracing experiments could be done in situ to determine whether the model is accurately predicting the sediment transport pathways. Similarly field measurements such as tidal current data could be used to calibrate and validate the vertical velocity profiles simulated by the 3D hydrodynamic model. Accurate knowledge of the flow structure at different depths at the same location would enable the model to be calibrated more accurately and would further improve the accuracy of the morphodynamic models which rely on accurate hydrodynamic data.

- The sediment transport modelling done here with SISYPHE is coupled with the 2D and 3D hydrodynamics. TELEMAC3D also possesses an inbuilt sediment transport module which can be used to model sediment transport processes without the need for coupling with SISYPHE. These different sediment transport models could be compared with each other and with the 2D sediment transport models and field observations. Modelling over longer

time periods would also provide useful information about the migratory behaviour of sandbanks.

- Wave conditions play a significant role in sandbank and coastline evolution. The models developed here could be further improved by implementing storm wave conditions to study the impact of storm waves on sandbank morphology and their recovery response to large storm waves.

- Sandbanks are a global feature on many continental shelves. It would be beneficial to see how the model developed here could be applied to other study sites. Expansion of the domain to cover larger areas of the North Sea would also provide useful insight into the interaction between global tidal currents and the local regional currents and the impact this could have on sediment pathways. The future of coastal management could follow a more integrated approach whereby different modelling tools are used together to model different aspects of coastal morphology. For example, the 3D hydrodynamic model developed here could be integrated into a different sediment transport model that simulates sandbank evolution.

- With climate change and sea level rise at the forefront of society thinking, it would prove a simple but useful avenue to expand and explore the developed model. The effects of sea level rise could be implemented into hydrodynamic models to determine the impact this on tidal velocities, sediment transport pathways and sandbank morphology.

Appendices

A TELEMAC2D Steering File

```
/ ------------------------------------------------------------------
/                    TELEMAC2D - HYDRODYNAMICS
/                    NORTH SEA SANDBANKS
/ ------------------------------------------------------------------
/
/ ------------------------------------------------------------------
/                    1. GENERAL INFORMATION/SETUP
/ ------------------------------------------------------------------
/
  TITLE                                  = 'North Sea Sandbanks'
  TIMESTEP                               = 60
  DURATION                               = 432000
  GRAPHIC PRINTOUT PERIOD                = 432000
  LISTING PRINTOUT PERIOD                = 60
/
  INFORMATION ABOUT SOLVER               = YES
  MASS BALANCE                           = YES
/
/ ------------------------------------------------------------------
/                    2. INTERNAL COUPLING
/ ------------------------------------------------------------------
/
  COUPLING WITH                          = SISYPHE,TOMAWAC
  COUPLING PERIOD FOR SISYPHE            = 1
  COUPLING PERIOD FOR TOMAWAC            = 1
  SISYPHE STEERING FILE                  = SIS_NS5.cas
  TOMAWAC STEERING FILE                  = TOM_NS5.cas
/
/ ------------------------------------------------------------------
/                    3. FILE INPUTS/OUTPUTS
/ ------------------------------------------------------------------
/
  GEOMETRY FILE                          = NorthSeaGeometry.slf
  BOUNDARY CONDITIONS FILE               = NorthSea_BC_1.cli
/
  VARIABLES FOR GRAPHIC PRINTOUTS        = 'B,U,V,S,H'
  RESULTS FILE                           = NorthSeaResults_COUPLED.slf
/
/ ------------------------------------------------------------------
/                    4. BOUNDARY CONDITIONS
/ ------------------------------------------------------------------
/
  PRESCRIBED ELEVATIONS                  = 0;0;0;0
  PRESCRIBED VELOCITIES                  = 0;0;0;0
  PRESCRIBED FLOWRATES                   = 0;0;0;0
/
/ ------------------------------------------------------------------
/                    5a. INITIAL CONDITIONS - STANDARD
/ ------------------------------------------------------------------
/
  COMPUTATION CONTINUED                  = NO
  INITIAL CONDITIONS                     = 'TPXO SATELLITE ALTIMETRY'
  MINOR CONSTITUENT INTERFERENCE         = YES
  ORIGINAL DATE OF TIME                  = 2017;05;23
  ORIGINAL HOUR OF TIME                  = 00;00;00
/
/ ------------------------------------------------------------------
/                    5b. INITIAL CONDITIONS - HOTSTARTED
/ ------------------------------------------------------------------
/
  COMPUTATION CONTINUED                  = YES
```

```
    INITIAL TIME SET TO ZERO                                = YES
    PREVIOUS COMPUTATION FILE                               = 'NorthSeaResults_HOTSTART.slf'
    ORIGINAL DATE OF TIME                                   = 2017;05;28
    ORIGINAL HOUR OF TIME                                   = 00;00;00
/
/ ------------------------------------------------------------------
/                       6. TIDAL CONDITIONS
/ ------------------------------------------------------------------
/
    TIDAL DATABASE                                          = 2
    BINARY DATABASE 1 FOR TIDE                              = 'D:\tpxo7.2\h_tpxo7.2'
    BINARY DATABASE 2 FOR TIDE                              = 'D:\tpxo7.2\u_tpxo7.2'
/
    OPTION FOR TIDAL BOUNDARY CONDITIONS                    = 1;1;1;1
    OPTION FOR LIQUID BOUNDARIES                            = 2;2;2;2
    GLOBAL NUMBER OF THE POINT TO CALIBRATE HIGH WATER       = 24522
    GEOGRAPHIC SYSTEM                                       = 2
    ZONE NUMBER IN GEOGRAPHIC SYSTEM                        = 31
    COEFFICIENT TO CALIBRATE SEA LEVEL                      = 0.07
    COEFFICIENT TO CALIBRATE TIDAL RANGE                    = 1.13
    COEFFICIENT TO CALIBRATE TIDAL VELOCITIES               = 0.85
/
/ ------------------------------------------------------------------
/                       7. PHSYICAL PARAMETERS
/ ------------------------------------------------------------------
/
    LAW OF BOTTOM FRICTION                                  = 2
    FRICTION COEFFICIENT                                    = 60.0
/
    TURBULENCE MODEL                                        = 1
    VELOCITY DIFFUSIVITY                                    = 2.5
/
    CORIOLIS                                                = YES
    CORIOLIS COEFFICIENT                                    = 1.146E-4
/
    WATER DENSITY                                           = 1025
/
/ ------------------------------------------------------------------
/                       8. NUMERICAL PARAMETERS
/ ------------------------------------------------------------------
/
    EQUATIONS                                               = 'SAINT-VENANT FE'
    DISCRETIZATIONS IN SPACE                                = 11;11
/
    ADVECTION                                               = YES
    TYPE OF ADVECTION                                       = 13;13
    SUPG OPTION                                             = 0;0
    PROPAGATION                                             = YES
/
    TREATMENT OF THE LINEAR SYSTEM                          = 2
    IMPLICITATION FOR VELOCITY                              = 0.75
    IMPLICITATION FOR DEPTH                                 = 0.75
    FREE SURFACE GRADIENT COMPATIBILITY                     = 0.1
/
    SOLVER                                                  = 1
    SOLVER ACCURACY                                         = 1E-6
    MAXIMUM NUMBER OF ITERATIONS FOR SOLVER                 = 500
/
    CONTINUITY CORRECTION                                   = YES
/
    PRECONDITIONING                                         = 2
    C-U PRECONDITIONING                                     = YES
/
    TIDAL FLATS                                             = YES
    OPTION FOR THE TREATMENT OF TIDAL FLATS                 = 1
    TREATMENT OF NEGATIVE DEPTHS                            = 2
    THRESHOLD FOR NEGATIVE DEPTHS                           = -0.01
    H CLIPPING                                              = YES
    MASS-LUMPING ON H                                       = 1
    MINIMUM VALUE OF DEPTH                                  = 0.01
/
    &FIN
```

B TELEMAC3D Steering File

```
/ ------------------------------------------------------------------
/                    TELEMAC3D - HYDRODYNAMICS
/                    NORTH SEA SANDBANKS
/ ------------------------------------------------------------------
/
/ ------------------------------------------------------------------
/                    1. GENERAL INFORMATION/SETUP
/ ------------------------------------------------------------------
/
    TITLE                                                = 'North Sea Sandbanks'
    TIMESTEP                                             = 10
    DURATION                                             = 432000
    ORIGINAL DATE OF TIME                                = 2017;05;23
    ORIGINAL HOUR OF TIME                                = 00;00;00
    GRAPHIC PRINTOUT PERIOD                              = 43200
    LISTING PRINTOUT PERIOD                              = 360
    NUMBER OF FIRST TIMESTEP FOR LISTING PRINTOUTS       = 0
    NUMBER OF FIRST TIMESTEP FOR GRAPHIC PRINTOUTS       = 0
/
    NON HYDROSTATIC VERSION                              = NO
    INFORMATION ABOUT SOLVER                             = YES
    MASS BALANCE                                         = YES
/
/ ------------------------------------------------------------------
/                    2. INTERNAL COUPLING
/ ------------------------------------------------------------------
/
    COUPLING WITH                                        = SISYPHE
    COUPLING PERIOD FOR SISYPHE                          = 1
    SISYPHE STEERING FILE                                = SIS_NS5.cas
/
/ ------------------------------------------------------------------
/                    3. FILE INPUTS/OUTPUTS
/ ------------------------------------------------------------------
/
    GEOMETRY FILE                                        = NorthSeaGeometry.slf
    BOUNDARY CONDITIONS FILE                             = NorthSea_BC_1.cli
    FORTRAN FILE                                         = mesh.transform.f
/
    2D RESULTS FILE                                      = R2D_NS_HOTSTART.slf
    3D RESULTS FILE                                      = R3D_NS_HOTSTART.slf
    VARIABLES FOR 2D GRAPHIC PRINTOUTS                   = 'B,U,V,S,H,TA1'
    VARIABLES FOR 3D GRAPHIC PRINTOUTS                   = 'U,V,W,Z,TA1'
/
/ ------------------------------------------------------------------
/                    4. MESH SETTINGS
/ ------------------------------------------------------------------
/
    MESH TRANSFORMATION                                  = 2
    NUMBER OF HORIZONTAL LEVELS                          = 10
/
/ ------------------------------------------------------------------
/                    5. BOUNDARY CONDITIONS
/ ------------------------------------------------------------------
/
    PRESCRIBED ELEVATIONS                                = 0;0;0;0
    PRESCRIBED VELOCITIES                                = 0;0;0;0
    PRESCRIBED FLOWRATES                                 = 0;0;0;0
/
/ ------------------------------------------------------------------
/                    6a. INITIAL CONDITIONS - STANDARD
/ ------------------------------------------------------------------
/
    COMPUTATION CONTINUED                                = NO
    INITIAL CONDITIONS                                   = 'TPXO SATELLITE ALTIMETRY'
    MINOR CONSTITUENT INTERFERENCE                       = YES
/
/ ------------------------------------------------------------------
/                    6b. INITIAL CONDITIONS - HOTSTARTED
/ ------------------------------------------------------------------
/
    COMPUTATION CONTINUED                                = YES
    INITIAL TIME SET TO ZERO                             = YES
    PREVIOUS COMPUTATION FILE                            = 'NorthSeaResults_HOTSTART.slf'
    ORIGINAL DATE OF TIME                                = 2017;05;28
    ORIGINAL HOUR OF TIME                                = 00;00;00
/
/ ------------------------------------------------------------------
/                    7. TIDAL CONDITIONS
/ ------------------------------------------------------------------
/
    TIDAL DATABASE                                       = 2
```

```
    BINARY DATABASE 1 FOR TIDE                          = 'D:\tpxo7.2\h_tpxo7.2'
    BINARY DATABASE 2 FOR TIDE                          = 'D:\tpxo7.2\u_tpxo7.2'
/
    OPTION FOR TIDAL BOUNDARY CONDITIONS                = 1;1;1;1
    GEOGRAPHIC SYSTEM                                   = 2
    ZONE NUMBER IN GEOGRAPHIC SYSTEM                    = 31
    COEFFICIENT TO CALIBRATE SEA LEVEL                  = 0.08
    COEFFICIENT TO CALIBRATE TIDAL RANGE                = 1.13
    COEFFICIENT TO CALIBRATE TIDAL VELOCITIES           = 0.85
/
/ ------------------------------------------------------------------
/                      8. PHSYICAL PARAMETERS
/ ------------------------------------------------------------------
    LAW OF BOTTOM FRICTION                              = 2
    FRICTION COEFFICIENT FOR THE BOTTOM                 = 60.0
    TURBULENCE REGIME FOR THE BOTTOM                    = 2
/
    LAW OF FRICTION ON LATERAL BOUNDARIES               = 0
    FRICTION COEFFICIENT FOR LATERAL SOLID BOUNDARIES   = 60.0
    TURBULENCE REGIME FOR LATERAL SOLID BOUNDAIRES      = 2
/
    HORIZONTAL TURBULENCE MODEL                         = 1
    VERTICAL TURBULENCE MODEL                           = 1
    COEFFICIENT FOR HORIZONTAL DIFFUSION OF VELOCITIES  = 2.5
    COEFFICIENT FOR VERTICAL DIFFUSION OF VELOCITIES    = 0.1
    VELOCITY VERTICAL PROFILES                          = 1
/
    CORIOLIS                                            = YES
    CORIOLIS COEFFICIENT                                = 1.146E-4
/
    AVERAGE WATER DENSITY                               = 1025
/
/ ------------------------------------------------------------------
/                         9. SEDIMENT
/ ------------------------------------------------------------------
    NUMBER OF TREACERS                                  = 'SAINT-VENANT FE'
    SEDIMENT                                            = 11;11
    INITAL VALUE OF TRACERS                             = 0.00
    CONSTANT SEDIMENT SETTLING VELOCITY                 = 0.108
    MEAN DIAMETER OF THE SEDIMENT                       = 350E-6
/
    COEFFICIENT FOR HORIZONTAL DIFFUSION OF TRACERS     = 1E-4
    COEFFICIENT FOR HORIZONTAL DIFFUSION OF TRACERS     = 1E-4
    PRECONDITIONING FOR DIFFUSION OF TRACERS            = 34
/
    SOLVER FOR THE DIFFUSION OF THE SEDIMENT            = 7
    OPTION OF SOLVER FOR THE DIFFUSION OF THE SEDIMENT  = 5
    SCHEME FOR ADVECTION OF TRACERS                     = 1
/
    TRACERS VERTICAL PROFILES                           = 1;1;1;1
    PRESCRIBED TRACER VALUES                            = 0;0;0;0
/
/ ------------------------------------------------------------------
/                    8. NUMERICAL PARAMETERS
/ ------------------------------------------------------------------
    ADVECTION STEP                                      = YES
    SCHEME FOR ADVECTION OF VELOCITIES                  = 1
    SCHEME FOR ADVECTION OF DEPTH                       = 5
    SCHEME FOR ADVECTION OF K-EPSILON                   = 2
/
    DIFFUSION STEP                                      = YES
    SCHEME FOR DIFFUSION OF VELOCITIES                  = 1
    SCHEME FOR DIFFUSION OF K-EPSILON                   = 1
/
    PROPAGATION STEP                                    = NO
/
    SOLVER FOR DIFFUSION OF VELOCITIES                  = 7
    SOLVER FOR PROPAGATION                              = 1
    SOLVER FOR VERTICAL VELOCITY                        = 1
```

```
    SOLVER FOR DIFFUSION OF K-EPSILON                          = 1
/
    ACCURACY FOR DIFFUSION OF VELOCITIES                       = 1E-6
    ACCURACY FOR PROPAGATION                                   = 1E-6
    ACCURACY FOR VERTICAL VELOCITY                             = 1E-6
    ACCURACY FOR DIFFUSION OF K-EPSILON                        = 1E-6
/
    PRECONDITIONING FOR DIFFUSION OF THE SEDIMENT              = 2
    PRECONDITIONING FOR DIFFUSION OF TRACERS                   = 2
    PRECONDITIONING FOR DIFFUSION OF VELOCITIES                = 2
    PRECONDITIONING FOR PROPAGATION                            = 2
    PRECONDITIONING FOR VERTICAL VELOCITY                      = 2
/
    MAXIMUM NUMBER OF ITERATIONS FOR ADVECTION SCHEMES         = 2
    MAXIMUM NUMBER OF ITERATIONS FOR PROPAGATION               = 2
    MAXIMUM NUMBER OF ITERATIONS FOR VERTICAL VELOCITY         = 2
    MAXIMUM NUMBER OF ITERATIONS FOR DIFFUSION OF VELOCITIES   = 2
    MAXIMUM NUMBER OF ITERATIONS FOR DIFFUSION OF K-EPSILON    = 2
    MAXIMUM NUMBER OF ITERATIONS FOR DIFFUSION OF SEDIMENT     = 2
/
    TIDAL FLATS                                                = YES
    OPTION FOR THE TREATMENT OF TIDAL FLATS                    = 1
    TREATMENT OF NEGATIVE DEPTHS                               = 2
    MINIMAL VALUE FOR DEPTH                                    = -0.01
    TREATMENT ON TIDAL FLATS FOR VELOCITIES                    = YES
    TREATMENT ON TIDAL FLATS FOR K-EPSILON                     = 1
/
    MASS-LUMPING FOR DEPTH                                     = 1
    MASS-LUMPING FOR VELOCITIES                                = 1
    MASS-LUMPING FOR DIFFUSION                                 = 1
/
    &FIN
```

C SISYPHE Steering File

```
/ ------------------------------------------------------------------------
/                    SISYPHE - MORPHODYNAMICS
/                    NORTH SEA SANDBANKS
/ ------------------------------------------------------------------------
/
/ ------------------------------------------------------------------------
/                    1. FILE INPUTS/OUTPUTS
/ ------------------------------------------------------------------------
/
  GEOMETRY FILE                                          = NorthSeaGeometry.slf
  BOUNDARY CONDITIONS FILE                               = NorthSea_BC_SIS.cli
  FORTRAN FILE                                           = noerod.f
/
  VARIABLES FOR GRAPHIC PRINTOUTS                        = 'B,U,V,S,H,E,CS*,QSBL,QSSUSP,TOB'
  RESULTS FILE                                           = NorthSeaResults_SIS_COUPLED.slf
/
/ ------------------------------------------------------------------------
/                    2. GENERAL SETUP
/ ------------------------------------------------------------------------
/
  MORPHOLOGICAL FACTOR                                   = 1
  MASS CONCENTRATION                                     = YES
/
/ ------------------------------------------------------------------------
/                    3. HYDRODYNAMIC PARAMETERS
/ ------------------------------------------------------------------------
/
  BED ROUGHNESS PREDICTION                               = NO
  BED ROUGHNESS PREDICTOR OPTION                         = 1
/
  RATIO BETWEEN SKIN FRICTION AND MEAN DIAMETER          = 3.6
  SKIN FRICTION CORRECTION                               = 1
/
/ ------------------------------------------------------------------------
/                    4. SEDIMENT PROPERTIES
/ ------------------------------------------------------------------------
/
  COHESIVE SEDIMENT                                      = YES
  NUMBER OF SIZE-CLASSES OF BED MATERIAL                 = 1
  SEDIMENT DIAMETERS                                     = 350E-6
  SEDIMENT DENSITY                                       = 2650
  SHIELDS PARAMETERS                                     = 0.0606
  SETTLING VELOCITIES                                    = 0.105
/
/ ------------------------------------------------------------------------
/                    5. BEDLOAD TRANSPORT
/ ------------------------------------------------------------------------
/
  BED LOAD                                               = YES
  BED-LOAD TRANSPORT FORMULA                             = 7
/
  SLOPE EFFECT                                           = YES
  FORMULA FOR SLOPE EFFECT                               = 1
  BETA                                                   = 0.85
  FRICTION ANGLE OF THE SEDIMENT                         = 40
  FORMULA FOR DEVIATION                                  = 2
  PARAMETER FOR DEVIATION                                = 0.85
/
  SEDIMENT SLIDE                                         = YES
/
  SECONDARY CURRENTS                                     = YES
  SECONDARY CURRENTS ALPHA COEFFICIENT                   = 1
/
/ ------------------------------------------------------------------------
/                    6. SUSPENDED LOAD
/ ------------------------------------------------------------------------
/
  SUSPENSION                                             = YES
  REFERENCE CONCENTRATION FORMULA                        = 3
  EQUILIBRIUM INFLOW CONCENTRATION                       = NO
  INITIAL SUSPENSION CONCENTRATIONS                      = 5.66E-6
/
  SOLVER FOR SUSPENSION                                  = 3
  SOLVER ACCURACY FOR SUSPENSION                         = 1E-6
  MAXIMUM NUMBER OF ITERATIONS FOR SOLVER FOR SUSPENSION = 100
/
  CORRECTION ON CONVECTION VELOCITY                      = NO
  TYPE OF ADVECTION                                      = 14
```

```
/
    OPTION FOR THE DISPERSION                          = 1
    DISPERSION ALONG THE FLOW                          = 1E-2
    DISPERSION ACROSS THE FLOW                         = 1E-2
/
/                    7. BED EVOLUTION EQUATION
/
    NON COHESIVE BED POROSITY                          = 0.4
/
    OPTION FOR THE TREATMENT OF NON ERODABLE BEDS      = 3
/
    TIDAL FLATS                                        = YES
    OPTION FOR THE TREATMENT OF TIDAL FLATS            = 1
    MINIMAL VALUE OF THE WATER HEIGHT                  = 1E-3
/
    &FIN
```

D TOMAWAC Steering File

```
/ TOMAWAC - WAVE CONDITIONS
/ NORTH SEA SANDBANKS
/
/ 1. GENERAL INFORMATION/SETUP
/
   TITLE                                          = 'North Sea Sandbanks'
   TIMESTEP                                       = 60
/
/ 2. FILE INPUTS/OUTPUTS
/
   GEOMETRY FILE                                  = NorthSeaGeometry.slf
   BOUNDARY CONDITIONS FILE                       = NorthSea_BC_TOM.cli
/
   2D RESULTS FILE                                = R2D_NS_TOM.slf
   GLOBAL RESULTS FILE                            = GLOBAL_NS_TOM.slf
   PUNCTAL RESULTS FILE                           = GLOBAL_NS_TOM.spe
   ABSCISSAE OF SPECTRUM PRINTOUT POINTS          = 432000
   ORDINATES OF SPECTRUM PRINTOUT POINTS          = 5858000
   VARIABLES FOR 2D GRAPHIC PRINTOUTS             = 'HM0,DMOY,TRP5,FX,FY,UX,UY'
   PERIOD FOR GRAPHIC PRINTOUTS                   = 60
   PERIOD FOR LISTING PRINTOUTS                   = 60
/
/ 3. DISCRETISATION
/
   MINIMAL FREQUENCY                              = 0.05
   FREQUENCIAL RATIO                              = 1.1007
   NUMBER OF FREQUENCIES                          = 12
   NUMBER OF DIRECTIONS                           = 12
   NUMBER OF TIMESTEP                             = 1
/
/ 4. BOUNDARY CONDITIONS
/
   TYPE OF INITIAL DIRECTIONAL SPECTRUM           = 6
   INITIAL SIGNIFICANT WAVE HEIGHT                = 1.5
   INITIAL PEAK FREQUENCY                         = 0.125
   INITIAL PEAK FACTOR                            = 3.3
   INITIAL ANGULAR DISTRIBUTION FUNCTION          = 1
   INITIAL WEIGHTING FACTOR FOR ADF               = 1.0
   INITIAL MAIN DIRECTION 1                       = 180
   INITIAL DIRECTIONAL SPREAD 1                   = 12
/
/ 5. INITIAL CONDITIONS
/
   TYPE OF BOUNDARY DIRECTIONAL SPECTRUM          = 6
   BOUNDARY SIGNIFICANT WAVE HEIGHT               = 1.5
   BOUNDARY PEAK FREQUENCY                        = 0.125
   BOUNDARY PEAK FACTOR                           = 3.3
   BOUNDARY ANGULAR DISTRIBUTION FUNCTION         = 1
   BOUNDARY WEIGHTING FACTOR FOR ADF              = 1.0
   BOUNDARY MAIN DIRECTION 1                      = 180
   BOUNDARY DIRECTIONAL SPREAD 1                  = 12
   LIMIT SPECTRUM MODIFIED BY USER                = YES
/
/ 6. OPTIONS
/
   MINIMUM WATER DEPTH                            = 0.05
   INFINITE DEPTH                                 = NO
   CONSIDERATION OF SOURCE TERMS                  = YES
   CONSIDERATION OF A WIND                        = YES
   BOTTOM FRICTION DISSIPATION                    = 1
   NUMBER OF BREAKING TIME STEPS                  = 5
   DEPTH-INDUCED BREAKING DISSIPATION             = 1
   &FIN
```

References

4C Offshore Ltd. Global Offshore Renewable Map - 4C Offshore, 2018. URL https://www.4coffshore.com/offshorewind/. xx, 12, 13

C. L. Amos and E. L. King. Bedforms of the Canadian eastern seaboard: A comparison with global occurrences. *Marine Geology*, 57(1):167–208, 1984. ISSN 0025-3227. doi: http://dx.doi.org/10.1016/0025-3227(84)90199-3. URL http://www.sciencedirect.com/science/article/pii/0025322784901993. 3, 4, 11

R. Ata. Telemac2d User Manual. Technical report, 2017. 47

T. Awk. Tomawac User Manual. Technical report, 2017. 47

R. Belderson, N. Kenyon, and M. Johnson. Bedforms. In A. H. Stride, editor, *Offshore tidal sands : processes and deposits*, chapter 3, pages 27–57. Chapman and Hall, London, 1982. 8

S. Berne. Offshore sands. In G. Middleton, editor, *Encyclopedia of Sediments and Sedimentary Rocks*, pages 492–499. Kluwer Academic Publishers, 2003. 3, 4, 9

S. Berne, A. Trentesaux, A. Stolk, T. Missiaen, and M. de Batist. Architecture and long term evolution of a tidal sandbank: The Middelkerke Bank (southern North Sea). *Marine Geology*, 121(1-2):57–72, oct 1994. ISSN 0025-3227. doi: 10.1016/0025-3227(94)90156-2. URL https://www.sciencedirect.com/science/article/pii/0025322794901562. 26

G. Besio. *Modelling of tidally generated large scale bedforms*. PhD thesis, University of Genoa, 2004. 29

G. Besio, P. Blondeaux, and G. Vittori. A three-dimensional model of sand bank formation. *Ocean Dynamics*, 55(5):515–525, dec 2005. ISSN 1616-7228. doi: 10.1007/s10236-005-0027-0. URL https://doi.org/10.1007/s10236-005-0027-0. 4, 13, 14, 29

G. Besio, P. Blondeaux, and G. Vittori. On the formation of sand waves and sand banks. *Journal of Fluid Mechanics*, 557:1–27, 2006. doi: 10.1017/S0022112006009256. 29, 30

G. Besio, P. Blondeaux, M. Brocchini, S. J. M. H. Hulscher, D. Idier, M. A. F. Knaapen, A. A. Németh, P. C. Roos, and G. Vittori. The morphodynamics of tidal sand waves: A model overview. *Coastal Engineering*, 55(7–8): 657–670, 2008. ISSN 0378-3839. doi: http://dx.doi.org/10.1016/j.coastaleng.2007.11.004. URL http://www.sciencedirect.com/science/article/pii/S0378383907001597. 29

BOC Metocean B.V. Met Ocean Data, 2020. URL https://app.metoceanview.com/hindcast/sites/nsea/54/2#! 183

S. M. Brooks. Coastal changes in historic times - linking offshore bathymetry changes and cliff recession in Suffolk. Technical report, London, 2010. 2, 39, 79

N. Carbajal and Y. Montano. Comparison between Predicted and Observed Physical Features of Sandbanks. *Estuarine, Coastal and Shelf Science*, 52 (4):435–443, 2001. ISSN 0272-7714. doi: http://dx.doi.org/10.1006/ecss.2000.0760. URL http://www.sciencedirect.com/science/article/pii/S0272771400907601. 3, 4, 28

A. P. Carr. Evidence for the sediment circulation along the coast of East Anglia. *Marine Geology*, 40(3):M9–M22, 1981. ISSN 0025-3227. doi: http://dx.doi.org/10.1016/0025-3227(81)90134-1. URL http://www.sciencedirect.com/science/article/pii/0025322781901341. 21

V. N. D. Caston. Linear sand banks in the southern North Sea. *Sedimentology*, 18:63–78, 1972. doi: 10.1111/j.1365-3091.1972.tb00003.x. xv, xx, 6, 7, 20, 82, 83

V. N. D. Caston and A. H. Stride. Tidal sand movement between some linear sand banks in the North Sea off northeast Norfolk. *Marine Geology*, 9(5):M38–M42, 1970. ISSN 0025-3227. doi: http://dx.doi.org/10.1016/0025-3227(70)90018-6. URL http://www.sciencedirect.com/science/article/pii/0025322770900186. 19, 26

Centre for Environment Fisheries and Aquaculture Science. North Sea and English Channel Sediment Particle Size Analysis, 2017. URL http://data.cefas.co.uk/#/View/698. 175, 176

A. Chadwick, C. Fleming, and D. Reeve. *Coastal engineering : processes, theory and design practice*. London : Spon, London, 2012. 1

F. Charru, B. Andreotti, and P. Claudin. Sand Ripples and Dunes. *Annual Review of Fluid Mechanics*, 2013. ISSN 0066-4189. doi: 10.1146/annurev-fluid-011212-140806.

A. Chatzirodou, H. Karunarathna, and D. E. Reeve. Investigation of deep sea shelf sandbank dynamics driven by highly energetic tidal flows. *Marine Geology*, 380:245–263, 2016. ISSN 0025-3227. doi: http://dx.doi.org/10.1016/j.margeo.2016.04.011. URL http://www.sciencedirect.com/science/article/pii/S0025322716300652. 40

N. Chini, P. Stansby, J. Leake, J. Wolf, J. Roberts-Jones, and J. Lowe. The impact of sea level rise and climate change on inshore wave climate: A case study for East Anglia (UK). *Coastal Engineering*, 57(11):973–984, 2010. ISSN 0378-3839. doi: https://doi.org/10.1016/j.coastaleng.2010.05.009. URL http://www.sciencedirect.com/science/article/pii/S0378383910000815. 38

M. B. Collins, S. J. Shimwell, S. Gao, H. Powell, C. Hewitson, and J. A. Taylor. Water and sediment movement in the vicinity of linear sandbanks: the Norfolk Banks, southern North Sea. *Marine Geology*, 123(3):125–142, 1995. ISSN 0025-3227. doi: http://dx.doi.org/10.1016/0025-3227(95)00010-V. URL http://www.sciencedirect.com/science/article/pii/002532279500010V. 3, 4, 11, 26, 80, 83

Collins English Dictionary. Sandbank definition and meaning, 2017. URL https://www.collinsdictionary.com/dictionary/english/sandbank.

B. Cooper. A synthesis of current knowledge on the genesis of the Great Yarmouth and Norfolk Bank Systems. The Crown Estate. Technical report, feb 2008. xx, 82, 83, 84

C. Coughlan, C. E. Vincent, T. J. Dolphin, and J. M. Rees. Effects of tidal stage on the wave climate inshore of a sandbank. *Journal of Coastal Research*, (SPEC. ISSUE 50):751–756, 2007. URL https://www.scopus.com/inward/record.uri?eid=2-s2.0-77956848944&partnerID=40&md5=4c218767509a85ee693cfed637f5c946. 35

C. Coughlan, C. Vincent, and T. Dolphin. Sediment transport modeling to investigate the links between the movements of sandbanks and local beach variability. *Coastal engineering*, 2008. ISSN 01613782.

H. de Swart and B. Yuan. Dynamics of offshore tidal sand ridges, a review. *Environmental Fluid Mechanics*, 2018. doi: 10.1007/s10652-018-9630-8. 4, 11, 43

A. S. de Winter, A. M. R. Bakker, H. W. van den Brink, R. Haarsma, A. Stepek, I. L. Wijnant, and R. C. Large-scale winds in the southern North Sea region: the wind part of the KNMI'14 climate change scenarios. *Environmental Research Letters*, 10(3):35004, 2015. ISSN 1748-9326. URL http://stacks.iop.org/1748-9326/10/i=3/a=035004.

S. Deleu, V. Van Lancker, D. Van den Eynde, and G. Moerkerke. Morphodynamic evolution of the kink of an offshore tidal sandbank: the Westhinder Bank (Southern North Sea). *Continental Shelf Research*, 24(15):1587–1610, oct 2004. ISSN 0278-4343. doi: 10.1016/J.CSR.2004.07.001. URL https://www.sciencedirect.com/science/article/pii/S027843430400161X.

S. Dey. *Fluvial hydrodynamics : hydrodynamic and sediment transport phenomena*. Heidelberg, Germany : Springer, 2014.

T. J. Dolphin, C. E. Vincent, C. Coughlan, and J. M. Rees. Variability in Sandbank Behaviour at Decadal and Annual Time-Scales and Implications for Adjacent Beaches. *Journal of Coastal Research*, pages 731–737, feb 2007. ISSN 07490208, 15515036. URL http://www.jstor.org/stable/26481681. 33, 34

D. B. Duane, M. Field, E. P. Meisburger, D. J. P. Swift, and S. J. Williams. Linear shoals on the Atlantic inner continental shelf, Florida to Long Island. *Shelf Sediment Transport: Process and Pattern*, pages 447–498, 1972. 8

K. R. Dyer and D. A. Huntley. The origin, classification and modelling of sand banks and ridges. *Continental Shelf Research*, 19(10):1285–1330, 1999. ISSN 0278-4343. doi: http://dx.doi.org/10.1016/S0278-4343(99)00028-X. URL http://www.sciencedirect.com/science/article/pii/S027843439900028X. xv, 3, 4, 9, 10, 11, 31

P. P. G. Dyke. *Modeling Coastal and Offshore Processes*. Imperial College Press, 2007. ISBN 9781860946752. URL https://books.google.co.uk/books?id=zsFuQgAACAAJ.

L. S. Esteves, J. J. Williams, and M. A. Lisniowski. Measuring and modelling longshore sediment transport. *Estuarine, Coastal and Shelf Science*, 83(1):47–59, 2009. ISSN 0272-7714. doi: http://dx.doi.org/10.1016/j.ecss.2009.03.020. URL http://www.sciencedirect.com/science/article/pii/S0272771409001413.

I. Fairley, I. Masters, and H. Karunarathna. Numerical modelling of storm and surge events on offshore sandbanks. *Marine Geology*, 371:106–119, 2016. ISSN 0025-3227. doi: http://dx.doi.org/10.1016/j.margeo.2015.11.007. URL http://www.sciencedirect.com/science/article/pii/S0025322715300669. 40

A. Figueiredo Jr, D. Swift, Stubblefield, and T. Clarke. Sand ridges on the inner atlantic shelf of north america: morphometric comparisons with huthnance stability model. *Geo-Marine Letters*, 1:187–191, 09 1981. doi: 10.1007/BF02462432. 9

E. Garel. Tidally-averaged Currents and Bedload Transport over the Kwinte Bank, Southern North Sea. *Journal of Coastal Research*, Special Is(51):87–94, 2010. ISSN 07490208, 15515036. URL http://www.jstor.org/stable/40928821. 39

E. Garel, W. Bonne, and M. B. Collins. Offshore Sand and Gravel Mining. In *Encyclopedia of Ocean Sciences*, pages 4162–4170. 2009. ISBN 9780123744739. doi: 10.4043/4495-MS. 14

H. Gerritsen, R. J. Vos, T. van der Kaaij, A. Lane, and J. G. Boon. Suspended sediment modelling in a shelf sea (North Sea). *Coastal Engineering*, 41(1-3):317–352, sep 2000. ISSN 0378-3839. doi: 10.1016/S0378-3839(00)00042-9. URL https://www.sciencedirect.com/science/article/pii/S0378383900000429?via%3Dihub. 79, 80

A. Giardino, D. Van den Eynde, and J. Monbaliu. Wave effects on the morphodynamic evolution of an offshore sand bank. *Journal of Coastal Research*, Special Is(51):127–140, 2010. 38

K. Glock, M. Tritthart, H. Habersack, and C. Hauer. Comparison of hydrodynamics simulated by 1d, 2d and 3d models focusing on bed shear stresses. *Water*, 11, 01 2019. doi: 10.3390/w11020226. 43

N. M. Grunnet and B. G. Ruessink. Morphodynamic response of nearshore bars to a shoreface nourishment. *Coastal Engineering*, 52(2):119–137, 2005. ISSN 03783839. doi: 10.1016/j.coastaleng.2004.09.006. 31

M. Hanley, S. Hoggart, D. Simmonds, A. Bichot, M. Colangelo, F. Bozzeda, H. Heurtefeux, B. Ondiviela, R. Ostrowski, M. Recio, R. Trude, E. Zawadzka-Kahlau, and R. Thompson. Shifting sands? Coastal protection by sand banks, beaches and dunes. *Coastal Engineering*, 87:136–146, may 2014. ISSN 0378-3839. doi: 10.1016/J.COASTALENG.2013.10.020. URL https://www.sciencedirect.com/science/article/pii/S0378383913001762?showall=true.

K. Hasselmann, T. Barnett, E. Bouws, H. Carlson, D. Cartwright, K. Enke, J. Ewing, H. Gienapp, D. Hasselmann, P. Kruseman, A. Meerburg, P. Muller,

D. Olbers, K. Richter, W. Sell, and H. Walden. Measurements of wind-wave growth and swell decay during the joint north sea wave project (jonswap). *Deut. Hydrogr. Z.*, 8:1–95, 01 1973. 185

A. Hequette and D. Aernouts. The influence of nearshore sand bank dynamics on shoreline evolution in a macrotidal coastal environment, Calais, northern France. *Continental Shelf Research*, 30(12):1349–1361, 2010. ISSN 0278-4343. doi: http://dx.doi.org/10.1016/j.csr.2010.04.017. URL http://www.sciencedirect.com/science/article/pii/S0278434310001561.

J.-M. Hervouet. *Hydrodynamics of Free Surface Flows: Modelling With the Finite Element Method*. John Wiley & Sons, 2007. 47

J. M. Horillo-Caraballo. *Investigation of the long-term evolution of the offshore sandbanks at Great Yarmouth, UK*. PhD thesis, The University of Nottingham, 2005. 30, 31

J. Horrillo-Caraballo and D. Reeve. Long-Term Evolution of Offshore Sandbank Morphology: Case Study: Great Yarmouth Sandbanks, U.K., feb 2005. URL https://doi.org/10.1061/40855(214)37. 30

J. M. Horrillo-Caraballo and D. E. Reeve. Morphodynamic behaviour of a nearshore sandbank system: The Great Yarmouth Sandbanks, U.K. *Marine Geology*, 254(1–2):91–106, 2008. ISSN 0025-3227. doi: http://dx.doi.org/10.1016/j.margeo.2008.05.014. URL http://www.sciencedirect.com/science/article/pii/S002532270800176X. 36, 37

J. Houbolt. Recent sediments in the Southern Bight of the North Sea. *Geologie en mijnbouw : tijdschrift van het Nederlandsch Geologisch-Mijnbouwkundig Genootschap.*, 47(4):245–273, 1968. ISSN 0016-7746. 4, 8, 19, 20, 26

M. Howarth and J. Huthnance. Tidal and residual currents around a Norfolk Sandbank. *Estuarine, Coastal and Shelf Science*, 19(1):105–117, jul 1984. ISSN 0272-7714. doi: 10.1016/0272-7714(84)90055-6. URL https://www.sciencedirect.com/science/article/pii/0272771484900556. 23

HR Wallingford. The TELEMAC-MASCARET modelling system, 2016. URL http://www.opentelemac.org/index.php/presentation. 46

S. J. M. H. Hulscher. Tidal-induced large-scale regular bed form patterns in a three-dimensional shallow water model. *Journal of Geophysical Research: Oceans*, 101(C9):20727–20744, 1996. doi: 10.1029/96JC01662. URL https://agupubs.onlinelibrary.wiley.com/doi/abs/10.1029/96JC01662. 25, 33

S. J. M. H. Hulscher and G. M. van den Brink. Comparison between predicted and observed sand waves and sand banks in the North Sea. *Journal of geophysical research*, 106(C5):9327–9338, 2001. ISSN 0148-0227. 4, 25, 28

S. J. M. H. Hulscher, H. E. de Swart, and H. J. de Vriend. The generation of offshore tidal sand banks and sand waves. *Continental Shelf Research*, 13(11):1183–1204, 1993. ISSN 0278-4343. doi: http://dx.doi.org/10.1016/0278-4343(93)90048-3. URL http://www.sciencedirect.com/science/article/pii/0278434393900483. 24, 25

D. A. Huntley, J. M. Huthnance, M. B. Collins, C.-L. Liu, R. J. Nicholls, C. Hewitson, M. O. Green, K. R. Dyer, and C. F. Jago. Hydrodynamics and Sediment Dynamics of North Sea Sand Waves and Sand Banks [and Discussion]. *Philosophical Transactions of the Royal Society of London. Series A: Physical and Engineering Sciences*, 343(1669):461–474, 1993. doi: 10.1098/rsta.1993.0059. 4, 24

J. Huthnance. Tidal current asymmetries over the Norfolk Sandbanks. *Estuarine and Coastal Marine Science*, 1(1):89–99, jan 1973. ISSN 0302-3524. doi: 10.1016/0302-3524(73)90061-3. URL https://www.sciencedirect.com/science/article/abs/pii/0302352473900613. 22

J. Huthnance. On the formation of sand banks of finite extent. *Estuarine, Coastal and Shelf Science*, 15(3):277–299, sep 1982a. ISSN 0272-7714. doi: 10.1016/0272-7714(82)90064-6. URL https://www.sciencedirect.com/science/article/pii/0272771482900646. 9, 22, 24

J. M. Huthnance. On one mechanism forming linear sand banks. *Estuarine, Coastal and Shelf Science*, 14(1):79–99, 1982b. ISSN 0272-7714. doi: http://dx.

doi.org/10.1016/S0302-3524(82)80068-6. URL http://www.sciencedirect.com/science/article/pii/S0302352482800686. 22, 25, 39

D. Idier and D. Astruc. Analytical and numerical modeling of sandbanks dynamics. *Journal of Geophysical Research C: Oceans*, 108(3):1–5, 2003. URL https://www.scopus.com/inward/record.uri?eid=2-s2.0-0142028729&partnerID=40&md5=01b820f4e81da1dafc8c02e785a617ed. 28

D. Idier, F. Paris, G. L. Cozannet, F. Boulahya, and F. Dumas. Sea-level rise impacts on the tides of the European Shelf. *Continental Shelf Research*, 137:56–71, apr 2017. ISSN 0278-4343. doi: 10.1016/J.CSR.2017.01.007. URL https://www.sciencedirect.com/science/article/pii/S0278434317300250. 39

G. Jacoub, P. K. Stansby, J.-M. Hervouet, C. Villaret, and M. Benoit. Offshore sandbank morphodynamics modelling with sea level rise, 2007. URL http://ima.org.uk/_db/_documents/Jacoub.pdf. 34

C. Jenkins, J. Eggleton, J. Albrecht, J. Barry, G. Duncan, N. Golding, and J. O'Connor. North Norfolk Sandbank and Saturn Reef cSAC/SCI Management Investigation Report. Technical report, 2015. 79, 83, 175

G. Jenkins, J. Murphy, D. Sexton, J. Lowe, P. Jones, and C. Kilsby. UK Climate Projections: Briefing report. Technical report, Met Office Hadley Centre, Exeter, 2010. 38

JNCC. SAC selection - 1110 Sandbanks which are slightly covered by sea water all the time, 2017a. URL http://jncc.defra.gov.uk/ProtectedSites/SACselection/habitat.asp?FeatureIntCode=H1110. 12

JNCC. Annex I Sandbanks in Offshore Waters, 2017b. URL http://jncc.defra.gov.uk/page-1452. 12

J. W. Kamphuis. Comparison of two-dimensional and three-dimensional beach profiles. *Journal of Waterway, Port, Coastal, and Ocean Engineering*, 121(3):155–161, 1995. doi: 10.1061/(ASCE)0733-950X(1995)121:3(155). URL https://ascelibrary.org/doi/abs/10.1061/%28ASCE%290733-950X%281995%29121%3A3%28155%29. 27

H. Karunarathna, J. Horrillo-Caraballo, Y. Kuriyama, H. Mase, R. Ranasinghe, and D. E. Reeve. Linkages between sediment composition, wave climate and beach profile variability at multiple timescales. *Marine Geology*, 381, 2016. ISSN 00253227. doi: 10.1016/j.margeo.2016.09.012.

N. Kenyon and B. Cooper. Sand banks , sand transport and offshore wind farms. *Strategic Environmental Assessment (SEA)*, (May):106, 2005. ISSN 1469-8714. doi: 10.13140/RG.2.1.1593.4807. 31

A. A. Khan and W. Wu. *Sediment transport : monitoring, modeling, and management*. Hauppauge, New York : Nova Science Publishers Inc., 2013.

M. A. F. Knaapen. Sandbank occurrence on the Dutch continental shelf in the North Sea. *Geo-Marine Letters*, 29(1):17–24, 2009. ISSN 1432-1157. doi: 10.1007/s00367-008-0105-7. URL http://dx.doi.org/10.1007/s00367-008-0105-7. 37

G. V. Kozyrakis, A. I. Delis, G. Alexandrakis, and N. A. Kampanis. Numerical modeling of sediment transport applied to coastal morphodynamics. *Applied Numerical Mathematics*, 104, 2016. ISSN 01689274. doi: 10.1016/j.apnum.2014.09.007.

C. Kuang and P. Stansby. Sandbanks for coastal protection: implications of sea-level rise. Part 2: current and morphological modelling, 2006a. 32

C. Kuang and P. Stansby. Sandbanks for coastal protection: implications of sea-level rise. Part 3: wave modelling, 2006b. 32, 33

J. Lanckneus, G. De Moor, and A. Stolk. Environmental setting, morphology and volumetric evolution of the Middelkerke Bank (southern North Sea). *Marine Geology*, 1994. ISSN 00253227. doi: 10.1016/0025-3227(94)90153-8. 26

M. Larson and N. C. Kraus. Analysis of cross-shore movement of natural longshore bars and material placed to create longshore bars. Technical report, US Army Corps of Engineers, Washington DC, 1992.

M. Lewis, S. Neill, and A. Elliott. Interannual Variability of Two Offshore Sand Banks in a Region of Extreme Tidal Range. *Journal of Coastal Research*, 300, 2014. doi: 10.2112/JCOASTRES-D-14-00010.1. 11, 12, 40

Z. Liu. *Sediment Transport*. 1st edition, 1998.

Z. Liu and D. Xia. A preliminary study of tidal current ridges. *Chinese Journal of Oceanology and Limnology*, 3(1):118–133, 1985. ISSN 0254-4059. 3, 4

Marine Conservation Society. Briefing: Site integrity and sandbanks, 2017. URL https://seas-at-risk.org/images/pdf/Other_pdfs/Site_-integrity_and_sandbanks_fin.pdf.

O. Mattic. Telemac3d User Manual. Technical report, 2017. 47

I. N. McCave. Grain-size trends and transport along beaches: Example from eastern England. *Marine Geology*, 28(1):M43–M51, 1978. ISSN 0025-3227. doi: https://doi.org/10.1016/0025-3227(78)90092-0. URL http://www.sciencedirect.com/science/article/pii/0025322778900920. 21

M. Nabi, H. J. De Vriend, E. Mosselman, C. J. Sloff, and Y. Shimizu. Detailed simulation of morphodynamics: 3. Ripples and dunes. *Water Resources Research*, 2013. ISSN 00431397. doi: 10.1002/wrcr.20457. 40

National Research Council Canada. Blue Kenue™: software tool for hydraulic modellers, 2019. URL https://nrc.canada.ca/en/research-development/products-services/software-applications/blue-kenuetm-software-tool-hydraulic-modellers. 84

Natural Environment Research Council. Download UK Tide Gauge Network data, 2018. URL https://www.bodc.ac.uk/data/hosted_data_systems/sea_level/uk_tide_gauge_network/. 96

S. P. Neill and J. D. Scourse. The formation of headland/island sandbanks. *Continental Shelf Research*, 29(18):2167–2177, 2009. ISSN 0278-4343. doi: http://dx.doi.org/10.1016/j.csr.2009.08.008. URL http://www.sciencedirect.com/science/article/pii/S0278434309002507. 38

B. Neumann, A. T. Vafeidis, J. Zimmermann, and R. J. Nicholls. Future Coastal Population Growth and Exposure to Sea-Level Rise and Coastal Flooding - A Global Assessment. *PLOS ONE*, 10(3):e0118571, mar 2015. ISSN 1932-6203. doi: 10.1371/journal.pone.0118571. URL http://dx.plos.org/10.1371/journal.pone.0118571. 1

North Norfolk District Council. Bacton to Walcott Coastal Management, 2018. URL https://www.north-norfolk.gov.uk/sandscaping. 14

North West Shelf Operational Oceanographic System. Waterlevel (obs-matroos), 2018. URL http://noos.eurogoos.eu/observations/nl-matroos-obs/. 96

T. Off. Rhythmic Linear Sand Bodies Caused by Tidal Currents1. *AAPG Bulletin*, 47(2):324–341, 1963. ISSN 0149-1423. doi: 10.1306/BC743989-16BE-11D7-8645000102C1865D. URL https://doi.org/10.1306/BC743989-16BE-11D7-8645000102C1865D. 3, 18

Oregon State University. The OSU TOPEX/Poseidon Global Inverse Solution - TPXO, 2010. URL http://volkov.oce.orst.edu/tides/global.html. 89

S. Pan, N. MacDonald, J. Williams, B. A. O'Connor, J. Nicholson, and A. M. Davies. Modelling the hydrodynamics of offshore sandbanks. *Continental Shelf Research*, 27(9):1264–1286, 2007. ISSN 0278-4343. doi: http://dx.doi.org/10.1016/j.csr.2007.01.007. URL http://www.sciencedirect.com/science/article/pii/S0278434307000337. 35

Y. Pan, C. Kuang, J. Zhang, Y. Chen, X. Mao, Y. Ma, Y. Zhang, Y. Yang, and R. Qiu. Postnourishment Evolution of Beach Profiles in a Low-Energy Sandy Beach with a Submerged Berm. *Journal of Waterway, Port, Coastal, and Ocean Engineering*, 143(4):05017001, 2017. ISSN 0733-950X. doi: 10.1061/(ASCE)WW.1943-5460.0000384. URL http://ascelibrary.org/doi/10.1061/%28ASCE%29WW.1943-5460.0000384.

G. Parker, N. W. Lanfredi, and D. J. Swift. Seafloor response to flow in a southern hemisphere sand-ridge field: Argentine inner shelf. *Sedimentary Geology*, 33(3):195 – 216, 1982. ISSN 0037-0738. doi: https://doi.

org/10.1016/0037-0738(82)90055-0. URL http://www.sciencedirect.com/science/article/pii/0037073882900550. 9

C. Pattiaratchi and M. Collins. Mechanisms for linear sandbank formation and maintenance in relation to dynamical oceanographic observations. *Progress In Oceanography*, 19:117–176, 1987. doi: 10.1016/0079-6611(87)90006-1. 4, 23, 24

R. Pingree. The Formation Of The Shambles And Other Banks By Tidal Stirring Of The Seas. *Journal of the Marine Biological Association of the United Kingdom*, 58:211–226, 1978. doi: 10.1017/S0025315400024504. 8

D. Reeve, B. Li, and N. Thurston. Eigenfunction Analysis of Decadal Fluctuations in Sandbank Morphology at Great Yarmouth. *J. Coast. Res.*, 17, 2001. 28

D. E. Reeve, J. M. Horrillo-Caraballo, and V. Magar. Statistical analysis and forecasts of long-term sandbank evolution at Great Yarmouth, UK. *Estuarine, Coastal and Shelf Science*, 79(3):387–399, 2008. ISSN 0272-7714. doi: http://dx.doi.org/10.1016/j.ecss.2008.04.016. URL http://www.sciencedirect.com/science/article/pii/S0272771408001807. 36

A. H. W. Robinson. Ebb-flood channel systems in sandy bays and estuaries. *Geography*, 45(3):183–199, 1960. ISSN 00167487. URL http://www.jstor.org/stable/40565158. 18

A. H. W. Robinson. Residual currents in relation to shoreline evolution of the East Anglian coast. *Marine Geology*, 4(1):57–84, 1966. ISSN 0025-3227. doi: http://dx.doi.org/10.1016/0025-3227(66)90037-5. URL http://www.sciencedirect.com/science/article/pii/0025322766900375. 18, 21

A. H. W. Robinson. Erosion and accretion along part of the Suffolk coast of East Anglia, England. *Marine Geology*, 37(1):133–146, 1980. ISSN 0025-3227. doi: https://doi.org/10.1016/0025-3227(80)90014-6. URL http://www.sciencedirect.com/science/article/pii/0025322780900146. 21

I. Robinson. Chapter 7 Tidally Induced Residual Flows. *Elsevier Oceanography Series*, 35:321–356, jan 1983. ISSN 0422-9894. doi: 10.1016/S0422-9894(08)

70505-1. URL https://www.sciencedirect.com/science/article/pii/S0422989408705051. 23

P. C. Roos and S. J. M. H. Hulscher. Large-scale seabed dynamics in offshore morphology: Modeling human intervention. *Reviews of Geophysics*, 41(2), 2003. doi: 10.1029/2002RG000120. URL https://agupubs.onlinelibrary.wiley.com/doi/abs/10.1029/2002RG000120. 29

P. C. Roos, S. J. M. H. Hulscher, M. A. F. Knaapen, and R. M. J. Van Damme. The cross-sectional shape of tidal sandbanks: Modeling and observations. *Journal of Geophysical Research: Earth Surface*, 109(F2), 2004. doi: 10.1029/2003JF000070. URL https://agupubs.onlinelibrary.wiley.com/doi/abs/10.1029/2003JF000070. 4, 29

R. Sanay, G. Voulgaris, and J. C. Warner. Tidal asymmetry and residual circulation over linear sandbanks and their implication on sediment transport: A process-oriented numerical study. 112(C12):– n/a, 2007. ISSN - 2156-2202. 36

Service Hydrographique et Océanographique de la Marine. Information géographique maritime et littorale de référence, 2012. URL https://data.shom.fr. 96

T. Silva, L. Biermann, and J. Rees. Suspended Sediment Climatologies around the UK. Technical report, Centre for Environment Fisheries and Aquaculture Science, 2016. URL https://assets.publishing.service.gov.uk/government/uploads/system/uploads/attachment_data/file/584621/CEFAS_2016_Suspended_Sediment_Climatologies_around_the_UK.pdf. xvii, 176, 177

G. Smith. North Sea sandbanks, 2013. URL http://www.naval-history.net/Map24NorthSeaSandbanks.htm. xv, 81

J. D. Smith. Geomorphology of a Sand Ridge. *The Journal of Geology*, 77(1): 39–55, 1969. ISSN 0022-1376. doi: 10.1086/627407. URL http://www.jstor.org/stable/30062237. 5, 19

P. Stansby, C. Kuang, D. Laurence, and B. Launder. Sandbanks for coastal protection: implications of sea-level rise. Part 1: application to East Anglia, 2006. 32, 33, 116

A. H. Stride. Current-swept sea floors near the southern half of Great Britain. *Quarterly Journal of the Geological Society*, 119(1-4):175–197, 1963. ISSN 0370-291X. doi: 10.1144/gsjgs.119.1.0175. URL https://jgs.lyellcollection.org/content/119/1-4/175. 17, 18, 20

A. H. Stride, R. Belderson, N. Kenyon, and M. Johnson. Offshore tidal deposits. In A. H. Stride, editor, *Offshore tidal sands : processes and deposits*, chapter 5, pages 95–125. Chapman and Hall, London, 1982. ISBN 0412129701. 21, 22

D. J. Swift. Tidal sand ridges and shoal-retreat massifs. *Marine Geology*, 18(3):105–133, mar 1975. ISSN 0025-3227. doi: 10.1016/0025-3227(75)90007-9. URL https://www.sciencedirect.com/science/article/pii/0025322775900079.

A. Talmon, N. Struiksma, and M. V. Mierlo. Laboratory measurements of the direction of sediment transport on transverse alluvial-bed slopes. *Journal of Hydraulic Research*, 33(4):495–517, 1995. doi: 10.1080/00221689509498657. URL https://doi.org/10.1080/00221689509498657. 61

P. Tassi. Sisyphe User Manual. Technical report, 2017. 47

P. Tonnon, L. van Rijn, and D. Walstra. The morphodynamic modelling of tidal sand waves on the shoreface. *Coastal Engineering*, 54(4):279–296, apr 2007. ISSN 0378-3839. doi: 10.1016/J.COASTALENG.2006.08.005. URL https://www.sciencedirect.com/science/article/pii/S0378383906001256. 34

H. H. van der Veen and S. J. M. H. Hulscher. Predicting the occurrence of sand banks in the North Sea. *Ocean Dynamics*, 59(5):689, 2009. ISSN 1616-7228. doi: 10.1007/s10236-009-0204-7. URL http://dx.doi.org/10.1007/s10236-009-0204-7. 33

H. H. van der Veen, S. J. M. H. Hulscher, and M. A. F. Knaapen. Grain size dependency in the occurrence of sand waves. *Ocean Dynamics*, 56(3):228–

234, 2006. ISSN 1616-7228. doi: 10.1007/s10236-005-0049-7. URL http://dx.doi.org/10.1007/s10236-005-0049-7. 3, 33, 79

J. van der Zanden, D. A. van der A, D. Hurther, I. Cáceres, T. O'Donoghue, S. Hulscher, and J. S. Ribberink. Bedload and suspended load contributions to breaker bar morphodynamics. *Coastal Engineering*, 129:74–92, 2017. ISSN 0378-3839. doi: https://doi.org/10.1016/j.coastaleng.2017.09.005. URL http://www.sciencedirect.com/science/article/pii/S0378383916303672. 41

M. J. van Duin, N. R. Wiersma, D. J. Walstra, L. C. van Rijn, and M. J. Stive. Nourishing the shoreface: Observations and hindcasting of the Egmond case, The Netherlands. *Coastal Engineering*, 51(8-9):813–837, 2004. ISSN 03783839. doi: 10.1016/j.coastaleng.2004.07.011.

B. van Maanen, R. J. Nicholls, J. R. French, A. Barkwith, D. Bonaldo, H. Burningham, A. Brad Murray, A. Payo, J. Sutherland, G. Thornhill, I. H. Townend, M. van der Wegen, and M. J. A. Walkden. Simulating mesoscale coastal evolution for decadal coastal management: A new framework integrating multiple, complementary modelling approaches. *Geomorphology*, 256: 68–80, 2016. ISSN 0169-555X. doi: http://dx.doi.org/10.1016/j.geomorph.2015.10.026. URL http://www.sciencedirect.com/science/article/pii/S0169555X15301914. 2

M. Viitak, I. Maljutenko, V. Alari, Ülo Suursaar, S. Rikka, and P. Lagemaa. The impact of surface currents and sea level on the wave field evolution during st. jude storm in the eastern baltic sea. *Oceanologia*, 58(3):176 – 186, 2016. ISSN 0078-3234. doi: https://doi.org/10.1016/j.oceano.2016.01.004. URL http://www.sciencedirect.com/science/article/pii/S0078323416000063. 171, 172

C. Villaret, J. M. Hervouet, R. Kopmann, U. Merkel, and A. G. Davies. Morphodynamic modeling using the Telemac finite-element system. *Computers and Geosciences*, 2013. ISSN 00983004. doi: 10.1016/j.cageo.2011.10.004. 123

M. Visser, W. de Ruijter, and L. Postma. The distribution of suspended matter in the Dutch coastal zone. *Netherlands Journal of Sea Research*, 27(2):127–143,

jun 1991. ISSN 0077-7579. doi: 10.1016/0077-7579(91)90006-M. URL https://www.sciencedirect.com/science/article/pii/007775799190006M. 176

T. Wahl, I. D. Haigh, P. L. Woodworth, F. Albrecht, D. Dillingh, J. Jensen, R. J. Nicholls, R. Weisse, and G. Wöppelmann. Observed mean sea level changes around the North Sea coastline from 1800 to present. *Earth-Science Reviews*, 124(Supplement C):51–67, 2013. ISSN 0012-8252. doi: https://doi.org/10.1016/j.earscirev.2013.05.003. URL http://www.sciencedirect.com/science/article/pii/S0012825213000937. 39

J. J. Williams, N. J. MacDonald, B. A. O'Connor, and S. Pan. Offshore sand bank dynamics. *Journal of Marine Systems*, 24(1–2):153–173, 2000. ISSN 0924-7963. doi: http://dx.doi.org/10.1016/S0924-7963(99)00085-8. URL http://www.sciencedirect.com/science/article/pii/S0924796399000858. 27

B. Yuan and H. E. de Swart. Effect of sea level rise and tidal current variation on the long-term evolution of offshore tidal sand ridges. *Marine Geology*, 390: 199–213, aug 2017. ISSN 00253227. doi: 10.1016/j.margeo.2017.07.005. 11, 42

B. Yuan, H. E. de Swart, and C. Panadès. Modeling the finite-height behavior of offshore tidal sand ridges, a sensitivity study. *Continental Shelf Research*, 137:72–83, apr 2017. ISSN 0278-4343. doi: 10.1016/J.CSR.2017.02.007. URL https://www.sciencedirect.com/science/article/pii/S0278434316305581. 41, 42

J. T. Zimmerman. Dynamics, diffusion and geomorphological significance of tidal residual eddies. *Nature*, 290(5807):549–555, 1981. ISSN 00280836. doi: 10.1038/290549a0. 21